# Dynamics of Compact Objects in Dense Stellar Clusters and the Implications for Gravitational Wave Detections.

Jordan Owen Barber

A thesis submitted for the degree of Doctor of Philosophy

Cardiff University
March 31st 2025

# Summary of thesis

Dense stellar clusters, such as globular clusters, are gravitationally bound groups of stars that evolve through numerous few-body interactions. The evolution of these clusters is closely linked to the dynamics of the black holes within them, leading to the formation of binary black hole systems and black hole-star systems; as well as driving binary black holes to merger. To better understand these dynamics, it is essential to use sophisticated simulation codes that accurately model the stellar evolution, setting the black hole mass distribution, and the gravitational interactions within clusters.

Chapter 1 introduces some of the physics surrounding black hole formation and subsequent evolution, both from single stars, and stellar binaries. We then discuss how the dynamics of black hole interactions couples with the evolution of the host stellar cluster; highlighting the effect of dynamics on the binary black hole orbital properties. The second half of the chapter reviews the current state of cluster simulation codes, with a particular focus on $N$-body methods, which are central to the work presented in this thesis.

In Chapter 2 we examine the role of primordial binaries within stellar clusters. We begin by simulating the isolated formation of a population of binary black holes using the rapid population synthesis code `COMPAS`. Using theoretical arguments, we then make predictions for the subsequent evolution of these binaries within a star cluster and compare the results to those from $N$-body simulations. We conclude this chapter with an analysis of the types of interactions expected within clusters, concluding that binary-binary encounters are likely the dominant form of interactions in clusters with $v_{\rm esc} \lesssim 100$ km s$^{-1}$ and large primordial binary fractions.

Chapter 3 presents a detailed analysis of data from 34 $N$-body cluster simulations produced using the new $N$-body code `PeTar`. These simulations cover a range of initial cluster masses, half-mass densities and metallicities, and include models both with and without primordial binaries. We investigate the orbital properties of merging binary black holes, their system multiplicity, and track the evolutionary history of particularly massive black holes. For each cluster, we compute both the number of mergers and the cluster's merger efficiency, comparing these against results from more approximate methods.

Building on this, Chapter 4 focuses on black hole-star binaries. We analyse their presence in our cluster models, explore their orbital properties, and search for systems that could resemble the three Gaia black hole systems that have recently been observed.

Finally Chapter 5 offers concluding remarks and a summary of the key findings from the thesis, along with discussions for the individual works presented throughout.

# Contents

# List of Figures

# List of Tables

All we have to decide is what to do with the time that is given to us.
- Gandalf, The Fellowship of the Ring by J.R.R Tolkien

# Collaborative work

Portions of this thesis are, to a great extent, adopted word-by-word from published collaborative work. The breakdown of these works is described below:

- Chapter 2 is drawn from Barber et al. (2023). This was work performed with Fabio Antonini and Debatri Chattopadhyay and published in **Monthly Notices of the Royal Astronomical Society**. I was the lead author for this work and performed all the analysis.
- Chapter 3 is drawn from Barber & Antonini (2025). This work was performed with Fabio Antonini and published in **Monthly Notices of the Royal Astronomical Society**. I was the lead author for this work and performed all of the analysis.
- Chapter 4 is drawn from Fantoccoli et al. (2025). This work was performed with Federico Fantoccoli, Fabio Antonini, Fani Dosopolou and Debatri Chattopadhyay and published in **Monthly Notices of the Royal Astronomical Society**. I was the second author for this work and supervised the first author, personally producing all the simulations used in this study and performing the majority of the analysis.

I am the sole author for all other work presented in this thesis.

# Scientific Acknowledgements

I am funded by the STFC grant ST/T50600X/1. The majority of the simulations in this work have been run using the Cardiff HPC System Hawk, and I acknowledge the support of the Supercomputing Wales project, which is part-funded by the European Regional Development Fund (ERDF) via Welsh Government. The simulations in this work have been performed using the following the codes: `COMPAS` (Team COMPAS: Riley, J. et al., 2022; Vigna-Gómez et al., 2018; Stevenson et al., 2017), `PeTar` (Wang et al., 2020b), `BSE` (Hurley et al., 2002; Banerjee et al., 2020), `SSE` (Hurley et al., 2000), `COSMIC` (Breivik et al., 2020), and `cBHBd` (Antonini & Gieles, 2020b).

I would like to thank Long Wang for his assistance in setting up, and running the `PeTar` simulation code, as well as Mark Gieles and Dani Marín Pina for our many useful comments and insightful discussions.

Finally, I would like to thank my thesis reviewers, Vivien Raymond and Sebastian Kamann, for their careful reading of my thesis and for the engaging and insightful discussion that followed.

# Acknowledgements

First and foremost I would like to express my sincerest gratitude to my PhD supervisor, Fabio Antonini, who has supported, guided and encouraged me throughout this journey. I have learned so much from him over these three and a bit years, and I would not be the researcher I am today without his mentorship. For that, I cannot thank him enough.

I am also grateful to the rest of my supervisory team, Stephen Fairhurst and Emyr Macdonald, for their helpful feedback and suggestions, always ensuring that I stayed on track and made the most of my PhD experience. I would like to extend my thanks to Debatri Chattopadhyay, who was instrumental in guiding me in the early stages of the PhD, assisting me with my first simulation runs, and supporting the work that lead to my first published paper. I must also thank Patrick Sutton, who supervised both of my undergraduate dissertations, helping develop my early research skills and build the confidence to continue onto the PhD in the first place.

To the rest of the Cardiff GEI group, I am incredibly thankful to have been a part of such a supportive and inspiring community. It has been a privilege to meet and work alongside you all.

Throughout my time in Cardiff, both during my undergraduate and PhD, I have been fortunate to make so many friends that have shaped me into who I am today. It would be impossible to give you all the proper recognition you deserve but know that I am forever grateful!

To Sama, you have become such a close friend, and I will sincerely miss sharing an office with you, especially having our chats, which so often turned into rants about one thing or another. I wish you all the success in completing your PhD and expect to see you running the collaboration in a few years. You know you'll always have my vote. To Alex, I am always impressed by your knowledge, and I feel like every conversation with you teaches me something new, usually meaning that I realise another way how my code is wildly inefficient. I will miss our morning political discussions and catching up on the latest shenanigans of your D&D campaign. To Ben, I will never tire of watching you completely destroy my Tetris solve times, it has been a pleasure getting to know you and I wish you all the best for the future.

To Will and Terri, you were among the first friendly faces I encountered, back when we would eat lunch huddled in the postdoc's office. It has been a pleasure to know both of you and and I wish you all the best for the future.

To the players in the GW D&D group: Ali, Abhinav, Alex, Sama, Ben, Michael, Vassilis, Nikitha, Meryl and Sam, thank you for indulging me every week for nearly two years and giving me the much needed break away from work.

To the rest of those that came before: Jakob, Sander, Virginia and Phil, it was a pleasure getting to know you all on nights out in the Flute, and conference trips abroad, thank you for making this PhD journey so enjoyable, and I wish you nothing

but success and good fortunes.

To my non-GW friends, James, Charlie, Tom and Adib, thank you for supporting me throughout my academic career. I greatly appreciate it, and here's to many more board game nights and bouldering sessions.

My wonderful family deserves so much thanks because, without their support, I would not be here today. To Mum and Terry, you have always pushed me to work hard and do my best. To my siblings, Ryan, Chloe, and Rosie, thank you for your continued support over the years. I would also like to give my gratitude to Chrissy's Family who have continued to support and encourage me through my university years.

Last, but certainly not least, I owe a tremendous debt of gratitude to my partner, Chrissy, who has been my biggest source of comfort and support throughout my PhD. Nothing in this thesis could have been possible without you by my side.

# List of acronyms

| | |
|---|---|
| AD | Anderson-Darling |
| AGN | Active galactic nucleus |
| BBH | Binary black hole |
| BH | Black hole |
| CCSNe | Core-collapse supernova |
| CDF | Cumulative distribution |
| CE | Common envelope |
| CO | Compact object |
| COM | Centre of mass |
| DCO | Double compact object |
| ECSNe | Electron capture supernova |
| GR | General theory of Relativity |
| GS | Giant star |
| GW | Gravitational wave |
| He | Helium |
| HG | Hertzsprung gap |
| IMBH | Intermediate mass BH |
| KAGRA | Kamioka Gravitational-Wave Detector |
| LIGO | Laser Interferometer Gravitational-Wave Observatory |
| MS | Main sequence |
| MT | Mass transfer |
| NS | Neutron star |
| PN | Post-Newtonian |
| PPI | Pulsational pair instability |
| RLO | Roche lobe overflow |
| SMBH | Supermassive BH |
| SN | Supernova |
| UCSNe | Ultra stripped supernova |
| WD | White dwarf |
| ZAMS | Zero-age main sequence |

# Chapter 1

# Introduction

## 1.1 Black holes

Of the four fundamental forces that govern our Universe, perhaps the most familiar is the force of gravitation. Throughout history there have been numerous attempts to describe this force empirically, however, the first mathematically rigorous theory came in 1687 with Sir Isaac Newton's "Law of Universal Gravitation" (Newton, 1687). Using this theory astronomers were able to compute the motion of the celestial bodies to unparalleled accuracy. According to Newton, the force of gravitational attraction between two bodies of mass $m_1$ and $m_2$ is proportional to the product of their masses and inversely proportional to the square of their separation $R = |\vec{r}_2 - \vec{r}_1|$

$$\vec{F}_{\mathrm{g}} = \frac{G m_1 m_2}{|\vec{r}_2 - \vec{r}_1|^3} \cdot (\vec{r}_2 - \vec{r}_1) \ , \tag{1.1}$$

where $G$ is the gravitational constant.

Almost 100 years later in 1784, English philosopher John Mitchell used this law to envision a massive stellar body, producing such a large gravitational force that the escape velocity of a particle on its surface would exceed that of light (Mitchell, 1784). He further described how, even though these "dark stars" would not emit any observable light, their presence may be inferred through observation of a star moving as though in a binary system, but without a visible companion star. Although this is the earliest notion of what we now refer to as a black hole (BH), the idea remained relatively untouched until the turn of the twentieth century and the reimagining of our theory of gravity.

In 1915 Albert Einstein presented his General theory of Relativity (GR) (Einstein, 1915), reconciling gravity into his previously published Special Theory of Relativity (Einstein et al., 1905). In GR we shift our idea of gravity to spacetime distortions caused by the presence of massive bodies. The observed "gravitational attraction" is then simply a consequence of objects moving on geodesics through this curved spacetime. Within the mathematical framework of GR the concept of a BH arises

simply as a non-trivial solution to Einstein's field equations. However, these objects were still mostly considered a mathematical curiosity of the theory until the 60s when it was shown that these BH spacetimes are actually generic solutions to GR. This realisation was swiftly followed by the first indirect evidence for a BH, Cygnus-X1, an X-ray source believed to be composed of a BH orbited by a blue supergiant variable star (HDE 226888) (Bowyer et al., 1965). It was not until 2015 that we got the first direct evidence for the existence of BHs through the observation of gravitational waves (GWs) from a merging binary black hole (BBH) (Abbott et al., 2016a). Finally, in 2019 the first direct image of a BH was produced by the Event Horizon Telescope Collaboration et al. (2019), depicting the shadow of the BH on the surrounding superheated plasma.

Astrophysically there a likely several mechanisms that can lead to the formation of a BH. Some alternative theories propose that BHs may have formed via gravitational collapse of extreme densities fluctuations in the early universe (Carr & Hawking, 1974; Chao, 1984; Carr et al., 2016; Choudhury & Sami, 2025), although, there has been no observational evidence supporting these ideas. It is generally well accepted that the vast majority of stellar mass BHs are the remnants of the gravitational collapse of massive stars (Bond et al., 1984a). The resulting BH's mass is highly dependent on the mass and metallicity of the progenitor star, as well as the modelling of the supernova (SN) (Heger et al., 2003; Mapelli et al., 2010; Fryer et al., 2012; Mirabel, 2017; Farmer et al., 2019). Since this process imposes an upper limit on the BH mass, it cannot account for the existence of supermassive BHs (SMBHs) ($M > \mathcal{O}(10^6\ \mathrm{M}_\odot)$), which are thought to exist in the centres of most galaxies (Rees, 1984; Shields, 1999; Kormendy, 2013). One possible explanation for the growth of these SMBHs is repeated BBHs mergers, an idea that has gained a lot of traction in recent years thanks to the GW observations of distant BBH inspirals.

GWs are another prediction from Einstein's GR, and in general are produced due to any non-symmetric, relative motion between masses. Unlike the electromagnetic force, which at leading order arises from an oscillating dipole moment, GWs are emitted first at quadrupolar order. Monopole radiation is forbidden by the local conservation of mass-energy in GR, since the mass-energy of an isolated system cannot vary in time. Likewise, dipole radiation vanishes because the conservation of total 4-momentum ensures that the system's centre of mass (COM) evolves at constant velocity, yielding a static dipole moment. Therefore the lowest non-vanishing radiative contribution in the multipole expansion of the gravitational field arises at quadrupolar order. Many astrophysical phenomena are predicted to produce GWs, however for the work in this thesis we are concerned with the production of GWs from binary star systems, specifically BBH systems. As two BHs orbit one another they radiate away both energy and angular momentum in the form of GWs; this corresponds to a decrease in the binary semi-major axis ($a$) and eccentricity ($e$) respectively. Given enough time the binary will radiate all its energy away and the two BHs will coalesce,

resulting in a single more massive BH. Owing to the non-linear nature of Einstein's field equations, the analytical calculation for the strength of this GW radiation is non-trivial in the relativistic limit (close to the time of merger). However, since a bound BBH will spend most of its life in the non-relativistic regime, Peters & Mathews (1963) showed that the rate at which a binary radiates energy can be estimated by averaging over one orbital period. Following this we can compute an estimate for the timescale over which the binary radiates away all its energy and eventually merges. This is commonly referred to as the "GW timescale" ($t_{\rm GW}$) or "delay time" ($t_{\rm delay}$) and was derived in Peters (1964)

$$t_{\rm GW} = \frac{12}{19}\frac{c_0^4}{\beta} \times \int_0^{e_0} \frac{de \cdot e^{29/19}[1 + (121/304)e^2]^{1181/2299}}{(1-e^2)^{3/2}} \ , \tag{1.2}$$

where

$$\beta = \frac{64}{5}\frac{G^3 m_1 m2 (m_1 + m_2)}{c^5} \ , \tag{1.3}$$

and

$$c_0 = \frac{a_0}{e_0^{12/19}} \frac{(1-e_0^2)}{\left[1 + \frac{121}{304}e_0^2\right]^{870/2299}} \ , \tag{1.4}$$

is computed from the initial conditions of the binary, $a = a_0$ and $e = e_0$.

The GWs produced from the binary propagates through the Universe, its intensity falling according to the inverse square law, until eventually reaching Earth. Importantly, our current GW detectors are specifically sensitive to the amplitude of the incoming GW, which in turn is proportional to the square root of the intensity. Since most sources are likely to be distant; by the time the signal reaches us it has become so weak that only the final few (loudest) cycles are observable with our current generation of detector. There are three main collaborations currently on the search for GWs from merging binaries: the Laser Interferometer Gravitational-Wave Observatory (LIGO) scientific collaboration (LSC) operates two detectors situated on opposite ends of the continental United States; the Virgo Collaboration has a detector in Pisa, Italy; and the Kamioka Gravitational-Wave Detector (KAGRA) collaboration has a detector in the Kamioka Observatory[1]. Collectively these three collaborations form the LIGO-Virgo-KAGRA (LVK) collaboration, which schedules and performs joint observing runs, sharing data in order to better localise sources and boost a detected signal's SNR.

When a signal is observed in these detectors, a series of sophisticated post-processing analyses is performed to extract posterior probability distributions for the parameters of the source binary. In total there are 15 parameters that describe

[1] A fifth detector named GEO600 was also built by a British-German collaboration, and is also a member of the LSC. However since its sensitivity is typically too low for BBH detections, it is now mainly used as a testing ground for new technologies.

the signal from a merging, quasi-circular BBH, which can be divided into extrinsic and intrinsic parameters. The intrinsic parameters comprise the primary and secondary component masses ($m_1$, $m_2$), as well as the three spin components for each BH ($S_{1:\mathrm{x,y,z}}$ and $S_{2:\mathrm{x,y,z}}$). The remaining seven are extrinsic parameters, consisting of the right ascension ($\alpha$), declination ($\delta$), and luminosity distance ($d_\mathrm{L}$) which together describe the location of the BBH relative to the Earth; the inclination ($\iota$), GW polarisation ($\psi$), and orbital phase ($\phi$) which describe the BBH's orientation with respect to Earth; and finally the time of merger ($t_\mathrm{c}$). In the context of this work, we are most concerned with the intrinsic properties, as these depend on the possible formation scenario of the source binary. We provide further details on the effects of different formation channels in Section 1.1.1. Another important feature of GW signal analysis is the ability to decompose a GW signal into a sum over spin-weighted spherical harmonic modes Thorne (1980), with the dominant contribution typically coming from the $(\ell, m) = (2, 2)$ mode. The remaining higher-order modes are generally subdominant, but their inclusion can reveal additional information about the properties of the source. In particular, these modes can carry signatures of orbital precession, where the component spins are misaligned with the orbital angular momentum vector causing the orbital plane to precess, and residual eccentricity in the binary. Both of these properties manifest as amplitude and phase modulations of the "standard" quasi-circular signal and are indicative of the BBH's evolution, making them ideal parameters to probe a source binary's formation and dynamical history (see Section 1.1.1 for further discussion).

The first GW was detected on the 14th September 2015 (Abbott et al., 2016a) by the LIGO detectors in the first observing run following their advanced LIGO upgrade. The GW was found to originate from a $36^{+5}_{-4}$ $\mathrm{M}_\odot$ + $29^{+4}_{-4}$ $\mathrm{M}_\odot$ BBH at a luminosity distance $410^{+160}_{-180}$ Mpc (Abbott et al., 2016b). Flash-forward to present day and the LVK collaboration now has $> 250$ publicly announced detections, and is currently in the midst of its fourth observing run(Abbott et al., 2019, 2021; The LIGO Scientific Collaboration et al., 2021).There have been numerous studies attempting to understand the observed population of merging BBHs, in particular to explain the likely astrophysical processes which cause such binaries to form. As more GW signals are detected we can begin to look into the population properties of the observed BHs, from which we aim to better understand the contribution to BBH formation from different astrophysical channels.

### 1.1.1 Binary black hole formation mechanisms

Broadly speaking, the processes that form a merging BBH can be split into two channels, an isolated evolution channel and a dynamical channel. Through the isolated channel, two massive stars are born in a bound binary and subsequently co-evolve in the absence of strong external interactions, for example in the galactic field. During

their evolution they likely undergo some period of common envelope (CE) evolution, which effectively shrinks the binary separation (e.g., Tutukov & Yungelson, 1973; Dominik et al., 2012; Ivanova et al., 2013; Glanz & Perets, 2021). Alternatively the binary's orbit may tighten through stable mass transfer (MT) episodes, where matter flows from one star to its companion over extended periods (e.g., Van Den Heuvel et al., 2017; Pavlovskii et al., 2017; Neijssel et al., 2019; Shao & Li, 2022). Additionally, chemically homogenous evolution, driven by efficient rotational mixing in rapidly spinning massive stars, can lead to the formation of close BBH systems without significant expansion of the stellar radii (e.g., Mandel & de Mink, 2016; Marchant et al., 2016; du Buisson et al., 2020; Riley et al., 2021). Eventually each star will collapse into a BH, and provided the binary remains bound following the SN kicks, the resulting BBH may merge within a Hubble time (e.g., Hurley et al., 2002; Belczynski et al., 2002; De Mink & Belczynski, 2015; Belczynski et al., 2016; Spera et al., 2019; Mapelli, 2020; Belczynski et al., 2020; Broekgaarden et al., 2021; Costa et al., 2021; Qin et al., 2023). A merging BBH formed through this isolated mechanism is expected to exhibit some key signatures in its GW signal. If we can extract these from the data, we can gain insight into the formation and evolution of the source of a observed GW. We now discuss these expected features.

In the previous section, we explained the likely formation of a single BH through the collapse of a massive star. Whilst this holds true for most stars, there are additional processes that must be considered for very massive stars with a helium (He) core $\gtrsim 30$ $M_\odot$. Specifically, it has been found that for He cores $> 60$ $M_\odot$ the core temperature becomes so high that energetic gamma-ray photons begin rapidly producing electron-positron pairs. This then reduces the radiation pressure which supported the star against gravitational collapse, and as a result the star becomes unstable and begins to contract, leading to the rapid burning of Oxygen and Silicon within the stellar envelopes (Ober et al., 1983; Bond et al., 1984b; Yungelson et al., 2008; Chen et al., 2014; Garba et al., 2022). This processes is aptly termed "pair-instability" and results in the complete destruction of the star leaving no remnant compact object (CO). There is an exception to this in extremely massive stars with cores $\gtrsim 130$ $M_\odot$, at which point the gravitational attraction on the outer stellar layers is so great that the star directly collapses to a BH (Heger et al., 2003).

Finally, for He cores between $\sim 30 - 60$ $M_\odot$ the star experiences several pair instability phases in oscillatory pulses. Although these pulses are too weak to fully unbind the star, they facilitate mass ejection ultimately resulting in a remnant BH which is significantly less massive than would otherwise be expected, this process is termed pulsational pair instability (PPI) (Barkat et al., 1967; Woosley et al., 2007; Belczynski et al., 2016; Spera & Mapelli, 2017; Woosley, 2017, 2019; Farmer et al., 2019; Stevenson et al., 2019; Marchant et al., 2019; Woosley & Heger, 2021). It can clearly be seen then that assuming solely a isolated evolution we should expect a "gap" in the BH mass distribution owing to pair instability and it has been shown

that, in terms of the BH mass, this gap is defined as $\sim 45-130$ M$_\odot$ (Woosley et al., 2002, 2007; Belczynski et al., 2016; Woosley, 2017, 2019; Woosley & Heger, 2021).

As well as impacting the individual component masses of a binary, the isolated evolution channel also is also expected to affect the binary properties. As previously discussed, the emission of GW radiation rapidly removes angular momentum from the system decreasing the eccentricity of a binary. In addition, there can be phases of MT and CE during a binary's stellar evolution which also reduce the eccentricity of the binary (Glanz & Perets, 2021). Ultimately, this results a binary with $e \sim 0$ once it enters the LIGO-Virgo frequency band ($\approx 10$ Hz). Concerning the spins of the binary components, whilst the magnitude of the resultant BH spins is mostly unconstrained and depends on the angular momentum of the progenitor star(Fuller & Ma, 2019; Fuller et al., 2019; Olejak & Belczynski, 2021; Marchant et al., 2024), there is expected to be a strong alignment of both spins with the orbital angular momentum, since the only way to induce a misalignment is through the BH natal kicks (Rodriguez et al., 2016c). Finally, it is expected that whilst the mass-ratio ($q = m_1/m_2$) is typically $\gtrsim 0.1$, there is some preference towards $q \sim 1$ (Giacobbo & Mapelli, 2018; Giacobbo et al., 2018).

The dynamical channel involves the formation and evolution of a BBH within a dense stellar system, where the binary experiences many gravitational encounters with other BHs and stars. Through these interactions BBHs can be formed, disrupted, and have their orbital properties altered through dynamical hardening. In certain cases, these encounters can bring a BBH into a regime where it is able to merge within a Hubble time. Since this mechanism requires dynamically active environments, the cores of dense stellar clusters such as globular clusters ($10^4$ M$_\odot \lesssim M_{\rm cl} \lesssim 10^6$ M$_\odot$) (e.g., Coleman Miller & Hamilton, 2002; Rodriguez et al., 2016b; Askar et al., 2017; Samsing, 2018; Hong et al., 2018; Rodriguez et al., 2018a,b; Sedda et al., 2019; Anagnostou et al., 2020; Antonini & Gieles, 2020a; Arca Sedda et al., 2021; Leveque et al., 2023; Torniamenti et al., 2024; Arca Sedda et al., 2023a), nuclear clusters ($10^6$ M$_\odot \lesssim M_{\rm cl} \lesssim 10^8$ M$_\odot$) (e.g., Miller & Lauburg, 2009; Antonini & Perets, 2012; Antonini & Rasio, 2016; Bartos et al., 2017; Mapelli et al., 2021; Atallah et al., 2023; Rodriguez et al., 2022) and open clusters ($10^2$ M$_\odot \lesssim M_{\rm cl} \lesssim 10^4$ M$_\odot$) (e.g., Banerjee, 2017; Di Carlo et al., 2019, 2020, 2021; Rastello et al., 2021; Torniamenti et al., 2022; Banerjee, 2022) are ideal locations. Nuclear clusters may also house an active galactic nucleus (AGN), where an accretion disc has formed around the central SMBH. In this case there are additional dynamical processes that can lead to a BBH forming and merging within the AGN disk, such as torques exerted on the BBH by the surrounding dense gas, and binary accretion effects (e.g., Stone et al., 2017; Bartos et al., 2017; McKernan et al., 2018; Gröbner et al., 2020; Fabj & Samsing, 2024).

Merging BBHs from the dynamical channel are also expected to leave signatures of their evolution in the GW signal. Firstly, the component masses are not limited

by the PPI, since the remnant BH of one merger can go on to form a new BBH which may also be driven to merger. These "hierarchical" mergers can keep occurring provided there are still BHs in the cluster, and the merger remnant BH is not ejected by the GW recoil kick. This can thus form BHs with no upper limit mass, as well as potentially filling the mass-gap left by the isolated channel. A dominant form of interactions in clusters are dynamical exchanges, where there is new binary paring following some $N \geq 3$ body encounter. These encounters yield an isotropic spin angle distribution and can also lead to very highly eccentric systems which maintain some of their eccentricity in the LIGO-Virgo band, these are typically called "GW captures".

The relative importance of the two formation channels in producing a detectable population of BBHs depends on two key factors: the proportion of stars that form in dense star clusters (and its redshift dependence), and the efficiency of both stellar evolution and dynamical processes in driving BBHs to merge. Most massive binaries are located in clusters and associations, which include both bound and unbound systems. However, the majority of these binaries are not gravitationally bound to one another, and in many cases, the surrounding stellar densities are too low for dynamical interactions to play a significant role in their evolution (Krumholz et al., 2019). As a result, most massive stars can be considered as evolving in the field of the galaxy, only influenced by their closest stellar companions with the majority of BH progenitors found in binary or higher-multiplicity systems (e.g., Sana et al., 2012; Moe & Di Stefano, 2017).

In contrast, within dense star clusters, dynamical processes can significantly enhance the merger rate of BBHs, making this channel a potentially important contributor to the observed BBH population. In addition, observations of young open clusters have found a binary fraction of $> 70\%$ among O/B type stars (Sana et al., 2012), which suggests that dense stellar clusters likely form with some initial population of *"primordial"* binaries[2]. These primordial binaries will initially evolve according to a purely isolated channel; however, while they remain in the cluster they can experience dynamical encounters with other members, which can alter their orbital properties (e.g., Samsing et al., 2014). This provides a mix of both formation channels. Although there has been extensive theoretical work on how dynamical encounters might influence the number and properties of detected BBHs (Goodman & Hut, 1993; Miller & Hamilton, 2002; Samsing & D'Orazio, 2018), reaching a clear conclusion remains challenging. This is mainly due to the complexity involved in simulating the relevant parameter space for star clusters in a self-consistent and accurate way.

[2]In the literature they are sometimes also referred to as "original" binaries.

### 1.1.2 Black holes in star clusters

Dynamical stellar systems are classified as collisional or collisionless systems, with the split determined by the relative importance of particle interactions to the evolution of the overall system. The evolution of a collisional system is driven by the frequent interactions between its constituent particles. Conversely in a collisionless system, the constituent particles evolve predominantly under the influence of the smooth gravitational field of the global system.

To make the distinction, we consider the 2-body relaxation time $t_{\rm relax}$ of a system of $N$ particles

$$t_{\rm relax} \simeq \frac{0.1N}{\ln(N)} t_{\rm cross} \ , \tag{1.5}$$

where $t_{\rm cross} = R/v$ is the crossing time of the system, $R$ is the radius of the system and $v$ is the average speed of a particle. Comparing $t_{\rm relax}$ to a Hubble time ($t_{\rm H}$), we define a collisional stellar system as having $t_{\rm relax} < t_{\rm H}$ and a collisionless system as having $t_{\rm relax} \gtrsim t_{\rm H}$. For a globular cluster which typically contains $N \sim 10^5$ stars and $t_{\rm cross} \approx 1$ Myr, the relaxation time is $t_{\rm relax} \approx 900$ Myr marking these as collisional systems. While open clusters are also collisional due to their short relaxation times, nuclear star clusters lie on the boundary between the collisional and collisionless regimes, with $t_{\rm relax} \sim 1 - 10$ Gyr. Many nuclear clusters therefore still experience dynamical evolution driven by two-body relaxation. To study such systems in a consistent framework alongside globular and open clusters, it is necessary to have utilise N-body simulations with $> 10^6$ particles.

Since a globular cluster is a collisional system, its evolution is driven by the frequent interactions of its stellar components. In particular these interactions lead to a number of important dynamical processes such as dynamical friction, three/four-body encounters and binary hardening; all of which are crucial in the dynamical formation of merging BBHs.

Dynamical friction describes the deceleration (drag) of a massive stellar object due to its gravitational deflections of the background field of lighter stars. For a stellar object with mass $M$ and relative velocity $v$, the deflection angle for an impact parameter $b$ is given by the gravitational focusing

$$\theta(b) \approx \frac{2GM}{bv^2} \ , \tag{1.6}$$

where each encounter transfers momentum to the lighter star. Integrating over all impact parameters, from the closest strong encounters at $b_{\rm min}$ to the distant weak encounters at $b_{\rm max}$ we account for contributions of small and large angle deflections. The cumulative effect of every deflection yields a net frictional force effectively slowing the massive body and causing it to spiral into the cluster core (Chandrasekhar, 1943). Since this focussing term is proportional to the mass of the perturbing object,

the strongest friction force is experienced by the heaviest objects in the cluster first, e.g., massive giant stars (GSs) and BHs.

This process is referred to as mass segregation and results with an over density of massive objects in the cluster core where their close proximity allows them to more readily interact. It is during these interactions within the core that we are more likely to see three-body and four-body encounters between BHs. These encounters are chaotic and have a variety of different end states depending on the initial conditions of the interaction (e.g., Antognini & Thompson, 2016; Samsing, 2018; Zevin et al., 2019; Marín Pina & Gieles, 2024), however, of particular note is the possibility of binary formation (e.g., Aarseth & Heggie, 1976; Goodman & Hut, 1993; Heggie & Hut, 2003; Ginat & Perets, 2024; Atallah et al., 2024).

A binary within a star cluster can either be hard or soft, depending on the ratio of its binding energy to the average kinetic energy of the surrounding stars. For a given binary we can define a cut-off semi-major axis value called the hard/soft limit ($a_{\rm h}$)

$$a_{\rm h} \simeq \frac{G\mu}{\sigma^2} \ , \tag{1.7}$$

where $\mu = m_1 m_2/(m_1 + m_2)$ is the reduced mass of the binary and $\sigma$ is the velocity dispersion of the surrounding stars. A binary with separation $a$, is then classified as a *hard* binary if $a < a_{\rm h}$ or as a *soft* binary if $a > a_{\rm h}$. Binary formation of two initially unbound particles requires some way to shed energy from the system. In the Newtonian point mass limit, this requires a third body to be involved in the interaction. In this way we have three single particles which undergo a close 3-body encounter, resulting in two particles forming a bound binary, and transferring the excess energy to the third body which kicks it to infinity. For the binary to form, the interacting particles must have been energetic enough for the third body to be ejected, and therefore their kinetic energies need to be at least as large as the average kinetic energy of the surrounding stars. Since we define the hard/soft limit as a binary binding energy equal to this average kinetic energy it is clear that most binaries must form with separations close to $a_{\rm h}$. The dynamics of hard and soft binaries has been well studied, going all the way back to the 70's, especially understanding how they interact with other cluster stars (e.g., Heggie, 1975; Hills, 1975; Hut & Bahcall, 1983; Spitzer, 1987; Quinlan, 1996). It was shown by Heggie (1975) that on average, through binary-single interactions a hard binary tends to harden (tighten) whilst a soft binary tends to be disrupted. Furthermore they found that during a resonant encounter[3], a hard binary loses, on average, 40% of its binding energy. Including fly-by interactions into the average yields an average energy loss of 20% (Spitzer, 1987; Heggie & Hut, 1993; Quinlan, 1996; Portegies Zwart et al.,

[3]These are complex interactions where the binary temporarily captures the single star, forming a triple system for several orbits.

2010).

There are some important caveats to note at this point. Firstly, close to $a_{\rm h}$ the distinction between a hard and soft binary becomes ambiguous, and the statistical statements made in Heggie (1975) may not hold. In this regime it is important to consider individual encounters, which may push a binary across the hard/soft binary in either direction. In fact, Goodman & Hut (1985) showed that a binary forming around $a_{\rm h}$ has a $\sim 10\%$ probability of surviving successive encounters, tightening the binary to the extent that the probability of ionisation $\sim 0$. Secondly, the statement of the average binding energy lost during an encounter is found in the equal mass regime ($m_1 = m_2$), and there has been recent work testing the validity of this statement in the non-equal mass case (e.g., Forastier et al., 2024).

Numerous previous studies have shown the important role BHs play on the long-term evolution of a stellar cluster (Spitzer, 1987; Binney & Tremaine, 1987; Wang, 2020; Antonini & Gieles, 2020a), and in particular how BBHs play a crucial role as an energy source for the cluster. The core of a cluster is a highly dynamical environment, with numerous encounters between stellar objects. Assuming a cluster with no primordial binaries, the interactions in the core are predominantly between single bodies which gradually reduce the net kinetic energy of the core. This leads to a contraction of the core, commonly referred to as core collapse. The now denser core facilitates more frequent strong encounters and eventually the formation of a binary. Subsequently, this binary hardens through 3-body interactions, each resulting in the transfer of energy from the binary to the third body. This causes the binary semi-major axis to shrink (hardening the binary), while the excess energy is pumped into the third body. Since this process ultimately increases the net kinetic energy of the core, it halts the core collapse. The binary will continue to harden until it is eventually either disrupted, or driven to merger. At this point the cluster core will resume its collapse until another binary is formed to halt it again. Given the short evolutionary timescales for O/B type stars, BHs are formed early on in the clusters lifetime and since they are the most massive objects in the cluster they dominate the strong encounters. Thus, the first binaries to be formed in the core are typically BBHs which subsequently interact with the other BHs.

Clearly, binaries are important for the survival of a cluster, however it takes some time for them to form dynamically. In addition they will number few, Marín Pina & Gieles (2024) showed that binary-binary encounters are efficient at destroying binaries which efficiently restricts the number of binaries within the core at any given time to $\mathcal{O}(1)$. On the other hand, the existence of primordial binaries provides a source of massive binaries right from the beginning, which facilitates the formation of numerous BBHs within $\mathcal{O}(1-10)$ Myr. Naturally the presence of primordial binaries can halt the core collapse much sooner than when they are not included (Trenti et al., 2007; Pavlík & Vesperini, 2021). Observational data further supports this idea. Only a small fraction of Milky Way globular clusters exhibit a steep central

brightness cusp indicative of a collapsed core, with Djorgovski & King (1986) finding only 20% of clusters in their survey are core-collapsed. This implies that most of their observed clusters remain non-collapsed despite ages and relaxation times that would otherwise predict collapse. This discrepancy strongly suggests an internal energy source. Primordial binaries are the most probable candidate for this energy source since they are able to inject energy and re-expand cluster cores through many-body encounters, maintaining relatively large core radii (Goodman & Hut, 1989).

Importantly, while primordial binaries are formed across a range of initial stellar masses, it was shown by Wang et al. (2021) that the secular evolution of a cluster is almost entirely driven by the BBHs and so for the purposes of numerical simulations, low-mass binaries can be mostly ignored until the BH population has been depleted. The existence of primordial binaries also increases the probability of binary-binary encounters in the core. These are more complex interactions than binary-single encounters and have additional possible end-states, in particular the formation of a stable triple system (Zevin et al., 2019).

### 1.1.3 Observational history of BHs in star clusters

For decades, globular clusters were believed to be largely devoid of stellar-mass BHs. This view was rooted in early theoretical arguments based on mass segregation and the so-called Spitzer instability (Spitzer, 1987), which suggested that BHs, being more massive than the average stellar population, would quickly sink to the centre of the cluster and dynamically decouple from the rest of the system (Kulkarni et al., 1993). This decoupled BH sub-cluster was expected to undergo core collapse and efficiently eject its members through strong dynamical interactions, leading to the rapid depletion of BHs on timescales significantly shorter than the cluster's age. Early dynamical simulations supported this view, and for a long time, there was little observational evidence to suggest otherwise.

This picture began to change in the past decade. The first strong observational evidence for retained BHs in a globular cluster came from Strader et al. (2012), who used deep radio observations to identify two candidate stellar-mass BHs in the Milky Way globular cluster M22. These BHs exhibited flat-spectrum radio emission consistent with low-level accretion, marking the first detection of such objects in a cluster environment. This discovery was followed by the spectroscopic detection of a detached stellar-mass BH binary in NGC 3201 by Giesers et al. (2018), who measured large radial velocity variations in a visible main-sequence companion, implying the presence of a $\sim 4.4\,\mathrm{M}_\odot$ dark companion. Subsequent observations by Giesers et al. (2019) reported two additional BH candidates in the same cluster, suggesting that multiple BHs could coexist in a single globular cluster.

These discoveries prompted renewed theoretical investigation. Modern simulations have since overturned earlier assumptions about universal BH ejection. For

instance, Monte Carlo cluster evolution models by Morscher et al. (2015) showed that up to hundreds of BHs can be retained in realistic globular cluster conditions for many Gyr. These models demonstrated that the Spitzer instability does not necessarily lead to full BH depletion, and that BHs can instead remain dynamically mixed with the rest of the cluster over long timescales. Similarly, Weatherford et al. (2020) used observational constraints and $N$-body-inspired models to infer that several Galactic globular clusters may currently host BH subsystems containing total BH masses exceeding $10^3\,\mathrm{M}_\odot$.

In addition to radio and spectroscopic detections, recent astrometric data from the Gaia satellite has opened a new window into BH discovery. The Gaia satellite was a space observatory which operated from 2013 to March 2025, making observations in the extended visible light band (near-Infrared to near-Ultra Violet). Using astrometry to measure the orbital motions of luminous stars around unseen companions, Gaia is able to identify candidate BH-star binary systems (Chawla et al., 2022). Several candidate BH–luminous star binaries have been identified this way in the field population of the Milky Way (e.g. El-Badry et al., 2023b,a; El-Badry, 2024), some of which may reside in dynamically old environments or could have been formed within dense stellar clusters (See Chapter 4 for in-depth study on Gaia-BH binaries). However, in general the formation environment of these systems, and their link to dense stellar clusters remains unclear. This method holds promise for uncovering further BH populations in stellar systems where traditional accretion-based detection methods may fail.

The implication of all these findings is significant: not only do stellar-mass BHs survive in globular clusters, but they may also play an important dynamical role in the long-term evolution of the cluster. BHs can act as a central energy source, stalling or even reversing core collapse, as well as driving the formation of compact object binaries, including those detectable via gravitational waves. The updated observational picture, combined with more sophisticated simulations, has led to a notable shift in our understanding of BH retention in star clusters.

## 1.2 Simulating star clusters

Current star cluster simulations generally fall into one of three categories based on the algorithms and methods used: $N$-Body simulations, Monte Carlo methods, and semi-analytical methods. This name order also typically represents the methods in decreasing computation time but decreasing accuracy. Furthermore, semi-analytical and Monte Carlo methods are generally able to efficiently explore a much larger region of the cluster parameter space, and are currently the only way to realistically simulate clusters with $> \mathcal{O}(10^6)$ particles. In the following sections we will explain these methods in a more detail.

### 1.2.1 $N$-Body methods

Some of the earliest $N$-body simulations date back to the 60s with the work of Von Hoerner (1960) and Aarseth (1963, 1966) who ran models with up to $N = 16$ and $N = 100$ particles respectively (Dehnen & Read, 2011). Since then there have been significant developments in both numerical techniques and computing hardware which enabled progressively more massive simulations up to $N \lesssim 10^6$ particles. With each development there has been a significant amount of work using these $N$-body codes to better understand the evolution of stellar clusters across a wider range of initial conditions (e.g., Terlevich, 1987; Aarseth & Heggie, 1998; Aarseth, 1963; Portegies Zwart et al., 2001; Wang et al., 2016; Rastello et al., 2021; Rizzuto et al., 2021; Torniamenti et al., 2022; Arca Sedda et al., 2023b; Rantala et al., 2024). Currently there are three main $N$-body codes which are commonly used in the literature; the $N$-body family initially started by Sverre Aarseth with the current generation code `NBODY7` (Aarseth, 1999, 2012), `BIFROST` which makes use of a symplectic integrator (Rantala et al., 2021, 2023), and `PeTar` which takes a hybrid approach by splitting the interactions into particle-particle and particle-tree interactions (Wang et al., 2020b). Whilst these codes exploit different numerical techniques for computational efficiency, they all work on the same principle.

Lets assume we have an isolated system of $N$ point-like particles which are only interacting through Newtonian gravitational attraction. We know the Newtonian gravitational force between any two particles is given by Eq 1.1, and so by extension the total gravitational force that a particle experiences from all other particles in the system, $\vec{F}_{\mathrm{g}_i}$, is given by

$$\vec{F}_{\mathrm{g}_i} = \sum_{j \neq i}^{N} \frac{G m_i m_j}{|\vec{r}_j - \vec{r}_i|^3} \cdot (\vec{r}_j - \vec{r}_i) \ , \tag{1.8}$$

and the equations of motion for the system are given by

$$\frac{d^2 \vec{r}_i}{dt^2} = \sum_{j \neq i}^{N} \frac{G m_j}{|\vec{r}_j - \vec{r}_i|^3} \cdot (\vec{r}_j - \vec{r}_i) \ . \tag{1.9}$$

An $N$-body algorithm is merely attempting to solve this set of non-linear differential equations. In theory there are no approximations involved in the direct calculation, and so the result is the most accurate representation for the evolution of that system. In practice, things are more complicated. For starters, it is clear that Eq 1.9 suffers from numerical singularities when the separation between any two particles, $|\vec{r}_j - \vec{r}_i|$, approaches 0. Thus, a commonly used fix is to introduce a "softening" parameter, $\varepsilon$, which suppresses the gravitational force for very close encounters (Aarseth, 1963). Eq 1.9 then becomes

$$\frac{d^2\vec{r}_i}{dt^2} = \sum_{j\neq i}^{N} \frac{Gm_j}{(|\vec{r}_j - \vec{r}_i|^2 + \varepsilon^2)^{3/2}} \cdot (\vec{r}_j - \vec{r}_i) \ , \tag{1.10}$$

where $\varepsilon > 0$. It is important to note that this method is not appropriate in cases where close encounters between particles are frequent and dynamically important such as in collisional stellar systems. The introduction of a softening parameter suppresses the gravitational force at short separations, which biases the dynamics by underestimating the strength and frequency of close interactions.

Another problem arises from the uncertainties introduced by numerical integration methods. In part this is due to the use of discrete time steps to approximate the continuous Newtonian equations of motion (Eq 1.9). Over time the uncertainties from this approximation compound and eventually lead to a drift in the energy and momentum of the system. This problem is much more significant for close interactions, where a high time step resolution is required to accurately simulate the orbits. There is also the issue that in general an $N$-body system is naturally chaotic and so similar initial conditions will exponentially diverge from each other over time. One option is to use smaller time steps for these strong encounters, thus reducing the approximation, however this results in a large increase of the computational time. This is especially true if applied to all interactions in the system as this would then provide unnecessarily high resolution for weak, distant interactions. Modern codes tend to opt for variable time stepping methods, where the close interactions are integrated with small time steps, and the weaker, distant ones with longer time steps. However this can still be computationally expensive for very small time steps, as such it is important to choose an integration scheme which efficiently reduces these errors (Zwart & Boekholt, 2014). A common approach is to consider higher order derivatives of the particle position in the numerical integration since this will reduce the individual error over a given time step $\Delta t$. Most modern $N$-body codes use the fourth-order Hermite scheme, which includes corrections up to the acceleration derivative (jerk) of the particles.

An alternative approach is to switch to a symplectic integration scheme. Integration schemes typically come in two flavours; symplectic integrators and non-symplectic integrators. A symplectic integrator works by reformulating the problem in terms of an approximate Hamiltonian of the system which can then be solved exactly. Since by construction these symplectic integrators are canonical transformations, a result of this approach is the long term conservation of energy and total angular momentum for the system. It is important to note that a symplectic integrator still suffers from numerical uncertainties over short timescales, and as such is not well suited to accurately follow chaotic close interactions. Like in the non-symplectic case, these errors can be reduced by taking a smaller time step, however these quickly become unfeasible small, drastically increasing the computational time.

Clearly a correct choice of time step is key to producing an efficient, accurate code, however, the dynamics within a star cluster occur over a wide range of timescales, from days (binary orbital periods), to Myr (the particle crossing time for a globular cluster), to Gyr (2-body relaxation of the cluster) (Wang et al., 2020b). Whilst one option is to introduce a variable individual time stepping scheme, where every particle is assigned its own time step for the dynamical calculations; this introduces a large amount of computational overhead. The better, and more widely used, approach is to utilise a *block time step* scheme. In this approach, the particles are grouped into a hierarchy of time steps according to some defined criterion, with particles in the same group evolved simultaneously. Unfortunately there are also issues that arise here due to the time symmetry of the scheme, and when particles can change groups, however the details are not in the scope of this work and those interested can find further details in Makino et al. (2006); Dehnen & Read (2011).

In all of the schemes described so far, a major problem has been the computational cost of integration over small time steps. While there are ways to reduce the number of calculations which require these small time steps, it is in general not possible to completely avoid them. For example, in the case of very close interactions where the particles move on tight orbits, the divergence in the force calculation necessitates a small time step to accurately resolve the interaction. Previously, we discussed the idea of softening the force calculation (see Eq 1.10) and while this does remove the divergence, it simply sends the force to $\sim 0$ and so does not accurately model these close encounters. This is especially a problem in a collisional system where these close encounters are particular important in driving the global evolution of a cluster. Instead we can perform a coordinate transformation of the force such that we remove this divergence, we can then solve these transformed equations to resolve the encounter and then transform back to the physical coordinate system. This process is called regularisation. There have been many regularisation schemes over the years but some of the most commonly used methods in modern codes are the Kustaanheimo & Stiefel regularisation (KS; Kustaanheimo et al., 1965), Algorithmic Regularisation (AR; Mikkola & Tanikawa, 1999) and SlowDown Algorithmic Regularisation (SDAR; Wang et al., 2020a).

Hybrid $N$-body models are the final scheme which we discuss since it pertains to the main simulation code used throughout the work presented in this thesis, `PeTar`. Regardless of the integration scheme or time stepping used, one key limiting factor for direct $N$-body (particle-particle) methods is the poor computational cost scaling with number of particles. In a direct method, we must compute $N - 1$ force calculations for each of the $N$ particles in the system, and so the the computational complexity scales with $\mathcal{O}(N^2)$. Clearly this quickly becomes prohibitively expensive for large $N$. Moreover, this does not take into account the additional computational expense of many tight orbital systems requiring many small time steps. This is one of the reasons the first one million particle simulation presented in Wang et al.

(2016) proved to be such an accomplishment. One way to reduce this computational complexity is to recognise that for a given particle, the weak interactions from distant particles can be grouped together and approximated as an interaction with a single large particle at the group's center of mass. This basic concept is typically referred to as a tree method and was proposed in Barnes & Hut (1986), where they showed that the computational complexity only follows $\mathcal{O}(N\log(N))$. There has since been developments creating a hybrid method where, for each particle, the interactions with nearby neighbours are computed via a direct particle-particle method, while the distant interactions are approximated in a particle-tree method ($P^3T$ Oshino et al., 2011). This idea was recently implemented in a new hybrid $N$-body code (`PeTar` Wang et al., 2020b) and since it also follows a $\mathcal{O}(N\log(N))$ complexity, we are now able to explore more massive clusters, with large initial binary fractions, requiring much less computational time compared with other direct $N$-body methods.

In this section we have discussed some of the many algorithms and schemes that are essential for the efficient and accurate simulation of $N$-body systems. However we should be clear that this is not an exhaustive list since that would far exceed the purposes of this thesis. In addition, it is important to note that modern $N$-body codes will often use a combination of these methods to maintain accurate results. For a more technical discussion of a specific code mentioned so far we refer the reader to respective code's technical paper listed previously. Finally for the interested reader we direct you to the following references for a more thorough coverage of the historical developments as well as a more detailed discussion of the various methods implemented: Hockney & Eastwood (1988); Aarseth (1999); Heggie & Hut (2003); Aarseth & Aarseth (2003); Trenti & Hut (2008); Dehnen & Read (2011); Wang et al. (2015).

### 1.2.2 Semi-analytical & Monte-Carlo algorithms

Here we discuss the methods underpinning semi-analytical codes (e.g., `cBHBd`) and Monte Carlo cluster codes (e.g., `CMC` & `MOCCA`) used in rapidly simulating star clusters.

Although $N$-body methods are often referred to as the "gold standard" for simulating collisional systems, especially star clusters, the excessive computational cost and general complexity for massive clusters necessitates alternative approaches. One such group of codes utilises an orbit averaged Monte-Carlo method, first developed by Hénon (1971b,a), and improved upon in Stodolkiewicz (1982, 1986). This method operates under three key assumptions:

1. The system is spherically symmetric[4],

2. The dynamical evolution of the system is driven by 2-body relaxation, and

[4]This is likely an oversimplification, particularly during the early stages of a clusters evolution, when it may exhibit significant asymmetry or even a fractal-like substructure (e.g., Küpper et al., 2011; Di Carlo et al., 2019)

3. The cluster is sufficiently massive that the relaxation timescale is significantly longer than the typical orbital timescale.

Over some time step $t_{\rm cross} < \Delta t \ll t_{\rm relax}$, the cluster can be considered in a steady state where the particle interactions are negligible and we can analytically define the energy ($E$) and angular momentum ($J$) for every particle in the cluster. It is further assumed that $E$ and $J$ are conserved over $\Delta t$. The effect of perturbations from the many weak interactions on a given particle will slowly accumulate over a relaxation timescale such that it is necessary to consider its impact. The approach, is then to assume that all the perturbations can be considered as a single effective perturbation from the particle's nearest neighbour.

Presently, there are two active groups utilising the Hénon method; the Cluster Monte Carlo (`CMC`) group (Joshi et al., 2000, 2001; Fregeau & Rasio, 2007; Chatterjee et al., 2010; Goswami et al., 2012; Pattabiraman et al., 2013; Rodriguez et al., 2022) and the Monte Carlo Cluster Simulator (`MOCCA`) group (Giersz, 1998; Giersz & Spurzem, 2000; Giersz, 2006; Giersz et al., 2008; Hypki & Giersz, 2013); both of which have had substantial updates and improvements since their conception. Of these developments a notable mention for both codes is the better modelling of strong interactions, which were previously not well approximated by this statistical approach. Both codes have implemented the `fewbody` integrator (Fregeau et al., 2004) to compute direct integration of the strong interactions between up to four particles. These Monte-Carlo codes are both faster than direct $N$-body codes, and able to explore very massive clusters $N > 10^6$. However, they are only approximate solutions, and make many assumptions regarding the interactions and dynamical evolution of the cluster. Whilst these two codes tend to agree with each other it is still necessary to validate these methods against results from $N$-body codes in the region where this is feasible.

Similar to the Monte Carlo codes, semi-analytical codes work under some assumptions regarding the dynamical evolution of a cluster and how it couples with the BH interactions within the system. In particular they rely on Hénon's principle, which states that over a relaxation time, the heat generation within the cluster core represents a constant fraction of the total energy in a cluster (Hénon, 1975). As we discussed in Section 1.1.2, the main energy source in a cluster comes from the dynamics of the BHs (Breen & Heggie, 2013). Since this energy generation is dependent on the global cluster properties, $M_{\rm cl}$ and $t_{\rm relax}$ (which is in turn related to $M_{\rm cl}$ and $r_{\rm h}$), we can couple the evolution of the cluster to the evolution of the total BH mass ($M_{\rm BH}$) within the cluster. Ultimately this means that we can simply solve a series of coupled first-order differential equations for $M_{\rm cl}$, $r_{\rm h}$, and $M_{\rm BH}$ to recover their time evolution. Whilst these methods are again more approximate than the Monte-Carlo methods since we are simply evolving the bulk properties of the cluster, they are significantly faster and require much fewer computational resources. This

allows a broader search of the parameter space as well as quick simulation of millions of cluster realisations. Similar to Monte-Carlo codes, it is important to validate the results from these codes against the more accurate $N$-body codes in regions of the parameter space where this is feasible. In practice, these comparisons have shown fairly good agreement with $N$-Body simulations in predicting the global evolution of the cluster properties (Antonini & Gieles, 2020b), although the detailed dynamical features, such as retention fractions and timing of interactions, may differ due to the simplifying assumptions inherent in semi-analytical models.

In the work presented in this thesis we utilise the semi-analytical code `cBHBd` and more details regarding the intricacies of the code can be found in Antonini & Gieles (2020b).

### 1.2.3 Stellar evolution codes

Since dense stellar clusters are ultimately a product of their constituent stars, it is important to consider not only the cluster dynamics but also the stellar evolution of its members. Detailed modelling of stellar structure and evolution is its own comprehensive field, relying on hydrostatic/hydrodynamic simulations (often in 1D, assuming spherical symmetry) (Martin et al., 2018). However, these codes typically require hours per star, making it impractical to embed them directly in cluster simulations. Instead, one can take the results of detailed runs and fit analytic formulae that approximate a star's evolutionary track for given initial parameters. Such "parametrised" stellar evolution codes reduce the runtime per star to $\mathcal{O}(< 1\text{ s})$, enabling both stellar population studies and integration into larger simulations.

This approach extends naturally to binaries: each star evolves independently until interactions (e.g. MT, CE) become important, at which point additional fitting formulae predict MT rates, envelope ejection, supernova outcomes, etc.(Hurley et al., 2002). These rapid binary population synthesis codes can evolve tens of thousands of systems in the time it would take a detailed code to process a single star. As a result, both direct $N$-body and Monte Carlo cluster codes integrate such modules to evolve their stellar and binary components without prohibitive computational cost. Today there are many different binary population synthesis codes to choose from, and while they often build on one another, they can yield varying results. In the paragraphs that follow, we briefly introduce some of the more common implementations that we have utilised throughout this thesis.

`BSE` (Binary Stellar Evolution Hurley et al., 2002) is the original rapid binary evolution code and is still widely used today, although it has received numerous updates to include improved fitting formulae and new stellar prescriptions. It models single star evolution using analytical polynomial fits to detailed stellar evolution tracks and includes simplified prescriptions for binary interactions. Ultimately this results in an extremely fast code, capable of modelling $\mathcal{O}(1)$ binary a second. Although

the original version contains now outdated prescriptions, for our studies we used an updated version implemented by Banerjee et al. (2020), which incorporated revised wind mass-loss rates, updated SN remnant prescriptions, and fallback dependent natal kicks. We have utilised this updated `BSE` code for studies presented in Chapters 3 and 4 predominantly as a module installed with the `PeTar` codebase.

`MOBSE` Giacobbo et al. (Massive Objects in Binary Stellar Evolution 2018); Giacobbo & Mapelli (Massive Objects in Binary Stellar Evolution 2018) is a modern extension of `BSE` designed to better model the most massive stars. It adopts metallicity dependent stellar wind prescriptions, and incorporates new models for core-collapse, electron capture and PPI SN. Note that while later updates to `BSE` has caught up to some of the changes presented in `MOBSE`, `MOBSE` still leads to more realistic treatment of very massive star evolution as well as resulting BH and neutron star (NS) mass distributions (Giacobbo et al., 2018). We use `MOBSE` in Chapter 3, to compare against results from `BSE`.

`COSMIC` (COmpact-object Synthesis and Monte Carlo Investigation Code Breivik et al., 2020) is an open source binary population code tailored to CO progenitors. Whilst it is explicitly based on the same framework as the updated `BSE` Banerjee et al. (2020), it operates within a `Python` wrapper which massively improves the user accessibility of the code. In practice, `COSMIC` retains `BSE`'s computational speed but can produce different results if the prescription parameters are not configured identically to a similarly updated `BSE` model. `COSMIC` was used alongside the `BSE` module within `PeTar`, for the study in Chapter 4.

`COMPAS` (Compact Object Mergers: Population Astrophysics and Statistics Team COMPAS: Riley, J. et al., 2022; Vigna-Gómez et al., 2018; Stevenson et al., 2017) is a modern open-source rapid population code, with its core structured as a modular `C++` suite that implements single star and binary star evolution in an object-orientated design. This code is designed for studying CO formation and evolution and as such contains updated SN and fallback prescriptions, as well as modelling the evolution of COs post-collapse such as the formation of pulsars (Chattopadhyay et al., 2020). In addition, `COMPAS` is very user friendly, and along with an extensive configuration setup, it allows for ranges of values for some parameters. This enables users to set up parameter grids, useful for exploring complex combinations of parameters with ease. `COMPAS` is widely used for modelling GW progenitors and was the primary code utilised in Chapter 2 of this thesis. In practice, `COMPAS` yields results comparable to other modern `BSE`-based codes, but it uses up-to-date stellar tracks and is designed to be easily extended with new physics.

Ultimately there are multiple different binary population synthesis codes on offer, with each receiving numerous updates since their conception to add new physics or improve existing prescriptions, although these come at varying regularity. Whilst they rely on the same idea of using fitting formulae for rapid modelling, they vary in the exact physics included and how up-to-date the fitting formulae are, with different

versions of the same code sometimes containing very different options. Comparison studies have shown that different binary population synthesis codes can yield different predictions if their underlying assumptions or evolutionary prescriptions differ (Toonen et al., 2014). Meanwhile, when two codes are run with identical input physics they generally produce statistical similar results. Therefore, when interpreting dynamical simulation results (i.e., binary merger rates, CO populations), it is crucial to consider which evolutionary code, and exactly which version, you are using since this sets the underlying physics, with the code specific assumptions possibly significantly impacting the conclusions.

## 1.3 Thesis structure

The direct detection of GWs from merging BBHs by the LIGO/Virgo/KAGRA collaboration has opened a new window into CO astrophysics (The LIGO Scientific Collaboration et al., 2021). Yet the relative contributions of isolated binary evolution versus dynamical assembly in dense stellar environments remain uncertain. Globular clusters and other dense stellar systems are promising sites for dynamical BBH formation via close encounters, three-body processes, and exchange interactions (e.g., Portegies Zwart et al., 2004; Rodriguez et al., 2016a; Arca Sedda et al., 2023b). To interpret the growing GW catalogue, and to use BBHs as probes of stellar evolution, and dynamics, it is therefore crucial to understand how cluster properties such as mass, density, metallicity, and primordial binary fraction, influence BBH formation rates, mass distributions, and merger timescales.

Despite significant progress, key open questions persist. For example, what fraction of stellar-mass black holes are retained in clusters after natal kicks, and how does their retention couple with the cluster core dynamics and BBH formation (Morscher et al., 2015)? How do primordial binaries versus dynamically formed binaries contribute to the observed BBH population (Askar et al., 2017; Heggie et al., 2006; Wang et al., 2021)? What is the role of cluster-driven processes, such as mass segregation, 2-body relaxation, and core collapse, in shaping the mass and eccentricity distributions of merging BBHs, as well as the wider BH population?

The main aim of this thesis is then to address these gaps by combining state-of-the-art numerical techniques with updated stellar and binary evolution physics. Specifically, we employ direct $N$-body simulations and multiple rapid population synthesis codes to investigate how choices of stellar evolution prescriptions affect BH retention, BBH formation, and GW merger predictions. By systematically varying both cluster parameters and stellar evolution prescriptions, this work aims to improve our understanding of both lone BH and BBH formation and evolution within dense stellar clusters. Our simulations add to the decades of previous $N$-body models, further exploring sparse areas of the parameter space and pushing into unexplored regions.

In Chapter 2 we utilise the rapid binary population synthesis code `COMPAS` (Team COMPAS: Riley, J. et al., 2022; Vigna-Gómez et al., 2018; Stevenson et al., 2017) to model the evolution of an isolated population of binary stars from zero-age main sequence (ZAMS) through to a possible double compact object (DCO). We then consider how the resultant population of BBHs should evolve when placed in a highly dynamical environment, using our theoretical understanding of how dense stellar clusters evolve. We will highlight the importance that primordial binaries play in shaping the binary distributions of merging BBHs and in determining the types of interactions we can expect within dense stellar clusters.

Chapter 3 builds on the work performed in Chapter 2, testing some of the conclusions that we arrived at using the new hybrid $N$-body code `PeTar` (Wang et al., 2020b) which directly models the gravitational forces between stellar systems in real star cluster environments. We have produced a new suite of 34 $N$-body models exploring regions of the parameter space that are mostly sparsely or previously unexplored. Subsequently, we perform a detailed analysis of the population of merging BBHs and show how there is a clear delineation between the evolution of primordial binaries and dynamical binaries in these clusters.

Chapter 4 takes these same 34 simulations and considers the formation and evolution of Gaia-like BH-binaries. These are characterised as binaries containing only a single BH which are observed by the Gaia satellite. Here we study the binary properties and evolutionary history of BH-main sequence (MS), BH-GS, BH-white dwarf (WD) and NS-star binaries in our stellar cluster simulations.

Finally Chapter 5 concludes this thesis, summarising the work presented and its importance in the further understanding of BBHs in stellar clusters.

# Chapter 2

# Binary black hole mergers in dense stellar clusters the importance of primordial binaries

As discussed in Chapter 1, star clusters likely form with a large fraction of massive stars initially in pairs. Owing to their mass, these primordial binaries evolve and collapse into BHs over $\mathcal{O}(10)$ Myr, which is a relatively short timescale compared with the evolutionary time of the cluster as a whole. Some of these primordial binaries will remain bound throughout all of their binary stellar evolution, resulting in a BBH. Thus it is likely that early in a star cluster's lifetime, they contain a significant population of BBHs, which would subsequently drive the cluster evolution through encounters. In addition, at least some of these primordial BBHs will reach a stage where their evolution is dominated by their GW emission coalescing and contributing to the total merging population.

In this chapter we investigate to what extent primordial binaries shape both the total BBH population, and the subset which contributes to the merging population, some of which may be observable with our current detectors. Since these massive stars collapse on short timescales, we can make the assumption that the dynamics of a cluster do not affect the primordial binaries during their stellar evolution periods, and only consider the dynamics from the global cluster after the BBHs are formed. The benefit of this is that we can model the binary stellar evolution in isolation using population synthesis codes and then take the resulting BBH when considering the subsequent interactions within a cluster. In addition, although primordial binaries can be formed of all stellar masses including low mass stars, it has been shown that the low mass binaries have almost no influence on the secular evolution of the cluster until the BH population has been depleted (Wang et al., 2021). As such it is not necessary to consider the effect of the lower mass binaries on the cluster until after the BHs have been removed from the cluster. Thus in the following work we ignore any primordial binaries in the smaller mass range, and only consider those that could

produce at least one BH.

Also in Chapter 1 we highlighted the important role of BBHs for the long-term evolution of a star cluster. Since massive primordial binaries would provide a source of many BBHs, the fraction of primordial binaries is clearly an important parameter to consider. Currently it is not clear if the fraction we see within young clusters can be applied across all clusters, so it is beneficial to consider a range of initial binary fractions, in particular looking at the two extreme ends (100% and 0%). In this work, we assume that there is a 100% binary fraction amongst massive stars.

## 2.1 Isolated Binary Population Study

We use the fast binary population synthesis code `COMPAS` (Team COMPAS: Riley, J. et al., 2022; Vigna-Gómez et al., 2018; Stevenson et al., 2017) to investigate the properties of the black hole and binary black hole population due to stellar evolution for different stellar metallicities. It should be noted that this is only a simplistic model as it does not take into account the dynamical interaction of binaries with the rest of the cluster, nor does it consider the evolution of the cluster itself. These are discussed in later sections.

Comparing the BH natal kicks against a range of escape velocities (1 km $s^{-1}$ to $2.5 \times 10^3$ km $s^{-1}$) we start by investigating here the expected retention fraction of BHs and BBHs within different clusters, owing just to stellar evolution. This range of escape velocities spans open clusters, globular clusters and nuclear clusters, allowing us to assess how the BH populations may vary across these environments.

We consider a wide range of cluster escape velocities, which cover open clusters, globular clusters, as well as nuclear clusters (Antonini & Rasio, 2016; Harris et al., 2006). It is important to note that, realistically, the escape velocity is an evolving quantity dependent both on the age of the cluster and the position within the cluster. For the work in this paper, we are only concerned with the initial stellar evolution forming BBHs and then the immediate consequences on the BBH populations. Thus, it is suitable to only consider the initial escape velocity of the cluster and assume that it is not time-dependent during this early stage. In terms of position, all escape velocities are treated as the cluster central escape velocity going to infinity unless stated otherwise.

### 2.1.1 Initial Conditions

We run thee models setting the metallicity to $Z = 0.01$, $Z = 0.001$ and $Z = 0.0001$ respectively. Throughout the paper we will refer to the $Z = 0.01$ model as an approximately "Solar" metallicity model while the other two models are considered "sub-Solar" metallicity models. Each model simulates $10^5$ binaries, evolving the stars from the ZAMS until CO formation, or until a Hubble time has passed. The

evolution model is broadly similar to the widely used `BSE` population synthesis code (Hurley et al., 2000, 2002). We sample the primary stellar mass from a Kroupa (2001) IMF between 20 $M_\odot$ to 150 $M_\odot$ since this lower limit of 20 $M_\odot$ is approximately the minimum stellar mass required to form a BH. The upper limit was left as the default value used by `COMPAS`.

Once $10^5$ primary masses have been assigned, the mass of the secondary star is drawn from a uniform mass ratio ($q$) distribution in the range 0.01 to 1 as found by Sana et al. (2012). Selecting the secondaries in this manner allows the possibility for a secondary mass less than the minimum primary mass of 20 $M_\odot$, in fact, $\approx 61\%$ of all systems have an initial secondary mass smaller than 20 $M_\odot$ across all three models. In these systems, the secondary star is unlikely to form a BH at the end of its evolution, and so they only contribute a single BH to the population.

With the binary masses chosen, the initial orbital period is drawn from a Sana et al. (2012) distribution,

$$f_{\rm p}(\log_{10} P) = 0.23 \times (\log_{10} P)^{-0.55} \ , \tag{2.1}$$

with the minimum period $\log(P_{\rm min}/{\rm days}) = 0.15$ and the maximum period set such that the distribution is normalised to 1 (Oh et al., 2015). The binary eccentricity is also drawn from the Sana et al. (2012) distribution,

$$f_{\rm p}(e) \propto e^{-0.45} \ , \tag{2.2}$$

between 0 and 1, independent of the period. We assume the default `COMPAS` prescriptions for MT, CE evolution and Roche lobe overflow (RLO); which are detailed in Table 2.1. Finally, natal kicks of compact objects formed through core-collapse supernova (CCSNe) are drawn from a Maxwellian distribution with $\sigma = 265$ km s$^{-1}$ (Hobbs et al., 2005), and electron capture supernova (ECSNe) and ultra stripped supernova (UCSNe) have a Maxwellian $\sigma = 30$ km s$^{-1}$ (Pfahl et al., 2002a; Podsiadlowski et al., 2004). We assume a fallback kick prescription for the BH natal kicks (Fryer, 1999), whereby we first calculate the NS kick from the Maxwellian distribution, and then scale this by the fraction of mass that falls onto the proto-compact-object (the fallback fraction) $f_{\rm b}$. This gives a final BH kick as

$$v_{\rm BH} = v_{\rm NS}(1 - f_{\rm b}) \ , \tag{2.3}$$

where $v_{\rm NS}$ is the drawn natal kick for a NS. Since the timescale of a typical SN is much shorter than the evolutionary timescales used in `COMPAS`; the SN are treated as instantaneous events which affect the binary orbital parameters (Team COMPAS: Riley, J. et al., 2022).

The resulting binary parameters are calculated following Appendix B of Pfahl et al. (2002b) which accounts for the natal kick, instantaneous mass loss, interaction

between the SN blast wave and the binary companion, and finally any change to the binary COM velocity (Blaauw, 1961; Hills, 1983; Brandt & Podsiadlowski, 1995; Kalogera, 1996; Tauris & Takens, 1998; Hurley et al., 2002). As described in Pfahl et al. (2002b), the binary is only flagged as gravitationally unbound if the final eccentricity following the SN is greater than 1.

Table 2.1: Perscriptions assumed for mass transfer and common envelope evolution of the binary. Note that most of these are the default prescription for `COMPAS`; the full list of default settings is detailed in Table 1 of Riley et al. (2022).

| Description | Value/Range | Fiducial parameter settings |
|---|---|---|
| Mass transfer stability criteria | $\zeta$-prescription | See Vigna-Gómez et al. (2018) and references therein |
| Mass transfer accretion rate | Thermal timescale | Limited by thermal timescale for stars (Vigna-Gómez et al., 2018; Vinciguerra et al., 2020) |
| | Eddington-limited | Accretion rate is Eddington-limited for compact objects |
| Non-conservative mass loss | Isotropic re-emission | Massevitch & Yungelson (1975); Bhattacharya & van den Heuvel (1991) Soberman et al. (1997); Tauris & Van Den Heuvel (2006) |
| Case BB mass transfer stability | Always stable | Based on Tauris et al. (2015, 2017); Vigna-Gómez et al. (2018) |
| Circularisation at the onset of RLO | On | Instantly circularise to periapsis (see Section 4.2 of Riley et al. (2022)) |
| CE prescription | $\alpha - \lambda$ | Based on Webbink (1984); De Kool (1990) |
| CE efficiency $\alpha$-parameter | 3.0 | See section 4.2.4 of Riley et al. (2022) |
| CE $\lambda$-parameter | $\lambda_{\text{fixed}} = 0.5$ | |

### 2.1.2 BBH Properties

In this section, we discuss the mass and orbital properties of the BBH population in more detail.

#### 2.1.2.1 Mass and orbital separation

One immediate result found from these simulations is that the fraction of systems that form BBHs increases for lower metallicity models; 2.4%, 10.8%, and 15.1% for model $Z = 0.01$, $0.001$ and $0.0001$ respectively. This is in part due to the stronger stellar winds produced in high metallicity stars which increase the amount of mass loss during the stellar evolution. This extra mass loss at Solar metallicities increases the minimum stellar mass required to form a BH and therefore reduces the total number of BHs formed. In addition, the increased stellar mass loss leads to less massive BHs forming in general (Belczynski et al., 2010), which then receive higher natal kicks, since the fallback fraction is lower, which can more easily disrupt the binary.

The lower BH masses at higher metallicity are apparent in Fig. 2.1, where we see that for the solar metallicity model (bottom-left panel) $\simeq 99\%$ of all primary BHs have masses $\leq 17.3$ $M_\odot$. Meanwhile, both sub-solar metallicity models (top-left and center-left panels), have 50% of primary BH masses exceeding 21.1 $M_\odot$ and 22.9 $M_\odot$, respectively. Table 2.2 summarises the 50%, 75% and 99% percentiles of the primary and secondary BH mass distribution for all three models. Note that the binary components are characterised such that the primary BH is always the most massive BH.

The right column of Fig. 2.1 shows the semi-major axis, $a$, distribution of the BBHs at formation, for each model. We see that the range of separations does not vary significantly with metallicity, always being between $\simeq 10^{-2}$ AU to $\simeq 10^{4}$ AU. However, there is a clear bi-modality in the distribution which becomes more pronounced for higher metallicities. The bi-modality of these distributions represents the two possible pathways for forming a BBH from a primordial binary (Wiktorowicz et al., 2019). BBHs at larger separations, $\gtrsim 10^2$ AU are formed from initially wide stellar binaries where the individual stars can evolve without much interference from each other. On the other hand, BBHs in the lower separation peak are predominantly formed following a CE evolution (Paczynski, 1976). This latter form of evolution occurs when one of the stars expands to such an extent that it overflows its Roche lobe and begins to donate material to its companion. In the case where the receiving star is unable to accept all the material a CE is formed, which surrounds both of the binary components. A consequence of CE evolution is the shrinking of the binary separation due to drag forces between the binary components and the surrounding envelope. Provided the separation does not shrink to the point of the stellar cores merging, this can result in the formation of the tight BBHs seen in the lower peak

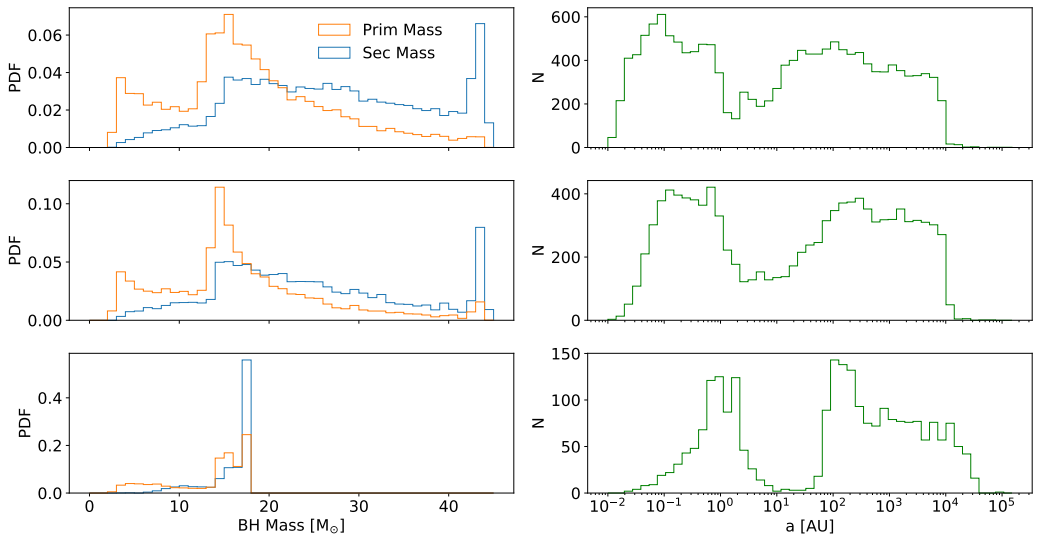


Figure 2.1: In the left column we show the primary (blue) and secondary (orange) BH mass distributions. The right column shows the binary separation. We plot these distributions, for three metallicity values, $Z = 0.0001$ (top row), $Z = 0.001$ (middle row), and $Z = 0.01$ (bottom row).

of the distribution (Livio & Soker, 1988; Xu & Li, 2010; Ivanova et al., 2013). It should be noted that it is possible for the stellar cores to avoid merger during the CE phase provided the envelope gets ejected before the cores have a chance to merge (Law-Smith et al., 2022). Another clear feature we find with the binary semi-major axis, is a preference for wider separations with higher metallicities, in particular, a pronounced reduction in number of binaries with separations $\leq 5 \times 10^{-1}$ AU at solar metallicity. The most likely cause for this comes from the increasing strength of the natal kick with increasing metallicity. As we have mentioned previously, higher metallicity stars tend to have stronger winds which efficiently strip material from the star and significantly reduce its mass. When this less massive star eventually undergoes a SN the remnant BH subsequently experiences a larger natal kick, since it is now both less massive and experiences less fallback. These larger natal kicks will typically widen a binary, thus yielding far fewer tight binaries compared to lower metallicities.

#### 2.1.2.2 Eccentricity

In Fig. 2.2 we plot the cumulative distribution of the BBH eccentricity distribution at formation. We see that the BBHs are predominantly low eccentricity with 50% of BBHs having an eccentricity below 0.187, 0.193 and 0.161 for metallicity models $Z =$ 0.0001, 0.001, and 0.01 respectively. The low eccentricities are a natural consequence of the circularising that occurs when the binary components interact through tides and mass transfer before a BBH is formed. In addition, we find that the BBH

Table 2.2: 50%, 75% and 99% percentiles for the primary and secondary BH masses for each of the three metallicity models

| Metallicity | BH type | 50% $M_\odot$ | 75% $M_\odot$ | 99% $M_\odot$ |
|---|---|---|---|---|
| 0.001 | Primary | 22.9 | 33.1 | 44.0 |
| | Secondary | 18.4 | 26.5 | 43.7 |
| 0.01 | Primary | 21.1 | 30.7 | 43.8 |
| | Secondary | 16.1 | 22.6 | 43.4 |
| 0.01 | Primary | 17.0 | 17.2 | 17.3 |
| | Secondary | 15.5 | 17.1 | 17.3 |

eccentricity distribution is mostly independent of the choice of metallicity. Although SN kicks may change the circularised binaries to become more eccentric, the fallback kick prescription ensures that most BBH progenitors have much smaller natal kick magnitudes (than their NS counterparts), preserving their smaller eccentricities.

#### 2.1.2.3 Time Delay

It is now helpful to look at the fraction of BBHs that would merge within a Hubble time, $t_{\rm H}$, based solely on the binary stellar evolution. To calculate the time delay ($t_{\rm delay}$), we numerically integrate the merger timescale given by (Peters, 1964) (Eq 1.2), for each BBH of $m_{1,\,2}$, eccentricity $e_0$, and semi-major axis $a_0$ in the population. Fig. 2.3 shows the cumulative distribution of the GW timescale for the three metallicities, along with the Hubble time $t_{\rm H} = 13.7$ Gyr line marked. We see that the higher the metallicity the lower the fraction of BBHs that can merge within a Hubble time. In particular, we find that fractionally 24%, 12% and 2.5% have $t_{\rm delay} \leq 13.7$ Gyr for metallicity models $Z = 0.0001$, 0.001, and 0.01 respectively.

## 2.2 BHs Retained in Clusters

### 2.2.1 Supernova kicks and Escape Velocity

To investigate the effect of stellar evolution on the BH populations inside star clusters we split the population into 3 distinct groups; single BHs, BBHs and BHs in binaries in which the other component is not a BH (i.e., it is either a star, a WD or a NS; we denote these binaries as BH-else). We further categorise the BBH population into hard and soft binaries; where a hard binary has a larger binding energy than the average kinetic energy of the surrounding stars. Thus, by interacting with surrounding stars and COs, a hard binary will on average become harder, i.e., its binding energy will increase. On the other hand, a soft binary will on average become softer and will eventually be dissociated by the encounters (Heggie, 1975).

As mentioned previously, the kicks received by binary components as a result of SN are the main source of binary disruption; and even for those BBHs that remain

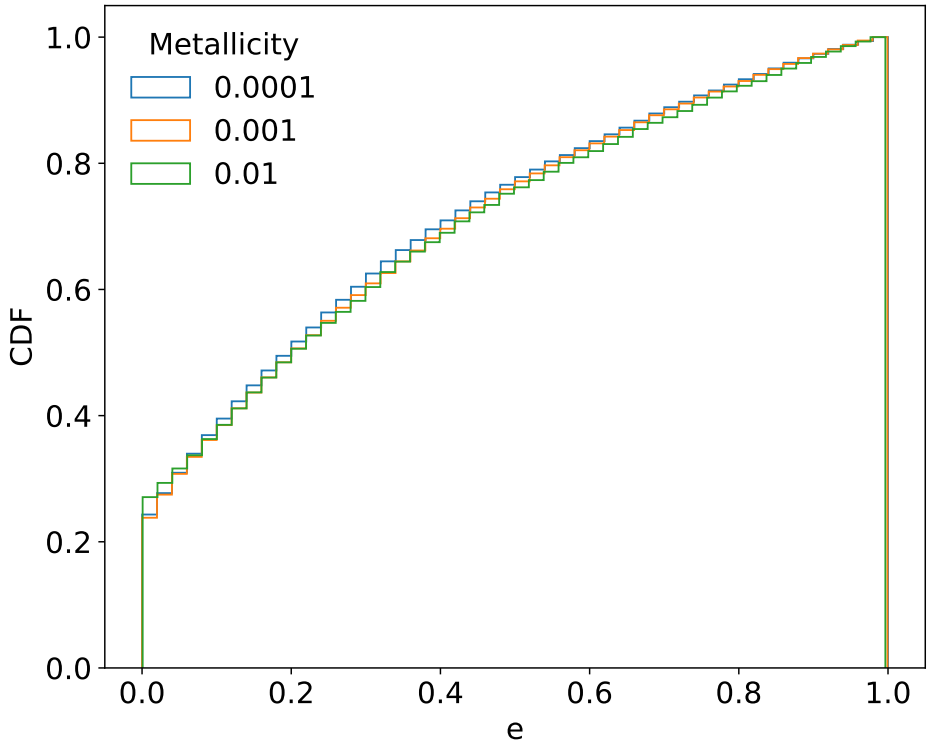


Figure 2.2: Cumulative distribution of the BBH eccentricities for the three metallicity models described in the text. We can see that there is very little difference between the models.

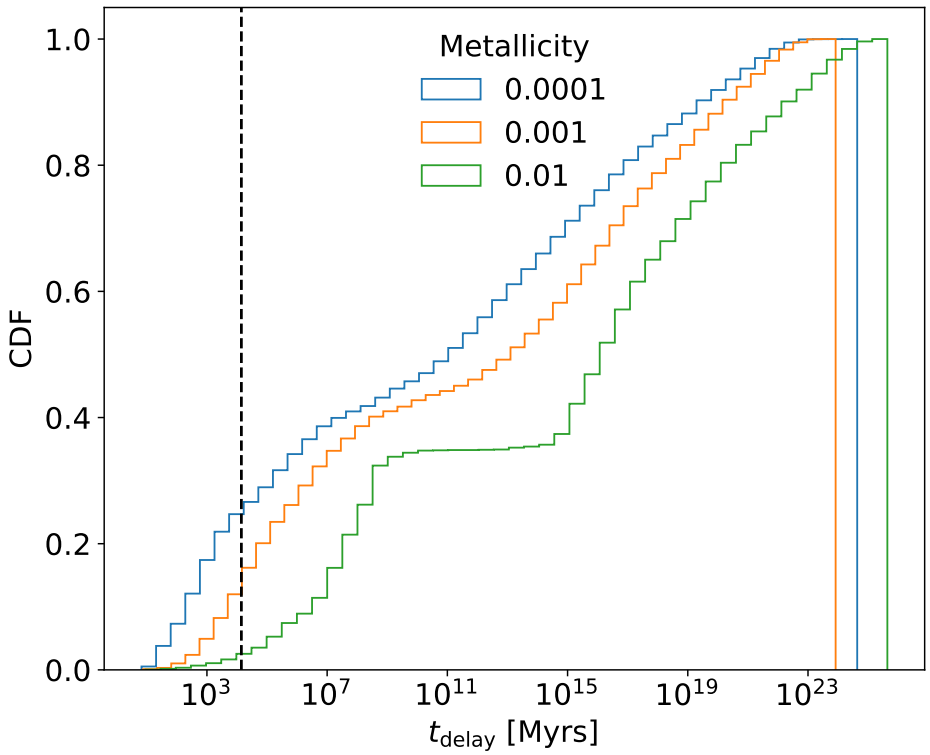


Figure 2.3: Time delay distribution for each metallicity model. We find that metallicity has a large impact when it comes to the number of BBHs that can merge in a Hubble time. Going from low metallicity to high metallicity the fraction of BBHs with $t_{\mathrm{delay}} \leq 13.7$ Gyr is 24%, 12% and 2.5%.

bound a kick will still be imparted to the binary COM and could be large enough to eject the binary from its host cluster. This is an important mechanism to consider since it will set the rest of the binary's evolution. If the binary is ejected from its cluster then it would continue to evolve in the external environment (e.g., the galactic field) without further dynamical interaction.

We find that the two sub-Solar metallicity models have similar disruption fractions, with 43% and 44% of the initial 100,000 binaries being disrupted due to the SN kicks. However, at solar metallicity, this fraction increases to 59% of binaries being disrupted. This is due to the larger winds involved at solar metallicity which ultimately produce less massive BHs than at sub-Solar metallicities; these smaller BHs then receive higher natal kicks.

At the end of the simulation, we identify the BHs that are in still bound binaries (either with another BH or a different type of stellar object), and the BHs that are now single, after being disrupted from their initial binary. For the range of potential cluster escape velocities (0 km $s^{-1}$ to 2500 km $s^{-1}$, defined at the start of this chapter), we compare against the COM kick of binaries with a BH or the component velocity of the single BH. We are then able to estimate the fraction of retained bound BBHs and retained single BHs.

In Fig. 2.4 we show the fraction of BHs retained by a range of cluster escape velocities; with the BH found as either a BBH, a single BH, or a BH-else. These are all normalised to the total number of retained BHs.

We see that in the $Z = 0.0001$ and $Z = 0.001$ models (top and middle panels), the BBHs are the dominant form of retained BHs up to $v_{\rm esc} \sim 40$ km $s^{-1}$, and $v_{\rm esc} \sim 20$ km $s^{-1}$ respectively, after which the single BHs become dominant. The BH-else binaries are a subdominant population at all values of $v_{\rm esc}$, with them only contributing between 10% to 15% of the retained BHs. In the $Z = 0.01$ model, BBHs are the dominant population only for escape velocities $v_{\rm esc} \leq 10$ km $s^{-1}$. Above this, the single BHs are the dominant population, approaching $\sim 90\%$ of the total population at the highest escape velocities.

An important point to note is that the relationship shown in Fig. 2.4 is only dependent on the escape velocity of the cluster and can therefore be applied to any cluster with that value of $v_{\rm esc}$ regardless of mass and size of the cluster.

When considering the retention fraction of the total binary (BBH and BH-else) populations and single BH populations we see a similar trend in the three models. Starting at the low escape velocities, the models show that the majority of the retained BHs are found in the binary population, with the single BH population becoming more dominant at higher escape velocities. This cutoff shifts slightly with the model's metallicity, with $v_{\rm esc} \gtrsim 30$ km $s^{-1}$ for the $Z = 0.0001$ model and $v_{\rm esc} \gtrsim 10$ km $s^{-1}$ for the $Z = 0.01$ model. Since we are only dealing with stellar evolution in these models, this trend implies that in the range where the binaries are dominant, the kick velocity required to break up a typical binary is greater than the escape

velocity of the cluster.

## 2.3 Black hole binary populations

We have discussed that for sub-Solar metallicities, the BH population for clusters with $v_{\rm esc} \lesssim 50$ km s$^{-1}$ is predominantly in the form of BBHs, which is likely to affect the properties of the subset of merging BBHs. In addition, since the evolution of a cluster is linked to its BH subsystem (Breen & Heggie, 2013; Chattopadhyay et al., 2022), the dominant presence of BBHs could impact the long-term evolution of the cluster. Thus, in what follows we investigate the properties of these *retained* BBHs. We subsequently look at the entire population of BBHs produced by the cluster, including ejected binaries, and consider their contribution to the merging BBH population.

### 2.3.1 Hard binaries

A binary is considered to be 'hard' when the binary binding energy is greater than the average kinetic energy of surrounding stars (Heggie, 1975). From this definition, we can find an expression for a cut-off semi-major axis at the hard/soft boundary

$$a_{\rm h} = \frac{G\mu}{\sigma^2} \ , \tag{2.4}$$

where $\mu = m_1 m_2/(m_1 + m_2)$ is the reduced mass of the binary and $\sigma$ is the average velocity dispersion of the cluster. The average velocity dispersion is initially proportional to the cluster escape velocity, with the exact factor dependent on the density profile assumed. We adopt the relation $v_{\rm esc} \approx 4.77\sigma$ (e.g., Antonini et al., 2019), which mimics a cluster King model with $W_0 = 7$.

It is important to consider that the definition of the hard/soft boundary in Eq 2.4 comes with some caveats. Notably, it is dependent on the distribution of energy between the binaries and singles within your cluster (Heggie, 1975) and the mass distribution of the single perturbers. Hence, we highlight that in Eq 2.4, we have assumed that the BBHs have reached equipartition with a single mass population of field stars. Another approach includes a factor of the average stellar mass of field stars $1/\langle m \rangle$, which, given the number of low-mass stars in a real cluster, would only increase the number of hard binaries (since $1/\langle m \rangle > 1$ for typical stellar mass distributions, where $\langle m \rangle$ is in solar masses). However, this value is subject to change as the stars and whole cluster evolve. Hence, for the remainder of this paper, we will use the definition in Eq 2.4 and classify a binary as hard if $a < a_{\rm h}$, with the knowledge that our results assume a lower estimate for the number of hard binaries.

We now consider the subpopulation of *hard* BBHs that are retained inside the cluster. We plot these as a subset of the retained BBHs and as a function of the cluster escape velocity in Fig. 2.4. In all models, we see that the majority of BBHs

are hard for low $v_{\rm esc}$, and that the sub-Solar model retains a high hard fraction for larger escape velocities than for the Solar metallicity. In particular, we see a $> 50\%$ hard fraction for $v_{\rm esc} \leq 24.1$ km s$^{-1}$ in the $Z = 0.01$ model; whereas the $Z = 0.0001$ model has $> 50\%$ for $v_{\rm esc} \leq 106.9$ km s$^{-1}$.

The reason for the increased hard binary fraction in the sub-Solar model can be explained simply by the separation distribution shown in Fig. 2.1.

We use Eq 2.4 with $m_1 = m_2 = 20$ M$_\odot$, and estimate a typical value for the hard/soft boundary at $v_{\rm esc} = 100$ km s$^{-1}$; we find $a_{\rm h} = 20$ AU. For Solar metallicity, 34.4 % of the BBHs have separations less than this and so are considered in the hard regime. On the other hand, for the sub-Solar metallicity, 52.8% of BBHs have separations below 20 AU. Clearly then, the sub-Solar models contain a higher proportion of tight BBHs and thus retain a large fraction of hard binaries at higher escape velocities. We also see this from the separation plot shown in Fig. 2.1. Although both metallicity models exhibit a bi-modality in the separation distributions, it is clear that the Solar metallicity is skewed more towards the second peak ($a > 20$ AU). At $v_{\rm esc} \gtrsim 400$ km s$^{-1}$, while the fraction of BBHs retained levels out for both metallicities in Fig. 2.4, the hard BBH fraction continues to decrease approaching zero. This is unsurprising, since the parameter $a_{\rm h}$ scales as $1/v_{\rm esc}^2$.

The results presented so far indicate that a significant fraction of the BHs retained in a cluster will be found in binaries with another BH and that a large fraction of these binaries will have separations below the hard/soft boundary $a_{\rm h}$ (especially for clusters with $v_{\rm esc} < 100$ km s$^{-1}$). Since hard binaries will on average become harder and remain bound during interactions with singles (Heggie, 1975), we should expect that a number of them will eventually merge due to energy loss by gravitational wave radiation. Hence, they will likely contribute to the population of merging BBHs from a cluster. Moreover, they will be important to the evolution of the cluster itself as they provide an efficient energy source during the early stages of cluster evolution.

### 2.3.2 Binaries ejected after one dynamical encounter

The small separation of hard binaries makes the likelihood of disruption due to binary-single interactions quite low. However, their large binding energies mean that the relative recoil kick the binary receives from strong 3-body interactions can be quite large. Through consideration of energy and momentum conservation and by assuming that the average binary-single interaction increases the binding energy of the binary by some fraction $\delta$, one finds an expression of a recoil kick velocity on the binary COM (Miller & Lauburg, 2009).

$$v_{\rm kick}^2 \simeq \delta q_3 \frac{G}{a} \frac{m_1 m_2}{m_{123}} \ , \tag{2.5}$$

where $m_{123} = m_1 + m_2 + m_3$ with $m_3$ the mass of the single perturber, $q_3 = m_3/(m_1 + m_2)$ which we assume to be $q_3 \approx 0.5$. The fraction of energy given by the binary

is typically averaged to $\delta = 0.2$ for binary-single encounters (Quinlan, 1996). By selecting the cases where $v_{\rm kick} \geq v_{\rm esc}$, we approximate the number of BBHs that would receive a recoil kick large enough to remove them from a cluster with escape velocity $v_{\rm esc}$. Within a globular cluster, we also expect binary-binary interactions, which are more complex than binary-single encounters, and it is thus non-trivial to extend our recoil kick expression to binary-binary interactions.

From Eq 2.5 we see that the harder a binary (i.e., the smaller is $a$) the larger the recoil kick experienced after an interaction. Thus, the condition $v_{\rm kick} \geq v_{\rm esc}$ is equivalent to a condition on the semi-major axis of the binary. By rearranging Eq 2.5 for $a$ and defining $a = a_{\rm ej}$ when $v_{\rm kick} = v_{\rm esc}$, the final relation for the critical semi-major axis value below which a binary is ejected is

$$a_{\rm ej} = 0.1 \frac{G}{v_{\rm esc}^2} \frac{m_1 m_2}{m_{123}} \ , \tag{2.6}$$

where $a_{\rm ej} < a_{\rm h}$ by definition.

Given that the recoil kick is also dependent on the mass of the perturber, we choose $m_3$ by randomly sampling the mass distribution of the retained single BHs for each escape velocity and metallicity model. In this way, we can further mimic the interactions that would likely occur if these BH populations were situated within a real cluster. The subset of hard BBHs that are retained after a single interaction is shown in Fig. 2.4 as dotted purple lines.

Although the population of BBHs that are ejected after their first encounter are not going to play much of a role in the overall cluster evolution, they still contribute to the population of merging BBHs. Either they were already tight enough to merge, and the interaction causes the merger to occur sooner (by reducing the separation), or the decreased semi-major axis and newly drawn eccentricity caused by the interaction, now place the binary in a regime where it can merge within a Hubble time. This population would be of particular interest as their binary properties will be set mostly by stellar evolution but include some influence due to the single interaction which ejects them. The longer a primordial binary remains in the cluster, the more interactions it will experience, and thus its orbital properties will become more akin to a dynamically formed binary.

When we take into account the tight BBHs that are ejected after a single interaction, we see in both metallicity models, the remaining hard BBH population in low mass clusters goes down significantly. In the sub-Solar model, low mass clusters with $v_{\rm esc} < 7$ km s$^{-1}$, we see more than half of the retained hard BBHs get ejected after their first interaction. As the escape velocity increases, fewer BBHs get ejected due to their first recoil kick. This is in part because the higher escape velocity requires an equivalently large recoil kick to eject the binary; but also, as for higher escape velocities the parameter $a_{\rm h}$ gets smaller, meaning fewer BBHs are hard and so the interaction is much more likely to either widen the binary or disrupt it completely.

In the Solar model we similarly see that the higher the escape velocity, the fewer BBHs are ejected due to the first interaction. However, we see that for $v_{\rm esc} < 28$ km s$^{-1}$ more than half of the BBHs are removed due to that first strong encounter while for $v_{\rm esc} > 160$ km s$^{-1}$ none of the first recoil kicks are able to eject the BBHs. This is slightly lower than the upper bound in the sub-Solar model where we see a few BBHs still ejected due to the interaction, up to an escape velocity $v_{\rm esc} = 280$ km s$^{-1}$.

In all the models, there is a certain escape velocity above which the fraction of retained BHs that are in BBHs levels out, while the subset of those that are in hard BBHs continues to drop; this is due to the relation between the hard/soft boundary and the escape velocity of the cluster, $a_{\rm h} \propto 1/v_{\rm esc}^2$ from Eq 2.4. The semi-major axis cut-off for a hard binary is getting larger still and thus fewer binaries are considered hard as the escape velocity continues to increase.

It is clear that in both metallicities models, we should expect low-mass clusters to eject a significant fraction of their hard BBH population relatively early in the cluster's evolutionary timescale. Since these ejected BBHs will typically have small separations, they are likely to make a significant contribution to the BBH merger rate for these clusters.

### 2.3.3 In-cluster binaries unaffected by dynamics

So far we have shown that for low metallicity clusters, the BH population due to stellar evolution and simplistic dynamics is predominantly in the form of hard BBHs. Given these binaries are tightly bound, it seems probable that some fraction of systems may merge before the next strong interaction interferes with the system. To investigate this, we compare the merger timescale Eq 1.2 (Peters, 1964) with the interaction timescale for every hard BBH retained within various combinations of cluster mass ($M_{\rm cl}$) and half-mass radii ($r_{\rm h}$).

#### 2.3.3.1 Timescales

To calculate the timescale for the binaries to experience a first encounter, we again make the assumption that the encounter removes a fraction $\delta$ of the binary binding energy. We then have the rate of energy loss from the binary given by $\dot{E}_{\rm bin} \simeq \delta E_{\rm bin}/t_{\rm int}$ (Heggie & Hut, 2003), from which we have the interaction timescale for a single binary (Antonini & Gieles, 2020b)

$$t_{\rm int} \simeq \delta \frac{G m_1 m_2}{2a} \dot{E}_{\rm bin}^{-1} \, . \tag{2.7}$$

We assume that the dynamical hardening of BBHs in the cluster core drives the cluster heating and that every binary contributes approximately the same amount of energy to the cluster. Then, we can equate the binary hardening rate to the cluster heating rate $N_{\rm bin}\dot{E}_{\rm bin} = \dot{E}$, where $N_{\rm bin}$ is the number of binaries in the cluster.

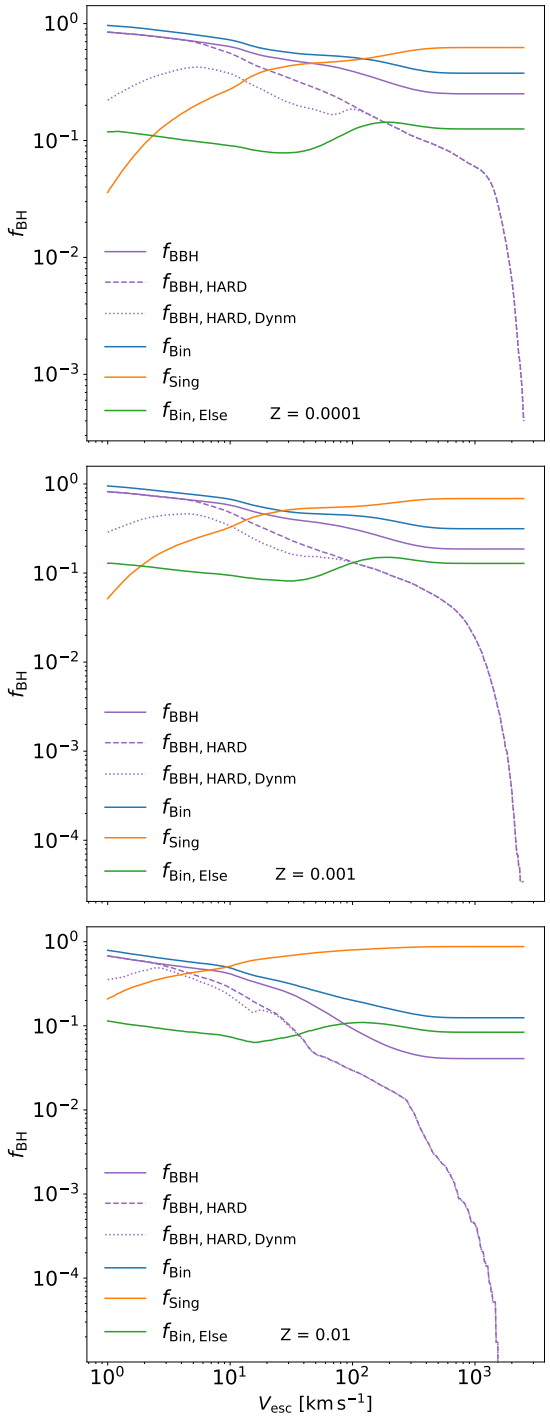


Figure 2.4: We show the fraction of BHs ($f_{\rm BH}$) retained as either single BHs (orange line, $f_{\rm sing}$) or as part of a binary (blue line, $f_{\rm bin}$). We further split the binaries into the BBH fraction ($f_{\rm BBH}$, solid purple line) and the binaries containing only one BHs ($f_{\rm Bin,Else}$, green line). For the BBH group we also show the subfraction of *hard* BBHs ($f_{\rm BBH,\,HARD}$, purple dashed line) where $a \leq a_{\rm h}$, with $a_{\rm h}$ defined in Eq 2.4. Finally, we show the expected number of BBHs that would remain bound to the cluster following an interaction ($f_{\rm BBH,HARD,Dynm}$, purple dotted line). The upper panel shows the metallicity model 0.001, the middle panel 0.01 and the lower panel 0.1.

From which we can further relate the heat generation to the global cluster properties (Hénon, 1961; Breen & Heggie, 2013)

$$\dot{E} = \zeta \frac{|E|}{t_{\rm rh}} \ , \tag{2.8}$$

where $E \simeq -0.2GM_{\rm cl}^2/r_{\rm h}$ is the total energy of the cluster and $\zeta \approx 0.2$ (Hénon, 1961, 1965; Gieles et al., 2011). The cluster relaxation time is given by

$$t_{\rm rh} = 0.138\sqrt{\frac{M_{\rm cl}r_{\rm h}^3}{G}}\frac{1}{\langle m_{\rm all}\rangle \psi \ln\Lambda} \ , \tag{2.9}$$

where $\langle m_{\rm all}\rangle = 0.809$ M$_\odot$ is set to the average stellar mass initially in the cluster, which is calculated using a Kroupa (2001) IMF between 0.08 M$_\odot$ and 150 M$_\odot$. $\ln\Lambda$ is the Coulomb logarithm which we set to a constant $\ln\Lambda = 10$, and $\psi$ depends on the mass spectrum within the half-mass radius. For a single component cluster, $\psi = 1$, but in what follows, we adopt $\psi = 5$. This takes into account that in the early evolution of the cluster (first $\sim 100$ Myr) the mass function contains more massive stars and $\psi$ is high.

Combining Eq 2.8 and Eq 2.7 we arrive at an expression for the expected total timescale between all interactions, $t_{\rm int}$, in terms of the cluster half-mass relaxation time ($t_{\rm rh}$)

$$t_{\rm int} \simeq 25\delta \frac{m_1 m_2}{M_{\rm cl}^2}\frac{r_{\rm h}}{a}N_{\rm bin}t_{\rm rh} \ . \tag{2.10}$$

We note that the derivation of Eq 2.10 makes the assumption that the cluster has undergone several relaxation times, such that it has reached a state of balanced evolution (Hénon, 1961; Breen & Heggie, 2013). Once in this state, we can relate the heat generation due to BBHs in the cluster core to the global properties of the cluster itself as in Breen & Heggie (2013). As before, we set $\delta = 0.2$ which is the expected averaged value for binary-single interactions. However, we note that $\delta$ should be a distribution of values, and that the average is expected to be somewhat higher for binary-binary interactions (Zevin et al., 2019). Here, we ignore these complications and continue with a fixed value.

It is important to consider that our assumption of all primordial binaries contributing equally to the heating of the cluster all the time is likely not realistic. It is more feasible that only a fraction of the primordial binaries are directly contributing to the heating at any given time, and so our assumption is producing a conservative, lower estimate for the interaction timescale. As a comparison we completed the analysis shown in the following section also assuming that none of the primordial binaries reach the core and so the interaction rate can simply be computed as (e.g., Spitzer, 1987)

$$t_{\rm int} \approx 2 \times 10^7 \zeta^{-1} \left(\frac{n}{10^6\ {\rm pc}^{-3}}\right)^{-1} \left(\frac{\sigma}{30\ {\rm km\ s}^{-1}}\right) \left(\frac{m_*}{m_3} 10\right)^{1/2} \left(\frac{a}{0.04\ {\rm AU}}\right)^{-1} \left(\frac{m_{12}}{20\ {\rm M}_\odot}\right)^{-1} {\rm yr}\ . \tag{2.11}$$

Here we have the number density of the cluster, $n$, the average star mass in the cluster, $m_*$, and the constant $\zeta \leq 1$ which parameterizes the difference from cluster equipartition (we set $\zeta = 1$ for this simple check). Using this alternative approach to the interaction timescale we found very little effect on the population fractions of the BBHs defined in the following section (Fig. 2.5). Similarly, we only found slight differences in the merging population (Fig. 2.6). Since we would draw the same conclusions on the BBH populations using either approach for interaction timescale, we continue this work assuming $t_{\rm int}$ as defined in Eq 2.10.

### 2.3.4 Merging population

With the consideration made in the previous sections, we are able to make the distinction between three distinct BBH populations. The first population, Pop I, are the tightest binaries, and they experience no dynamical encounters before they merge. These BBHs fall into one of two categories. One possibility is that they are ejected from the cluster by the SN kick of one of the binary components, continuing to evolve in the galactic field until they merge within a Hubble time. The other option is that the BBH remains in the cluster, however, its GW timescale is shorter than the typical interaction timescale of the cluster, hence it will merge before it can experience a strong encounter that significantly affects the binary properties (Section 2.3.3). Clearly, this population of merging BBHs should closely resemble that of the isolated binary formation channel, since its properties are solely dictated by the stellar evolution of the binary.

We define Pop II BBHs as those that will experience a single strong interaction[1] that ejects them from the cluster, i.e., $a \leq a_{\rm ej}$ (Section 2.3.2). Meanwhile, Pop III are the remaining *hard* BBHs that will experience multiple strong encounters inside the cluster, i,e., $a_{\rm ej} < a \leq a_{\rm h}$.

Fig. 2.5, shows the fraction of BBHs split into these populations across a range of cluster escape velocities. It should be noted that one extra population of BBHs that is not plotted here are the soft BBHs, where $a > a_{\rm h}$, since these binaries are likely to be disrupted and contribute to the single BH population. However, we know from Fig. 2.4 that these become the dominant form of BBHs in very massive clusters with high escape velocity. The definition of Pop I, Pop II and Pop III relies on the calculation of the cluster interaction timescale, which is dependent on both

[1]We note that for these `COMPAS` models we do not consider the effect of 3-body interactions prior to the BH formation.

the cluster mass and the half mass density. Therefore, we are unable to simply plot the fraction of BBHs against the cluster escape velocity as we had previously done in Fig. 2.4. Instead, we show the relationship between the fraction of these populations against varying cluster half mass density with fixed cluster mass, $M_{\rm cl} = 10^5$ M$_\odot$ (left panels) and vice-versa with fixed density of $\rho = 1200$ M$_\odot$ pc$^{-3}$ (right panels). For a given cluster mass and density, we also compute the cluster escape velocity which is plotted on the main x-axis (with the corresponding varying cluster mass and half mass density shown on the secondary x-axis).

It is possible for all three of these populations to contribute to the subpopulation of merging BBHs under slightly different conditions, and thus we investigate how the contribution of each population changes across the range of escape velocities used in Fig. 2.5. By definition, Pop I BBHs all merge either before an interaction or outside the cluster after being ejected by the SN kicks, hence in Fig. 2.6 we divide up the Pop I BBHs into outside and inside mergers. For a sub-Solar metallicity model, $Z = 0.0001$ and fixed $\rho$ (upper right panel), we see that at low escape velocities, $v_{\rm esc} < 21.3$ km s$^{-1}$, the Pop I mergers are dominated by outside mergers. Meanwhile, in the Solar model with fixed $\rho$ (lower right panel), the outside Pop I mergers remain dominant up to $v_{\rm esc} = 191.5$ km s$^{-1}$, above which point the mergers from Pop I become dominated by inside mergers. This difference between metallicities is likely a result of the larger SN kicks imparted on the BBHs at Solar metallicities. This means that it is much easier for the Pop I binaries to be ejected at lower escape velocities in the Solar metallicity case, thus leading to more outside mergers. When the cluster mass is kept constant (left panels) we see that in the Solar model (lower panels) the Pop I mergers are always outside the cluster. On the other hand, for the sub-Solar model (upper left panels) the outside mergers are almost always dominant.

For the other two populations, Pop II and Pop III, we must calculate what fraction of them will undergo a merger within a Hubble time and thus how they will contribute to the merging population. Recall that we define Pop II BBHs as binaries whose semi-major axis is smaller than some cut-off value, $a < a_{\rm ej}$, where $a_{\rm ej}$ is defined by Eq 2.6 and describes the separation at which a single strong interaction ejects the BBH from the cluster. Naturally then, for this population to merge either the binary properties as set by the stellar evolution place the BBH in a merging regime or the single strong interaction adjusts the properties such that the BBH can now merge in a Hubble time. Assuming either of these scenarios we set upper and lower limits on the number of expected mergers from Pop II.

We first estimate the lower limit of mergers from Pop II by assuming the interaction does not affect the binary properties, and so they are set solely by the stellar evolution. With these parameters we calculate the GW timescale from Eq 1.2, and check how many would merge within a Hubble time. For the upper limit, we account for the effect the single strong interaction has on the binary. We assume that the encounter reduces the binary binding energy by 20% and draw a new eccentricity

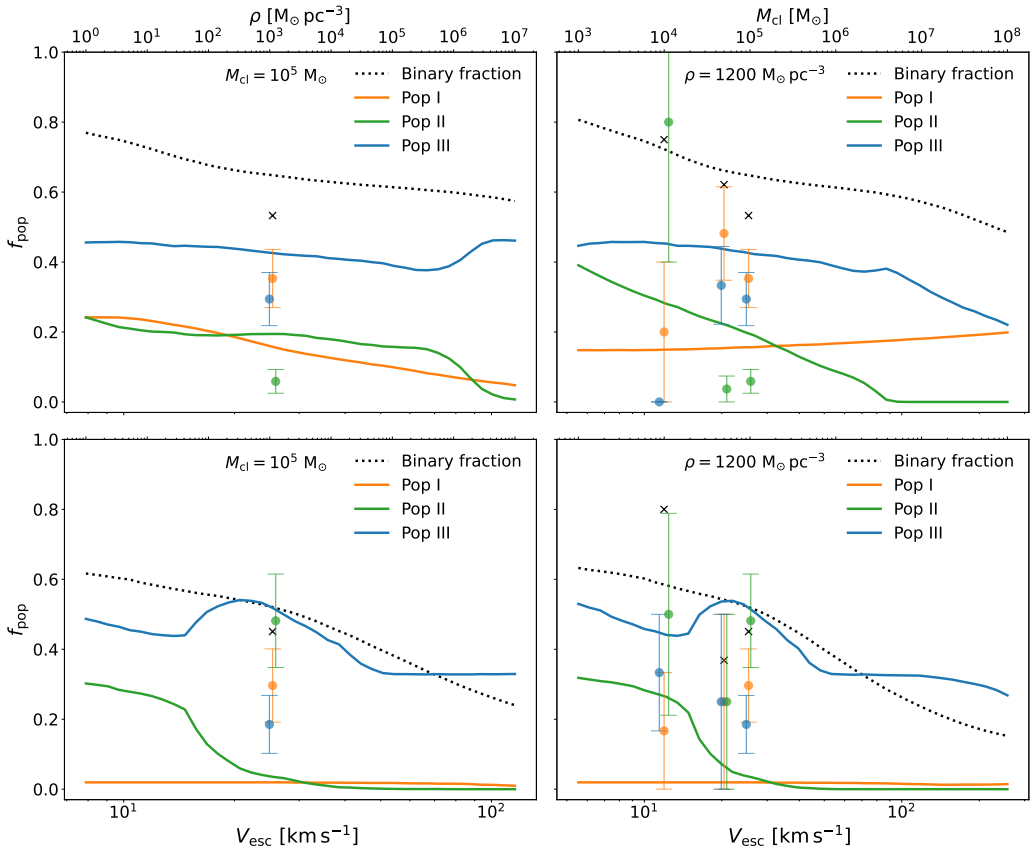


Figure 2.5: Here we show the primordial BBH population split into three subpopulations based on the binary separation. Pop I (orange lines) are BBHs that experience no interactions before they merge (either outside the cluster or before an encounter in the cluster). Pop II (green lines) are BBHs that experience one strong interaction that ejects them from the cluster and Pop III (blue lines) are hard BBHs that experience more than one encounter in the cluster. In addition, we show the overall retained BH-binary (binary with at least one BH) fraction (black dashed line) across the range of escape velocities. In the left panels we fix the cluster mass at $M_{\rm cl} = 10^5$ M$_\odot$ and vary the cluster density from $\rho = 1$ M$_\odot$ pc$^{-3}$ to $10^7$ M$_\odot$ pc$^{-3}$. The right panels show a fixed density of $\rho = 1200$ M$_\odot$ pc$^{-3}$ while varying the cluster mass from $M_{\rm cl} = 10^3$ M$_\odot$ to $10^8$ M$_\odot$. We show the results for a sub-Solar metallicity model ($Z = 0.0001$) in the top panels, and for a Solar metallicity model ($Z = 0.01$) in the bottom panels. Finally, the coloured points represent the corresponding populations as found in the $N$-body models and similarly the black crosses are the retained BH-binary fraction of the cluster.

by averaging 10 random samples from a thermal eccentricity distribution. The upper limit for mergers can then be found by how many merge within a Hubble time. We show these limits in Fig. 2.6 (the green lines). Note that the values shown in Fig. 2.6 are normalised by the total number of BBHs across the simulation since the total fraction of merging BBHs is dependent on whether you take the upper or lower limit for the Pop II mergers. In the sub-Solar model, when the cluster mass is kept constant, we see that the fraction of Pop II mergers gradually increases until a maximum of 18% at 76 km s$^{-1}$ after which is rapidly drops towards zero. This increase in dominance is likely due to the shortened interaction timescale at higher densities. For some of the tight binaries that remain in the cluster, this means that they are no longer able to merge before an interaction timescale. Essentially this is a shift from "inside" Pop I mergers to Pop II mergers.

This is supported by the fact that we see the those "inside" Pop I mergers drop to zero at the same time as Pop II grows. However, this growing number of Pop II mergers will always be turned around if the density (and thus the escape velocity) continue to increase, since $a_{\rm ej} \propto \frac{1}{v_{\rm esc}^2}$. Therefore, since the $a_{\rm ej}$ cut-off value decreases for larger $v_{\rm esc}$ the Pop II binaries close to $a_{\rm ej}$ will fall into the Pop III group as they no longer receive a large enough kick to escape the cluster on a single interaction. When we instead keep the density constant (upper right panel) we see that the fraction of Pop II mergers has a fairly consistent slight downward trend up to 100 km s$^{-1}$ after which point it drops quickly to zero. This difference with the fixed mass case discussed previously can likely be explained by the different trends we see in Fig. 2.5. There we see that the fixed density case sees the Pop II fraction simply start at 40% of the BBH population and then quickly fall to zero as the cluster mass increases. On the other hand the fixed mass case (upper left) sees the Pop II fraction hover around 20% of the BBH population across almost the entire range of densities considered. Interestingly, this difference in trend is not particularly seen in the Solar model (lower panels of Fig. 2.5) where instead fixing either the cluster mass or the density has negligible effect on the trend of the Pop II fraction. This then is carried through to the mergers in the Pop II group, where we see at Solar metallicity (lower panels of Fig. 2.6) the same distribution of Pop II mergers when we fix density and mass respectively.

In the case of Pop III mergers, they exist in the cluster for more than a single interaction and since they are still hard binaries we can assume that each successive interaction shrinks the semi-major axis, until it reaches $a_{\rm ej}$ at which point the subsequent interaction ejects the binary. In the process of the many encounters leading to $a_{\rm ej}$ it is possible that one of the interactions leads to a merger before the binary reaches $a_{\rm ej}$. However, it is difficult to consider this as it is very dependent on each individual encounter. Thus, we opt to compute a lower limit on the mergers. Assuming that all the Pop III binaries are able to shrink to $a_{\rm ej}$ without merging earlier, we then consider the final encounter in the same way as for Pop II mergers, and

see how many mergers occur within a Hubble time. It should be noted that we do account for the number of interactions that it will take to reach $a_{\rm ej}$ from the binaries initial separation, and this is factored into the time to merger. Although this population originates from the primordial population, the longer they remain within the cluster the more interactions they experience which will change the binary orbital parameters. Over enough encounters the orbital properties of the binary would more closely resemble that of a purely dynamically formed BBH. However, this theoretical treatment of potential interactions has a couple of caveats. Firstly, we do not consider 3-body interactions on a binary until it has formed a BBH. Secondly, we do not consider exchanges of binary components from these encounters, which would in turn mean a change in the component mass.

In Fig. 2.6 we also show the fraction of mergers coming from Pop III, and we see that in both models (and in both variations of fixed $\rho$ and fixed $M_{\rm cl}$) this population doesn't contribute to the mergers until $\approx 25$ km s$^{-1}$. In the Solar models (lower panels), Pop III quickly becomes the dominant contributor to the mergers (by $\approx 40$ km s$^{-1}$). In addition, we see that at Solar metallicity, both when fixing density and cluster mass, the contribution from Pop III eventually levels out at $\approx 32\%$ of the initial BBHs formed. At sub-Solar metallicity (upper panels), we see that while Pop III does eventually become the dominant source of mergers there is still a significant amount of Pop I and Pop II mergers.

### 2.3.5 Comparison to $N$-body simulations

So far we have assumed a simplistic cluster model where we only start to consider the dynamics of the cluster after the stars have evolved and formed the BH populations. This is useful to estimate the effect of the stellar evolution on the BBH population and specifically on the subpopulation of merging BBHs. However, in reality, the dynamics of the cluster during the period of stellar evolution may impact the BH populations. To investigate this we utilise the high-performance hybrid $N$-Body code, `PeTar` (Wang et al., 2020b; Nitadori & Aarseth, 2012), which allows us to populate a star cluster with some given density profile, and evolve the stars (both single and those in binaries) whilst still considering the dynamical interactions of the surrounding cluster. In comparison to direct $N$-body codes, `PeTar` combines the particle-tree particle-particle method (Oshino et al., 2011) and the slow-down algorithmic regularisation method (`SDAR`) (Wang et al., 2020a) with parallelisation using a hybrid parallel method based on the `FDPS` framework (Iwasawa et al., 2016, 2020; Namekata et al., 2018). This allows the simulations to be much quicker than other direct $N$-body codes whilst also giving us the option to simulate massive star clusters with binary fractions approaching 100% (Wang et al., 2021). Stellar evolution in PeTar follows the updated single and binary stellar evolution packages (Banerjee et al., 2020; Hurley et al., 2000) where we choose all the stellar parameters to mimic

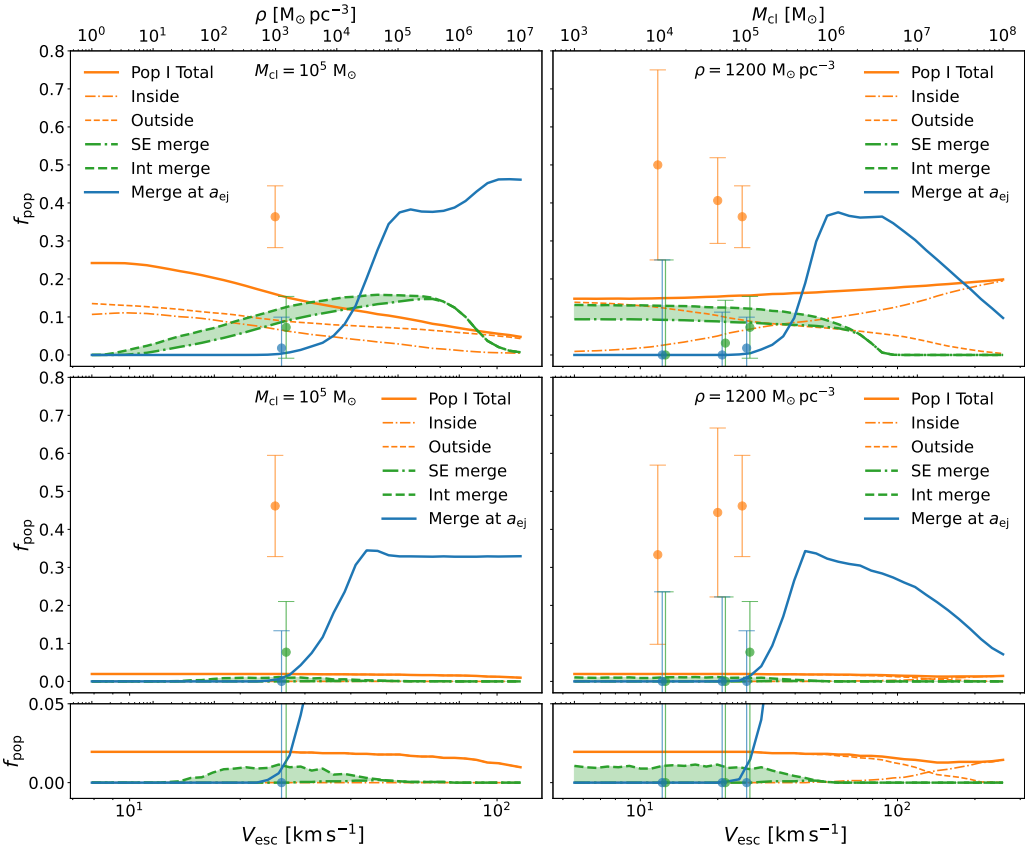


Figure 2.6: We show the fraction of merging BBHs normalised by the total number of BBHs, split between three populations (Pop I, Pop II and Pop III) defined in the text and caption of Fig 2.5. The top row shows the sub-Solar model and the middle row shows the Solar model.

For Pop I mergers (orange lines), we show the number of mergers inside the cluster (dashed-dot lines), outside the cluster (dashed lines) and the total number (solid lines). Since Pop II mergers experience a single encounter which ejects them from the cluster, we compute two limits for the mergers. The first a lower estimate assuming the orbital properties from the stellar evolution (SE merge, dashed-dot line), and the then an upper limit assuming a single interaction which increases the binding energy by 20% and produces an eccentricity kick which is drawn from a thermal distribution (Int merge, dashed line). Between these limits we show the green shaded region. Finally, for Pop III mergers we compute an upper estimate, assuming that the BBHs undergo multiple interactions until the separation shrinks to $a_{\rm ej}$. At which point we compute the effect of the interaction on the binary orbital properties. We show (in corresponding colours) the results from our $N$-body simulations, including both the mergers that occur within the simulation time (1 Gyr), and those escaped systems that would merge within a Hubble time according to Eq 1.2. Since the Pop I and Pop II distributions are difficult to distinguish in the Solar metallicity case; in the bottom panels we zoom in on the Solar models (middle panels) over the range $f_{\rm pop} = [0, 0.05]$.

those used in the COMPAS runs.

We run 6 different cluster models, 3 at the sub-Solar metallicity $Z = 0.0001$ and 3 at Solar metallicity, for three different cluster masses; $M = 10^4$ $M_\odot$, $5 \times 10^4$ $M_\odot$ and $1 \times 10^5$ $M_\odot$ (see Table. 2.3). For all these models we keep the density fixed at $\rho_h \approx 1200$ $M_\odot$ $pc^{-3}$ . Each cluster is initialised with a King (1966) model where the concentration parameter is set to $W_0 = 7$ and the stellar masses drawn from a Kroupa (2001) IMF with a range of 0.08 $M_\odot$ to 150 $M_\odot$. We then set the initial binary fraction such that all stars $M > 20$ $M_\odot$ are placed in a binary, with the partner star randomly selected from a uniform q-distribution between 0.1 and 1. We then adjust the binary period and eccentricity according to the extended Sana et al. (2012) distribution described in Oh et al. (2015) which matches the adjustment made for the binaries in the COMPAS models.

Each model is simulated for 1 Gyr which gives more than enough time for all the primordial binaries to either form a compact object binary or to be disrupted due to the interactions, and for the clusters to have significantly evolved through dynamics. From the data, we extract the binary information at the time that each BBH is formed and run the same population tests as we did for the COMPAS models to separate these BBHs into the same population groups. The key difference here is that by using a self-consistent cluster model we can take into account the dynamical interactions within the cluster, as well as the evolution of the cluster itself before the formation of the BHs. We note that an alternative approach to this analysis would be to track the evolution of these BBHs post-formation within the N-body simulations, then identifying mergers as they happen up to the end of the simulation. This is a more sophisticated approach which accurately models the subsequent dynamical evolution of the BBHs. This is beyond the scope of this chapter, however we utilise this approach in Chapter 3.

This allows us to get a more accurate picture of these populations in a more realistic setting. The cluster mass and half-mass radii can simply be read from the data at the time of the BBH formation; however, to calculate the escape velocity for a specific binary at this time, we must take into account its position within the cluster and find the average velocity dispersion of the surrounding stars. From this we can find the escape velocity of the cluster using the relation $v_{esc} \simeq 4.77\sigma$ for a King density profile with $W_0 = 7$ (as used for the COMPAS Model).

We show the results of these $N$-body simulations as markers on Fig. 2.5 and Fig. 2.6. These markers are not in a one-to-one correspondence with the COMPAS results, since the binary stellar evolution code used is subtly different in PeTar compared to COMPAS. It is also important to note that the uncertainty in the data for the smallest cluster we simulated, at $v_{esc} = 14$ km $s^{-1}$, is very large since we are dealing with a relatively low number of statistics here, less than ten binaries. From Fig. 2.5, one of the key differences we see between the PeTar results and the COMPAS results is the slight reduction in the number of pop III binaries. This suggests some dynamical

interactions during the stellar evolution phase of the binaries, disrupt some of these wider BBHs.

In order to better quantify the effect of dynamics on the binary population during the period of stellar evolution, we use the independent binary stellar evolution tool in `PeTar` to evolve a population of binaries drawn from the same initial distributions as those used in the cluster simulations. We then compare the separation and eccentricity distributions for the formed BBH in each case (with dynamics and isolated); these comparisons are shown in Fig. 2.7. From the comparison of the separation distributions it is clear that the dynamical environment causes two main effects; most importantly, the disruption of the wider binaries $\gtrsim 10$ AU and secondly, the hardening of the tighter binaries. This results in the separation distribution shifting to smaller $a_{\rm BBH}$. The eccentricity distribution is not overly affected by the introduction of dynamics.

These $N$-body runs have shown us that, dynamical encounters prior to the formation of BHs tend to slightly reduce the prevalence of the wider Pop III binaries. However, these still account for at least $\sim 20\%$ of the BBH population in our models (excluding the single case of 0 binaries in the sub-Solar metallicity model in which we are dealing with very low number statistics $< 5$). Therefore, it still seems that our method for splitting the BBH population is applicable even when considering early dynamics in the cluster.

In addition, we investigate the number of actual mergers that occur in the simulations until the final integration time of 1 Gyr, and including those that occur within the ejected population in less than the Hubble time.

After identifying the mergers in the simulations, we then look back to the time of BBH formation for each of these binaries so that we can characterise them into the three populations. In addition, for BBHs that still exist at the end of the simulation and have escaped the cluster, we calculate the time delay using Eq 1.2, and check if they would merge within a Hubble time. We plot these points on top of the `COMPAS` results in Fig. 2.6 normalised to the initial number of BBHs that are formed from the primordial population; and also quote the merger counts in Table 2.3. As was the case for Fig. 2.5, the markers on Fig. 2.6 are not in a one-to-one correspondence with the `COMPAS` results.

We see a clear dominance of mergers from Pop I in every model, especially for the most massive $10^5$ $M_\odot$ cluster where the errors are smaller. We also note that we find a significantly higher fraction of Pop I mergers in the $N$-body runs than we had predicted from the `COMPAS` models. Pop III mergers are non-existent within the solar metallicity models, and there is only a single merger found in the most massive cluster at sub-solar metallicities. Pop II mergers are also very sub-dominant, always around 5 times fewer than Pop I mergers. We discuss possible reasons for this discrepancy near the end of this section.

In Table 2.3 we also show counts for the number of mergers from the dynamical

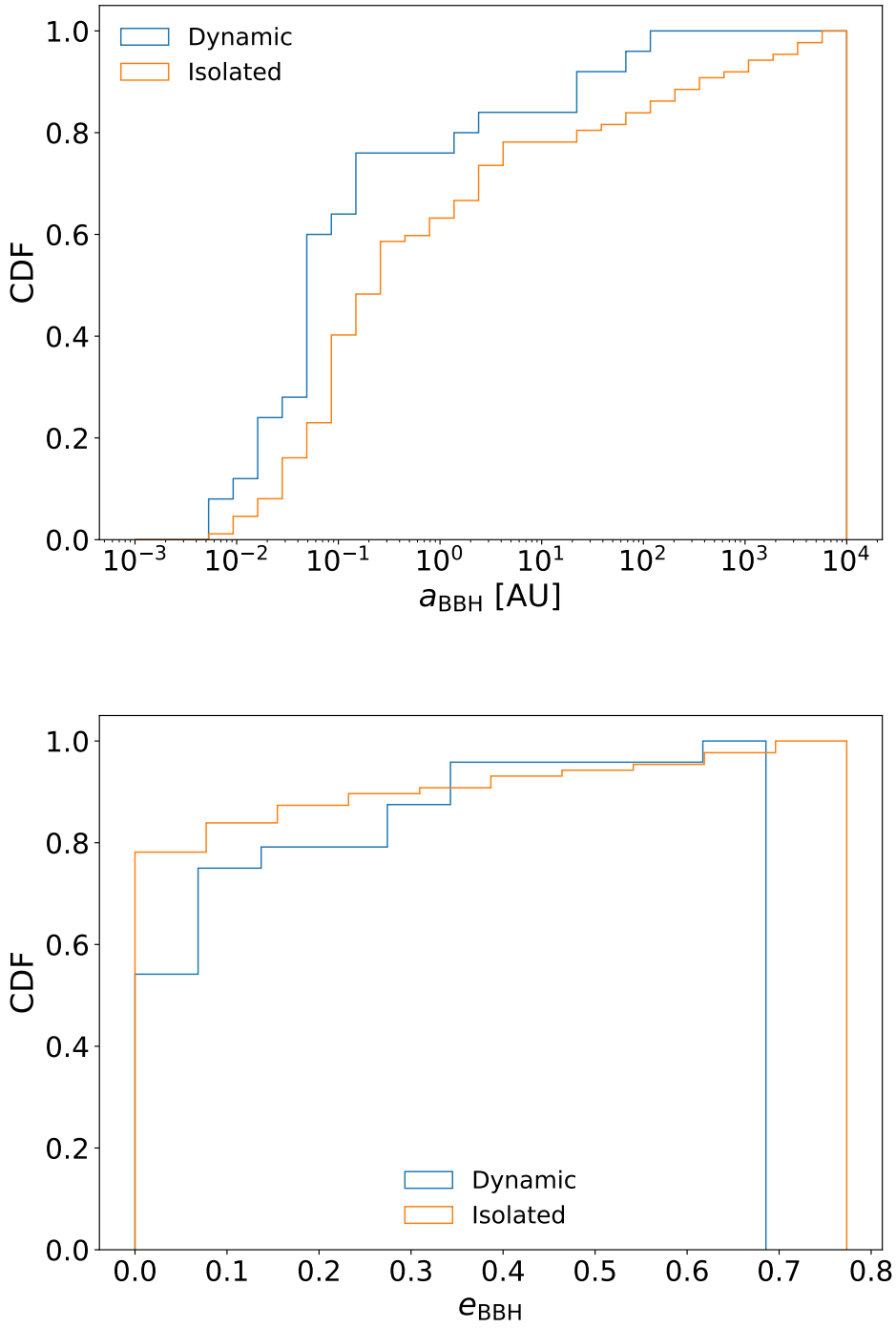


Figure 2.7: We compare the separation (upper panel) and eccentricity (lower panel) distributions when considering only binary stellar evolution, and in the context of a dynamical environment. We see that there is very little effect on the eccentricity of the formed BBHs; however, the separation of the BBHs is typically reduced when dynamics are introduced. These plots show results only from the Solar metallicity models.

population. Note that this population includes binaries formed through exchanges at any point in the stellar evolution. We find that these are a minority of mergers compared to the those from the primordial population. The final column of Table 2.3 shows the number of single BHs left in the cluster at the end of the simulation, 1 Gyr. These might still contribute to the dynamical population of merging BBHs. If we assume that the remaining BHs will interact dynamically to form BBHs and that these BBHs will merge within a Hubble time, then we can estimate an upper limit for the number of mergers we expect from the dynamical channel. This needs to take into account, however, that a binary will eject approximately $\sim 5$ other BHs before merging (Breen & Heggie, 2013). We can conclude that the dynamical channel is still expected to produce fewer mergers compared to the primordial channel.

We consider the future evolution of BBH populations we have defined and conclude that it should be expected for dynamical interactions to ultimately have a larger contribution to the formation of BBHs, since a significant fraction of Pop III binaries will likely experience an exchange at some time. This exchange will likely manifest as a binary-binary interaction and will add to the number of binaries that are formed through captures of the single BHs still in the cluster. The dominance of dynamically formed binaries in these clusters is consistent with previous studies (Di Carlo et al., 2020; Rastello et al., 2021; Torniamenti et al., 2022) where their $N$-body simulations showed that the dynamical population was almost always larger than the "original" population [2], typically by about a factor of three.

When we look at the merging population we find that the reverse is true, dynamical interactions appear to be less important, with the BBH mergers predominantly arising from the binary population that is mostly unaffected by dynamical interactions. This is also consistent with Di Carlo et al. (2020); Rastello et al. (2021); Torniamenti et al. (2022), who all find that the "original" binaries are more efficient at merging compared to BBHs formed through exchanges. It should be noted that the prevalence of original BBH mergers in our $N$-body models is even more pronounced which stems from a different time delay distribution of the BBHs at formation (see the solid lines on the left panel of Fig. 2.8). When we compare this plot against the same made for the `COMPAS` results, Fig. 2.3 (re-plotted on the right panel of Fig. 2.8), we see that at every metallicity the proportion of BBHs that merge within a Hubble time is larger than found using `COMPAS`, with the difference more extreme for higher metallicities. This explains why the $N$-body points shown in Fig. 2.5 and Fig. 2.6 don't match the fractions predicted from `COMPAS`. It is necessary to check whether this difference in $t_{\rm delay}$ is arising from the slightly different stellar evolution routines of both codes, or simply from the dynamical environment of the stellar cluster. Therefore, we also complete an "isolated" run in `PeTar`, with the same initial stellar conditions as the $N$-body runs but without the dynamics of the

[2] In these studies, primordial binaries are termed original, whilst dynamical binaries are referred to as "exchange" binaries.

stellar cluster. The resulting $t_{\rm delay}$ distribution is shown in the left panel of Fig. 2.8, with the dotted lines showing the distribution for the isolated simulation run. We see that the dynamical environment of the star cluster does impact the $t_{\rm delay}$ distribution compared to the isolated run, however the isolated run in `PeTar` is still not able to recover a distribution similar to that found for `COMPAS`. Therefore, we conclude that the main cause of the discrepancy between the $N$-body points and the `COMPAS` lines shown in Fig. 2.5 and Fig. 2.6 must result from the slightly different stellar evolution routines. As we discussed in Chapter 1, `COMPAS` is a modern population synthesis code specifically designed for modelling COs formation, and differs from `BSE` with the inclusion of more up-to-date prescriptions, in particular relating to the accurate modelling of massive star evolution, SN, and SN remnant formation.

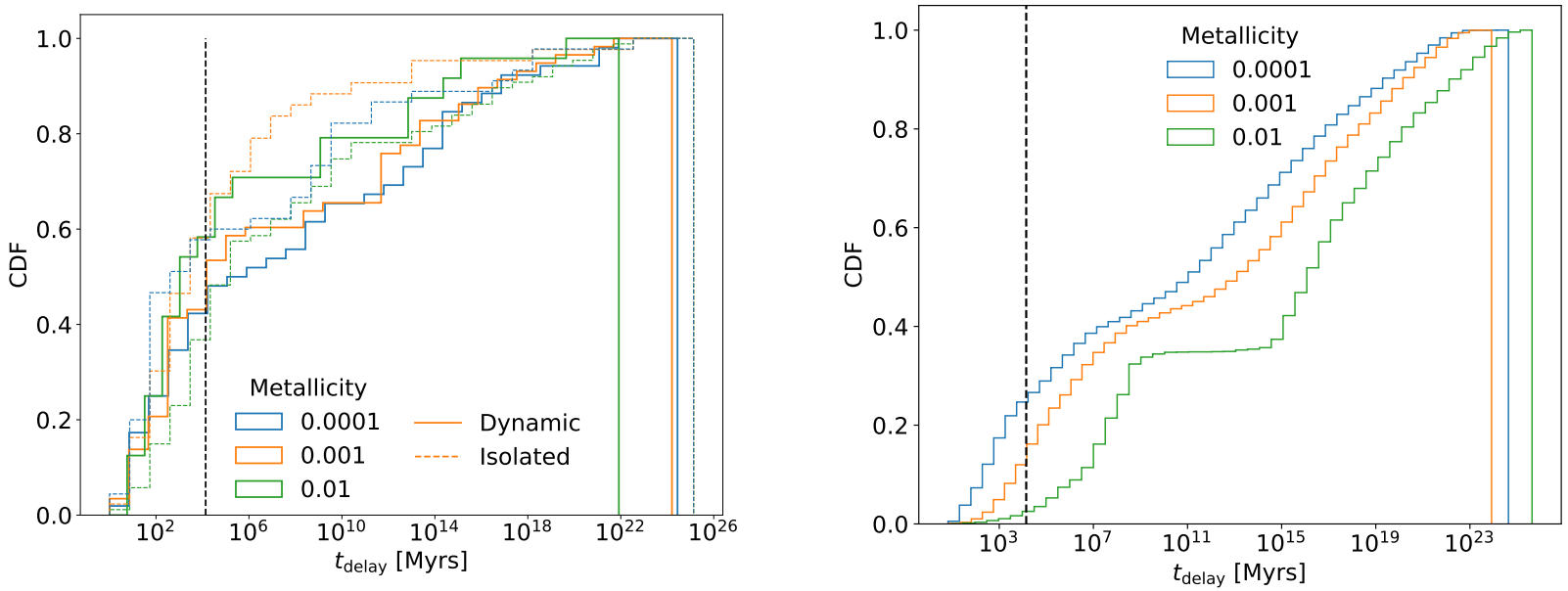


Figure 2.8: On the left panel we compare the time delay distribution across three metallicities for the primordial binary population found in the $N$-body results (Solid lines). We only show the results from the $10^5$ $M_\odot$ clusters at each metallicity. We also show the time delay distribution found using the `PeTar` code without dynamics (dashed lines). Comparing the dashed and solid lines we can see how much of the difference the dynamical environment of the cluster makes on the BBHs formed. We also note that these distributions differ from the time delay distributions that we previously showed for the `COMPAS` results (Fig. 2.3). We have re-plotted the `COMPAS` distributions here in the right panel for ease of comparison.

Table 2.3: A count of mergers found within $N$-body simulations that were run up to 1 Gyr. Here the primordial binaries are separated in the three populations based on their orbital parameters at BBH formation. We also give the number of mergers among BBHs that form through dynamical interactions, and the number of lone BHs remaining at the end of the simulation, $N_{\rm BH}$.

| Metallicity | Mass | Primordial | | | Dynamical | $N_{\rm BH}$ |
|---|---|---|---|---|---|---|
| $Z_\odot$ | $M_\odot$ | Pop I | Pop II | Pop III | | |
| 1 $Z_\odot$ | 10000 | 2 | 0 | 0 | 0 | 1 |
| | 50000 | 4 | 0 | 0 | 0 | 23 |
| | 100000 | 12 | 2 | 0 | 4 | 50 |
| 0.1 $Z_\odot$ | 10000 | 2 | 0 | 0 | 1 | 3 |
| | 50000 | 10 | 1 | 0 | 3 | 29 |
| | 100000 | 24 | 5 | 1 | 6 | 70 |
| 0.01 $Z_\odot$ | 10000 | 4 | 0 | 0 | 1 | 2 |
| | 50000 | 13 | 1 | 0 | 2 | 34 |
| | 100000 | 20 | 4 | 1 | 6 | 95 |

### 2.3.6 Varying stellar properties

We vary some stellar properties, notably the natal kick prescription and the chemically homogeneous evolution assumption, and rerun the analysis performed in Section 2.3.4. Table 2.4 details the different models that we run.

We find very little difference between Mod1, Mod2 and Mod3 suggesting that the choice of chemically homogeneous evolution does not affect the population fractions of the BBHs. Furthermore, we also see negligible variation for the BBH mass, semi-major axis, eccentricity and mass ratio distributions across Mod1, Mod2 and Mod3.

The choice of BH kick prescription has a dramatic effect on the populations and the BH parameters, as can be expected; since the size of the SN kicks is one of the main determinants of whether a binary is a) disrupted following stellar evolution and b) if it remains within the cluster following the BH formation. We investigated three prescriptions for the BH natal kicks; firstly, the "Fallback" model Mod1, where the BH kick is scaled by the amount of material that falls back onto the BH. This is what has been used in producing the results up until now. Secondly, we used the "Reduced" kick model (Mod5), where we assume that the BHs receive the same momentum kick as a typical NS, and so the drawn kick magnitude is scaled by the

Table 2.4: Stellar evolution variations compared to the previous models shown above

| Model | Variation |
|---|---|
| Mod1 | Standard parameters described above |
| Mod2 | Chemically homogeneous evolution - Optimistic |
| Mod3 | Chemically homogeneous evolution - Pessimistic |
| Mod4 | BH kick prescription - No kicks |
| Mod5 | BH kick prescription - Reduced (equal momentum) |

ratio $M_{\rm NS}/M_{\rm BH}$. Lastly, we use a zero-kick model (Mod4) where the BHs receive no kicks from the SN, although it is still possible for them to experience some kicks due to the MT during the explosion.

We show the population fractions from these results in Fig. 2.9 where we have set the metallicity to $Z = 0.0001$. When we assume the BHs receive no natal kick (upper panels) we see that the fraction of Pop III BBHs falls rapidly with increasing density and cluster mass which is a very different relation to what we had seen when using the fallback models previously (and in the lower panels). Meanwhile, the relationship between the Pop I fraction and the Pop II fraction with cluster density and mass remain largely the same as in the fallback case, although their respective fractions are slightly lower. This greater dominance in the Pop III BBHs across the escape velocity range is most likely due to the increased number of BBHs that can remain bound following the BH natal kicks (since these are now zero). Although it is true that the zero kicks should also mean that the number of Pop I and Pop II BBHs should also be increased; Pop III will benefit the most since they have larger separations and thus would be easier to disrupt following a kick.

The reduced kick model (middle panels) is particularly interesting since it has the most apparent change in relationship. In this case the Pop III BBHs actually start as the minority population and increase in fraction with increasing density and cluster mass. This is contrary to what we see for the fallback kick and zero kick models where the general trend is a decrease in Pop III dominance with escape velocity. This difference is likely arising due to the fact that the reduced prescription for kicks will generally produce larger BH kicks compared to the fallback prescription. These larger kicks are able to disrupt more of the wider Pop III BBHs than the fallback model, and this is reflected in the lower contribution to the BBH population. As the escape velocity increases we have the Pop II/Pop III cut off value, $a_{\rm ej}$ shrink and so the Pop II BBHs become classified as Pop III, this is the same as what we have discussed previously. However, in this case since we have fewer wider BBHs (those with separations close to the Pop III/soft BBH boundary $a_{\rm h}$), Pop III gains more members from Pop II than it loses as soft binaries. This explains why we see this increasing trend of dominance in the Pop III with reduced kicks compared to the opposite for the fallback and no kick prescriptions.

## 2.4 Importance of binary-binary interactions

Thus far we have shown that a significant fraction of the retained BHs are found in BBHs, the latter being the majority source for low $v_{\rm esc}$ clusters. This abundance of binaries in the cluster will in turn lead to a higher chance that any specific BBH experiences a binary-binary encounter during its lifetime in the cluster. These interactions are complex with a variety of possible outcomes, including exchanges of binary components and complete disruption of one or both binaries (Antognini &

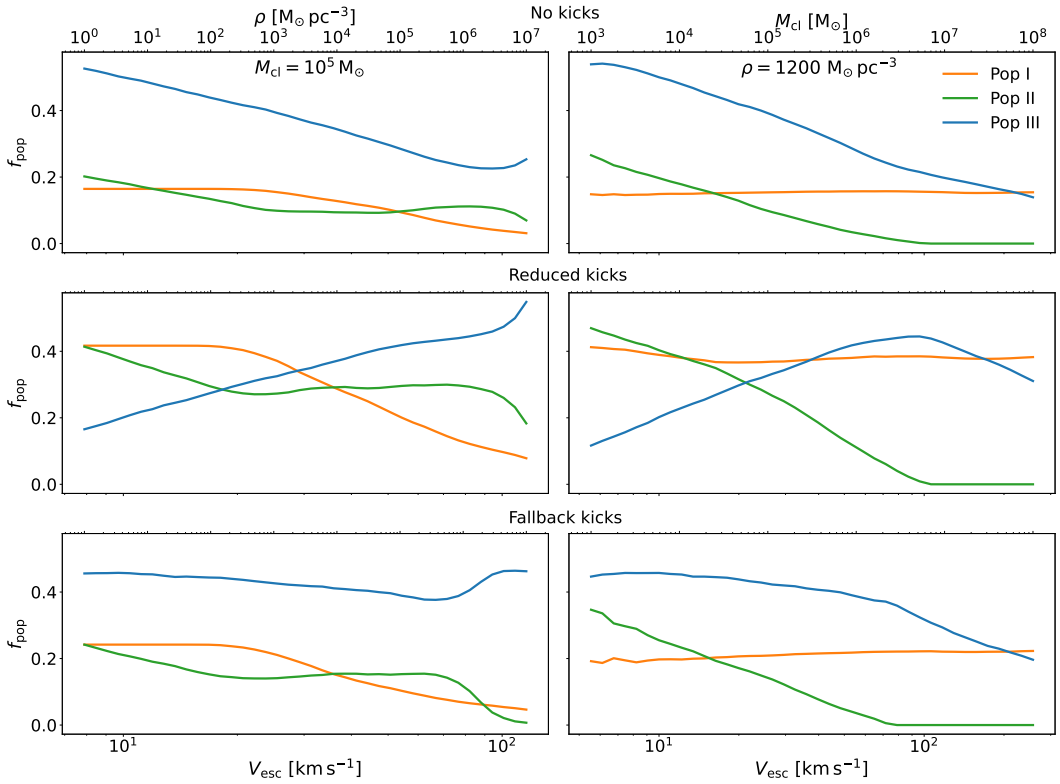


Figure 2.9: We show the BBH populations, described in the caption of Fig. 2.5, at metallicity $Z = 0.0001$ Z$_\odot$, assuming different prescriptions for the BH natal kicks. The upper panels show the case for zero natal kicks, the middle panels show the "reduced" model where kicks are scaled by the mass ratio of the BH to a typical NS. Finally, the lower panels show the "fallback" model which scales the kicks based on the amount of material falling onto the BH while it is forming, this is characterised by a fallback fraction $f_{\rm b}$. These populations are defined as described in the caption of Fig. 2.5. The right column of plots assumes a constant density $\rho = 1200$ M$_\odot$ pc$^{-3}$, whereas the left column assumes a constant cluster mass $M_{\rm cl} = 10^5$ M$_\odot$

.

Thompson, 2016; Zevin et al., 2019). All of which would naturally have implications on the properties of the BBH population. Therefore, we show the importance of binaries by quantifying the number of potential binary interactions we would expect given the population evolved with `COMPAS`, and making some assumptions regarding the host cluster.

We loosely follow the method shown in Atallah et al. (2023) to calculate the interaction rate between a target binary and a projectile "species", which we define as the binary or single population as required. Firstly, we set up some relationships for the cluster environment where we are to place our BHs. We assume a double King (1966) cluster sphere model where the inner sphere is a scaled-down version of the outer sphere. The inner sphere is taken as the BH sub-cluster which results from the BH mass segregation expected to form in these dense stellar environments (Breen & Heggie, 2013; Küpper et al., 2011). The outer sphere we take as the primary cluster which we assume to contain only one solar mass stars, such that the average stellar mass for the cluster is $\langle m_* \rangle = 1\ \mathrm{M}_\odot$. The two spheres are defined to be uncoupled so that they maintain independent velocity dispersion profiles. Under this assumption, the deviation from energy equipartition between the outer (primary) and inner (BH) cluster at $r = 0$ is defined by

$$\eta = \frac{\langle m_{\rm BH} \rangle \, \sigma^2_{\rm BH}(0)}{\langle m_* \rangle \, \sigma^2_{\rm cl}(0)} \ , \tag{2.12}$$

where $\langle m_* \rangle$ and $\langle m_{\rm BH} \rangle$ are the average masses in the primary and BH clusters. The choice of $\eta$ determines the energy shared between the two clusters, with $\eta = 1$ once full equipartition of energy is reached. In this state, the ratio of the velocity dispersion for each cluster scales with the ratio of the average masses $\frac{\sigma^2_{\rm BH}}{\sigma^2_*} = \frac{\langle m_* \rangle}{\langle m_{\rm BH} \rangle}$. Alternatively, we can set $\eta = \frac{\langle m_{\rm BH} \rangle}{\langle m_* \rangle}$ which is a state where the BHs have the same velocity dispersion as the stars.

In a similar vein to Atallah et al. (2023), we assume that the interaction between a target binary and the projectile species (singles or binaries) occurs within the BH sub-cluster. Then, by assuming equipartition between the target and projectile we can relate their respective velocity dispersions by

$$\begin{aligned} \sigma_{\rm p} &= \sigma_{\rm BH}, \\ \sigma_{\rm t} &= \sqrt{\frac{\langle m_{\rm p} \rangle}{m_{\rm t}}} \sigma_{\rm p} \ . \end{aligned} \tag{2.13}$$

We finally define the relative velocity dispersion in the relative motion frame as in Binney & Tremaine (2008).

$$\sigma_{\rm rel,p} = \sqrt{\sigma_{\rm t}^2 + \sigma_{\rm p}^2} = \sigma_{\rm BH}\sqrt{1 + \frac{\langle m_{\rm p}\rangle}{m_{\rm t}}} \ . \tag{2.14}$$

We define the escape velocity from the core of both clusters $v_{\rm esc}(\infty)$, with the total potential at the core $\Phi_{\rm tot}(0) = \Phi_{\rm cl}(0) + \Phi_{\rm BH}(0)$.

$$v_{\rm esc}(\infty) = \sqrt{-2(\Phi_{\rm cl}(0) + \Phi_{\rm BH}(0))} \ , \tag{2.15}$$

where the potential at infinity goes to 0. From King (1966) we can relate the central potential to the $W_0$ parameter by $\Phi(0) = -W_0\sigma^2$. Setting $W_0 = 7$ and substituting the velocity dispersion from Eq 2.12 with $\langle m_*\rangle = 1$ M$_\odot$ yields

$$v_{\rm esc}(\infty) = \sqrt{14\left(1 + \frac{\eta}{\langle m_{\rm BH}\rangle}\right)\sigma_*} \ . \tag{2.16}$$

Now we adapt the general interaction rate between a target binary and a projectile species, such that we integrate the interactions over our hard BBH and BH populations:

$$\begin{aligned} \Gamma_{\rm S} &\propto \sum_{i=0}^{N_{\rm S}} a_{\rm t}^2 \sigma_{\rm rel,S}\left[1 + \frac{G(m_{\rm t} + m_{\rm S,i})}{2a_{\rm t}\sigma_{\rm rel,S}^2}\right] \\ \Gamma_{\rm B} &\propto \sum_{i=0}^{N_{\rm B}} (a_{\rm t} + a_{\rm B,i})^2 \sigma_{\rm rel,B}\left[1 + \frac{G(m_{\rm t} + m_{\rm B,i})}{2(a_{\rm t} + a_{\rm B,i})\sigma_{\rm rel,B}^2}\right] \ , \end{aligned} \tag{2.17}$$

Where $a_{\rm t}$ and $a_{\rm B,i}$ are the target and projectile binary separations and $\sigma_{\rm rel,B}$ and $\sigma_{\rm rel,S}$ is the relative velocity dispersion assuming binary and single projectiles respectively. We can further integrate over the target binary semi-major axis and mass, which simply includes a second summation in Eq 2.17 over $a_{\rm t,j}$ and $m_{\rm t,j}$. In doing this we can estimate the total interaction rates for every BBH in the population with every other BBH and with every single BH in the population. The ratio of these two rates can give us a measure of the dominant form of interactions given our BH populations. Fig. 2.10 shows the ratio of the total interaction rate for every binary-binary ($\Gamma_{\rm B,tot}$) and binary-single ($\Gamma_{\rm S,tot}$) encounter in our population against the cluster escape velocity. We plot this curve at three metallicities $Z = 0.01,\ 0.001,$ and 0.0001 and distinguish the boundary line at $\Gamma_{\rm B,tot}/\Gamma_{\rm S,tot} = 1$ below which single interactions become more dominant in the population. In addition, we consider two possible states of the cluster; a state of energy equipartition where $\frac{\sigma_{\rm BH}^2}{\sigma_*^2} = \frac{\langle m_*\rangle}{\langle m_{\rm BH}\rangle}$ and a state where the velocity dispersion of the BHs and stars is equal. One would expect that as a stellar cluster evolves, it moves towards a state of energy equipartition.

Concentrating first on the case where the cluster has reached energy equipartition; the trivial takeaway from Fig. 2.10 is that binary-binary interactions dominate the

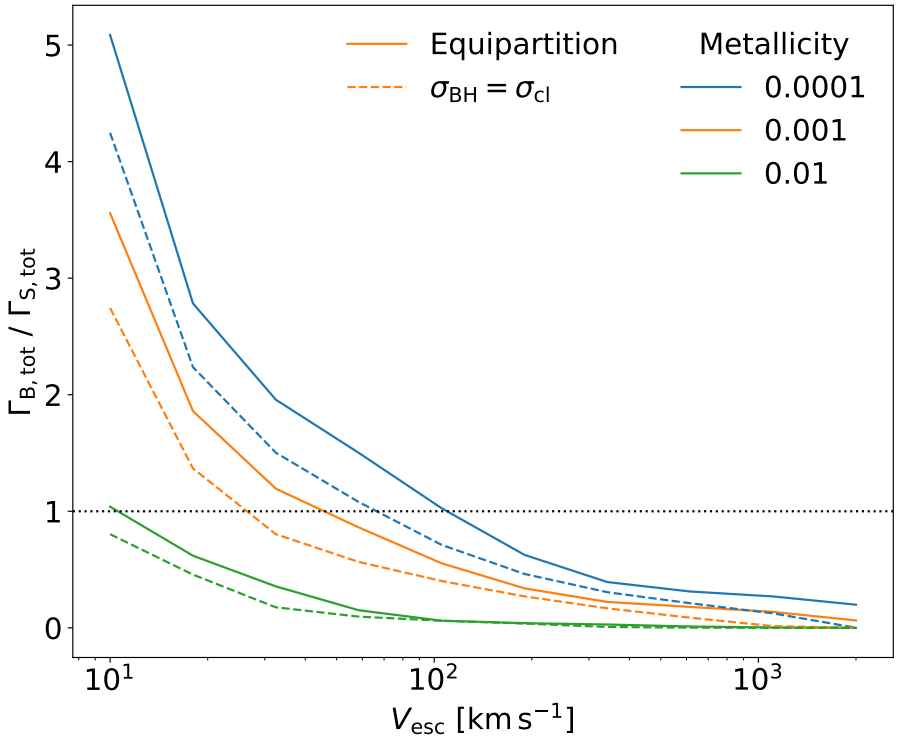


Figure 2.10: The ratio of the total number of binary-binary interactions to binary-single interactions, integrated over the entire hard BBH and single BH populations found using `COMPAS` (see Section 2.2). We show this ratio across three metallicities ($Z = 0.01,\ 0.001,$ and $0.0001$) and for two states of the cluster, energy equipartition and a state of equal velocity dispersion between BHs and stars. We also mark the boundary line of $\Gamma_{B,tot}/\Gamma_{S,tot} = 1$ below which binary-single interactions become the dominant form of encounter.

BBH encounters at low $v_{\rm esc}$.

As the escape velocity increases, and we begin to retain more single BHs within the cluster the number of potential binary-single encounters grows. In addition, the velocity dispersion of the cluster increases and as such the hard-soft boundary for the BBHs ($a_{\rm h}$) decreases and so does the number of hard binaries which can undergo a binary-binary encounter. The combination of these two effects leads to the ratio of $\Gamma_{\rm B,tot}/\Gamma_{\rm S,tot}$ decreasing as the escape velocity increases.

We see that the escape velocity where $\Gamma_{\rm B,tot}/\Gamma_{\rm S,tot}$ becomes less than one is dependent on the metallicity of the cluster, with the lower metallicity clusters maintaining a majority of binary-binary interactions for higher escape velocities. We also see that the escape velocity of the transition point, $\sim 100$ km s$^{-1}$ for the sub-Solar metallicity model, is larger than the escape velocity at which the single BH population becomes more numerous than the hard BBH population, 30 km s$^{-1}$ for the same model (see Fig. 2.4). This tells us that this transition point is not only dependent on the number count of single BHs to BBHs. For each interaction, we have a cross-section for the interaction $\Sigma_{\rm int} \propto k(a_{\rm t} + a_{\rm p})^2$ with $a_{\rm p} = 0$ when the projectile species are single BHs and $k = 2$ so that we include only strong interactions with the target binary. Naturally, the interaction cross-section for a binary-binary interaction is larger than for a binary-single interaction. Thus, for the binary-single interactions to become dominant, they not only need to outnumber the binary-binary interactions but outnumber them to such a degree that the extra encounters can make up for their lower cross-section. To better understand this cut-off, we investigated how the binary fraction, $N_{\rm bin}/(N_{\rm bin} + N_{\rm singles})$, evolves with $v_{\rm esc}$. We find that for every metallicity model the binary-single interactions become dominant below a binary fraction of 30%, which is consistent with recent work on the topic (Marín Pina & Gieles, 2024).

For each metallicity model in Fig. 2.10 we also consider the case where $\sigma_{\rm BH} = \sigma_*$. We see that in this scenario the transition point to dominant binary-single interactions is pushed to lower escape velocities for all models, while the general shape of the relationship between $\Gamma_{\rm B,tot}/\Gamma_{\rm S,tot}$ and $v_{\rm esc}$ remains almost unchanged compared to the equipartition case.

To investigate how the ratio $\Gamma_{\rm B,tot}/\Gamma_{\rm S,tot}$ depends on the properties of the target binary, we run further analyses and calculate the interaction rates for a given target BBH with our hard BBH and single BH populations.

Starting first by fixing the target BBH mass to the average BBH mass from our population, $\langle m_{\rm BBH} \rangle = 44$ M$_\odot$, and fixing the escape velocity, we draw 10,000 target separations uniformly across the range of hard BBH semi-major axis in our population. For each target binary, we calculate the averaged ratio of the interactions $\Gamma_{\rm B}/\Gamma_{\rm S}$, repeating this for five different values of $v_{\rm esc}$ and also for each of our metallicity models. Fig. 2.11 shows these results plotted against the semi-major axis of the target binary ($a_{\rm t}$), again with the cut-off value $\Gamma_{\rm B}/\Gamma_{\rm S} = 1$ marked.

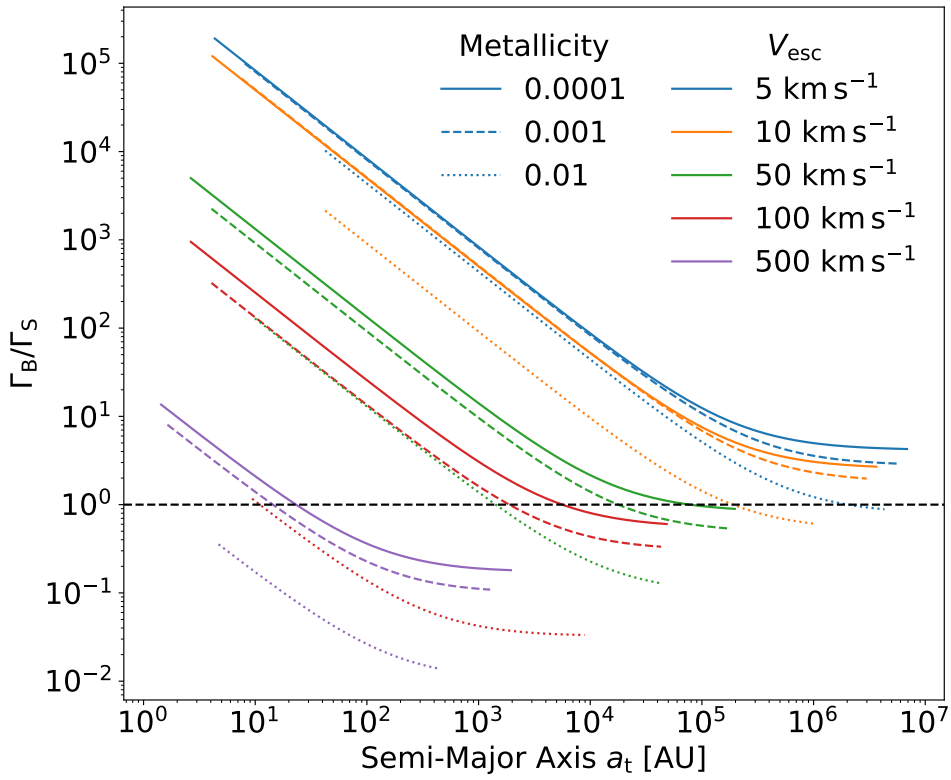


Figure 2.11: For our three metallicity models $Z = 0.01,\ 0.001,\ 0.0001$ we assume five cluster escape velocities, $v_{esc} = 5,\ 10,\ 50,\ 100,$ and 500 km s$^{-1}$ and then generate 10,000 target binaries drawing their separations from the range of semi-major axes in the retained hard BBH population. We then calculate the ratio of binary-binary and binary-single interaction rates for each target binary, integrating over the retained hard BBH and single BH populations. We finally show this ratio against the target semi-major axis for all three metallicities and all five escape velocities, in addition to plotting the boundary line at $\Gamma_B/\Gamma_S = 1$ below which the binary-single interactions are dominant

We see that for a given metallicity and escape velocity, the ratio of interactions increases for a smaller target separation, with the relationship at low $a_{\rm t}$ scaling proportional to $\left(1+\frac{\langle a_{\rm b}\rangle}{a_{\rm t}}\right)$. Looking to the other extreme of large $a_{\rm t}$, at all escape velocities and metallicities the ratio of interactions levels out. It can be shown that in this regime

$$\frac{\Gamma_{\rm B}}{\Gamma_{\rm S}} \simeq \frac{N_{\rm B}}{N_{\rm S}}\frac{\sigma_{\rm rel,B}}{\sigma_{\rm rel,S}} \ , \tag{2.18}$$

where we assume that the target separation is much larger than the average separation of the projectile binaries. Note that since here we are fixing the escape velocity of the cluster, Eq 2.18 is constant and so in the high $a_{\rm t}$ regime the key factor determining whether binary-single or binary-binary interactions are dominant comes down to which population is more numerous at this $v_{\rm esc}$. This explains why for low escape velocities, $v_{\rm esc} = 5$ km s$^{-1}$ and $v_{\rm esc} = 10$ km s$^{-1}$ where we are retaining many more hard BBHs than single BHs, the single interactions are never dominant, even at large $a_{\rm t}$.

As the cluster escape velocity increases, and so, in turn, does the velocity dispersion, we know that $a_{\rm h}$ for any given binary decreases which both limits the maximum separation of the target binary and lowers the number of hard BBH to be used as projectiles. In addition, the cluster retains more single BHs at higher escape velocity which naturally increases the binary-single interaction rate of the target binary. All of these aspects can be seen in Fig. 2.11, when comparing curves at increasing $v_{\rm esc}$. The key point here is that for a given target binary, the separation at which the binary-single interactions become dominant becomes smaller as the escape velocity of the cluster increases. In particular, for a metallicity $Z = 0.0001$, binary-binary interactions are the dominant form of encounter in clusters up to $v_{\rm esc} = 100$ km s$^{-1}$ for almost any target binary separation.

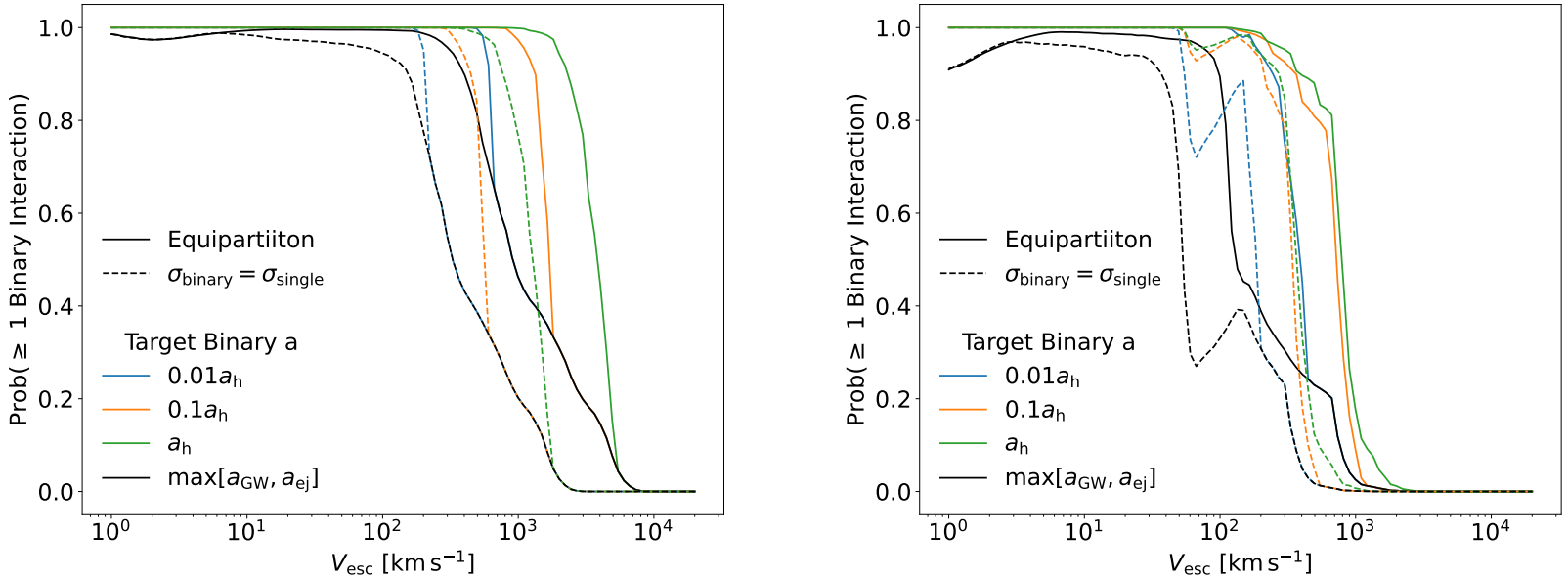


Figure 2.12: Probability to experience at least one binary-binary encounter in the chain of successive interactions a target binary undergoes before its separation reduces to $a_{\rm ej}$. The probability is computed as 1-$P$(All Singles), where $P$(All Singles) is the probability that the binary only interacts with singles. We show this probability by taking three values for the initial separation of the target binary in terms of the hard/soft boundary, $a_{\rm h}$, $0.1a_{\rm h}$ and $0.01a_{\rm h}$. We also compute the probability of the next encounter being a binary for a target binary with separation $a = \max[a_{\rm GW},\ a_{\rm ej}]$ where $a_{\rm GW}$ is the separation at which the binary energy loss is dominated by GW radiation. Finally, we perform the above analysis assuming two states for the overall cluster: a state of energy equipartition, and a state with the BH velocity dispersion equal to the stellar velocity dispersion. The left panel shows results for $Z = 0.0001$ while the right panel shows for $Z = 0.01$.

### 2.4.1 Probability of at least one binary-binary encounter

Whilst within the cluster, a hard BBH will undergo multiple encounters until it is either disrupted or ejected from the cluster. Although interactions with other binaries can cause some chaotic outcomes, it is typical to assume strong encounters with single BHs will result in the binary giving up about 20% of its energy, thus shrinking its semi-major axis. This tightening of the binary will continue with successive encounters until its separation reaches $a_{\rm ej}$ as defined in Eq 2.6 at which point the next single interaction will eject the binary from the cluster (Antonini & Rasio, 2016). However, when the cluster starts with a non-zero binary fraction, we can expect that there are many other BBHs (see Fig. 2.4) in the cluster which will complicate the simple picture above, since at any point along this chain of interactions, the target binary may interact with another binary. Strong binary-binary interactions will typically result in a greater change in the binding energy of one of the binaries, compared to a typical binary-single encounter. In addition to the increased effect of hardening, binary-binary interactions can also lead to exchanges of the binary components which results in essentially a new, dynamically formed, binary (Zevin et al., 2019).

Given our populations of BHs and BBHs formed solely from binary stellar evolution, we calculate the probability that a target binary interacts with at least one other binary before it can shrink its separation to $a_{\rm ej}$ (Eq 2.19). Here $P_{\rm int}$(All Singles) is the probability that the target binary receives only $N$ single interactions, where $N = \log\left(\frac{a_{\rm h}}{a_{\rm ej}}\right) / \log 1.2$ is the number of single interactions to reach $a_{\rm ej}$ from the initial separation $a_{\rm init}$

$$P_{\rm int}(\text{Binary}) = 1 - \text{P}_{\rm int}(\text{All Singles}) \ . \tag{2.19}$$

Using the interaction rates in Eq 2.17 we can define the probability for the next interaction to be with a single BH, given the current separation of the target binary

$$P_{\rm int}(\text{single}) = \frac{\Gamma_{\rm S}}{\Gamma_{\rm S} + \Gamma_{\rm B}} \ . \tag{2.20}$$

We then calculate this $P_{\rm int}$(single) $N$ times as the target binary's separation shrinks to $a_{\rm ej}$. The product of these probabilities then gives us the probability of only interacting with single BHs, $P_{\rm int}$(All Singles), which we put into Eq 2.19 to find the probability of at least one binary interaction. We perform this calculation for three distinct target binaries, all with $M_{\rm tot} = 44$ M$_\odot$, and separations as fractions of the hard/soft boundary, $0.01a_{\rm h}$, $0.1a_{\rm h}$ and $a_{\rm h}$. Fig. 2.12 takes the data from the $Z = 0.0001$ model and plots this probability for a range of cluster escape velocities, also taking the two possible assumptions about the cluster state, equipartition and equal velocity dispersion. We see that for low $v_{\rm esc}$ clusters the probability of encountering a binary before being ejected is $\approx 1$, while as the escape velocity increases this

probability drops off quite rapidly.

However, the probability of at least one binary encounter for a target binary initially at $a_{\rm h}$ remains almost certain up to a $v_{\rm esc} \simeq 10^3$ km s$^{-1}$. Calculating the number of single interactions required for a binary to shrink from $a_{\rm h}$ to $a_{\rm ej}$, we find that it takes $\sim 30$ encounters. Since $a_{\rm h}$ and $a_{\rm ej}$ both scale with $1/v_{\rm esc}^2$, this number of encounters is independent of the cluster. Thus, even at the highest escape velocities, it would still take 30 encounters to reach $a_{\rm ej}$ and so even if every interaction in that chain had a 90% chance of being with a single BH, the probability of all 30 being encounters involving a single BH is still only 4%.

When the cluster escape velocity increases, the target binary enters a regime with $a_{\rm ej} < a_{\rm GW}$, where $a_{\rm GW}$ is defined as the separation at which the GW radiation dominates the energy loss of the binary (Antonini & Rasio, 2016)

$$a_{\rm GW} = 0.05 \left(\frac{M_{\rm tot}}{20\ {\rm M}_\odot}\right)^{3/5} \left(\frac{q}{(1+q)^2}\right)^{1/5} \left(\frac{\sigma_{\rm rel}}{30\ {\rm km\ s^{-1}}}\right)^{1/5} \left(\frac{10^6\ {\rm M}_\odot\ {\rm pc}^{-3}}{\rho}\right)^{1/5} {\rm AU}\ . \quad (2.21)$$

Once in this regime, the number of single interactions that the binary experiences starts to decrease with increasing $v_{\rm esc}$. Since $a_{\rm GW}$ is only weakly dependent on cluster properties $\sigma_{\rm rel}$ and $\rho$ compared to the binary hard/soft boundary $a_{\rm h}$ rapidly approaches $a_{\rm GW}$ as $v_{\rm esc}$ increases. The BBH now needs to experience fewer single encounters before it eventually reaches $a_{\rm GW}$ and then merges before another interaction. Thus, the total probability that at least one of the interactions is with another binary decreases. We see this at the high $v_{\rm esc}$ regime of Fig. 2.12, with the probability of each target binary eventually decreasing. In Fig. 2.12 we have also calculated the probability that the next encounter would be with a binary if the target binary has a separation $a = \max(a_{\rm GW},\ a_{\rm ej})$.

# Chapter 3

# Formation and evolution of binary black holes in $N$-body simulations of star clusters with up to two million stars

Recent years have seen several important improvements in the modelling of massive star clusters. $N$-Body simulations are starting to push the number of particles above the $N = 10^5$ limit (Wang et al., 2015; Banerjee, 2022; Arca sedda et al., 2024) with the first million particle N-body simulation performed in Wang et al. (2016). A particular point of development moves $N$-body codes from complete particle-particle calculations to a hybrid particle-tree, particle-particle method which includes a regularisation scheme for the closest interactions (Iwasawa et al., 2015, 2017; Rantala et al., 2020, 2021, 2023). In this work, we use the highly efficient hybrid $N$-body code `PeTar` recently developed by Wang et al. (2020b). This code combines the particle-tree particle-particle method (Oshino et al., 2011) and the slow-down algorithmic regularisation method (SDAR Wang et al., 2020a) to efficiently simulate the evolution of star clusters, while Stellar evolution is modelled using the single and binary stellar evolution packages (`SSE` and `BSE` respectively; Hurley et al., 2000, 2002; Banerjee et al., 2020). This allows us to simulate clusters starting with masses and half-mass densities larger than has been previously explored and up to $10^6$ $M_\odot$ and $10^5$ $M_\odot$ $pc^{-3}$, respectively. This region of parameter space has thus far been sparsely sampled by previous work; some work started at slightly higher densities but at much smaller cluster mass (Rastello et al., 2021; Rizzuto et al., 2021; Arca Sedda et al., 2023c; Rantala et al., 2024). The wide range of initial conditions we consider in this work allows us to address two important questions: (i) what is the effect of dynamical encounters on the rate and properties of BBH mergers; and (ii) how these scale with the mass and density of the host cluster. More generally, we

test our theoretical understanding of BBH formation in dynamical environments using $N$-body simulations that take into account both gravitational interactions and stellar evolution processes and that contain a realistic initial population of stellar binaries.

## 3.1 Methods

To study the formation mechanisms of BBHs we run 34 $N$-body cluster models. We use the high-performance hybrid $N$-body code `PeTar` (Wang et al., 2020b), which combines the particle-tree particle-particle method ($P^3T$; Oshino et al., 2011) and the slow-down algorithmic regularisation method (`SDAR` Wang et al., 2020a) with parallisation via a hybrid parallel method based on the `FDPS` framework (Iwasawa et al., 2016, 2020; Namekata et al., 2018). In addition to OpenMP and MPI processes for parallisation, we chose a `PeTar` configuration which accelerates the long-range force calculation with Nvidea P100 GPUs. `PeTar` is computationally much more efficient than standard direct $N$-body codes (Wang et al., 2020b), allowing us to explore a broader parameter space of initial conditions than previous work and to include high binary fractions approaching 100% for massive stars.

A drawback of `PeTar` is that it does not directly include post-Newtonian (PN) terms in the equations of motion, unlike some other $N$-body codes (Aarseth, 2012). Mergers through GW radiation are modelled by computing the semi-major axis and eccentricity evolution described as in Peters (1964) (Eq 1.2)

To determine whether a binary merges, `PeTar` compares the GW timescale to the binary integration time-step. This time-step depends on strength of the perturbation from the binaries neighbours and the slowdown factor for the binary. The stronger the perturbation, the smaller this time-step becomes. When the GW timescale becomes shorter than the integration time-step, the binary is considered to have merged before the next time-step. Once these criteria are satisfied, the binary position is evolved in space until the time of merger, and as such we can find the actual position of a BBH merger in our clusters.

Within the simulation we include stellar evolution of the stars using the single and binary stellar evolution packages (`SSE` and `BSE` respectively; Hurley et al., 2000, 2002; Banerjee et al., 2020). Within `BSE`, compact objects can merge through GW emission. This is accounted for by computing the semi-major axis and eccentricity evolution using Eq 1.2.

We consider a binary as *ejected* from the cluster if the following two conditions are satisfied. Firstly, we impose a distance criterion $r_{\rm COM} > 20 r_{\rm h}$, where $r_{\rm COM}$ is the COM position of the binary and $r_{\rm h}$ is the cluster half-mass radius at any given time. Secondly, there is an energy criterion $K_{\rm COM} + \Omega_{\rm COM} > 0$, where $K_{\rm COM}$ and $\Omega_{\rm COM}$ are the kinetic energy and potential energy of the binary COM, respectively.

In this work we use `PeTar` to explore astrophysically motivated initial cluster

conditions in areas of the parameter space where there has been a lack of previous simulations.

### 3.1.1 Initial Conditions

We generate the cluster initial conditions using `McLuster`(Wang et al., 2019; Küpper et al., 2011). For every cluster we adopt a King density profile (King, 1966) with a concentration parameter $W_0 = 8$ and assume that the cluster is not in any larger galactic tidal field. This value of $W_0$ allows us to explore the dynamics within compact clusters. However, it is important to note that our results are sensitive on the choice of this parameter, since a large $W_0$ value models a cluster closer to core-collapse. This effectively sets the interaction timescale within the cluster core, where a large $W_0$ value describes a highly active core, and a lower value describes a dynamically quiet core. Although not the focus of this study, we also highlight that the choice of this parameter can significantly influence the formation of an intermediate mass BH (IMBH) (Rizzuto et al., 2021). Most models have an initial half-mass density $\rho_{\rm h} = 1.2 \times 10^3$ M$_\odot$ pc$^{-3}$ as this is a typical value found for globular clusters in the Galaxy (Harris, 2010). We also explore higher densities, $\rho_{\rm h} = 10^4$ M$_\odot$ pc$^{-3}$ and $\rho_{\rm h} = 10^5$ M$_\odot$ pc$^{-3}$, since clusters might have been much denser in the past, and vary the initial cluster mass from $10^4$ M$_\odot$ to $10^6$ M$_\odot$. We consider three values of metallicity: $Z = 0.01,\ 0.001$ and $0.0001$.

In order to characterise the effect of an initial binary population on the cluster evolution and BBH mergers, we consider clusters in which all BH stellar progenitors are initially in a binary – we refer to these initial binaries as primordial binaries. For most cluster models we consider two variations. One variation begins with no primordial binaries, whilst in the other we ensure that every star with initial mass $> 20$ M$_\odot$ is initialised in a binary. We opted against initialising lower mass binaries for three main reasons. Firstly, this work is focused on the effect of primordial binaries on the overall rate of BBH mergers and on the formation and evolution of BBHs, and these are unlikely to be affected by binaries with low mass components. Secondly, it has been suggested that once BHs have been formed in the cluster, the dynamical evolution of the cluster properties depends only on the number and properties of the massive binaries (Wang et al., 2021). Finally, the exclusion of lower mass binaries makes our simulations computational more efficient, reducing significantly the computing cost.

We sample the initial masses of the cluster stars from a Kroupa (2001) initial mass function between $M = 0.08$ M$_\odot$ and 150 M$_\odot$. Primordial binaries are then generated by taking every stellar mass $> 20$ M$_\odot$ and drawing from a uniform mass ratio ($q$) distribution $0.1 \leq q \leq 1$; the particle in the cluster with the closest mass to what was drawn is then chosen as the binary partner. The eccentricity for these binaries is then drawn from a Sana et al. (2012) distribution

$$f_{\rm e} = 0.55e^{-0.45} \ . \tag{3.1}$$

The binary period is set using the extended Sana et al. (2012) distribution described in Oh et al. (2015)

$$f_{\log_{10}(P)} = 0.23 \left[\log_{10}\left(\frac{P}{\rm days}\right)\right]^{-0.55} \ . \tag{3.2}$$

We also consider a single cluster variation where we set the binary period based on the Duquennoy & Mayor (1991) distribution. This allows us to determine whether our results are particularly sensitive to the choice of period distribution.

We draw the SN natal kicks from a Maxwellian distribution with $\sigma = 265$ km s$^{-1}$ (Hobbs et al., 2005) and assume a fallback kick prescription when scaling the kicks for BH formation (Fryer, 1999). In addition, we assume the rapid SN mechanism (Fryer et al., 2012) for CO formation, and strong PPI cut-off at 45 M$_\odot$ (Belczynski et al., 2020).

In Table 3.1 we summarise the initial conditions of all of our simulations. We also give the initial half-mass relaxation time for the cluster and the total physical time over which they are simulated. The half-mass relaxation time is given by (Spitzer & Hart, 1971)

$$t_{\rm rh} = \frac{0.138}{\langle m_{\rm all}\rangle \psi \log\Lambda}\sqrt{\frac{M_{\rm cl} r_{\rm h}^3}{G}} \ , \tag{3.3}$$

where $M_{\rm cl}$ and $r_{\rm h}$ are the initial cluster mass and half-mass radius respectively, $\langle m_{\rm all}\rangle$ is the average stellar mass within $r_{\rm h}$ computed from the starting conditions of each cluster simulation, $\log\Lambda$ is the Coulomb logarithm, and $\psi$ depends on the mass spectrum within the half mass radius which we set equal to 5 (e.g., Antonini et al., 2019). The final integration time of the simulations is chosen such that it is several times the initial relaxation time of the cluster. For the most massive clusters ($M_{\rm cl} = 5 \times 10^5$ M$_\odot$ and $10^6$ M$_\odot$), we make sure that the simulation runs for at least one initial relaxation time. This means that all cluster models have undergone significant dynamical evolution due to two-body relaxation by the end of the simulation.

We choose some naming scheme for our simulations based on the metallicity, mass and density of the initial cluster for ease of reference. From here on we refer to specific simulations based on this identifier and whether the model contains primordial binaries.

In Fig. 3.1 we present the initial cluster conditions ($\rho_{\rm h}$ and $M_{\rm cl}$) simulated in this study, compared to those produced in previous $N$-Body studies Banerjee (2020); Rastello et al. (2021); Di Carlo et al. (2021); Chattopadhyay et al. (2022); Arca Sedda et al. (2023c). The plot highlights that regions of high density and cluster

Table 3.1: Initial cluster conditions for our `PeTar` $N$-body simulations. Each model is given a unique name based on its initial setup (metallicity, initial cluster mass and density) with a -L added to models which are run for three Gyr instead of one Gyr. Each model contains two variations, one which starts with no binaries, and one which sets an initial binary fraction of 100% amongst massive stars (initial mass $\geq 20$ $M_\odot$). Finally, the * denotes a model with a Duquennoy & Mayor (1991) period distribution instead of the Sana et al. (2012) distribution used in all the other models.

| Model | Metallicity | Total Mass $M_\odot$ | Density $M_\odot$ pc$^{-3}$ | Half-Mass Relaxation Time Myr | Binary Fraction | End Time Myr | Binary Period Dist |
|---|---|---|---|---|---|---|---|
| Z1-M1-D3 | 0.01 | 10,000 | 1200 | 11.5 | 0<br>0.0025 | 1000 | Sana |
| Z1-M5-D3 | | 50,000 | 1200 | 47.0 | 0<br>0.0025 | 1000 | Sana |
| Z1-M10-D3 | | 100,000 | 1200 | 86.2 | 0<br>0.0026 | 1000 | Sana |
| Z1-M50-D3 | | 500,000 | 1200 | 253.7 | 0 | 608 | Sana |
| Z1-M100-D3 | | 1,000,000 | 1200 | 506.8 | 0 | 632 | Sana |
| Z2-M1-D3 | 0.001 | 10,000 | 1200 | 11.3 | 0<br>0.0025 | 1000 | Sana |
| Z2-M5-D3 | | 50,000 | 1200 | 49.4 | 0<br>0.0025 | 1000 | Sana |
| Z2-M5-D3-L | | 50,000 | 1200 | 49.4 | 0<br>0.0025 | 3000 | Sana |
| Z2-M10-D3 | | 100,000 | 1200 | 86.2 | 0<br>0.0026 | 1000 | Sana |
| Z2-M10-D3-L | | 100,000 | 1200 | 86.2 | 0<br>0.0026 | 3000 | Sana |
| Z2-M10-D3-L* | | 100,000 | 1200 | 86.2 | 0<br>0.0026 | 3000 | Duquennoy & Mayor |
| Z2-M10-D4 | | 100,000 | 10,000 | 24.4 | 0<br>0.0025 | 1000 | Sana |
| Z2-M1-D5 | | 10,000 | 100,000 | 0.561 | 0<br>0.0025 | 1000 | Sana |
| Z2-M5-D5 | | 50,000 | 100,000 | 2.78 | 0<br>0.0025 | 1000 | Sana |
| Z3-M1-D3 | 0.0001 | 10,000 | 1200 | 11.2 | 0<br>0.0025 | 1000 | Sana |
| Z3-M5-D3 | | 50,000 | 1200 | 47.7 | 0<br>0.0025 | 1000 | Sana |
| Z3-M10-D3 | | 100,000 | 1200 | 86.7 | 0<br>0.0025 | 1000 | Sana |
| Z3-M50-D3 | | 500,000 | 1200 | 253.7 | 0 | 568 | Sana |
| Z3-M100-D3 | | 1,000,000 | 1200 | 506.8 | 0 | 280 | Sana |

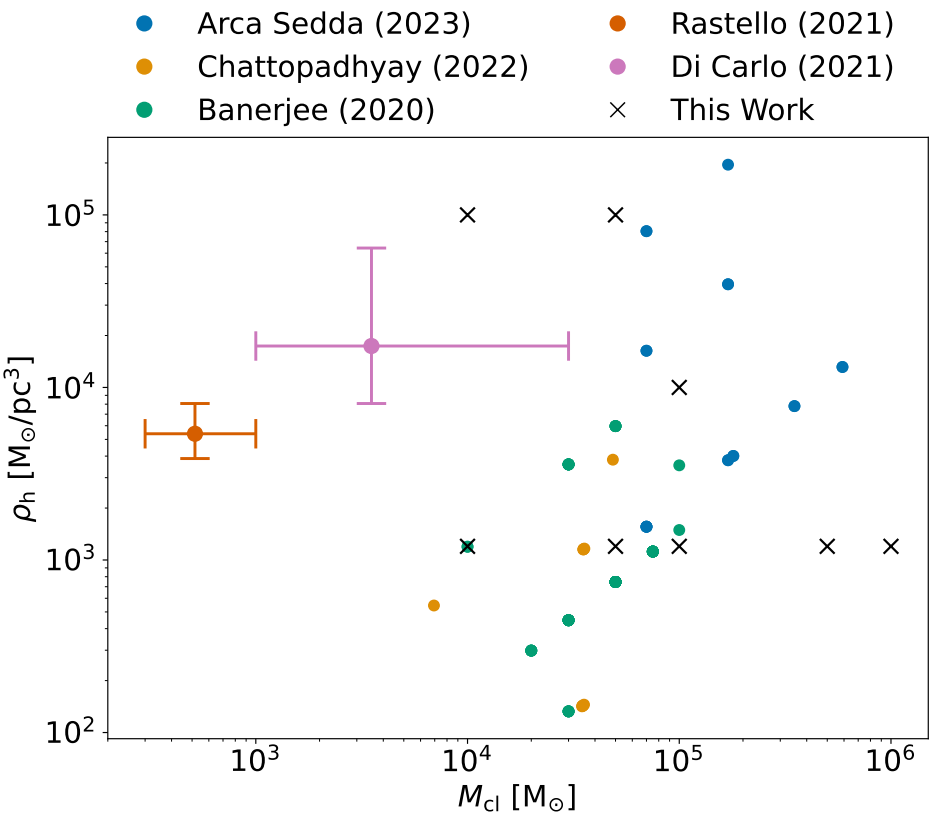


Figure 3.1: Comparison of the initial cluster properties ($\rho_h$ and $M_{cl}$) between the simulations in our work (black crosses) and previous studies; Arca Sedda et al. (2024) (blue dots), Chattopadhyay et al. (2022) (orange dots), Banerjee (2020) (green dots), Rastello et al. (2021) (red error bars) and Di Carlo et al. (2021) (pink error bars).

mass are relatively under-explored. Consequently, the work presented here provides a significant contribution to improving our understanding of these highly dynamic environments.

## 3.2 Binary black hole Formation and Merger

Through stellar evolution, the most massive stars become BHs within $\lesssim 5$ Myr whilst the smaller stars ($\sim 20$ M$_\odot$) collapse on a timescale $t \sim 15$ Myr, especially within metal rich environments. Once the BHs form inside the cluster they will either contribute to the single BH population or the BBH population[1]. BBHs are then either characterised as *hard* BBHs or *soft* BBHs depending on their binding energy compared to the average kinetic energy of stars in their immediate environment (Heggie, 1975). We define the hard/soft boundary as:

$$a_{\rm h} = \frac{G\mu}{\sigma^2} \ , \tag{3.4}$$

where $\mu$ is the reduced mass and $\sigma$ is the 1D velocity dispersion of the surrounding stellar objects, which is computed for each defined Lagrangian radii by `PeTar` in a data post-processing step. A binary with a separation $a < a_{\rm h}$ is considered a hard binary.

After all massive stars have collapsed to BHs, the number of single BHs and BBHs within a cluster will still evolve with time due to dynamical processes. New BBHs can be formed or disrupted through dynamical encounters, whilst existing BBHs may merge into a more massive BH. Dynamical encounters can also be responsible for ejecting both BHs and BBHs from a cluster (Morscher et al., 2015). In Fig. 3.2 we show the evolution of these two populations for cluster models Z3-M10-D3 (upper panels) and Z3-M5-D3 (lower panels), we then show cluster variations with and without primordial binaries on the left and right panels, respectively. In these plots we also show the subset of hard BBHs as well as the number of binaries containing only one BH (which we refer to as BH-Star binaries).

As expected, in all models we see the formation of the first BHs at $\approx 4$ Myr with a significant number of BBHs and BH-Star also forming at this time in models with a primordial binary population. In models without a primordial binary population, BBHs are formed through dynamical interactions in the cluster core. Three-body binary formation processes lead to the formation of the first BBHs in the cluster, which occurs approximately after a core-collapse time (Lee, 1995). After the first binary is formed, the number of BBHs within the cluster remains of $\mathcal{O}(1)$. A classical explanation for this is that once a BBH forms in the cluster core, it dominates the interactions, restricting further BBH formation and becoming a major energy source to the cluster (Heggie & Hut, 2003). However, recent work has suggested an

[1]For now, we ignore higher multiplicity systems i.e., triples, quadruples etc.

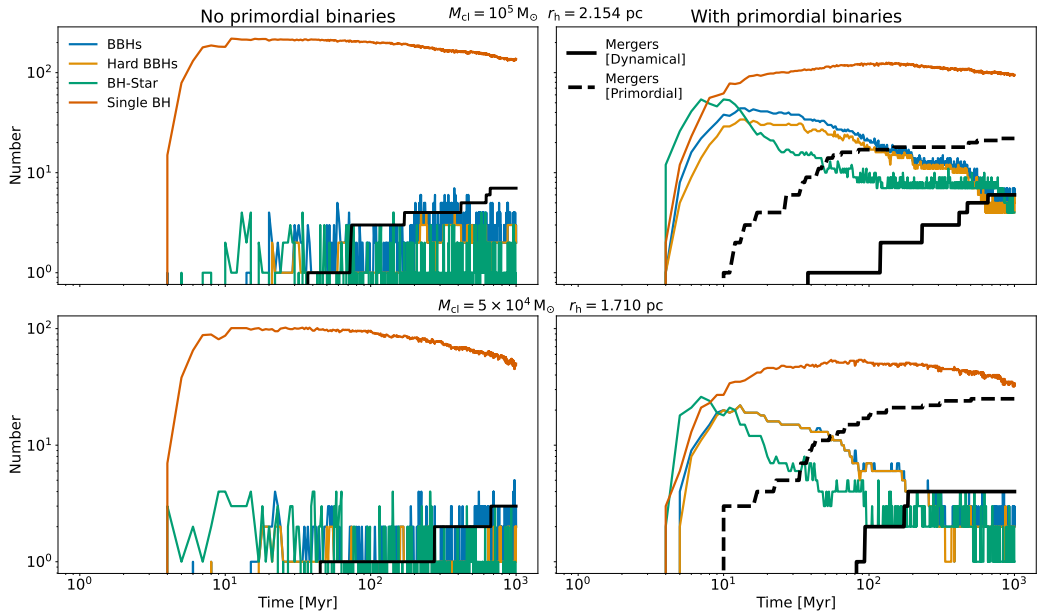


Figure 3.2: Number of BH and BBH population inside the cluster as a function of time. The BBH population is split into all BBHs, hard BBHs and binary systems containing only one BH. We over-plot the cumulative count of merging BBHs from the dynamically formed BBHs (solid line) and BBHs from the primordial binary population (dashed line). The upper panel shows Model Z3-M10-D3 while the bottom panel shows model Z3-M5-D3. We show both variations with (right) and without(left) a primordial binary population.

alternative explanation. When considering a high rate of binary-binary interactions in the core which efficiently ionise one of the binaries involved in the encounter (Marín Pina & Gieles, 2024) the long term formation of multiple binaries is limited.

Clusters with a primordial binary population (right panels of Fig. 3.2) form BBHs much earlier on. This is because primordial binaries with sufficiently massive components and that remain bound through stellar evolution, become BBHs after a time between 4 Myr to $\approx$ 10 Myr. At this time and in both cluster models, there are approximately as many BHs in BBHs as single BHs. It is expected that when a cluster contains a large number of BBHs, interactions between binaries can become the dominant form of encounters (see Chapter 2). These encounters are often chaotic with numerous potential end-states (Zevin et al., 2019), including being a mechanism for stable triple BH formation (Sigurdsson & Phinney, 1993), as discussed further in Section 3.2.1. But importantly, they often lead to the disruption or ejection of binaries, thus reducing the number of BBHs in the cluster. This is what we see in our models, to the extent that at the end of the simulation the number of BBHs is largely independent of whether the cluster originally had a primordial binary population. Table 3.2 summarises the end state for every cluster simulation we run, giving the final number of single BHs, BH-Star binaries and BBHs.

Fig. 3.2 also shows that in each simulation the hard BBHs represent a significant

Table 3.2: Here we show the end state information from our simulations. The first two columns denote the cluster model name (defined in Table 3.1) and whether this cluster is initialised with a primordial binary fraction. Columns 3 and 4 denote the number of BHs and BBHs within the cluster at the end of the simulation time, with the BBH column further split into the total number of BBHs, the number of hard BBHs and the number of binary systems with only one BH. Columns 5, 6 and 7 describe the merging BBHs coming from the primordial binaries, dynamically formed binaries and the combined total respectively. Each of these groups is further split into the total number for that group, the number of in-cluster mergers and the number of ejected mergers. The final column shows the total merger efficiency for each cluster.

| Model | | $N_{\rm sing}$ | $N_{\rm BHBs}$ Tot(Hard)Star | Primordial Mergers Tot(Incl)Ejec | Dynamical Mergers Tot(Incl)Ejec | Total Mergers Tot(Incl)Ejec | Merger Efficiency |
|---|---|---|---|---|---|---|---|
| Z1-M1-D3 | With Binaries | 4 | 1(1)0 | 2(0)2 | 0(0)0 | 2(0)2 | $2.0 \times 10^{-4}$ |
| | No Binaries | 0 | 1(1)0 | - | 2(2)0 | 2(2)0 | $2.0 \times 10^{-4}$ |
| Z1-M5-D3 | With Binaries | 23 | 1(1)2 | 4(0)4 | 0(0)0 | 4(0)4 | $8.0 \times 10^{-5}$ |
| | No Binaries | 28 | 1(1)1 | - | 3(2)1 | 3(2)1 | $6.0 \times 10^{-5}$ |
| Z1-M10-D3 | With Binaries | 50 | 1(1)7 | 14(6)8 | 4(3)1 | 18(9)9 | $1.8 \times 10^{-4}$ |
| | No Binaries | 95 | 2(1)2 | - | 7(6)1 | 7(6)1 | $7.0 \times 10^{-5}$ |
| Z1-M50-D3 | No Binaries | 404 | 1(1)4 | - | 3(3)0 | 3(3)0 | $6.0 \times 10^{-6}$ |
| Z1-M100-D3 | No Binaries | 780 | 0(0)3 | - | 0(0)0 | 0(0)0 | - |
| Z2-M1-D3 | With Binaries | 3 | 3(3)1 | 2(1)1 | 1(0)1 | 3(1)2 | $3.0 \times 10^{-4}$ |
| | No Binaries | 3 | 1(1)0 | - | 1(1)0 | 1(1)0 | $1.0 \times 10^{-4}$ |
| Z2-M5-D3 | With Binaries | 29 | 1(1)3 | 11(5)6 | 4(4)0 | 15(9)6 | $3.0 \times 10^{-4}$ |
| | No Binaries | 50 | 3(2)0 | - | 1(1)0 | 1(1)0 | $2.0 \times 10^{-5}$ |
| Z2-M10-D3 | With Binaries | 70 | 1(1)4 | 30(10)20 | 5(4)1 | 35(14)21 | $3.5 \times 10^{-4}$ |
| | No Binaries | 108 | 2(1)2 | - | 8(8)0 | 8(8)0 | $8.0 \times 10^{-5}$ |
| Z2-M5-D3-L | With Binaries | 5 | 2(2)4 | 8(5)3 | 6(6)0 | 14(11)3 | $2.8 \times 10^{-4}$ |
| | No Binaries | 28 | 2(2)0 | - | 4(3)1 | 4(3)1 | $8.0 \times 10^{-5}$ |
| Z2-M10-D3-L | With Binaries | 32 | 4(3)2 | 5(1)4 | 4(4)0 | 9(5)4 | $9.0 \times 10^{-5}$ |
| | No Binaries | 72 | 2(2)3 | - | 3(3)0 | 3(3)0 | $3.0 \times 10^{-5}$ |
| Z2-M10-D3-L* | With Binaries | 84 | 10(9)3 | 12(4)8 | 4(3)1 | 16(7)9 | $1.6 \times 10^{-4}$ |
| | No Binaries | 157 | 1(0)0 | - | 4(4)0 | 4(4)0 | $4.0 \times 10^{-5}$ |
| Z2-M10-D4 | With Binaries | 29 | 2(2)3 | 27(12)15 | 9(8)1 | 36(20)16 | $3.0 \times 10^{-4}$ |
| | No Binaries | 82 | 1(1)2 | - | 10(9)1 | 10(9)1 | $1.0 \times 10^{-4}$ |
| Z2-M1-D5 | With Binaries | 0 | 0(0)1 | 3(0)3 | 2(2)0 | 5(2)3 | $5.0 \times 10^{-4}$ |
| | No Binaries | 0 | 1(1)0 | - | 2(2)0 | 2(2)0 | $2.0 \times 10^{-4}$ |
| Z2-M5-D5 | With Binaries | 2 | 0(0)0 | 16(7)9 | 4(4)0 | 20(11)9 | $4.0 \times 10^{-4}$ |
| | No Binaries | 6 | 1(1)3 | - | 4(3)1 | 4(3)1 | $6.0 \times 10^{-5}$ |
| Z3-M1-D3 | With Binaries | 2 | 0(0)1 | 6(3)3 | 1(1)0 | 7(4)3 | $7.0 \times 10^{-4}$ |
| | No Binaries | 0 | 1(1)0 | - | 1(1)0 | 1(1)0 | $1.0 \times 10^{-4}$ |
| Z3-M5-D3 | With Binaries | 34 | 2(2)1 | 18(9)9 | 4(3)1 | 22(12)10 | $4.4 \times 10^{-4}$ |
| | No Binaries | 50 | 2(2)0 | - | 3(3)0 | 3(3)0 | $6.0 \times 10^{-5}$ |
| Z3-M10-D3 | With Binaries | 95 | 6(5)4 | 28(13)15 | 6(5)1 | 34(18)16 | $3.4 \times 10^{-4}$ |
| | No Binaries | 137 | 2(2)0 | - | 7(7)0 | 7(7)0 | $7.0 \times 10^{-5}$ |
| Z3-M50-D3 | No Binaries | 777 | 3(1)5 | - | 6(5)1 | 6(5)1 | $1.2 \times 10^{-5}$ |
| Z3-M100-D3 | No Binaries | 1641 | 0(0)0 | - | 0(0)0 | 0(0)0 | - |

subset of the overall BBH population. For clusters with a primordial binary population, this is a result of both stellar and dynamical processes. Firstly, primordial stellar binaries that form with relatively close separations are likely to undergo further stellar interactions, causing their orbits to shrink. This process ultimately leads to the formation of BBHs with high binding energies. Secondly, these interactions also disrupt the soft BBHs over time, which explains why the relative fraction of hard BBHs increases with time and why near the end of the simulations almost all BBHs in the cluster are hard (see Table 3.2). For clusters without primordial binaries, BBHs can only form through dynamical encounters involving more than two BHs. Fig. 3.2 and Table 3.2 show the evolution and final counts of BH-Star binaries, which whilst are not the focus of this chapter, they can be of interest for studies into quiescent BHs, especially in light of the recent Gaia Collaboration et al. (2024) BH observations (we study this population in detail in Chapter 4).

In Fig. 3.2 we also display the cumulative number of BBH mergers produced from each cluster simulation. We distinguish between two populations to which we will often refer to through the reset of the article: (1) BBH mergers in which the BH components formed from stars that were originally part of the same binary system; and (2) BBHs that paired through dynamical encounters. This distinction helps illustrate the different pathways through which BBH mergers can occur within the star cluster models. Interestingly, we see that the presence of primordial binaries has a negligible effect on the total number of mergers amongst the dynamically formed population (see also Table 3.2). Moreover, it has little effect on the time when the first and subsequent mergers amongst the dynamically formed population happen.

With Fig. 3.3 we show both variations of models Z3-M10-D3 (upper panels) and Z1-M10-D3 (lower panels). Here we plot the radial position of every BBH in the simulations, distinguishing between dynamically formed BBHs and those from the primordial population. For the ejected BBH population we extend their tracks using equation (1.2) either up to a Hubble time ($t_{\rm H}$) or until they reach coalescence. This allows us to include BBH mergers amongst the ejected population that occur after the end of the $N$-body simulation but within $t_{\rm H}$.

Considering the evolution of primordial BBHs, we see that in both models there are many BBHs which are ejected from the cluster shortly after being formed. Of these BBHs almost all of them go on to merge within $t_{\rm H}$. As discussed previously, dynamical encounters are a key mechanism for ejection of BHs and BBHs from a cluster; however, we find that these BBHs are ejected by the natal kick on one of the binary components. This early ejection from the cluster by a stellar evolution mechanism, provides a subpopulation of merging BBHs that likely show negligible effect from dynamics. Later in the lifetime of the cluster, we also find ejections of primordial BBHs, some of which also merge. These later ejections are due to dynamical encounters in the cluster.

As can be seen in Table 3.2, the primordial binary mergers are split roughly

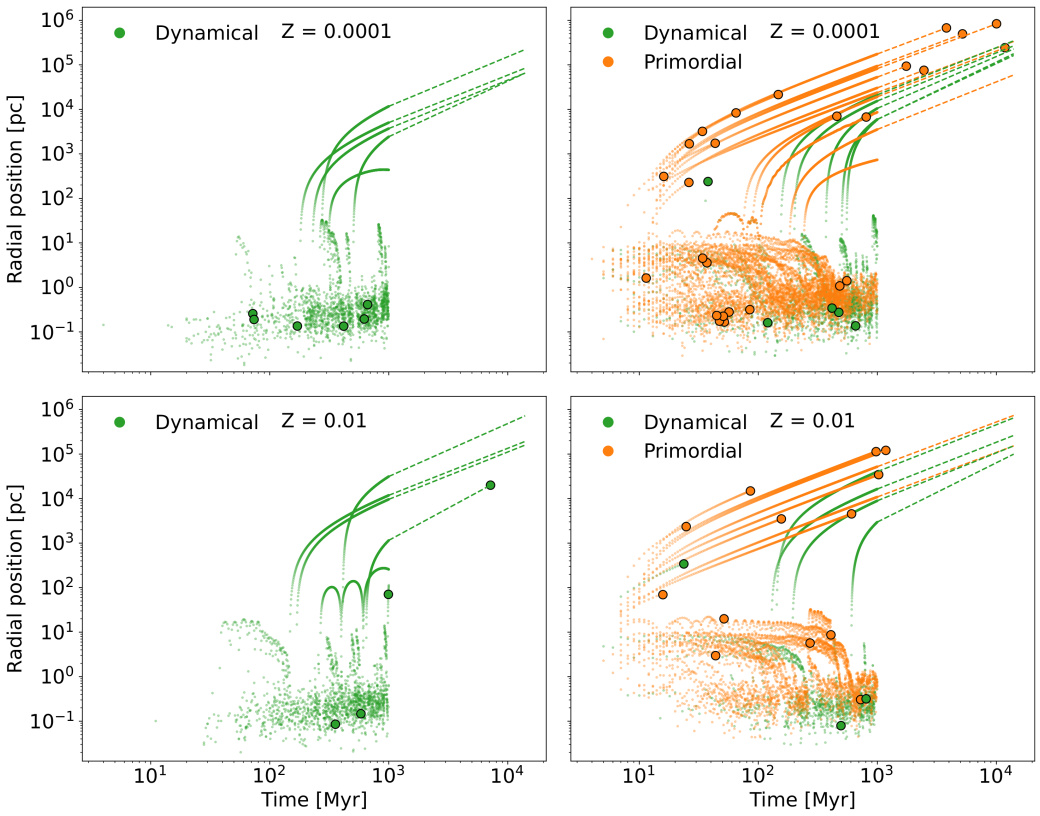


Figure 3.3: The evolution of the radial position of every BBH in the simulation. The top panels show model Z3-M10-D3 and the bottom panels show model Z1-M10-D3, whilst the columns, right/left, show the cluster variation with/without a primordial binary population. Here we distinguish between the dynamically formed BBHs and those from the primordial binary population and highlight the time when the BBH mergers occur (filled circles). For the ejected population, we compute their delay time and plot the future path up to merger or up to $t_{\rm H}$.

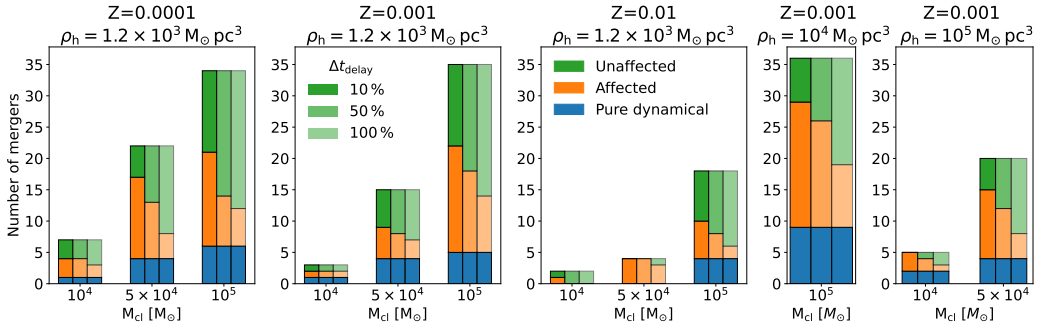


Figure 3.4: The number of mergers in our cluster models, split between the dynamical population and the primordial population. The primordial population is further split into "*affected*" and "*unaffected*" binaries according to the fractional change in delay time from a purely isolated evolution. We show these counts for three cut-off fractional change values in the delay time: 10%, 50% and 100%.

evenly between in-cluster mergers and ejected mergers in all models. In contrast, most dynamically formed BBHs merge inside the cluster. Moreover, we find that primordial BBHs are always the dominant source of mergers. We further discuss in-cluster and ejected mergers later in Section 3.3. In addition, we find that the Solar metallicity models produce fewer mergers in both the primordial and dynamical populations, overall, and in particular fewer incluster mergers, compared to sub-Solar models. This difference likely arises from the larger natal kicks at Solar metallicities (see Chapter 2). Stronger kicks eject more BHs and BBHs from the cluster and also tend to widen the orbits of surviving primordial binaries (see Fig 2.1), reducing the number that can merge within a Hubble time.

### 3.2.1 Effect of dynamics on the number of BBH mergers

We have shown that roughly half of the mergers amongst the primordial BBH population come from BBHs ejected by natal kicks shortly after formation, and thus likely contain no imprint from the dynamics of the cluster. On the other hand, the remaining BBH mergers that are produced by binaries that remain bound to the cluster after the SN kicks can show some imprint of the dynamical environment in which they evolved. To investigate the extent to which the cluster has affected the population of primordial BBH mergers, we take the primordial binaries in each cluster and evolve them using the stand-alone `BSE` code. The binary populations are simulated until merger and then the merger times are compared against the same specific binary in the cluster simulations.

Since the stellar evolution prescriptions are chosen identically to the corresponding full cluster simulation, any difference in the merger time for a specific binary can be attributed to the dynamics of the cluster altering the binary parameters. However, we do not account for the randomness of the drawn natal kick magnitude and

direction in our comparison and thus our results represent an upper estimate for the number of BBHs that are affected by dynamics.

When comparing the merger time for a specific binary, we define the fractional difference in merger time:

$$\Delta t_{\rm delay} = \frac{|t_{\rm d,isol} - t_{\rm d,cluster}|}{t_{\rm d,isol}} \ , \tag{3.5}$$

where $t_{\rm d,isol}$ is the merger time from the isolated binary simulation and $t_{\rm d,cluster}$ is the merger time in the cluster simulation. Note that here we are taking the absolute value of the difference since the dynamics of the cluster can either aid the merger of the binary or hinder it. We then make a choice for the boundary value of the fractional difference; if the computed fractional difference for a given BBH is larger than the cut-off value, we categorise the BBH as *affected* by the cluster. We choose three cut-off values, 10%, 50% and 100% – a 100% difference occurs when the inclusion in a cluster environment has changed a BBHs delay time by a factor of 2.

Fig. 3.4 shows the results of this comparison for a selection of our models across varying initial cluster mass, density and metallicity. We find that $\lesssim 20\%$ (for 100% change in delay time) of the primordial BBH mergers are characterised as affected by dynamics. Based on our theoretical understanding of BBH dynamics in clusters (Breen & Heggie, 2013; Rodriguez et al., 2018a), we would expect that as the mass and density of the cluster are increased the effect of dynamical encounters will become more important. On the contrary, our results appear to be mostly independent of cluster mass, density and metallicity, in the sense that the fraction of BBH mergers that have been significantly affected by dynamics remains similar across all models. For $M_{\rm cl} = 10^5$ M$_\odot$ and $Z = 0.001$, the fraction of mergers amongst the primordial binary population that have been significantly affected by dynamics (100% variation in delay time) is 0.2 for $\rho_{\rm h} = 1.2 \times 10^3$ M$_\odot$ pc$^{-3}$ and 0.15 for $\rho_{\rm h} = 10^5$ M$_\odot$ pc$^{-3}$. For $\rho_{\rm h} = 1.2 \times 10^3$ M$_\odot$ pc$^{-3}$ and $Z = 0.0001$, the fraction of affected mergers is 0.3 for $M_{\rm cl} = 10^4$ M$_\odot$ and 0.14 for $M_{\rm cl} = 10^5$ M$_\odot$. However, if we consider only a 10% variation in delay time; we find that the majority of BBHs in high density clusters ($\rho_{\rm h} = 10^4$ M$_\odot$ pc$^{-3}$ and $\rho_{\rm h} = 10^5$ M$_\odot$ pc$^{-3}$) are characterised as affected, compared with far fewer (typically around half) in lower density clusters. This suggests more dynamic activity in regard to weaker interactions in the high density clusters which produce only a small change in the properties of the primordial BBHs.

We have seen that our clusters contain a population of primordial BBHs which are ejected early on due to the large component natal kicks. Since these kicks are drawn randomly in both the stand-alone `BSE` code and `PeTar`, they could be the cause of the *affected* binaries we find in Fig. 3.4. We investigate this possibility by performing the same analysis, excluding this group of escaped BBHs. If the kicks were the most important factor, we should expect the fraction of affected binaries to decrease significantly in this new analysis, since the ejected population are the

binaries that receive the largest kicks. We find that there is effectively no difference in the fraction of affected mergers from the primordial binary population. Comparing to the values stated above: for $M_{\rm cl} = 10^5$ M$_\odot$ and $Z = 0.001$ we find the fraction of affected mergers is 0.38 at $\rho_{\rm h} = 1.2 \times 10^3$ M$_\odot$ pc$^{-3}$ and 0 at $\rho_{\rm h} = 10^5$ M$_\odot$ pc$^{-3}$. For $\rho_{\rm h} = 1.2 \times 10^3$ M$_\odot$ pc$^{-3}$ and $Z = 0.0001$, the fraction of affected mergers is 0.4 for $M_{\rm cl} = 10^4$ M$_\odot$ and 0.15 for $M_{\rm cl} = 10^5$ M$_\odot$. The small changes in the fraction of affected binaries compared to our former analysis (Fig. 3.4) likely implies that the larger effect on the binary properties is due to dynamical encounters.

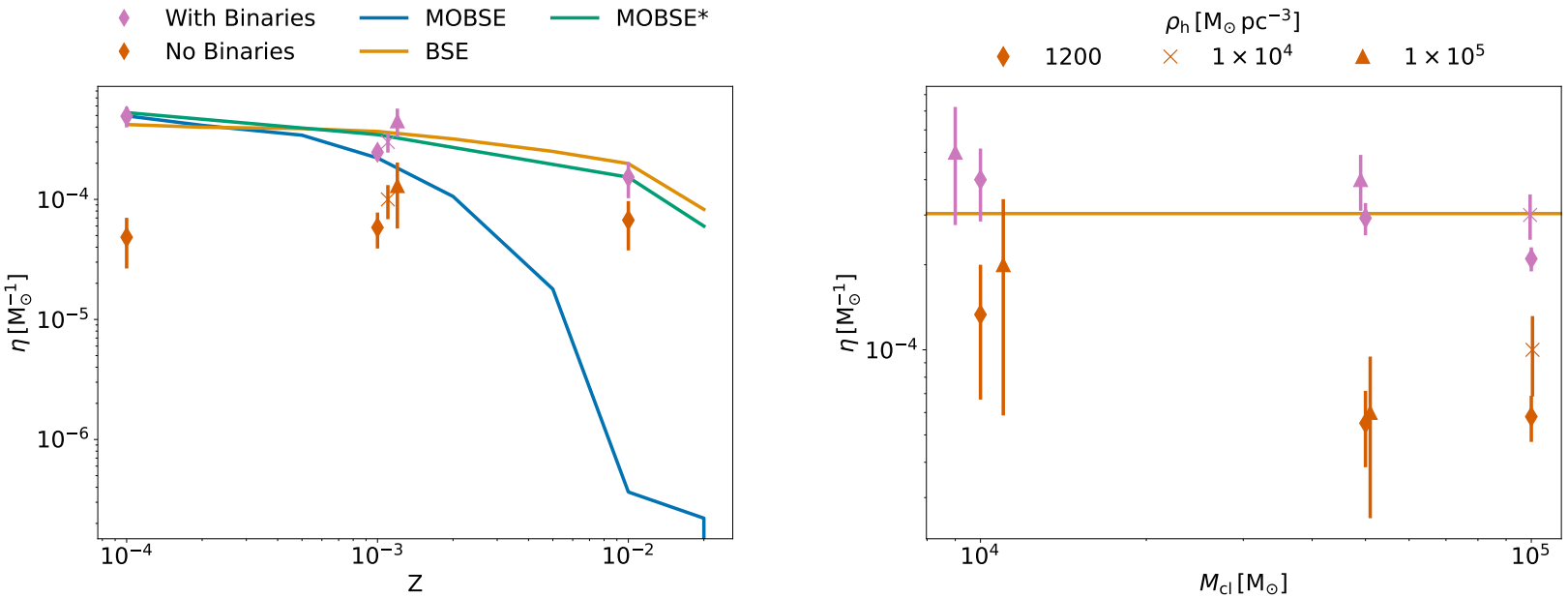


Figure 3.5: The merger efficiency as a function of metallicity (left panel) and initial cluster mass (right panel). We distinguish between the clusters with a primordial population and without by purple and orange markers respectively, whilst the initial cluster density is shown by marker type. We also over plot the merger efficiency from the stellar evolution codes `BSE` and `MOBSE` shown by orange and blue lines. Furthermore, we found a large discrepancy between these two codes at high metallicity owing to the treatment of HG stars during CE evolution. We show that resolving this discrepancy gives an adjusted `MOBSE`* relationship in green which is more consistent with the `BSE` results.

To determine the dependence of the number of BBH mergers on the cluster properties and how this number is affected by dynamical encounters, we compute the cluster merger efficiency ($\eta$).

$$\eta = \frac{N_{\rm merge}}{M_{\rm cl}} \ , \tag{3.6}$$

where $N_{\rm merge}$ is the number of mergers in the cluster. To compare against the expected efficiency from the isolated channel, we also simulate a population of binaries using two different binary evolution codes, `BSE` and `MOBSE` (Giacobbo et al., 2018; Giacobbo & Mapelli, 2018). The initial binary populations in these latter models were the same as the initial binaries in the cluster simulations. The left (right) panel of Fig. 3.5 shows $\eta$ as a function of metallicity (cluster mass), where we differentiate between clusters with primordial binaries and those without. We see that the merger efficiency of clusters with a primordial binary population broadly follows the same relationship as the same population simulated in isolation using `BSE`. We conclude that in our models, dynamical encounters have a small effect on the BBH merger rate.

In the left panel of Fig. 3.5 we see that the results obtained with `MOBSE` show a large disagreement with both the isolated `BSE` results and the cluster simulation results. This discrepancy is due to the treatment of Hertzsprung gap (HG) stars during a CE evolution phase. `BSE` allows for the possibility of binary survival when the CE is initiated by a star crossing the HG. In the standard version of `MOBSE`, instead, when a HG star enters a CE phase as a donor star, it is assumed that the stars merge. This assumption leads to a small number of systems surviving a CE phase at high metallicity – the rapid expansion of metal-rich stars in the HG that initiate a CE leads to stellar mergers due to the absence of a well-developed core-envelope structure.

In contrast, metal-poor stars remain relatively compact in the HG but expand more significantly in the subsequent stellar evolution phases. These facts fully explain the large difference in the merger efficiency obtained with `BSE` and `MOBSE` at $z > 0.001$. To further illustrate this, we evolve the same binary population with `MOBSE`, but now allowing the binaries to survive a CE phase that occurs during the HG (indicated as `MOBSE`$^*$ in Fig. 3.5). As expected, these new simulations recover a similar merger efficiency as found with `BSE` and the cluster models. Finally, in Fig. 3.5 we compare the merger efficiency between cluster models with and without primordial binaries and find that the former always show a high merger efficiency. The merging efficiency for each cluster simulation is summarised in Table 3.2.

The results discussed in this section and illustrated in Fig. 3.4 and Fig. 3.5 lead to the following conclusions: (i) most BBH mergers found in our models with a primordial binary population are not assembled dynamically, although a significant fraction of them are still affected by dynamical encounters (see Fig. 3.4); (ii) the

merger efficiency of our cluster models with an initial binary population is not significantly increased by dynamical encounters. This can be seen in Fig. 3.5 by comparing the value of $\eta$ for the isolated binary models and the cluster models; and (iii) the role of dynamical encounters in enhancing the merger rate of BBHs depends on the stellar evolution prescriptions used. Specifically, if stars are allowed to merge during a CE phase occurring when the donor is on the HG, dynamically assembled BBHs will dominate for $Z > 0.001$, while they remain a subdominant population at lower metallicities.

#### 3.2.1.1 Higher multiplicity systems

As previously shown, a fraction of the primordial BBH mergers are affected by the dynamics, and almost all dynamical BBH mergers occur in-cluster. Thus, it is reasonable to assume that at least some of these merging systems may participate to even higher multiplicity interactions involving triples, quadruples etc. We investigate this and find that $\lesssim 10\%$ of all primordial BBHs mergers occur in a triple BH system, with the rest occurring in binaries. On the other hand, the dynamically formed BBH mergers showed roughly equal numbers of mergers as a part of a stable triple and as a binary. We also find a small fraction of dynamical BBHs merging whilst part of a quadruple BH system. No higher multiplicity systems were found to contain merging BBHs.

Fig. 3.6 shows the fraction of merging BBHs that are found in each type of system, and we have further split up the dynamical BBH mergers in those from clusters with a primordial binary population and those without. We see that in clusters without primordial binaries the dynamical BBH mergers occur slightly more frequently within stable triple systems than in binaries.

The orbital properties of the stable triple systems that are formed dynamically in our models are shown in Fig. 3.7. These are obtained from the last $N$-body snapshot in which the binary was still present in the simulation. At this time, the exact merger time due to GW energy loss varied slightly between binaries, but it was always $\lesssim 1$ Myr. We consider the distribution of $M_3/\max(M_1, M_1)$, where $M_1$ and $M_2$ are the masses of the inner binary, and $M_3$ is the mass of the tertiary object on an outer orbit with semi-major axis $a_{\rm out}$ and eccentricity $e_{\rm out}$. The relative inclination between the inner and outer binary orbits is indicated as $i$. The analysis shown in Fig. 3.7 helps to understand whether the presence of a tertiary BH can affect the inner BBH evolution – lighter and more distant tertiary companions will have a smaller effect on the evolution of the binary. Interestingly, from the top panel of Fig. 3.7 we see that the most massive object of the triple is in most cases one of the binary components. We also find that both inner and outer orbits often have a significant eccentricity. The relatively small values of the ratio $a_{\rm out}/a_{\rm in} \lesssim 10^3$ indicate that at least in some cases we might expect the tertiary to have an effect on

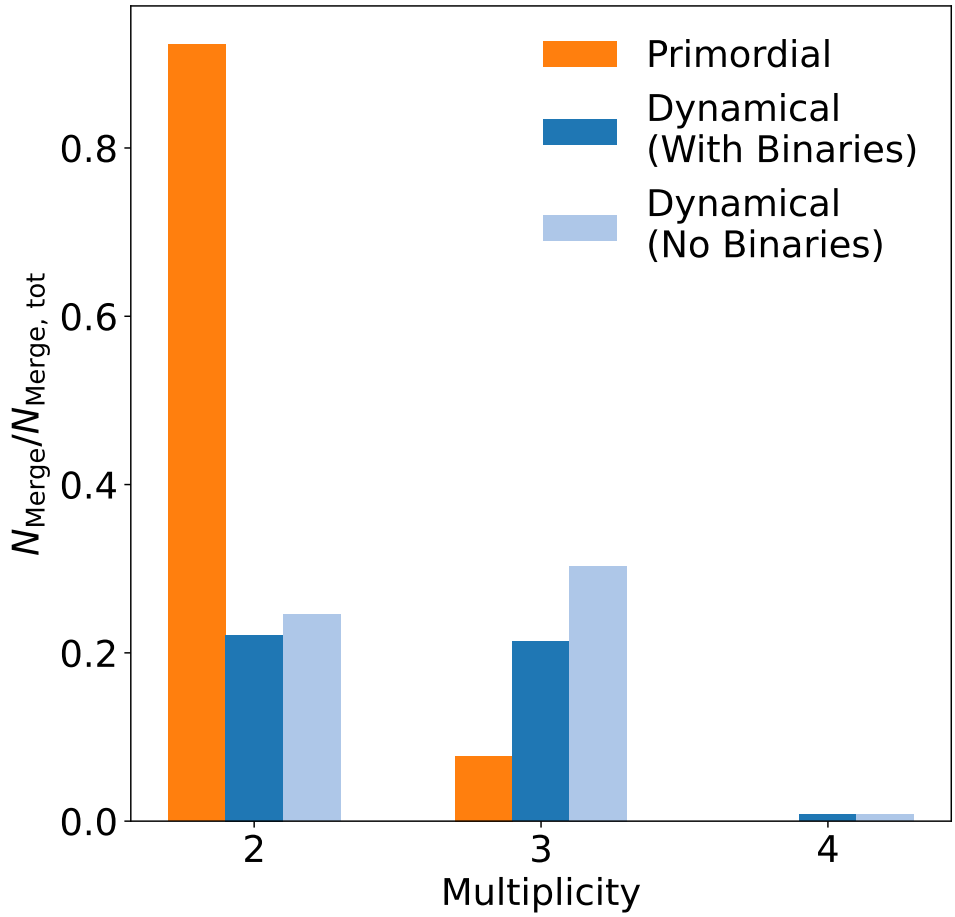


Figure 3.6: Fraction of mergers that are found in stable triples and quadruples just before merger. We distinguish between mergers from the primordial binary population and the dynamically formed population, as well as further splitting the dynamically formed binaries based on whether the cluster contained a primordial binary population. Higher multiplicity systems were searched also, however no mergers were found within them.

the evolution of the binary. However, we note that in order to address the impact on the BBH evolution, one should consider a more detailed analysis, taking into account relativistic effects acting on the inner binary orbit (e.g., Ford et al., 2000; Blaes et al., 2002).

### 3.2.2 Effect of dynamics on the properties of BBH mergers

We have shown in the previous sections that a significant fraction of primordial BBHs can be affected by dynamical encounters in the cluster, and that despite this the number of mergers is consistent with the same binaries evolving in isolation. However, it is likely that the binary orbital parameters of this affected population differ compared to the unaffected BBHs. To investigate this, we compute the distributions of component masses, mass ratio, merger time and eccentricity. We split up the mergers in dynamically formed BBHs, primordial BBHs that are affected by the cluster (where we take affected BBHs as those with $\Delta t_{\rm delay} \leq 50\%$) and primordial BBHs unaffected by the cluster. These distributions are plotted in Fig. 3.8.

For each parameter we take the affected and unaffected population and perform an Anderson-Darling (AD) k-sample test (Scholz & Stephens, 1987) to test whether the samples from the two populations are drawn from the same distribution. We opt for the AD test since this gives more weight to the tails of the distribution compared to other tests (such as the Kolmogorov-Smirnov test). The p-value from this test is shown on each of the distribution plots. Our results show that at the 95% level, the unaffected and affected population are sampled from different distributions for every parameter. Further, the secondary mass and eccentricity samples for the two populations are sufficiently different at the 99% level.

The bottom panel in Fig. 3.8 shows the eccentricity measured at the moment the binary decouples from the cluster dynamics, which is determined as described in Section 3.1. The distribution shows that the affected BBHs are typically more eccentric than the unaffected BBHs. This is likely due to dynamical encounters within the cluster. It is typically assumed that on average eccentricity induced through single-binary encounters should follow a thermal distribution (shown by the black line in the plot) (Heggie, 1975). However, we see that the affected BBH population does not follow this relation. A reasonable explanation for this is that dynamical encounters did not have enough time to fully thermalise the distribution before GW energy loss leads to orbital circularisation. However, the effect of encounters is still significant enough that the eccentricity distribution of the affected population can be distinguished from the unaffected one. As a caveat to this analysis, we stress that these differences might at least partly explained by the different natal kick magnitude and direction that are drawn randomly from the assumed distributions. However, following the analysis in Section 3.2.1 this is unlikely.

We now focus on the dynamical BBH population and their orbital parameters.

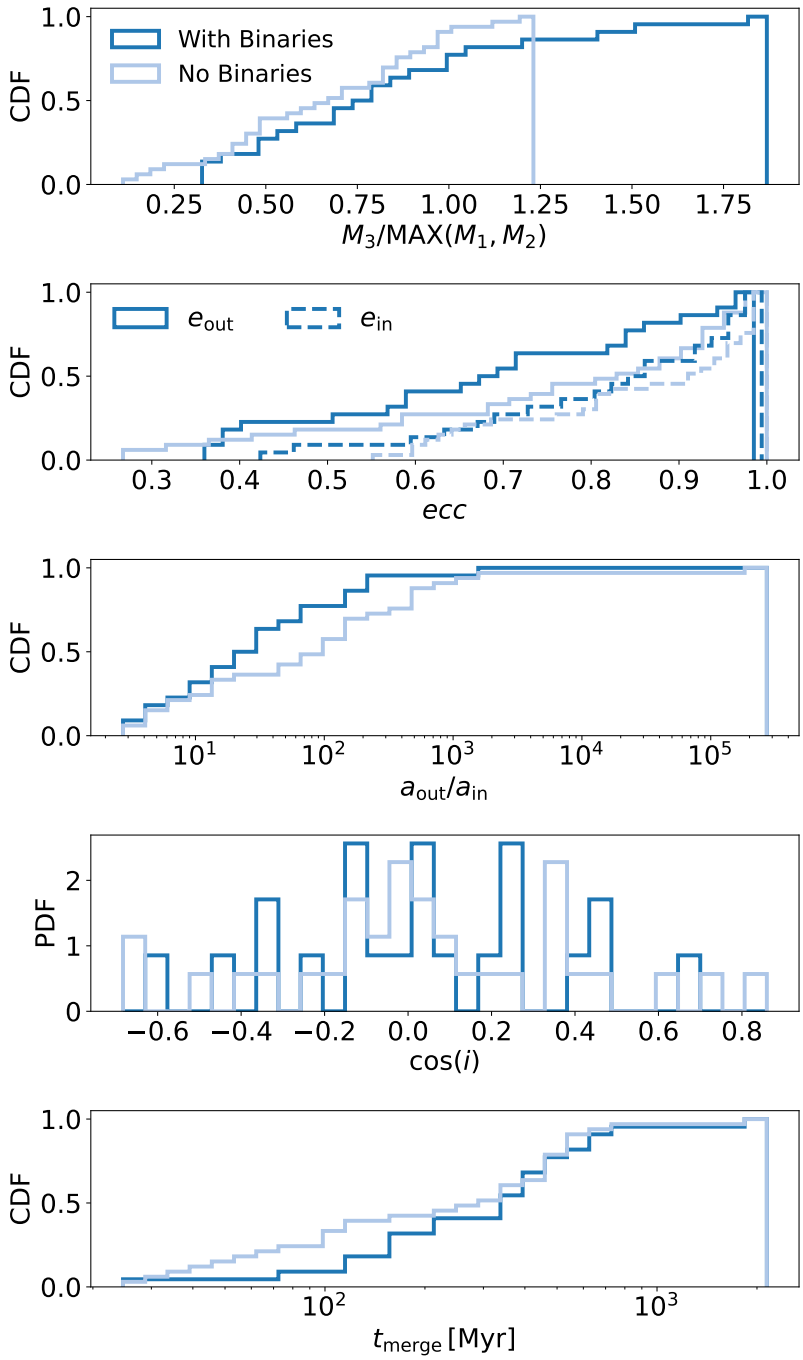


Figure 3.7: The orbital distributions for the stable triple systems that contain a dynamically formed BBH which merges within $t_H$. We split the dynamically formed BBHs into the population coming from clusters with a primordial binary population and those without.

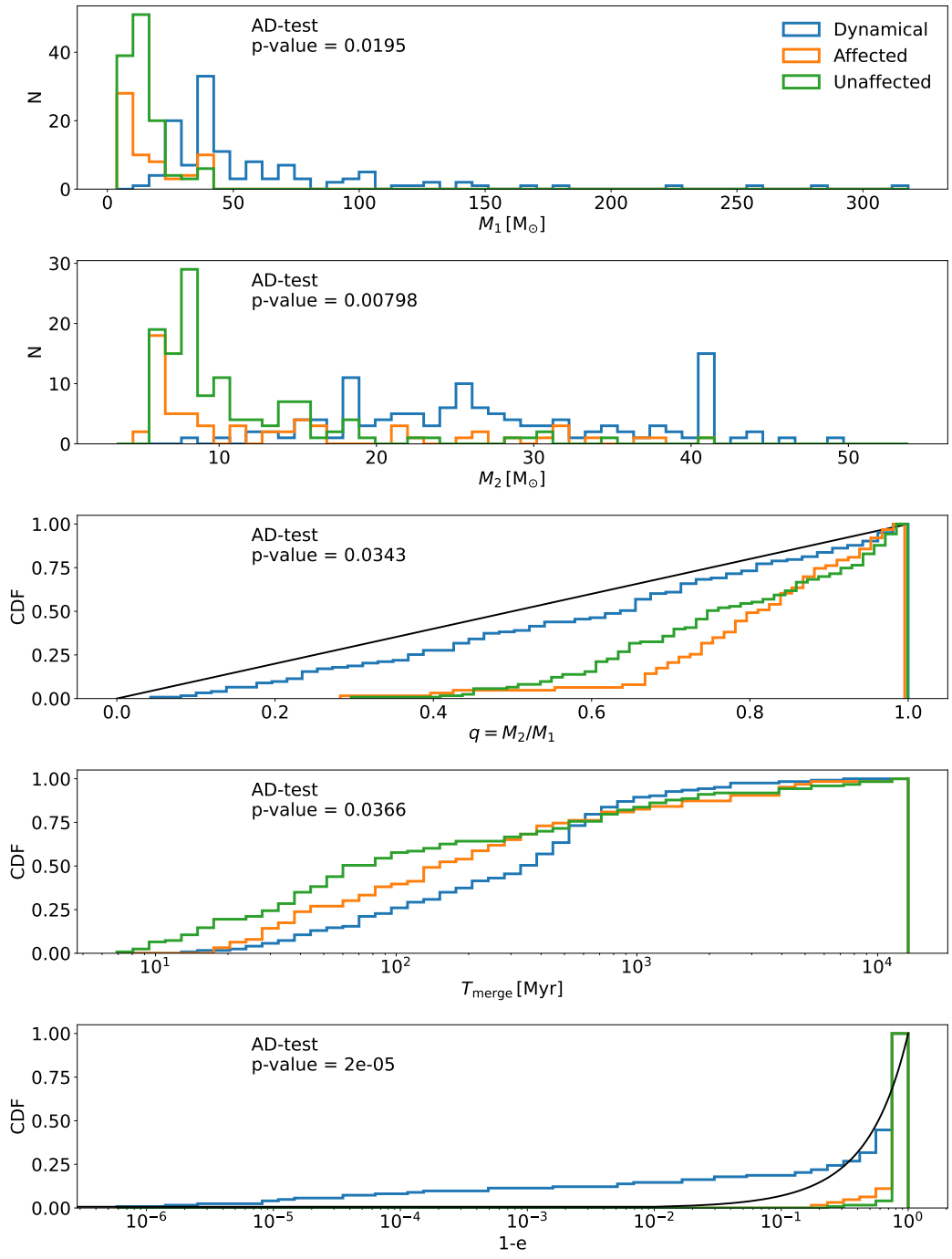


Figure 3.8: Distributions for the three merging populations - dynamically formed BBHs, affected primordial BBHs and unaffected primordial BBHs, from all simulations. Here we have taken the cut-off fractional change defining affected binaries as 50%. We note that for each distribution we perform a K-sample Anderson-Darling (Scholz & Stephens, 1987) test between the unaffected and affected populations, the p-value of the tests are shown on the corresponding panel. For the mass ratio and eccentricity panels, we plot the reference distributions $U(0,1)$ and $f(<e) \propto e^2$ respectively.

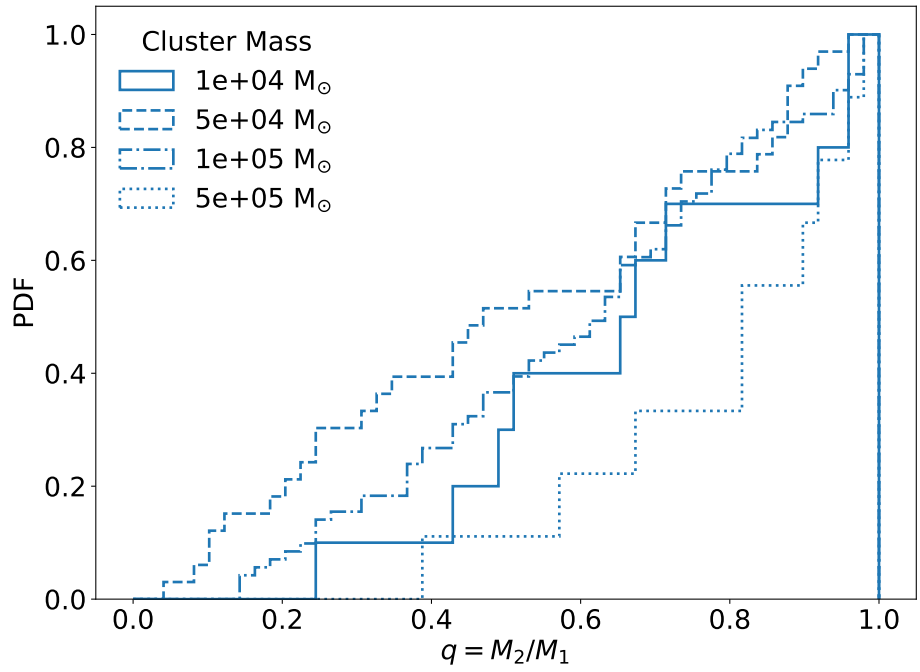


Figure 3.9: The cumulative distribution of the mass ratio ($q$) for dynamically formed merging BBHs. We show the combined distribution from all of our simulations, as well as the distribution for each initial cluster mass.

Several important results emerge from this analysis. First the mass-ratio distribution of merging BBHs (shown in Fig. 3.9) appears to contain more asymmetric binaries than the primordial BBH mergers, and it is nearly uniform between 0 and 1. Both of these results are somewhat surprising since three-body encounters are expected to favour the formation of binaries with nearly equal mass components (Rodriguez et al., 2016a; Park et al., 2017). Moreover, we find that the BBH eccentricity distribution is clearly over-thermal, in the sense that it contains more eccentric binaries than $N(< e) \propto e^2$; about 20% of the BBHs have $1 - e \lesssim 10^{-2}$. This is not surprising, however, because we are only considering those BBHs that merge within $t_{\rm H}$, which naturally favours the BBHs with the highest eccentricities due to the strong dependence of the GW merger timescale on $e$.

In addition, we investigate whether the presence of the primordial population affects the properties of the dynamically formed BBHs that go on to merge. We therefore split the dynamical BBH population depending on whether its host cluster contained a primordial binary population and again perform an AD k-sample test (Scholz & Stephens, 1987) between these two populations. Fig. 3.10 shows the results of these comparisons for the same parameters as in Fig. 3.8. Our tests suggest for each of the parameters the two populations of dynamical BBHs are drawn from the same distribution, and so the presence of the primordial population does not affect

the merging dynamical BBHs.

One of our cluster variations (Z2-M10-D3-L*) is initialised with a Duquennoy & Mayor (1991) binary period distribution. Although not the focus of this work, we investigated whether this choice led to any differences in the BBH properties. We found little to no difference in the BBH properties compared to clusters initialised with a Sana et al. (2012) period distribution.

## 3.3 In-cluster vs Ejected Mergers

$N$-body simulations provide a detailed understanding of the evolution of stellar populations within a cluster, requiring minimal assumptions about the properties and dynamical evolution of the BHs. As such, they represent the most reliable approach for advancing our understanding of BBH formation in dense stellar environments. However, due to the substantial computational demands of $N$-body simulations, approximate methods–such as those relying on Monte Carlo techniques and semi-analytical codes– are often used. These methods typically involve the following two assumptions (amongst other ones): (i) the only important interactions in the cluster core are those close interactions that involve binaries and single objects, i.e., interactions between binaries and singles and interactions between two binaries; (ii) these interactions are assumed to be strong interactions, which lead to an either a direct or a resonant encounter between the three BHs. Assumption (i) means that interactions involving higher multiplicity systems such as stable triples and quadruples are often neglected. Assumption (ii) implies that the effect of soft interactions–where the closest approach of the third BH to the binary is larger than $\sim 2$ times the binary semi-major axis–is also neglected.

Given these assumptions, the number of merging BBHs can be approximately derived. Moreover, one can derive the number of mergers that occur inside the cluster *vs* those that occur after being dynamically ejected from it. This distinction is a key to a full characterisation of the merging BBH population. For example, a fraction of in-cluster mergers are expected to have a residual eccentricity within the frequency band of current GW detectors. Moreover, mergers amongst the ejected and the in-cluster populations will have different redshift distributions, as in-cluster mergers occur earlier on during the evolution of the cluster (Rodriguez & Loeb, 2018).

In this section, we begin by reviewing the theory framework for the formation and evolution of BBHs in star clusters. We then compare these theoretical predictions with the outcomes of our cluster models, providing a testbed to evaluate and refine current theories.

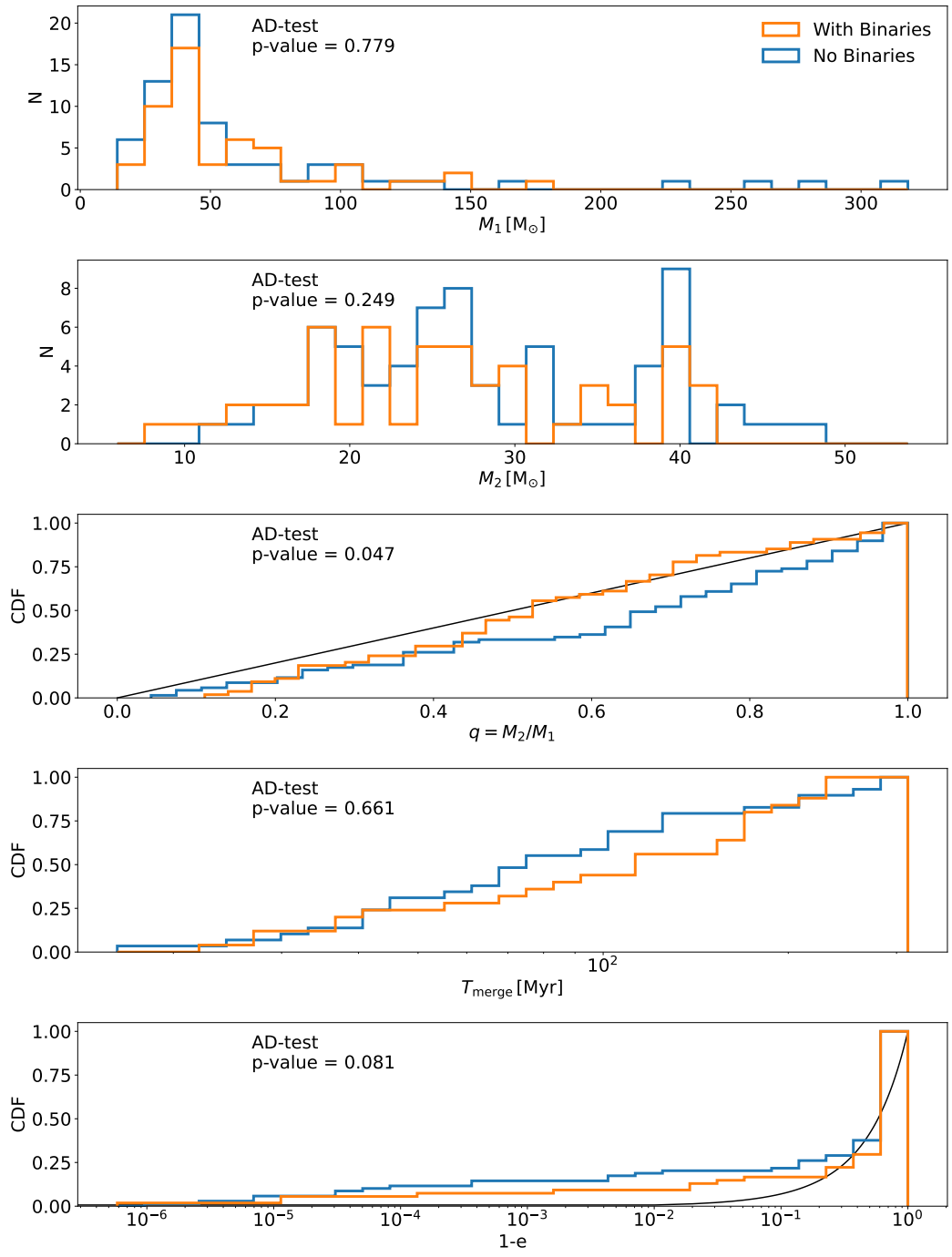


Figure 3.10: Distributions of dynamical formed BBHs from all clusters with and without a primordial binary population. We note that for each distribution we perform a two sample Anderson-Darling (Scholz & Stephens, 1987) test between the two populations, the p-value of the tests are shown on the corresponding panel. On the panels with mass ratio and 1-eccentricity we plot the reference distributions $U(0,1)$ and $f(<e) \propto e^2$ respectively.

### 3.3.1 Theory

Here we follow Samsing (2018) and Antonini & Gieles (2020b) to describe the evolution of BBHs due to binary-single interactions. We assume that after a hard BBH is formed in the core of a star cluster, it experiences a sequence of binary-single interactions with single BHs and stars. During a single interaction with a cluster member of mass $M_3$ the semi-major axis of the binary decreases from $a$ to $\epsilon a$. Then energy and momentum conservation imply that the binary experiences a recoil kick $v_{\rm bin}^2 = G\mu\frac{M_3}{M_{123}}\left(1/\epsilon a - 1/a\right) \approx 0.2G\mu\frac{M_3}{M_{123}}q_3/a$, where $\mu = M_1M_2/(M_1+M_2)$, $M_{123} = M_1+M_2+M_3$, $q_3 = M_3/(M_1+M_2)$, and we have assumed that in the interaction the binding energy of the binary increases by a fixed fraction $\approx 0.2$, i.e., $\epsilon \approx 1/(1+0.2)$ (e.g., Quinlan, 1996; Coleman Miller & Hamilton, 2002; Antonini & Rasio, 2016).

Setting $v_{\rm bin} = v_{\rm esc}$, with $v_{\rm esc}$ the escape velocity from the cluster, we obtain the limiting semi-major axis below which a three body interaction will eject the binary from the cluster:

$$a_{\rm ej} = \left(\frac{1}{\epsilon} - 1\right) G\frac{M_1M_2}{M_{123}}q_3/v_{\rm esc}^2 \ . \tag{3.7}$$

We have two possibilities, either the binary reaches $a_{\rm ej}$, and it is ejected from the cluster or it mergers before reaching $a_{\rm ej}$.

The total probability that a binary merges in between any two consecutive binary-single interactions, before reaching $a_{\rm ej}$, is obtained by integrating the differential merger probability per binary-single encounter, $d\mathcal{P}_{\rm GW} = P_{\rm GW}dN_3$, over the total number of binary-single interactions experienced by the binary (Samsing, 2018). Noting that $da/dN_3 = (\epsilon-1)a$, this leads to

$$\mathcal{P}_{\rm GW}(a_{\rm ej}) = \int_{a_{\rm h}}^{a_{\rm ej}} \frac{1}{\epsilon-1}\ell_{\rm GW}^2\frac{da}{a} \approx \frac{7}{10}\frac{1}{1-\epsilon}\ell_{\rm GW}^2(a_{\rm ej}) \ , \tag{3.8}$$

where $\ell_{\rm GW}$ is the value of $\ell = (1-e^2)^{1/2}$ below which the evolution of the binary becomes dominated by GW energy loss–we are assuming here that the binary receives a large angular momentum kick such that the phase space is stochastically scanned and uniformly covered by the periapsis values. Antonini & Gieles (2020b) showed that

$$\ell_{\rm GW} \simeq 1.3\left[\frac{G^4\left(M_1M_2\right)^2\left(M_1+M_2\right)}{c^5}\frac{t_{\rm rh}}{\zeta|E|}\right]^{1/7} a^{-5/7} \ , \tag{3.9}$$

where $\zeta \simeq 0.1$ and $E = -0.2GM_{\rm cl}^2/r_{\rm h}$, with $r_{\rm h}$ the half-mass radius of the cluster.

The total probability that a BBH will merge outside its parent cluster is given by the product of the probability that the binary reaches $a_{\rm ej}$ and the probability that it merges after being ejected (Antonini & Gieles, 2020b)

$$\mathcal{P}_{\rm ex}(a_{\rm ej}) = (1 - \mathcal{P}_{\rm GW}(a_{\rm ej}))\, P_{\rm ex} \ , \tag{3.10}$$

where $P_{\rm ex}$ is the probability that an ejected binary merges on a timescale shorter than $t_{\rm H}$:

$$P_{\rm ex}(a_{\rm ej}) = \ell^2_{\rm H}(a_{\rm ej}) \ , \tag{3.11}$$

and

$$\ell_{\rm H} \simeq 1.8 \left[\frac{G^3 M_1 M_2 (M_1+M_2)}{c^5} t_{\rm H}\right]^{1/7} a^{-4/7} \ . \tag{3.12}$$

Thus, for $\ell < \ell_{\rm H}$, an ejected binary merges in less than $t_{\rm H}$.

From the above considerations it follows that the fraction of in-cluster mergers to the total population of BBH mergers produced by a cluster is

$$\mathcal{F}_{\rm GW} = \frac{\mathcal{P}_{\rm GW}}{\mathcal{P}_{\rm GW} + \mathcal{P}_{\rm ex}} \ . \tag{3.13}$$

In Fig. 3.11 we plot this quantity as a function of cluster mass and for different values of $\rho_{\rm h}$. For the cluster models we considered, we should expect that the fraction of mergers that are produced inside the cluster varies between $\approx 0.25$ and 0.45. These fractions appear to be consistent with those obtained in previous work. For example, Rodriguez et al. (2018b) find that 55% of the mergers in their Monte Carlo models occur when the binary is still bound to its parent cluster.

### 3.3.2 Comparison to $N$-body models

We investigate the fraction of in-cluster mergers in our simulations for both primordial and dynamically formed BBH populations. To make comparisons against theoretical studies, here we simulate the same clusters using the fast cluster population model code `cBHBd` (Antonini & Gieles, 2020b). This code assumes no primordial binaries, and only considers BH-BH interactions through binary-single encounters. The basic theoretical framework is the one described above in Section 3.3.1. Using `cBHBd` we produce 1000 realisations of each of our cluster initial conditions (see Table 3.1), we then find the average number of in-cluster and ejected mergers as well as the average in-cluster fraction.

We show the number of in-cluster and ejected mergers from our simulations in the left panel of Fig. 3.12. For each model we show the cluster variations with and without primordial binaries and then split up the mergers based on whether they merged in-cluster or were ejected before merger. We also show the average number of in-cluster and ejected mergers from the `cBHBd` models for each cluster respectively. In the `PeTar` models with a primordial binary population, there is a similar number of ejected and in-cluster mergers. As explained above, most of these binaries are not

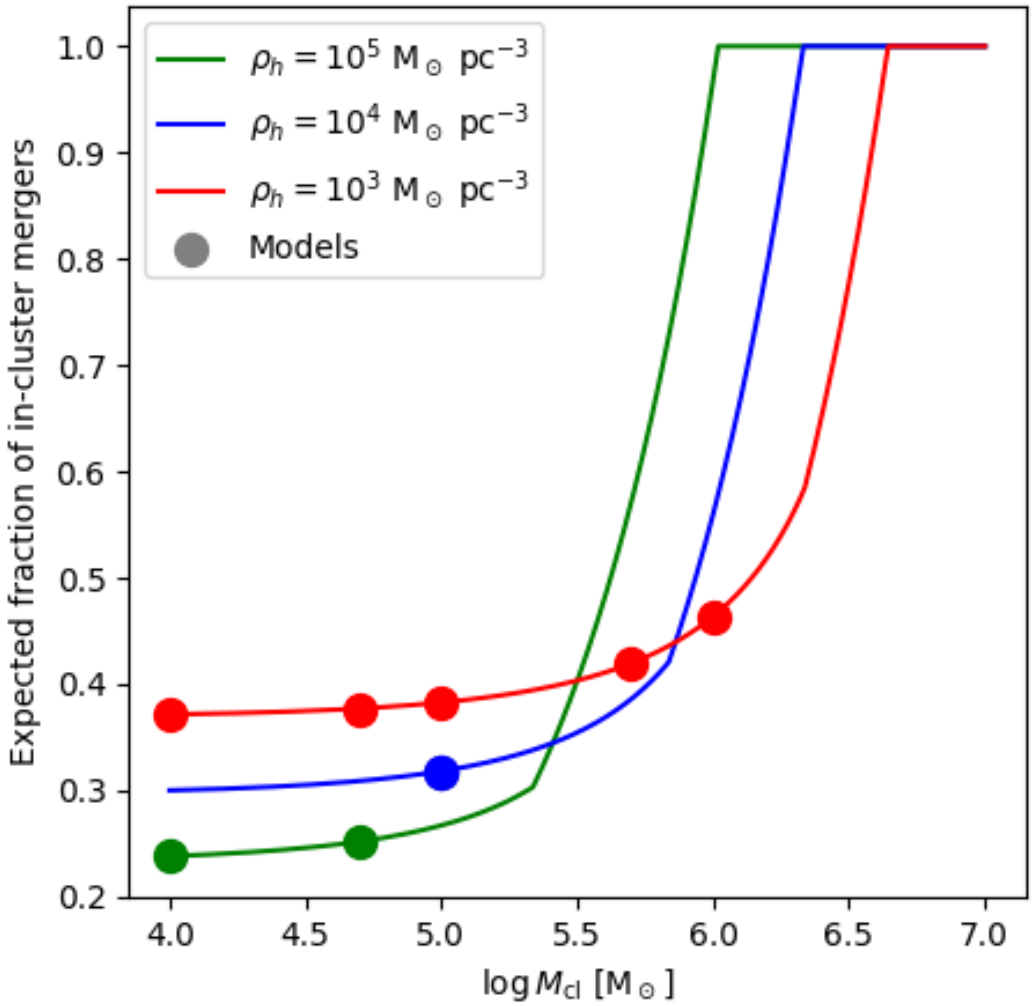


Figure 3.11: Expected fraction of in-cluster mergers as a function of cluster mass and density obtained from equation (3.13). The filled circles show the predicted fraction of in-cluster mergers for the initial values of $M_{\rm cl}$ and $\rho_{\rm h}$ we used in the $N$-body models.

ejected by dynamical encounters, but by a SN kick during BH formation. Clusters without primordial binaries exhibit almost no ejected mergers across all simulations. This shows that dynamically formed BBHs tend to merge within the cluster rather than being ejected. The low number of mergers amongst the ejected population aligns with the results from the `cBHBd` models, which predict only one merger out of approximately 10 cluster simulations. Following from this, we observe only six mergers, amongst the 17 cluster models that start without primordial binaries. In contrast, the predicted number of in-cluster mergers is much higher in the $N$-body simulations compared to the `cBHBd` models. In total, we find 63 in-cluster mergers, whereas the theoretical expectation is that we should find only $\mathcal{O}(1)$ merger.

In Fig. 3.12 we plot the in-cluster fraction ($N_{\rm incl}/N_{\rm tot}$) for each simulation. As we should expect based on Section 3.3.1, the `cBHBd` models give a $\sim 40\%$ in-cluster fraction. We note that the lower cluster mass models show results quite different from 40%, and that this is due to small number statistics due to the low number of mergers from these clusters. In the $N$-body models without primordial binaries, essentially all mergers occur inside the clusters. We conclude that the theory is in disagreement with the $N$-body model results and that this disagreement is due to the much larger number of in-cluster mergers produced in the $N$-body models than expected.

It is important to note the `cBHBd` is a theory based approach that makes specific assumptions about the state of the cluster and how the evolution of the cluster is linked to the formation and evolution of BBHs. In particular, it assumes that once a BBH is formed it only ever experiences strong binary-single interactions which either harden or disrupt the binary. Thus, it does not account for higher multiple interactions such as binary-binary interactions, nor does it consider the formation of higher multiplicity systems, i.e., triples or quadruples. We showed in Section 3.2.1.1 that roughly half of the dynamically formed BBH mergers occurred as the inner binary of a stable BH triple system, and also found quadruple systems in our models. When such higher multiplicity systems are present they dominate the dynamical interactions due to their large cross-section for gravitational encounters. Moreover, the effect of relatively soft interactions with the closest approach $r_{\rm p} > 2a$ are neglected in `cBHBd` (Forastier et al., 2024). As mentioned above, Monte Carlo codes make similar assumptions and also find results that are consistent with `cBHBd` (Fregeau & Rasio, 2007). In particular, the left panel of Fig. 3.12 shows that both `CMC` and `MOCCA` simulations predict approximately an order of magnitude fewer mergers than our $N$-body models. We conclude that these approximations might at least partly explain the discrepancy between the theory and the full $N$-body simulations.

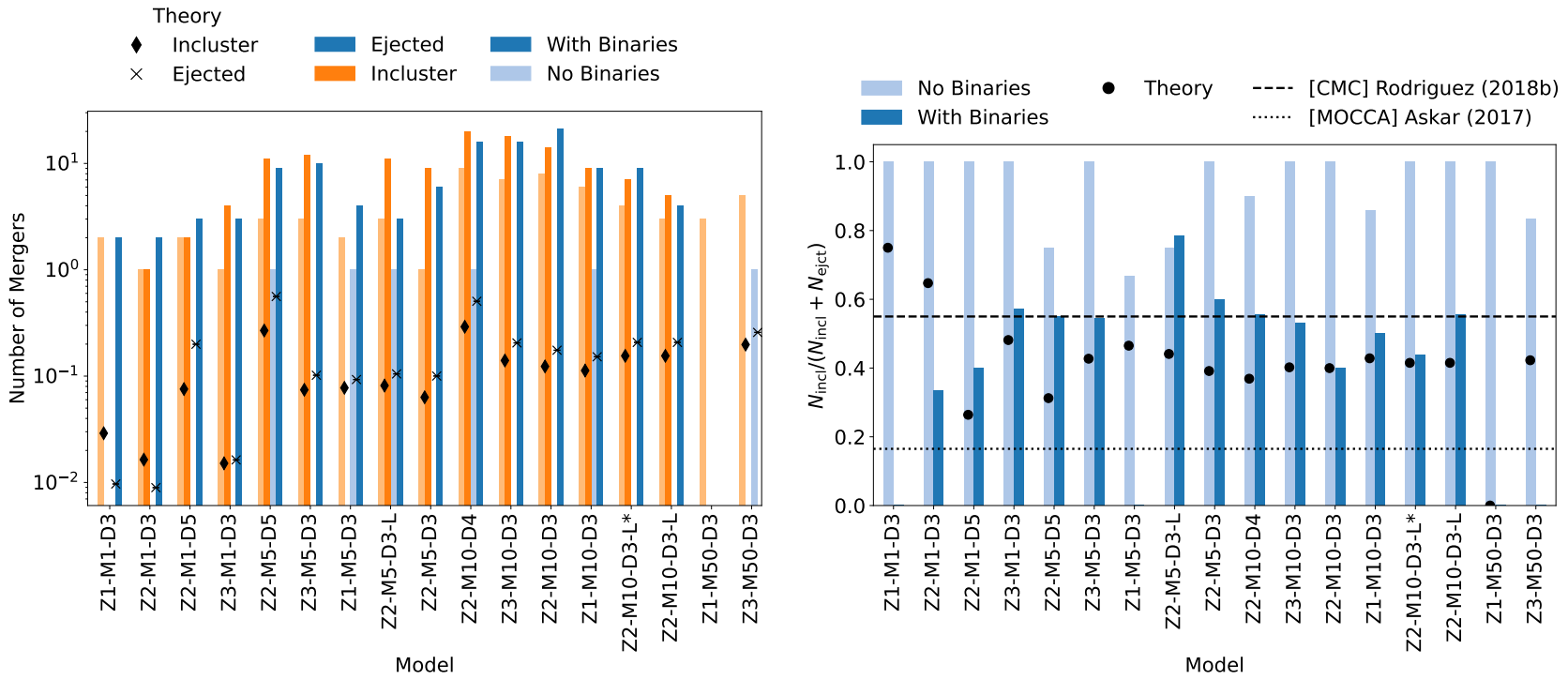


Figure 3.12: We show the number of ejected and in-cluster BBHs mergers occurring in all of our `PeTar` simulations. Ejected and in-cluster mergers are distinguished by blue and orange bars respectively, whilst the same cluster with and without primordial binaries are shown with darker and lighter shades. We further plot the results from theoretical models for the same initial cluster conditions. On the right panel we show the incluster merger fraction found in two previous studies (Rodriguez et al., 2018b; Askar et al., 2017) which use monte-carlo cluster codes `CMC` and `MOCCA` respectively.

To further investigate the in-cluster and ejected merging populations, we look at their radial position at the moment of merger normalised to the cluster core radius at that time. We split the mergers into the dynamically formed BBHs, the affected primordial BBHs and the unaffected primordial BBHs. Fig. 3.13 shows the cumulative distribution (CDF) of the radial distance for these mergers, where we have further split the distributions depending on the cluster properties. In the upper panel, we show the CDF for different initial cluster masses and in the lower panel we are comparing with cluster metallicity. In both plots we find that the cluster properties have little effect on the radial distribution of the mergers.

Focusing on the dynamically formed BBHs, 84% of the mergers in all simulations occurred within the cluster core, as opposed to 40% for the affected BBHs and 19% for the unaffected BBHs. This supports the idea that these dynamically formed BBHs are forming and merging in the most dynamically active region of the cluster, likely undergoing many encounters that involve higher multiplicity systems.

It is important to put our results into the context of previous star cluster studies. In Fig. 3.14 we plot the in-cluster merger fraction against the initial cluster mass and the initial cluster half-mass density alongside several previous studies. All the studies we compared against utilise a direct $N$-body code. Arca Sedda et al. (2024) use `NBODY6++` whilst both Chattopadhyay et al. (2022) and Banerjee et al. (2020) use `NBODY7`. These codes include post-Newtonian terms which allows for a self-consistent treatment of general relativistic effects. Fig. 3.14 shows that our simulations add to the suite of existing work, expanding and filling in more of the parameter space towards the highest mass and density values. Since we are interested in understanding the role of dynamics in BBH formation, we now consider models without primordial binaries, as any BBH in these models must have a dynamical origin.

Many previous studies explore non-zero primordial binary fraction amongst massive stars. Hence, we opt to compare only the in-cluster merger fraction for our clusters with no initial binaries against cluster with $f_{\rm bin} < 10\%$ amongst massive stars from the previous studies. We find that our results are broadly consistent with most previous studies across both cluster mass and density. The only exception are the simulations by Arca Sedda et al. (2024). These authors find that the fraction of in-cluster mergers is $\lesssim 50\%$ in their models. We are unsure about the cause for this difference, but note that all other published models we considered find in-cluster merger fraction that are much higher than found by Arca Sedda et al. (2024) and that are consistent with our results. For example, Chattopadhyay et al. (2022) found 3 ejected mergers in only one of their 11 cluster models. All mergers in their other models occurred inside the cluster. A key point we find is that in our simulations the in-cluster fraction for the dynamically formed BBHs has no dependence on the initial cluster mass or density. The work of Banerjee et al. (2020) and Chattopadhyay et al. (2022) also do not show any clear dependency, whilst Arca Sedda et al. (2024) find that the number of in-cluster mergers decreases with increasing cluster

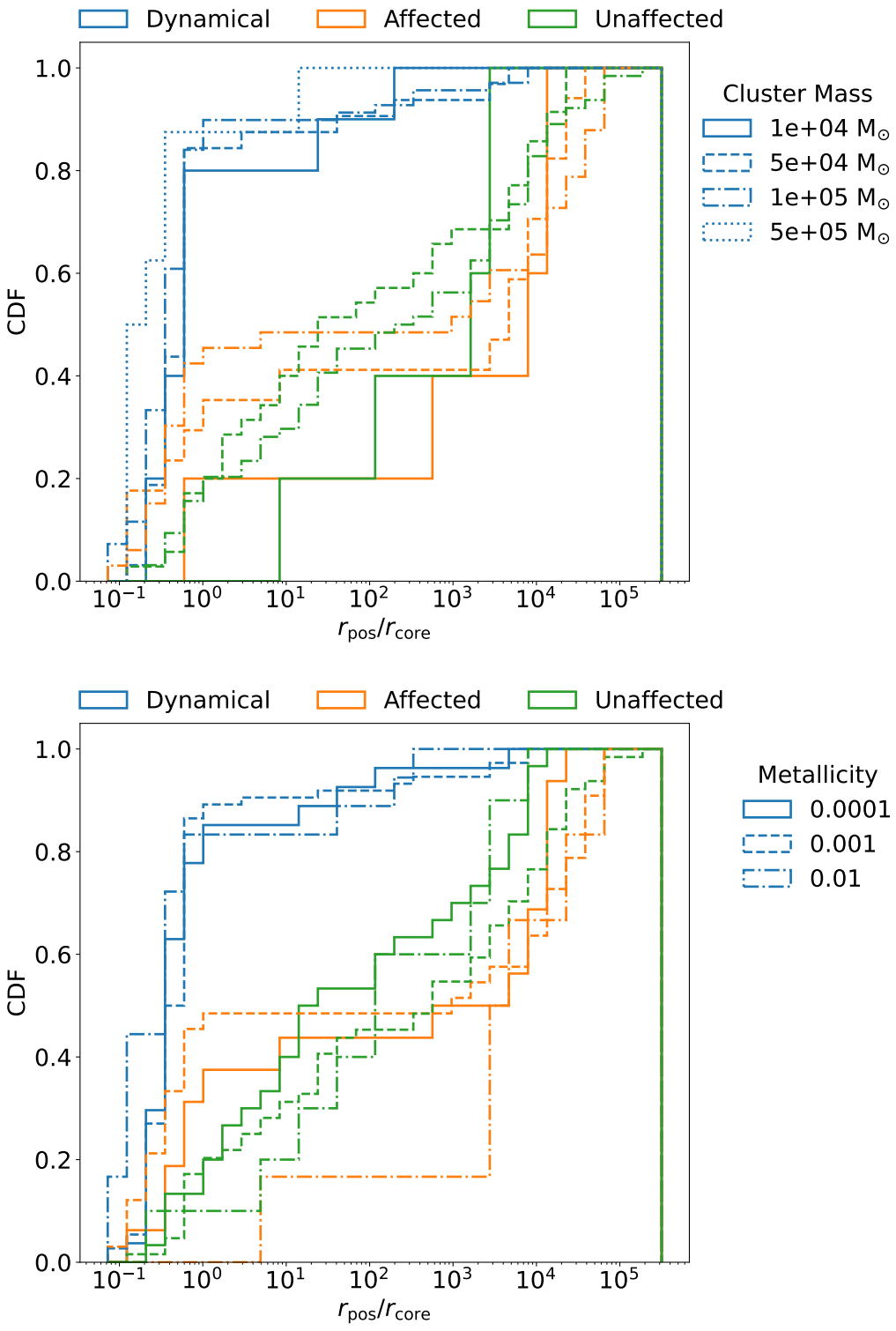


Figure 3.13: We show the CDF of the radial position for the affected, unaffected and dynamical BBH mergers in our simulations. The upper panel shows the distribution split by initial cluster mass, whilst the lower panel shows the distribution split by cluster metallicity.

mass and density.

## 3.4 Formation of high-mass black holes

In Fig. 3.15 we show the primary *vs* secondary mass for all of our BBH mergers split between the affected, unaffected and dynamical BBH populations. We find primary BHs with mass $> 100$ $M_\odot$. These masses exceed the assumed maximum BH mass that can be formed through stellar evolution in our models. This limit is imposed by the PPI prescription used in `BSE`, which here is at 45 $M_\odot$. The BHs with a mass above this limit must have been formed through consecutive mergers with either other BHs or stars (e.g., Zwart et al., 1999; Portegies Zwart et al., 2004; Mapelli, 2016; Di Carlo et al., 2019; González et al., 2021; Rizzuto et al., 2021). In fact, we find that the most massive BHs formed in our models first grow through accreting stars, and in a second stage through mergers with smaller BHs. These latter mergers are believed to be a key formation mechanism for intermediate and supermassive BH seed growth in massive clusters (Antonini et al., 2019; Chattopadhyay et al., 2023). However, they require clusters with large $v_{\rm esc}$ values (Antonini & Rasio, 2016). This is because the asymmetric emission of GWs during a BBH inspiral/merger induces a recoil kick on the remnant BH to conserve momentum. The strength of the kick depends on the mass ratio and spin alignment of the system but can be as large as $\mathcal{O}(10^3)$ km s$^{-1}$ (Schnittman & Buonanno, 2007). These recoil kicks are not accounted for in `PeTar`. Therefore, the chain of mergers would have been most likely interrupted after the first BH-BH merger. We can thus consider our simulations as an optimistic upper estimate of the number of mergers from the dynamical BBH population.

To better understand the formation of these massive BHs we first identify those that have been involved with at least one previous merger. Fig. 3.16 reproduces the scatter between primary and secondary masses, although now we identify two groups based on whether this is a first time merger, or a hierarchical merger where either the primary, secondary or both components have been involved in a previous merger. From Fig. 3.16, we can see the clear mass limit at 45 $M_\odot$ for the majority of the first time mergers. However, we also see two *first time* mergers which far exceed the PPI cut-off, one at $\approx 100$ $M_\odot$ and one at 225 $M_\odot$.

To investigate the formation of the 225 $M_\odot$ BH we track its evolution from the ZAMS of its stellar progenitor up to the end of the simulation. Firstly, we found this binary in the Z2-M5-D5 cluster model without primordial binaries, thus it is one of the clusters with the highest density. We further found that this massive BH was the result of eight previous stellar mergers which produced a 397 $M_\odot$ star which is then swallowed by a 26.7 $M_\odot$ BH. This results in a 225 $M_\odot$ BH which, following the merger with one final star of mass 2 $M_\odot$, forms a BBH and eventually merges. Notably, we find that the remnant of this BBH merger then goes on to form another merging BBH three more times. We note that a caveat to this evolutionary pathway

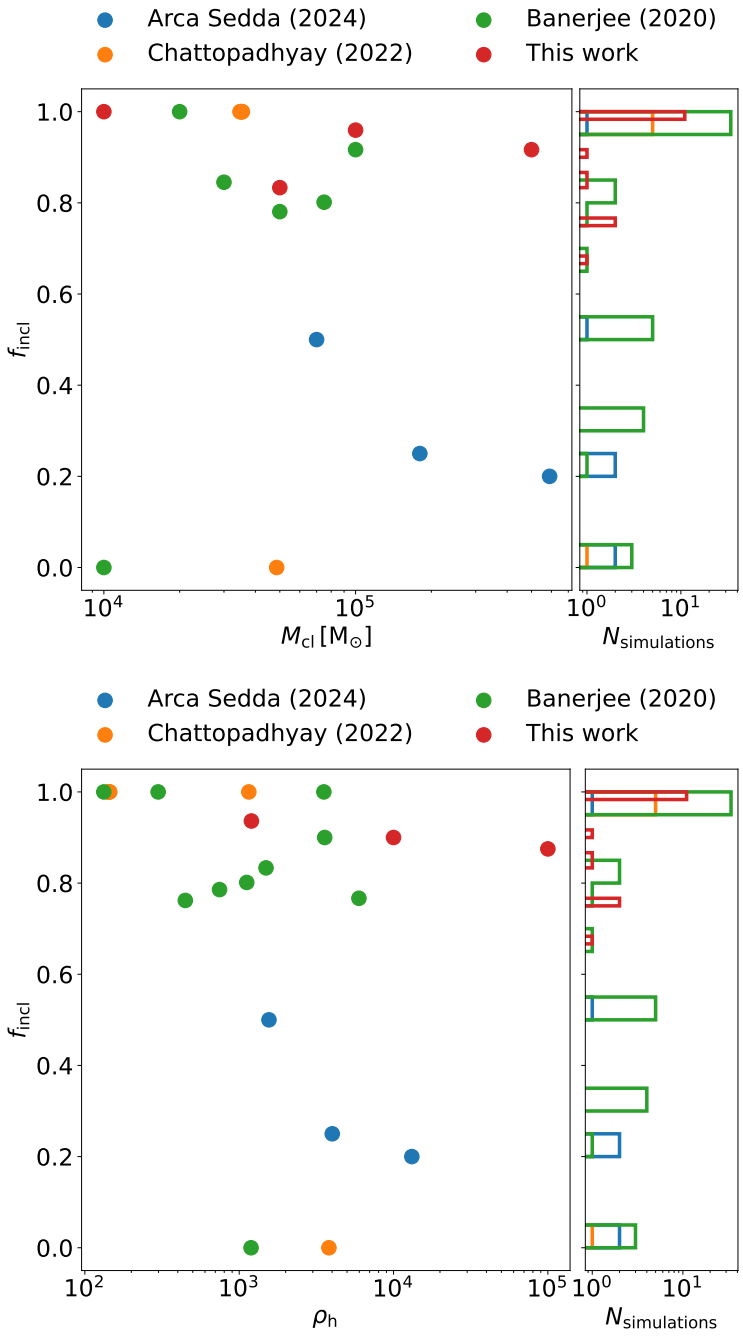


Figure 3.14: We show the in-cluster fraction of mergers against initial cluster mass (upper panel) and initial density at half mass radius (lower panel). In each plot we include only the clusters with lower primordial binary fraction ($\leq 0.1$) and have averaged over all other cluster parameters. We show our results (red) compared to previous works utilising other $N$-body codes Arca Sedda et al. (2024); Chattopadhyay et al. (2022); Banerjee (2020). To the right of each scatter plot we show a histogram of the incluster fraction from every simulation in each of the studies.

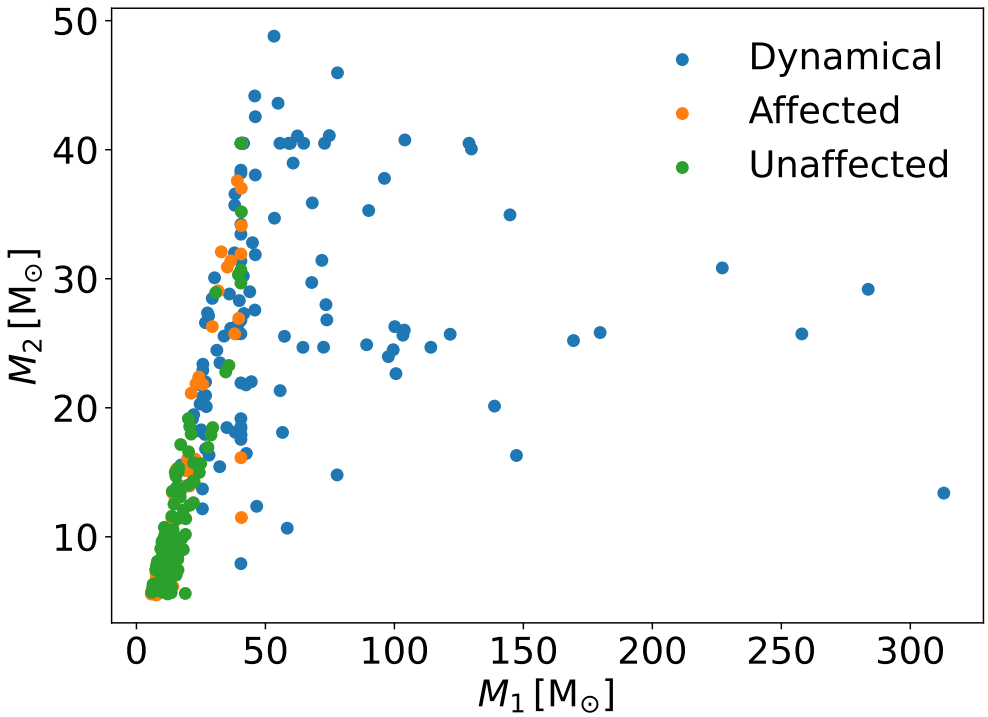


Figure 3.15: Comparing component masses for all of our BBH mergers, split between the three populations, dynamical binaries, affected primordial binaries and unaffected primordial binaries. Here we have taken the cut-off fractional change defining affected binaries as 50%.

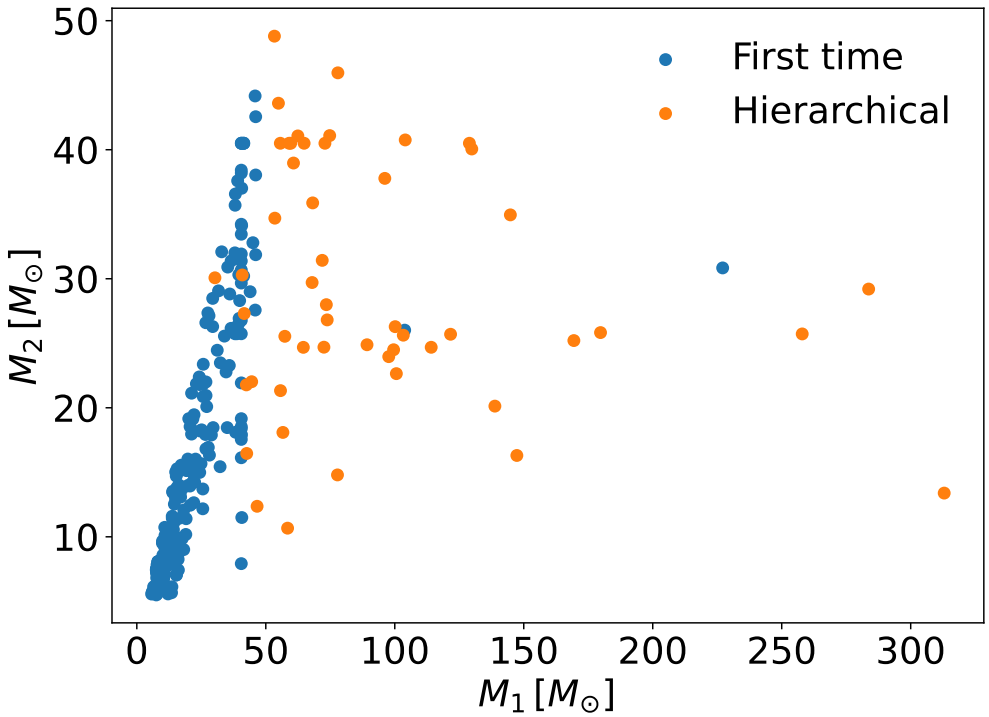


Figure 3.16: Comparing the component masses for all BBH mergers in our simulations, split by whether this is a first time merger (neither component has been in a BBH merger before) or a hierarchical merger (one or both components are remnants from a previous merger).

is the fact that `PeTar` does not currently model mass loss during stellar collisions. For massive stars with loosely bound envelopes it is likely that stellar collisions remove significant mass from the star, thus restricting mass growth. We show a schematic of these mergers in Fig. 3.17 along with the masses of all the components. We also note that in this case, GW recoil kicks are unlikely to be large enough to eject the remnant from the cluster due to the low mass ratio of the BBH (Holley-Bockelmann et al., 2008). Since this merger was found in a cluster with no primordial binaries, we then choose another hierarchical merger from a cluster model containing a primordial binary population to compare the evolutionary pathways. We opt for a hierarchical merger with $M_1 = 57.4$ $M_\odot$ and $M_2 = 25.5$ $M_\odot$. We find that the secondary BH is the result of the evolution of a primordial binary system, which undergoes some period of MT before one component forms a BH and then quickly merges with its companion star. On the other hand, the primary BH is the remnant of a previous BBH merger where the binary was from the primordial binary population, evolved together, formed a BBH and merged. The schematic from this merger chain is shown in Fig. 3.18.

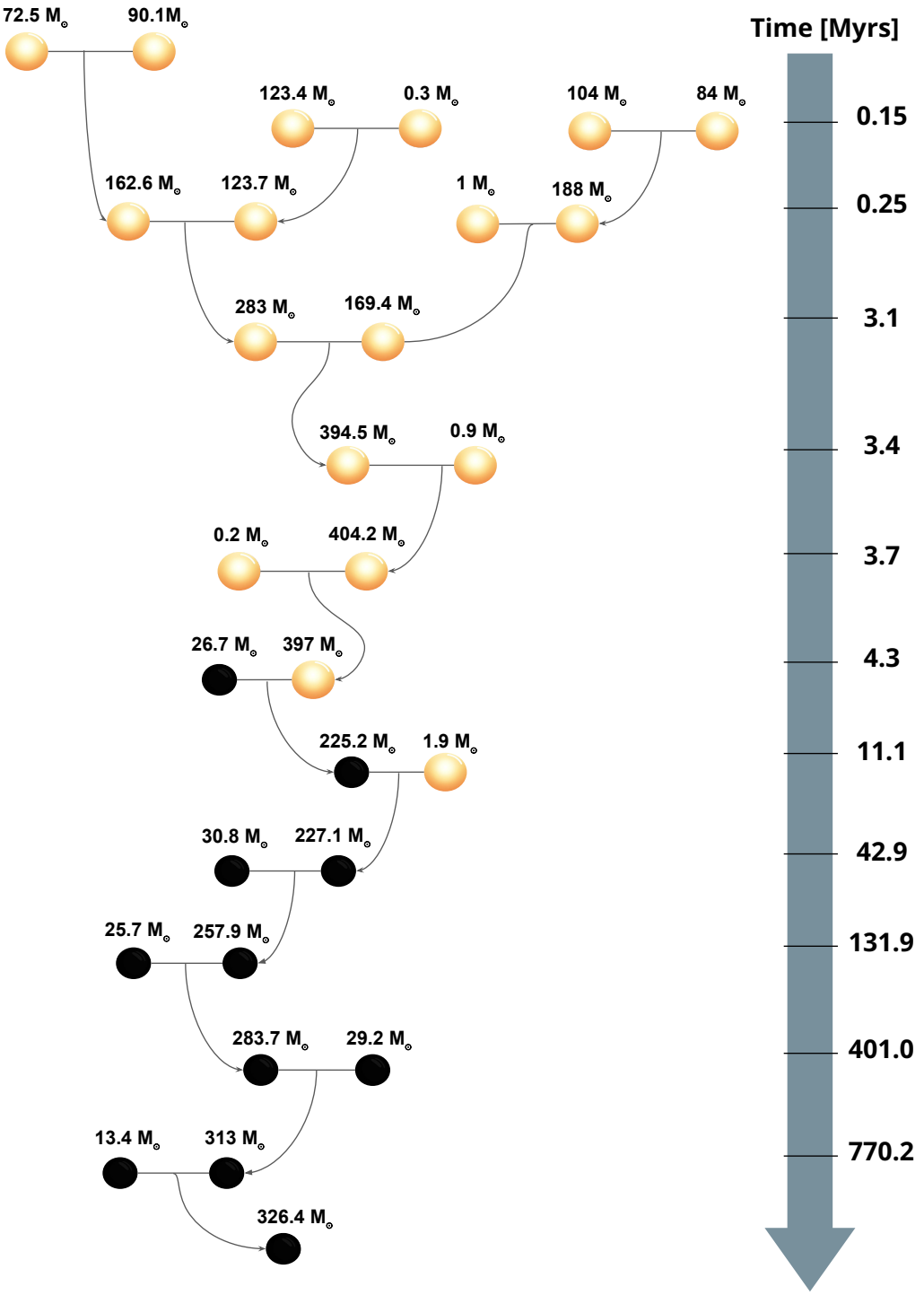


Figure 3.17: A schematic showing the chain of mergers leading to the formation of a massive BH in cluster model Z2-M5-D5.

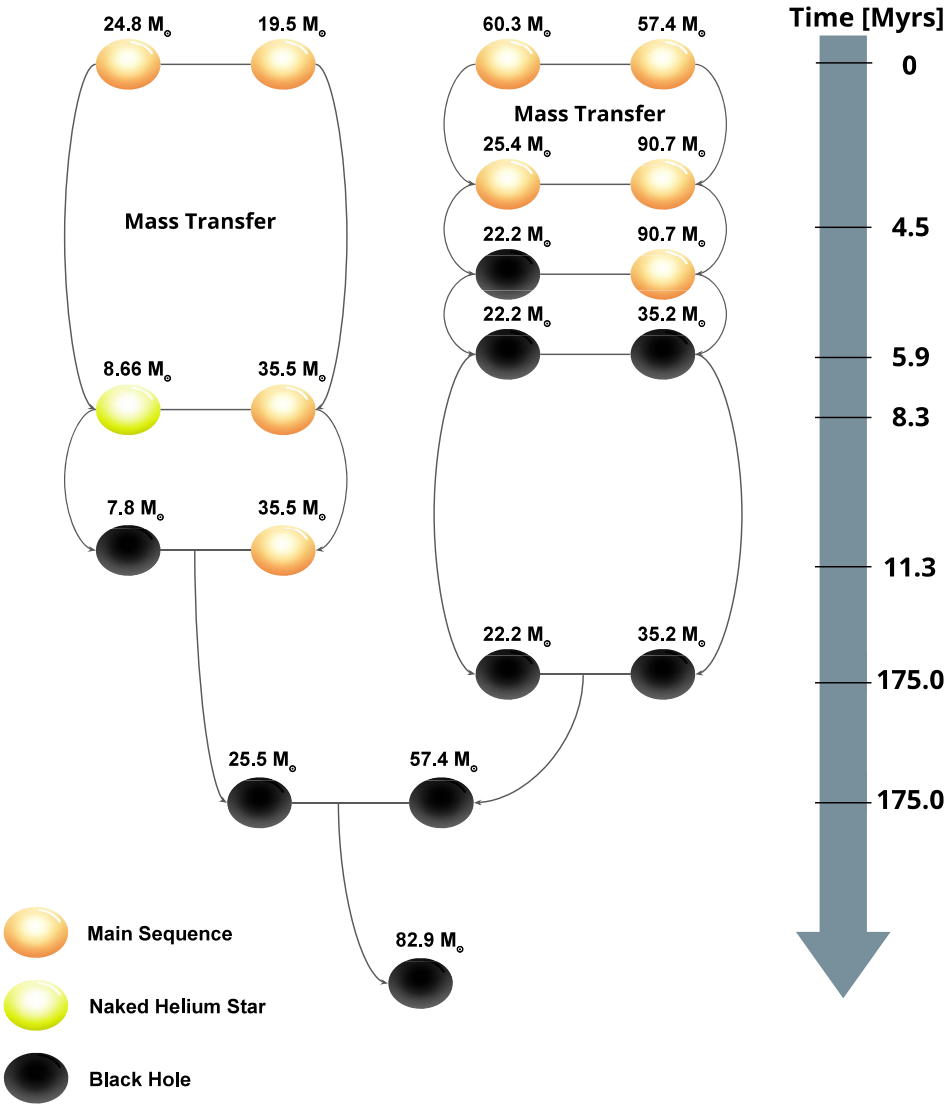


Figure 3.18: A schematic of the evolution of a primordial binary in model Z3-M5-D3 also leading to the formation of a massive BH. The primordial binary undergoes a MT episode during the stellar phases before merging as a BBH. The remnant BH stays within the cluster and goes on to form a new BBH which then merges within a Hubble time.

# Chapter 4

# Properties of black hole-star binaries formed in $N$-body simulations of massive star clusters: implications for Gaia black holes

BH binaries, particularly BH-star (BH-S) systems, have been essential for studying the formation and evolution of massive stars (e.g., Eggleton, 2006; McClintock & Remillard, 2006). Historically, most of our understanding on BHs has come from the study of X-ray binaries, where the BH mass could be dynamically measured (e.g., Özel et al., 2010; Farr et al., 2011). The detection of GWs in 2015 then opened the door to GW astronomy as a method to study BH populations. Finally, recent observations have now revealed a new family of quiescent (X-ray quiet) BHs in binary systems. These quiescent BHs, discovered through astrometry and radial velocity measurements (e.g., Thompson et al., 2019), have opened new windows into the study of non-interacting BH binaries. The Gaia satellite in particular has been instrumental in identifying these systems. Recently there have been three quiescent BH binaries found by the Gaia satellite: Gaia BH1 (El-Badry et al., 2023a; Chakrabarti et al., 2023), Gaia BH2 (El-Badry et al., 2023b; Tanikawa et al., 2023b), and Gaia BH3 (Gaia Collaboration et al., 2024). These systems, with some unique orbital characteristics and associations with distinct Galactic populations, challenge traditional models of BH formation, particularly those from the isolated binary evolution channel.

The observed properties of these three Gaia BHs are shown in Table 4.1. Gaia BH1 is a binary between a Sun-like star and a 10 $M_\odot$ BH, Gaia BH2 is a binary between a red giant star and a 9 $M_\odot$ BH, and Gaia BH3 comprised of a metal-poor

| | Stellar type | $M_{\rm BH}$ [$M_\odot$] | $M_*$ [$M_\odot$] | $a$ [$R_\odot$] | $P$ [days] | $e$ | [Fe/H] |
|---|---|---|---|---|---|---|---|
| Gaia BH1 | G-type main-sequence | $9.62^{+0.18}_{-0.18}$ | $0.93^{+0.05}_{-0.05}$ | $301.55^{+2.15}_{-2.15}$ | $185.59^{+0.05}_{-0.05}$ | $0.45^{+0.005}_{-0.005}$ | -0.2 |
| Gaia BH2 | Red giant | $8.94^{+0.34}_{-0.0.34}$ | $1.07^{+0.19}_{-0.19}$ | $1066.55^{+17.20}_{-17.20}$ | $1276.7^{+0.6}_{-0.6}$ | $0.5176^{+0.0009}_{-0.0009}$ | -0.2 |
| Gaia BH3 | G-type giant | $32.7^{+0.82}_{-0.82}$ | $0.76^{+0.05}_{-0.05}$ | $2477.035^{+58.058}_{58.058}$ | $4253.1^{+98.5}_{-98.5}$ | $0.7291^{+0.0048}_{-0.0048}$ | -2.6 |

Table 4.1: Main properties of Gaia BH1 (El-Badry et al., 2023a), Gaia BH2 (El-Badry et al., 2023b), and Gaia BH3 (El-Badry, 2024).

giant star with a 33 $M_\odot$ BH. Gaia BH1 and BH2 both contain large periods (186 days and 1280 days) and high eccentricities ($e \approx 0.45$ and $e \approx 0.5$) which are difficult for isolated mechanisms to reproduce. Nevertheless, there are studies investigating both isolated (Kotko et al., 2024; Kruckow et al., 2024; Gilkis & Mazeh, 2024) and dynamical mechanisms (Shikauchi et al., 2020; Rastello et al., 2023; Di Carlo et al., 2024; Tanikawa et al., 2023a) to form such systems. For Gaia BH3, it has been shown that it can be explained through both a low-metallicity isolated evolution (Iorio et al., 2024; El-Badry, 2024) and dynamical encounter in a globular cluster (Marín Pina et al., 2024). Interestingly, its low metallicity and chemical composition may also suggest that it is a part of the ED-2 stream, a remnant of a dissolved globular cluster (Balbinot, E. et al., 2024).

Given our new suite of $N$-body cluster simulations, presented in Chapter 3, we are in an ideal position to perform a investigation into the types of BH-S binaries which are formed in our massive clusters. In the sections that follow we have characterised the properties of BH-S binaries in our models. We have extended the explored parameter space to higher cluster masses and densities than has previously been studied (Rastello et al., 2023; Di Carlo et al., 2024; Tanikawa et al., 2023a), and investigated the possibility for the dynamics in our models to generate binaries with properties resembling those of the observed Gaia BHs.

## 4.1 Methods

### 4.1.1 Initial conditions

In this work we use the new suite of cluster simulations presented in Chapter 3 to perform a detailed search and analysis of BH-S binaries. Below we give a brief recap of the important initial conditions from our simulations. For a more detailed description of the `PeTar` code and the cluster initial conditions, refer back to Section 3.1.

- Initial cluster mass : $10^4\ M_\odot \leq M_{\rm cl} \leq 10^6\ M_\odot$
- Initial cluster half-mass density : $\rho_{\rm h} \in \{1200, 10^4, 10^5\}\ M_\odot\ {\rm pc}^{-3}$
- Stellar metallicity : $Z \in \{10^{-2}, 10^{-3}, 10^{-4}\}$.

For most cluster models we consider two variations, one with and one without

primordial binaries[1]. We note that since our primordial binaries are always set such that the primary mass is $\geq 20$ $M_\odot$, we are not considering the formation of BH-S binaries through exchanges that involve a primordial binary in which both components are low-mass stars. This is unlikely to affect significantly our results since such binaries are unlikely to undergo frequent dynamical interactions leading to an exchange of one of the components with a massive star or a BH. Due to their lower mass these binaries do not efficiently migrate to the cluster core where these interactions can take place (Spitzer, 1987). Instead, the majority of our BH-S binaries come from the primordial binary population, where the primary star forms a BH and remains bound to its companion star. We note that based on the initial mass ratio distribution we use, the minimum mass of the companion star is $M_{2,\rm min} = 2$ $M_\odot$, and that many of these BH-S systems will eventually evolve to BH-GS and potentially BBH systems. Ultimately it is important to understand that in our results might be underestimating the number of BH-S binaries formed by not considering primordial low-mass star binaries.

Stellar masses are set according to a Kroupa (2001) initial mass function with $0.08$ $M_\odot \leq M \leq 150$ $M_\odot$. The primordial binaries are initialised with a mass ratio drawn from a uniform distribution, $0.1 \leq q \leq 1$, an eccentricity drawn from a Sana et al. (2012) distribution (Eq 3.1) and a period distribution following the extended Sana et al. (2012) distribution from Oh et al. (2015) (Eq 3.2). We draw SN natal kicks from a Maxwellian distribution with $\sigma = 265$ km s$^{-1}$ (Hobbs et al., 2005) and assume a fallback kick prescription when scaling the kicks for BH formation (Fryer, 1999). In addition, we assume a Fryer et al. (2012) rapid SN engine for the CO remnant mass, and strong PPI cut-off at 45 $M_\odot$ (Belczynski et al., 2020). Unlike previous studies (Rastello et al., 2023; Di Carlo et al., 2024; El-Badry et al., 2022), we allowed the binary to survive without merging if a phase of CE evolution is initiated by a donor star that is on the HG.

The largest integration time simulated was 3 Gyr, and the majority of the simulations integrated for 1 Gyr. The final integration time of the simulations is chosen such that it is several times the initial relaxation time of the cluster. For the most massive clusters ($M_{\rm c} = 5 \times 10^5$ $M_\odot$ and $10^6$ $M_\odot$), we make sure that the simulation runs for at least half the initial relaxation time.

The first five columns of Table 4.2 are adapted from Table 3.1 and provide a breakdown of the cluster initial conditions for each of our simulations.

[1]These primordial binaries are the same as described in Chapter 3.

Table 4.2: Initial cluster conditions for our `PeTar` $N$-body simulations. Each model is given a unique name based on its initial setup (metallicity, initial cluster mass and density). Models with a -L added are run for 3 Gyr; Z1-M100-D3 and Z3-M50-D3 are terminated at 507 Myr, and Z3-M100-D1 and Z3-M100-D3 at 254 Myr. All the remaining models are evolved up to a maximum integration time of 1 Gyr. Each model contains two variations, one which starts with no binaries, and one which sets an initial binary fraction of 100% amongst massive stars (initial mass $\geq 20$ $M_\odot$).

| Model | Metallicity | Total Mass | Density | Binary Fraction | Primordial BH-MS(BH-GS)[BH-WD]NS-S | | | Dynamical BH-MS(BH-GS)[BH-WD]NS-S | | |
|---|---|---|---|---|---|---|---|---|---|---|
| | | $M_\odot$ | $M_\odot$ pc$^{-3}$ | | Ejected | Retained | Total | Ejected | Retained | Total |
| Z1-M1-D3 | 0.01 | 10,000 | 1200 | 0 | 0(0)[0]0 | 0(0)[0]0 | 0(0)[0]0 | 0(0)[0]0 | 0(0)[0]0 | 0(0)[0]0 |
| | | | | 0.0025 | 1(1)[0]0 | 2(2)[0]0 | 3(3)[0]0 | 0(0)[0]0 | 1(1)[0]0 | 1(1)[0]0 |
| Z1-M5-D3 | | 50,000 | 1200 | 0 | 0(0)[0]0 | 0(0)[0]0 | 0(0)[0]0 | 1(0)[0]0 | 0(0)[0]0 | 1(0)[0]0 |
| | | | | 0.0025 | 3(2)[1]4 | 7(3)[0]2 | 10(5)[1]6 | 0(0)[0]0 | 0(1)[0]0 | 0(1)[0]0 |
| Z1-M10-D3 | | 100,000 | 1200 | 0 | 0(0)[0]0 | 0(0)[0]0 | 0(0)[0]0 | 0(0)[0]0 | 0(0)[0]0 | 0(0)[0]0 |
| | | | | 0.0026 | 3(2)[1]5 | 29(25)[0]2 | 32(27)[1]7 | 1(0)[1]0 | 2(0)[0]0 | 3(0)[1]0 |
| Z1-M50-D3 | | 500,000 | 1200 | 0 | 0(0)[0]0 | 0(0)[0]0 | 0(0)[0]0 | 0(0)[0]0 | 0(0)[0]0 | 0(0)[0]0 |
| Z1-M100-D3 | | 1,000,000 | 1200 | 0 | 0(0)[0]0 | 0(0)[0]0 | 0(0)[0]0 | 0(0)[0]0 | 0(0)[0]0 | 0(0)[0]0 |
| Z2-M1-D3 | 0.001 | 10,000 | 1200 | 0 | 0(0)[0]0 | 0(0)[0]0 | 0(0)[0]0 | 0(0)[0]0 | 0(2)[0]0 | 0(2)[0]0 |
| | | | | 0.0025 | 2(1)[0]1 | 3(3)[0]0 | 5(4)[0]1 | 0(0)[1]0 | 1(0)[0]0 | 1(0)[1]0 |
| Z2-M5-D3 | | 50,000 | 1200 | 0 | 0(0)[0]0 | 0(0)[0]0 | 0(0)[0]0 | 0(0)[0]0 | 0(0)[0]0 | 0(0)[0]0 |
| | | | | 0.0025 | 2(0)[1]0 | 17(25)[0]0 | 19(25)[1]0 | 0(0)[0]0 | 0(0)[0]0 | 0(0)[0]0 |
| Z2-M5-D3-L | | 50,000 | 1200 | 0 | 0(0)[0]0 | 0(0)[0]0 | 0(0)[0]0 | 0(0)[0]0 | 0(0)[0]0 | 0(0)[0]0 |
| | | | | 0.0025 | 0(0)[2]0 | 21(24)[0]1 | 21(24)[2]1 | 0(0)[0]0 | 0(2)[0]0 | 0(2)[0]0 |
| Z2-M10-D3 | | 100,000 | 1200 | 0 | 0(0)[0]0 | 0(0)[0]0 | 0(0)[0]0 | 1(0)[0]0 | 1(1)[0]0 | 2(1)[0]0 |
| | | | | 0.0026 | 9(4)[1]9 | 47(49)[0]2 | 56(53)[1]11 | 0(0)[0]0 | 3(2)[0]0 | 3(2)[0]0 |
| Z2-M10-D3-L | | 100,000 | 1200 | 0 | 0(0)[0]0 | 0(0)[0]0 | 0(0)[0]0 | 3(0)[0]0 | 0(0)[0]0 | 3(0)[0]0 |
| | | | | 0.0026 | 4(0)[1]3 | 48(46)[0]7 | 52(46)[1]10 | 0(0)[0]0 | 1(1)[0]0 | 1(1)[0]0 |
| Z2-M10-D4 | | 100,000 | 10,000 | 0 | 0(0)[0]0 | 0(0)[0]0 | 0(0)[0]0 | 1(0)[0]0 | 2(1)[0]0 | 3(1)[0]0 |
| | | | | 0.0025 | 7(5)[1]4 | 32(41)[0]1 | 39(46)[1]5 | 0(0)[0]0 | 2(2)[0]0 | 2(2)[1]0 |
| Z2-M1-D5 | | 10,000 | 100,000 | 0 | 0(0)[0]0 | 0(0)[0]0 | 0(0)[0]0 | 0(0)[0]0 | 0(1)[0]0 | 1(0)[0]0 |
| | | | | 0.0025 | 2(2)[1]3 | 1(1)[0]0 | 3(3)[1]3 | 4(2)[1]0 | 1(2)[1]0 | 5(4)[2]0 |
| Z2-M5-D5 | | 50,000 | 100,000 | 0 | 0(0)[0]0 | 0(0)[0]0 | 0(0)[0]0 | 3(0)[1]0 | 1(2)[0]0 | 4(2)[1]0 |
| | | | | 0.0025 | 14(8)[6]2 | 5(12)[0]0 | 19(20)[6]2 | 3(0)[0]0 | 0(1)[0]0 | 3(1)[0]0 |
| Z3-M1-D3 | 0.0001 | 10,000 | 1200 | 0 | 0(0)[0]0 | 0(0)[0]0 | 0(0)[0]0 | 0(0)[0]0 | 2(1)[0]0 | 2(1)[0]0 |
| | | | | 0.0025 | 1(1)[0]0 | 7(7)[0]0 | 8(8)[0]0 | 0(0)[0]0 | 1(2)[0]0 | 1(2)[0]0 |
| Z3-M5-D3 | | 50,000 | 1200 | 0 | 0(0)[0]0 | 0(0)[0]0 | 0(0)[0]0 | 0(0)[0]0 | 1(1)[0]0 | 1(1)[0]0 |
| | | | | 0.0025 | 4(2)[1]3 | 34(34)[0]2 | 38(36)[1]5 | 0(0)[0]0 | 1(5)[0]0 | 1(5)[0]0 |
| Z3-M10-D3 | | 100,000 | 1200 | 0 | 0(0)[0]0 | 0(0)[0]0 | 0(0)[0]0 | 0(0)[0]0 | 0(0)[0]0 | 0(0)[0]0 |
| | | | | 0.0025 | 13(5)[1]6 | 58(66)[0]0 | 71(71)[1]6 | 1(0)[0]0 | 1(2)[0]0 | 2(2)[0]0 |
| Z3-M50-D3 | | 500,000 | 1200 | 0 | 0(0)[0]0 | 0(0)[0]0 | 0(0)[0]0 | 0(0)[0]0 | 0(0)[0]0 | 0(0)[0]0 |
| Z3-M100-D3 | | 1,000,000 | 1200 | 0 | 0(0)[0]0 | 0(0)[0]0 | 0(0)[0]0 | 0(0)[0]0 | 0(0)[0]0 | 0(0)[0]0 |
| Total | | 4,580,000 | | | 66(33)[17]40 | 311(338)[0]17 | 377(371)[17]57 | 19(2)[4]0 | 21(30)[1]0 | 40(32)[5]0 |

### 4.1.2 Classification and post-ejection evolution

In this section, we present the two classification criteria for the binaries. Firstly, we classify the binaries as *ejected* binaries and *retained* binaries. In this paper we will mostly focus on the ejected population, which are binaries that are ejected from the cluster either by a SN kick or through a dynamical interaction. We focus on the ejected binaries since they are more relevant to the halo/field population observed by Gaia. However, we also provide a less detailed description of the retained binaries. There are two conditions that must be fulfilled to classify a binary as ejected from the cluster: firstly, we impose $r_{\rm bin} > 20r_{\rm h}$, where $r_{\rm bin}$ is the position of the COM of the binary and $r_{\rm h}$ is the cluster half-mass radius at any given time. The second criterion is that the velocity of the COM of the binary is larger than the escape velocity from the cluster. If these conditions are both satisfied at a given evolutionary stage (e.g., BH-MS), then the binary is classified as ejected. For the remaining binaries we only include them in our retained binary population after imposing a condition that the binary survives inside the cluster until at least the next stage of stellar evolution, e.g., a MS star becoming a GS. Thus, a retained binary is a binary that is formed as a BH-type binary inside the cluster, and it evolves to another type within the cluster.

The second classification is to divide the ejected binaries in primordial and dynamical. Primordial are the binaries initially present in the cluster, though they may experience dynamical processes that change their orbit. Dynamical binaries are those in which the components are paired through gravitational encounters during the simulations. We take the binaries at the time of ejection and subsequently evolve them in isolation for a Hubble time, using the `COSMIC` code (Breivik et al., 2020). All the stellar evolution parameters in `COSMIC` are set to be exactly the same as in `PeTar` so that the stellar evolution is consistent through the evolution. However, we note that the isolated evolution of an ejected binary might not be a good approximation in some cases. If the binary is ejected in a stable multiple system (triple, quadruple or more), the isolated binary evolution set-up will ignore the effect of the tertiary (or other objects in a multiple system) on the binary evolution (Stegmann et al., 2022).

The total number of primordial and dynamical binaries for each of our simulations is provided Table 4.2, each split into the ejected and retained populations and then further split into the stellar type of the binary components. We consider binaries in which one component is a BH and the other component is either a MS star, a WD, or a GS. We also briefly consider binaries in which one component is a NS and the other is a star (either a MS or a GS). In the following sections we discuss, in detail, the properties of these systems.

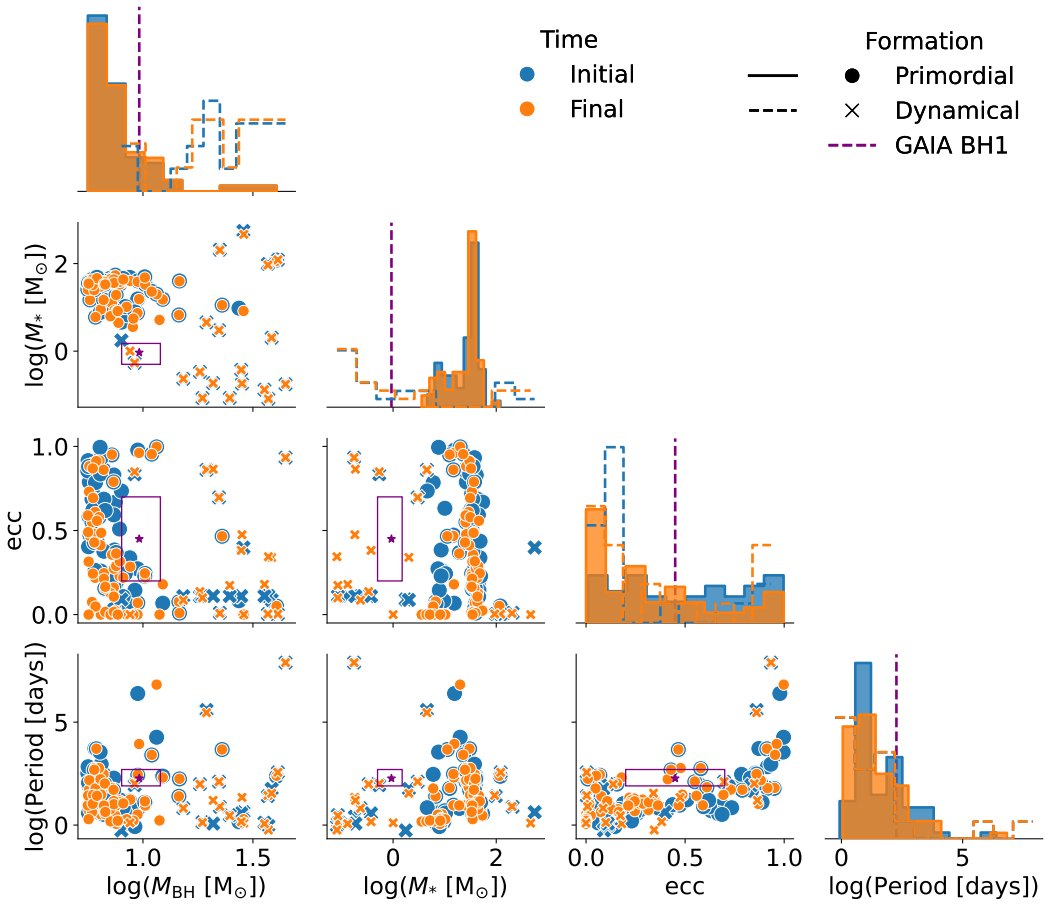


Figure 4.1: Component mass and orbital properties of the ejected BH-MS binaries. In the scatter(histogram) plots, dots(lines) and crosses(dashes) represent primordial binaries and dynamical binaries, respectively; binaries at the first BH-MS time are in blue and at the last BH-MS time in orange. The purple contours define the Gaia BH1 similarity region.

## 4.2 BH-MS binaries

In this section, we characterise the ejected BH-MS population; MS stars are defined following the `BSE` classification of stellar types in Hurley et al. (2002). The component mass and orbital properties of the ejected BH-MS binaries are shown in Fig. 4.1. We consider two evolutionary times when performing the analysis: (i) the first time the stellar component is on the MS, and (ii) the last time-step in which the stellar component is classified as a MS. The aim is to illustrate the range of parameter space that a system can explore throughout its lifetime as a BH-MS binary, considering that stellar evolution processes, tidal interactions, and mass transfer events may still influence the properties of the binary. The contours represent the 'region of similarity' in the parameter space for the Gaia BH1 system. They are defined by the following limits: $M_* \in [0.5, 1.5]$ $M_\odot$, $M_{\rm BH} \in [8, 12]$ $M_\odot$, $e \in [0.2, 0.7]$, $a \in [200, 600]$ $R_\odot$, $P \in [80, 500]$ days. These contours are much wider than the errors on the Gaia BH1-system parameters (reported in Table 4.1), typically smaller than 2%, and highlight the *Gaia BH1-like binaries* – for a similar analysis in lower mass cluster simulations see Rastello et al. (2023).

The distributions of the BH and MS star masses for dynamical and primordial binaries show that the two populations are well separated. For primordial binaries, the BH mass distribution is peaked around $M_{\rm BH} \simeq 7$ $M_\odot$, while for dynamically formed binaries the distribution is nearly uniform between 10 $M_\odot$ and 40 $M_\odot$. This discrepancy underlines the possibility for dynamically formed binaries to cover a wider range of mass ratios compared to primordial binaries. The MS mass distribution for dynamical and primordial binaries is also distinctly separated. The primordial binary distribution has a strong peak around $M_* \simeq 30$ $M_\odot$, while the dynamical population produces essentially no binaries near this peak, extending to both lower and higher masses and containing a large fraction of lower mass stars with a peak at around $M_* \simeq 0.45$ $M_\odot$. We find that 93% of the ejected BH-MS binaries are formed inside the cluster. It is important to clarify that we define "forming inside the cluster" with respect to the state of the binary at the time of ejection. If the binary is ejected as a BH-MS system then we say this has formed in the cluster. On the other hand if a binary is ejected as a MS-MS system, and subsequently one of the components collapses to form a BH, we class the resultant BH-MS binary as forming outside the cluster. The eccentricity and period distributions for primordial and dynamical binaries cover a similar range of values, with no differing features. Moreover, we do not find significant difference in the distributions between the initial and final time of the MS evolutionary stage.

Fig. 4.1 shows that the eccentricity distribution has a peak at $e \simeq 0$, and above $e \simeq 0$ the distribution appears nearly uniform. The peak could be due to a CE phase; 18% of BH-MS ejected system progenitors undergo a CE phase before ejection. As a caveat we note that post-CE systems might have eccentricities up to $\sim 0.2$, and that

the evolution in this phase remains uncertain (Kruckow et al., 2021). In addition to a CE phase, tidal forces in the binary contribute to the circularisation of the orbit (Hurley et al., 2002; Hut, 1981). The strength of both equilibrium and dynamical tides depends on the ratio between the radius of the star and the semi-major axis of the orbit ($R/a$), and the binary mass ratio. Given these scales, we can approximately track the impact of tides by searching for RLO events in the binary sample. During a RLO phase, the radius of one of the two stars (or both) strongly increases, enhancing the effects of tides and leading to orbital circularisation. We find that 68% of the ejected BH-MS binaries progenitors undergo at least one RLO phase before ejection. It is important to underline that all the BH-MS progenitors that undergo a CE phase, previously start a RLO overflow event. Therefore, the orbits of 26% of the systems that undergo a RLO is immediately circularised due to a CE phase. These binaries are the low eccentricity population shown in Fig. 4.1.

We note, however, that Sepinsky et al. (2007); Dosopoulou & Kalogera (2016a,b), showed that tidal interactions do not always result in rapid circularisation during the early stages of MT. As a result, MT at periastron in eccentric orbits may introduce significant eccentricities.

In addition, we underline that CE evolution and tides are not the only processes that affect the eccentricity distribution: the eccentricity distribution still remains nearly uniform due to kicks during BH formation (though attenuated in our prescription) or due to dynamical interactions in the cluster. Moreover, a more detailed analysis of the effect of tides and MT is needed to fully address their role in our models, but this is beyond the scope of this work.

After ejection, no BH-MS binary experiences a CE phase (the CE phase generally occurs as the star is leaving the MS). However, 32% of the ejected BH-MS had experienced at least one RLO event during the BH's formation; this shifts more binaries towards lower eccentricities in the final population, explaining the stronger peak at $e \sim 0$ in the orange distribution in Fig. 4.1.

As previously mentioned, the presence of a tertiary companion can alter the evolution of the inner BH-MS binary (or its progenitors), leading to a different evolutionary path. In addition, Tanikawa et al. (2023a) has shown that Gaia BH-like binaries are often found with an accompanying tertiary star. Therefore, we look for triple companions to the BH-MS binaries before the time of ejection. We find that 42% of the binaries have been in a stable triple system before they are ejected from the cluster. A *stable* triple is defined as a system that has an outer eccentricity $e < 1$. We find that 37% of the stable triples occur when the inner binary is a BH-MS. Moreover, in the majority of these systems (85%), the inner binary is dynamically formed. When analysing the properties of the triples in our models, we look at the last evolution snapshot in which the system is present in the simulation: they have an average semi-major axis ratio $a_{\rm in}/a_{\rm out} = 0.015$ (where $a_{\rm in}$ is the semi-major axis of the inner orbit and $a_{\rm out}$ of the outer orbit), and the average outer

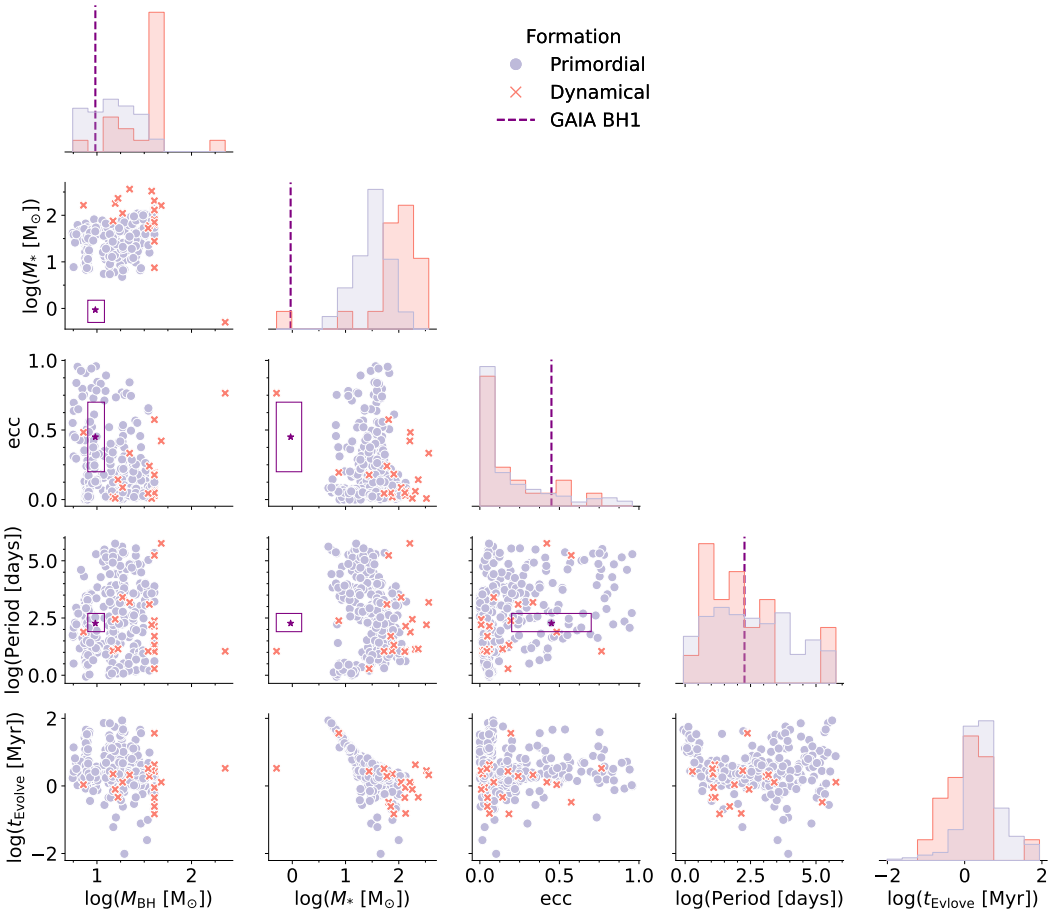


Figure 4.2: Properties of BH-MS retained binaries. Red dots and the blue crosses represent primordial binaries and dynamical binaries, respectively; the purple contours depict the Gaia BH1 similarity region. Here $t_{\rm evolve}$ represents the lifetime of the binary, i.e., the time between formation and when the stellar component evolves off the MS.

orbital eccentricity is $e = 0.93$.

Out of the 85 ejected BH-MS binaries, only 13 are found in stable triple systems. This implies that in at least 85% of cases, treating the binary as isolated is a reasonable approximation for its evolution after ejection from the cluster. We find that in 11 of the 13 ejected triple systems the inner binary is from the dynamical population. Thus, 58% of the ejected dynamical BH-MS binaries, and 3% of the ejected primordial BH-MS binaries are in a stable triple at ejection (See Table. 4.2 for total numbers). This suggests that the presence of a tertiary companion is a signature of dynamical formation in our models.

### 4.2.1 BH-MS retained binaries

We consider now the properties of the retained BH-MS binaries in our simulations, the properties of which are shown in Fig. 4.2. We note that we found no substantial change between the main properties of BH-MS binaries at the time of formation and at the last BH-MS time. Therefore, we show only the binaries taken at the final BH-MS time. However, we do keep the distinction between primordial and dynamical binaries and find that 94% of the binaries have a primordial origin, while 6% are formed dynamically.

The distributions shown in Fig. 4.2 are similar to those in Fig. 4.1. The BH mass distribution shows an evident cut-off at $\simeq 45$ $M_\odot$. This sharp mass limit is due to PPI SN that prevents the formation of any BHs above this mass value. The few binaries that cross the threshold have a dynamical origin, and are either formed through hierarchical BBH mergers or through the accretion of a massive star by a BH (see Chapter 3). It is important to point out that currently `PeTar` does not compute the GW recoil kick following a BBH merger. Therefore, some massive BHs formed through hierarchical mergers that we find, will likely be ejected from the cluster shortly after forming and thus not go on to form future binaries.

We note that the population of dynamically formed binaries contains a significant subpopulation with $M_* \lesssim 1$ $M_\odot$ – the median MS mass of this clump is $\simeq 0.44$ $M_\odot$. These binaries are formed early during the simulation and, in almost all cases, are immediately disrupted: the median formation time is $\simeq 4.11$ Myr from the beginning of the simulation, and the median disruption time is the same. Therefore, most of them undergo an immediate disruption after formation and are not shown in Fig. 4.2.

On the other hand, for ejected BH-MS binaries, the population of the corresponding low mass clump is made of 13 binaries: 3 binaries survive as BH-MS for an average time $\simeq 971$ Myr, the other 10 stay BH-MS until the end of the simulation. The most similar binary to Gaia BH1 (see Section 4.6.1) is part of this long-lived population.

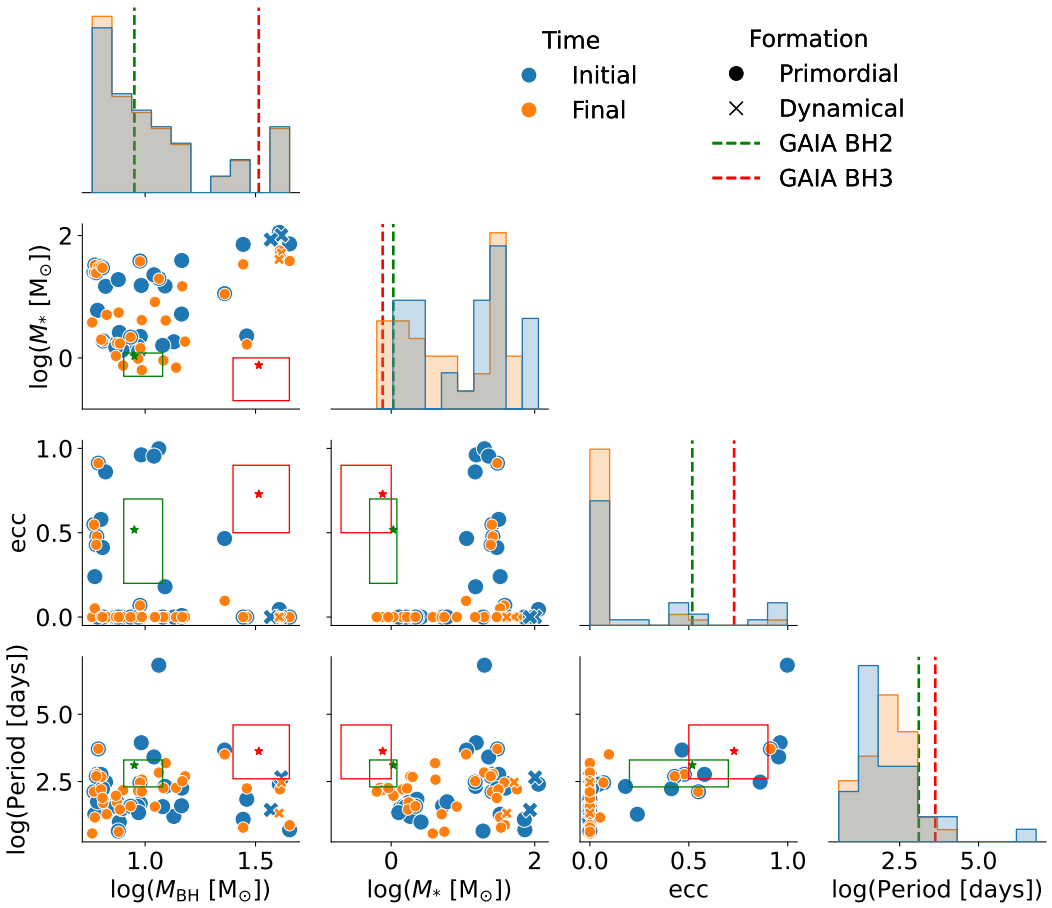


Figure 4.3: Properties of the BH-GS ejected binaries produced in our models. The dots and the crosses represent primordial binaries and dynamical binaries, respectively. The binaries at the first BH-GS time are shown in blue, the last BH-GS time is represented by orange colour. The green and red contours are the Gaia BH2 and Gaia BH3 similarity regions.

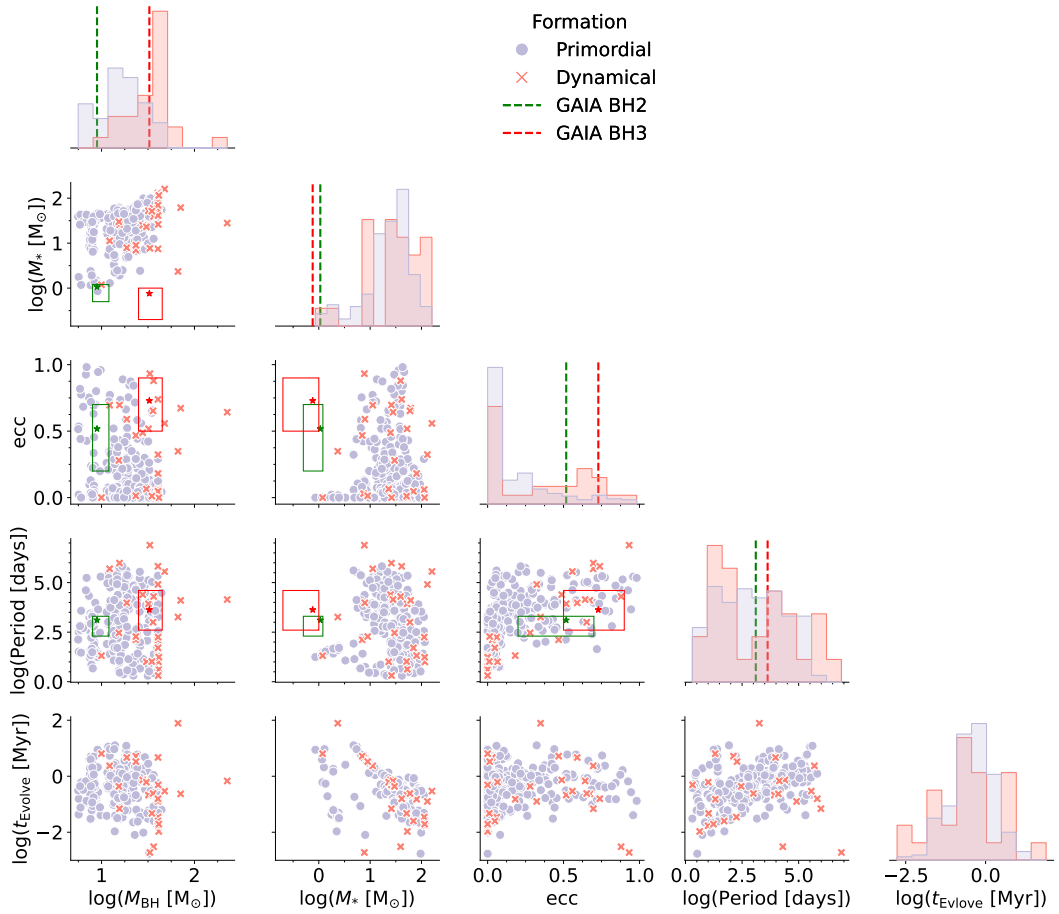


Figure 4.4: Properties of the retained BH-GS binaries. The red dots and the blue crosses represent primordial binaries and dynamical binaries respectively; the green and red contours are the Gaia BH2 and Gaia BH3 similarity region, respectively. Here $t_{\rm evolve}$ represents the lifetime of the binary, i.e., the time between formation and when the stellar component evolves off the giant phase.

## 4.3 BH-GS Binaries

In this section, we describe the BH-GS binary population in our models; GSs are defined following the `BSE` classification as stars with indices 3, 4, or 5 (e.g., Di Carlo et al., 2024). The results are reported in Fig. 4.3. The Gaia BH2 similarity region is defined as: $M_* \in [0.5, 1.2]$ $M_\odot$, $M_{BH} \in [8, 12]$ $M_\odot$, $e \in [0.2, 0.7]$, $a \in [238, 1088]$ $R_\odot$, $P \in [200, 2000]$ days, while for Gaia BH3 $M_* \in [0.2, 1]$ $M_\odot$, $M_{\rm BH} \in [25, 45]$ $M_\odot$, $e \in [0.5, 0.9]$, $a \in [560, 11760]$ $R_\odot$, $P \in [400, 40000]$ days; the same contours for Gaia BH3 are adopted in Marín Pina et al. (2024). All the ejected BH-GS binaries in our models are first ejected as BH-MS binaries and then evolve to a BH-GS binary outside the cluster.

From Fig. 4.3 it is evident that almost all the BH-GS ejected systems are from the primordial binary population with the BH mass peak at $M_{\rm BH} \simeq 8$ $M_\odot$, similarly to the BH-MS case; the eccentricity distribution has a strong peak near $e \simeq 0$. The only

systems that have $e > 0$ have a GS mass in the range $M_* \in [10, 35]$ $M_\odot$. Roughly half of these systems maintain a finite eccentricity up to the end of the BH-GS phase, in the other half the eccentricity drops to $e = 0$. As previously discussed for BH-MS binaries, the evolution towards $e \simeq 0$ is driven by tides and CE evolution. We find 63% of BH-GS progenitors undergo a RLO event that reduces the median of the eccentricities from $\simeq 0.21$ pre-RLO to $\simeq 0$ post-RLO, and 37% of the systems undergo a CE phase.

After ejection, 26% of BH-GS undergo a CE phase when they are classified as BH-GS and 49% experience a RLO phase. Moreover, in the vast majority of cases, the RLO phase occurs when the stellar companion is a HG star. Unlike the BH-MS case, the number of dynamically formed systems (2) is significantly lower compared to the primordial binaries (33), making it difficult to provide a meaningful comparison between the two populations.

As for the BH-MS binaries, we look for triple systems in our BH-GS sample. We consider the 35 ejected BH-GS binaries that are presented in Fig. 4.3 and we find that 37% of the BH-GS binaries have formed a stable triple system during their in-cluster evolution. These systems have a high average outer orbit eccentricity ($e = 0.94$), and an average semi-major axis ratio ($a_{\rm in}/a_{\rm out} = 0.004$).

Amongst the ejected population, we find that 13 BH-GS progenitors were in a stable triple system at the moment of ejection. These systems are the same triple systems with an inner BH-MS inner binary discussed in Section 4.2.

The BH-GS retained binaries are shown in Fig. 4.4. The distribution of BH masses show the same cut-off at 45 $M_\odot$ found in the BH-MS case (Fig. 4.2). The mass distribution of GSs is similar to the one found for BH-MS binaries, although we notice that the low mass part of the distribution is now mostly populated by primordial binaries. We note that the three BHs that have a mass above the PPI limit in the whole sample are part of the in-cluster population. The most massive amongst them has a mass of 225 $M_\odot$.

## 4.4 BH-WD binaries

In this section, we consider ejected BH-WD binaries. WD stars are defined following the `BSE` classification (indices 10, 11 and 12). The results are reported in Fig. 4.5.

The number of BH-WD binaries formed is given in Table 4.2; 22% of the ejected BH-WD binaries are formed before the ejection, the remaining are formed during the isolated evolution after ejection. Fig. 4.5 shows that, as expected, the properties of the binaries remain essentially the same during the lifetime of the systems. The BH mass distribution is peaked around $M_{\rm BH} \simeq 8$ $M_\odot$, with the exceptions being massive, dynamically formed systems. The WD masses are concentrated around $M_{\rm WD} \simeq 1.1$ $M_\odot$, with an extended lower mass tail. However, we note that this peak is likely strongly dependent on the max simulated time of our clusters (3 Gyr) since

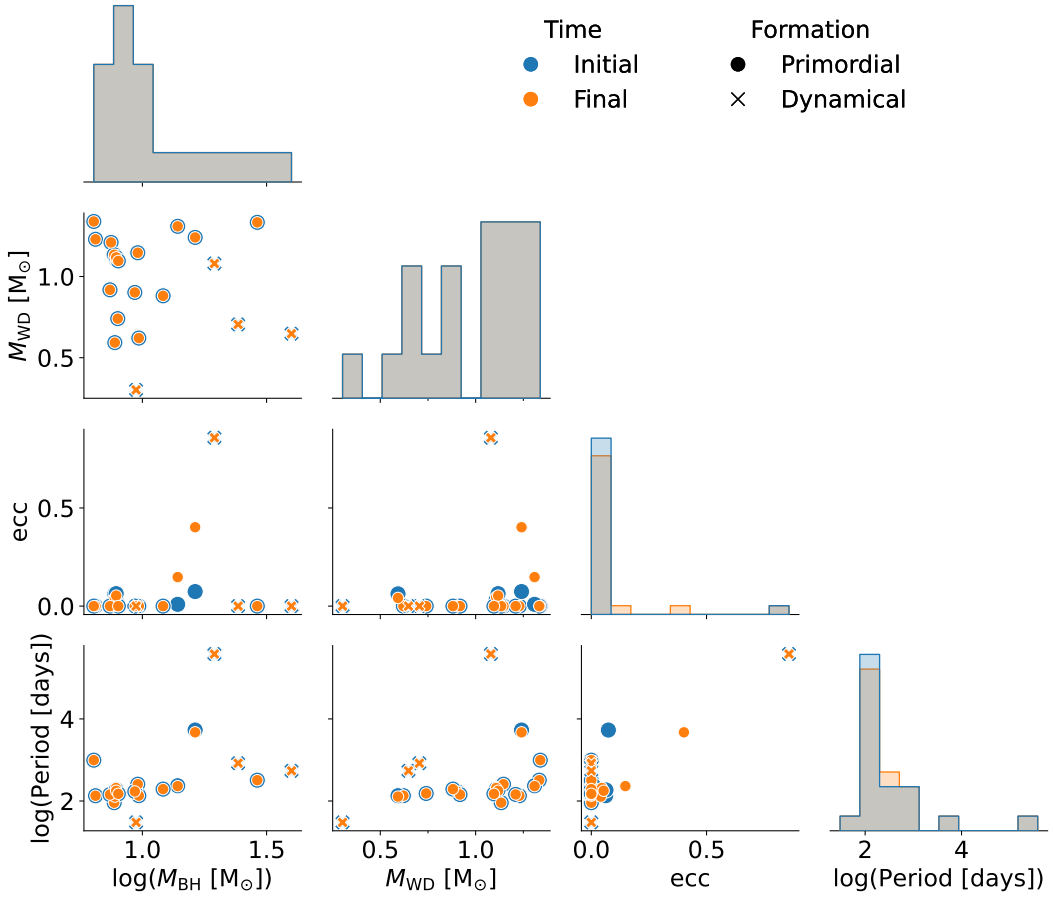


Figure 4.5: Properties of the BH-WD ejected binaries, the dots and the crosses represent primordial binaries and dynamical binaries respectively; the binaries at the first BH-WD time are shown in blue, the last BH-WD time is represented by orange colour.

there are many more low mass stars which have not had time to collapse into a WD. Similarly to the BH-MS and BH-GS systems, the eccentricity has a strong peak at $e \simeq 0$, and, as before, the reason are CE phase and tidal friction: 68% of the BH-WD progenitors experience at least one RLO event and 67% of the systems undergo a CE event before ejection, which reduces the eccentricity from a median $\simeq 0.18$ to $e \simeq 0$. During almost all the RLO events, the CE phase is present.

The percentage of BH-WD progenitors that undergo at least one CE is higher than for BH-MS and BH-GS. BH-WD binaries are more likely to undergo several CE and RLO phases during their evolution, therefore their eccentricity distribution is more strongly peaked at $e \sim 0$ than BH-MS and BH-GS binaries. Although, we note that the previously mentioned caveat should be considered here since BH-WD binaries that are formed after the current max simulation time will most likely form dynamically between a lone WD and BH. These binaries will then not experience CE or RLO phases.

The CE phase and tides alone could fully explain the eccentricity and period distributions in Fig. 4.5. There are two exceptions: a dynamically formed system and a primordial one. The former is formed dynamically, and its separation is sufficiently high to avoid CE or strong tides, the latter comes from the initial binary population, and is discussed below. We find that 19% of BH-WD systems are formed dynamically.

We study the possible impact of a tertiary in the formation of the ejected population of BH-WD systems: 4 (19%) BH-WD binaries have been in a stable triple system during their in-cluster evolution, with all the inner binaries from the primordial binary population. Only 1 BH-WD system progenitor was found in a stable triple system at the moment of ejection. The semi-major axis ratio at the last time the triple existed in the cluster model is $a_{\rm in}/a_{\rm out} = 0.04$, and the eccentricity of the outer orbit is $e = 0.95$.

The highly eccentric primordial binary mentioned previously is part of a stable triple during its in-cluster evolution: this system avoids a CE phase and the orbit becomes highly eccentric due to triple dynamics. In the other 3 stable triples, the inner binary undergoes a CE phase during which its orbit circularises and the period decreases. Because the distance of the tertiary to the inner binary is relatively large, it seems unlikely that after a CE phase the presence of the tertiary companion can significantly affect the binary evolution.

It should be stressed that the importance of the dynamical effects is strongly dependent on the characteristics of the triple system, such as the mass of the tertiary, the separation and the inclination. Moreover, the relativistic precession of the inner binary orbit can suppress the eccentricity evolution (Blaes et al., 2002), but this effect is not included in our simulations.

Finally, we looked for retained BH-WD binaries, and only found one dynamical binary with $M_{\rm WD} = 0.65$ M$_\odot$, $M_{\rm BH} = 67.92$ M$_\odot$, $e = 0.5$ and period = 10 days. Most BH-WD binaries that are formed in the models are immediately disrupted or

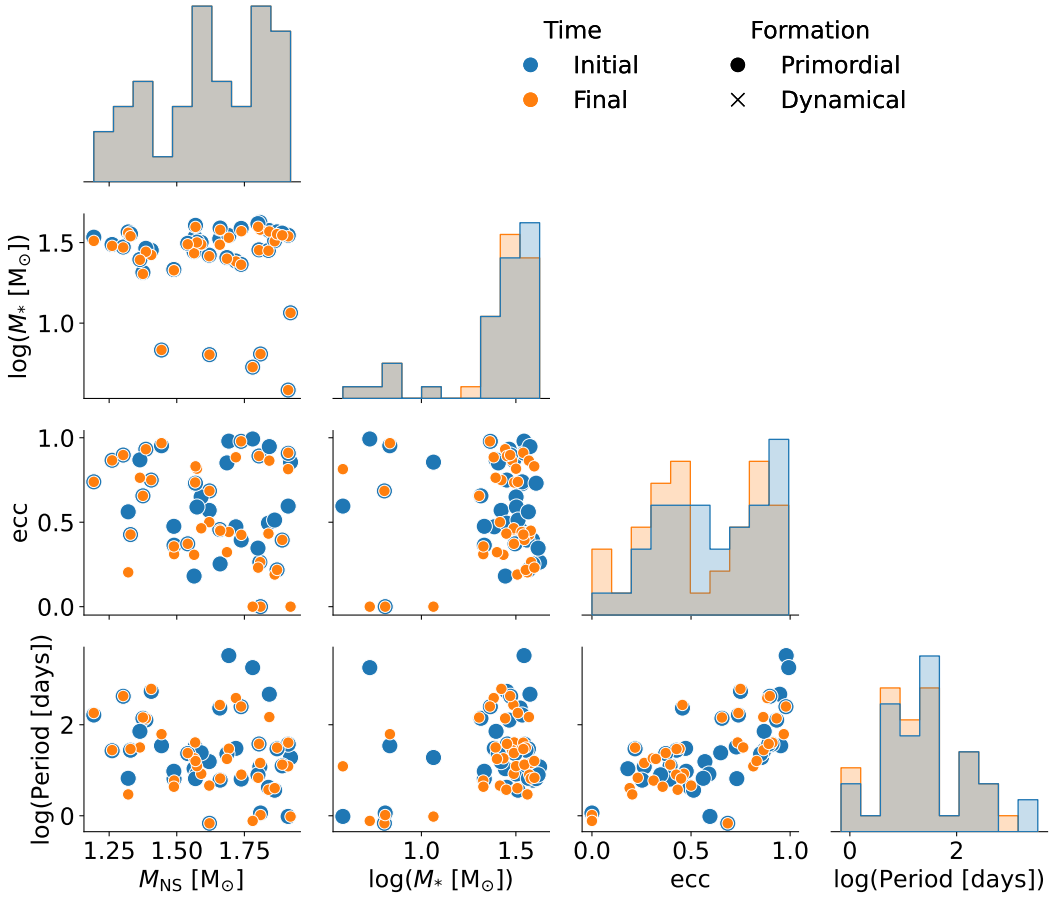


Figure 4.6: Properties of the ejected NS-S binaries. The binaries at the time the system is first classified as a NS-S are shown in blue, the last NS-S time is shown in orange. Note the absence of dynamically formed binaries.

ejected by dynamical encounters.

## 4.5 NS-S Binaries

In this section we consider NS-S binaries, where we account for both MS and GS companions. The binary properties for the ejected population are shown in Fig. 4.6. We find that in all but two of the ejected NS-S systems, the progenitor GS has collapsed to form the NS before the ejection from the cluster, and that they all come from the primordial binary population. The latter point can be explained by considering that it is more difficult for a NS to capture a companion through dynamical interactions as the central region of the cluster, where these interactions typically occur, is dominated by BHs until the end of the simulation.

The NS masses are distributed uniformly across the interval $M_{\rm NS} \in [1, 2]$ $M_\odot$, while the stellar mass distribution of the companion is peaked around $M_* \simeq 30$ $M_\odot$, with some less massive stars down to $M_* \approx 3$ $M_\odot$. The eccentricity distribution is closer to uniform compared to the BH-GS or BH-WD cases (see Section 4.3 and

Section 4.4). Several factors must be accounted for when considering the eccentricity distribution.

While NS-S progenitors maintain an almost circular orbit throughout their evolution, the NS natal kick increases the eccentricity of the binaries when the NS is formed. For this reason, we expect higher eccentricities than for BH-GS and BH-WD binaries. In the latter systems, CE and RLO occur shortly before the BH forms which circularises the binary, and then the reduced BH natal kick is not sufficient to produce a large spread in the eccentricity distribution. Moreover, due to the fallback prescription, a significant fraction of BHs can be formed without a natal kick.

We find that 37% of the ejected NS-S systems undergo a CE phase and that 97% experience a RLO event. In essentially all cases, the RLO and CE phases occur when the companion star is on the HG, and often the binary does not survive up to the GS phase of the companion. These behaviours explain the absence of the peak at $e \simeq 0$ in Fig. 4.6.

Although we find no ejected NS-S binaries in stable triple systems at the time of ejection, we do find that the 32% of the progenitor systems have been part of a stable triple system inside the cluster. We investigate these progenitor triple systems and find that they have an average semi-major axis ratio of $a_{\rm in}/a_{\rm out} = 0.0001$ – the smallest through all the type of triple systems studied in this article. In fact the average semi-major axis of the inner binary ($\simeq 100$ R$_\odot$) is more than five times smaller than for all the other triple systems previously mentioned ($\simeq 580$ R$_\odot$). Moreover, these NS-S progenitor triples have the largest average outer semi-major axis across all other triple systems, and the average outer eccentricity is $e_{\rm out} = 0.96$.

We show the properties of the retained NS-S binaries in Fig. 4.7 and similar to the ejected population, we find only systems from the primordial binary population. The distribution of the NS masses is uniform between 1.1 M$_\odot$ and 1.9 M$_\odot$, while the distribution of stellar masses (both MS and GS) is peaked around 30 M$_\odot$. The binary eccentricities are spread between 0 and 1, with a slight preference for high eccentricities likely due to the NS natal kick. The binary periods are found predominantly between 1 day and 100 days, peaking at around $\approx 18$ days. We only find 4 systems exceeding 100 days.

## 4.6 Application to Gaia Black holes

In this section we investigate the formation of Gaia BH-like systems (El-Badry et al., 2022, 2023b; El-Badry, 2024) in our simulations: We identify the top candidates within the sample, outline the formation pathways of these systems, and analyse the formation efficiencies of Gaia-like systems in our models. Similar studies can be found in Marín Pina et al. (2024), Rastello et al. (2023), Di Carlo et al. (2024) and Tanikawa et al. (2023a).

To quantify the capability of forming a certain type of systems in our simulations,

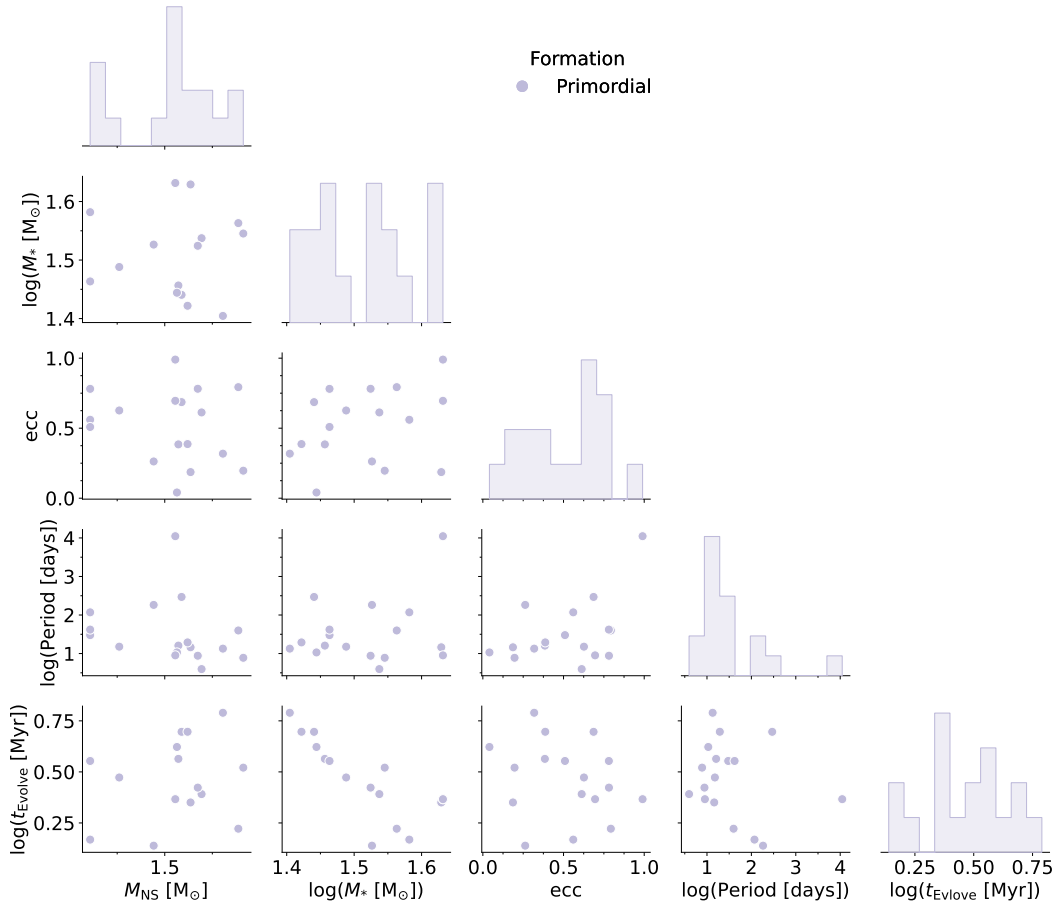


Figure 4.7: Properties of the retained NS-S binaries. We do not show the dynamically formed binaries as there are none in the sample. Here $t_{\rm evolve}$ represents the lifetime of the binary, i.e., the time between formation and when the stellar component evolves off the MS or giant phase.

we define the formation efficiency as:

$$\eta = N_{\rm BH-type}/M_{\rm tot} \ , \tag{4.1}$$

where $N_{\rm BH-type}$ is the number of binaries of a certain category (BH-MS, BH-GS or Gaia-like binaries) and $M_{\rm tot}$ is the total mass of the cluster in our simulations or of a certain type (e.g., clusters with the same metallicity or density). Here, Gaia-like binaries mean all binaries that fall within the contour similarity regions given in Fig. 4.1 and Fig. 4.3. As shown in these figures, there is no ejected binary that satisfies all observational constraints at once. It is also evident that the constraint on the eccentricity poses a strong limit for our sample. If we relax this analysis by removing completely the eccentricity constraint, we find that there are two systems that are within the Gaia BH1 similarity region, and two systems that lie within the Gaia BH2 similarity region. However, even after relaxing the eccentricity constraint, we do not find any Gaia BH3-like system and therefore only consider Gaia BH1 and BH2 in what follows.

The relaxation of the eccentricity constraint is justified by the considerable uncertainty in the prescription for binary eccentricity evolution within the `BSE` framework. In particular, after a phase of CE evolution the eccentricity of a binary is simply set to 0, which introduces very large uncertainties. On the other hand, the final period of a binary, which is also linked to the CE evolution, is computed using some known stellar prescriptions for its evolution during the CE. Whilst there are still uncertainties regarding these prescriptions we can be more confident with the final period value than the eccentricity value and thus opt to only relax the eccentricity constraint. Finally, we stress that for each system, we consider it within the similarity region if at any point during the evolutionary stage it is within the contours and not necessary at the first/last moment.

The two Gaia BH1-like ejected systems both have a dynamical formation. The first system is a dynamically formed binary from a dense ($\rho_{\rm h} = 10^5$ M$_\odot$ pc$^{-3}$), relatively low mass ($M_{\rm c} = 10^4$ M$_\odot$) cluster, with a sub-solar metallicity ($Z = 0.001$) and an initial binary population. The second system is also formed dynamically, and it is ejected from a low density ($\rho_{\rm h} = 1200$ M$_\odot$ pc$^{-3}$), intermediate mass ($M_{\rm c} = 10^5$ M$_\odot$) cluster, with sub-solar metallicity ($Z = 0.001$) and zero initial binary fraction (i.e. no primordial binaries). The second system is also the 'closest' to Gaia BH1 in parameter space, and it is further considered in 4.6.1. The efficiency for Gaia BH1-like systems considering the entire mass of the clusters ($M_{\rm tot} \simeq 4.6 \times 10^6$ M$_\odot$) is $\eta = 4.36 \times 10^{-7}$ M$_\odot^{-1}$ which is comparable to the value found by Rastello et al. (2023) in clusters with lower mass and density.

The two Gaia BH2-like systems have a primordial origin: the first system formed in a dense, intermediate mass cluster ($\rho_{\rm h} = 10^5$ M$_\odot$ pc$^{-3}$, $M_{\rm c} = 5 \times 10^4$ M$_\odot$), with sub-solar metallicity ($Z = 0.001$). This system is described in detail in section

4.6.2. The second system is also a primordial binary ejected from an intermediate dense cluster ($\rho_{\rm h} = 10^4$ M$_\odot$ pc$^{-3}$), with mass $M_{\rm c} = 10^5$ M$_\odot$, sub-solar metallicity ($Z = 0.001$). Considering the absence of a proper eccentricity constraint for these systems, it is important to underline that both Gaia BH2-like systems undergo at least one RLO and CE phase during their evolution. In particular, the second system escapes the cluster due to a BH natal kick. Its eccentricity at ejection is $e \simeq 0.5$, and it is subsequently circularised during a RLO event. We find that the formation efficiency for Gaia BH2-like systems is also $\eta = 4.36 \times 10^{-7}$ M$_\odot^{-1}$.

We quantify the formation efficiency of our models in producing BH-S binaries in Fig. 4.8. There we show the total production efficiency for all (ejected and retained) BH-S binaries and also for only ejected BH-S binaries. We then further plot the formation efficiency of ejected BH-MS and BH-GS binaries separately. We plot these efficiencies both as a function of $Z$ and $M_{\rm c}$, and separating clusters by $\rho_{\rm h}$. The efficiency shows a strong peak around $Z = 10^{-3}$, and decreases in high mass clusters for both ejected and retained binaries. There are no ejected or retained BH-S binaries in the highest mass clusters and there are two main reasons for this. First, the high mass of the cluster means a higher escape velocity, making it more difficult for binaries to be ejected in dynamical interactions. Secondly, the most massive simulations ($M_{\rm c} \geq 5 \times 10^5$ M$_\odot$) ran for a shorter time than the less massive ones ($\leq 608$ Myr), which leads to a lower number of binaries being produced dynamically per unit mass. Furthermore, we note that the efficiency production of ejected BH-S binaries increases with cluster density, but it remains nearly independent of density for the retained population. This suggests that retained BH-S binaries mostly form from the evolution of the primordial binary population with little effect from dynamics. Our previous analysis of the retained BH-MS and BH-GS binaries (Fig. 4.2 and Fig. 4.4 respectively) supports this since we show that they are predominantly formed from the primordial binary population.

### 4.6.1 Best Gaia BH1 match

When searching for Gaia BH1-like binaries, two distinct questions arise: is it *probable*, under our simulations, to form such a system, and is it *possible* at all to form the Gaia BH1 binary? The former adopts a statistical viewpoint, studying the density of simulated binaries within the defined similarity region. The later simply asks whether any single binary every resembles Gaia BH1 in our models, regardless of its rarity. In what follows we take this later approach. To identify the binary in our model that most closely resembles Gaia BH1, we follow Di Carlo et al. (2024). The distance between a point in the parameter space and a Gaia system is defined as $|x - x_{\rm Gaia}|/x_{\rm Gaia}$, where $x$ is the array of parameters of the binary and $x_{\rm Gaia}$ are the parameters for Gaia BH1 reported in Table 4.1. Following Di Carlo et al. (2024), we do not take the eccentricity of the binary into account for distance computation, as

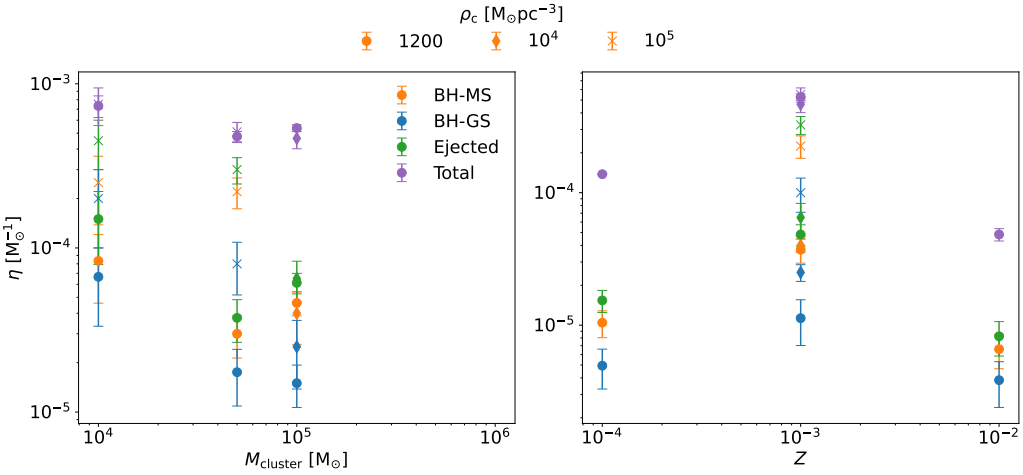


Figure 4.8: Here we show the formation efficiency of the ejected BH-S binaries split into BH-MS and BH-GS systems, as a function of initial cluster mass (left panel) and cluster metallicity (right panel). We distinguish between initial cluster half-mass density by varying marker symbols. For each cluster type we also show the formation efficiency for the ejected binary population and the total population (ejected + retained binaries).

| | $M_{BH}$ [$M_\odot$] | $M_*$ [$M_\odot$] | $a$ [$R_\odot$] | $P$ [days] | $e$ | $M_c$ [$M_\odot$] | $\rho_c$ [$M_\odot$ pc$^{-3}$] | $Z$ |
|---|---|---|---|---|---|---|---|---|
| Closest to Gaia BH1 | 9.16 | 0.54 | 197.32 | 103.12 | 0.85 | $10^5$ | 1200 | 0.001 |
| Closest to Gaia BH2 | 9.27 | 1.07 | 208.28 | 108.31 | 0.0 | $5 \times 10^4$ | $10^5$ | 0.001 |
| Closest to Gaia BH3 | 9.55 | 0.76 | 187.86 | 93.01 | 0.0 | $10^5$ | 1200 | 0.01 |

Table 4.3: Properties of the closest to Gaia BH systems as well as the key properties of the cluster where they are formed.

we assume that the eccentricities remain uncertain during `BSE` evolution as stated earlier.

The parameters of the closest system to Gaia BH1 are reported in Table 4.3. The system is a dynamically formed BH-MS binary which is formed early in the cluster ($\sim 6$ Myr) due to the encounter between a 12.7 $M_\odot$ naked He star and a low mass MS star ($M_* \simeq 0.5$ $M_\odot$). The He star rapidly ($t \simeq 0.02$ Myr) explodes in a SN, producing a kick that expands the orbit (from $a \simeq 32$ $R_\odot$ to $a \simeq 175$ $R_\odot$) and makes it highly eccentric (from $e \simeq 0$ to $e \simeq 0.85$). The SN remnant is a stellar-mass BH with $M_{BH} \simeq 9.5$ $M_\odot$. The system exists in the cluster for only $\approx 1$ Myr before it is ejected, with velocity $v_{esc} = 125.3$ km s$^{-1}$, and it continues to evolve in isolation. The binary then survives for nearly a Hubble time with its orbital properties largely unchanged. The evolution is schematically illustrated in Fig. 4.9. The estimate on the age of Gaia BH1 form Tanikawa et al. (2023a) is $\gtrsim 1$ Gyr. This is also compatible with our best candidate, whose properties after ejection are essentially unchanged up to a Hubble time.

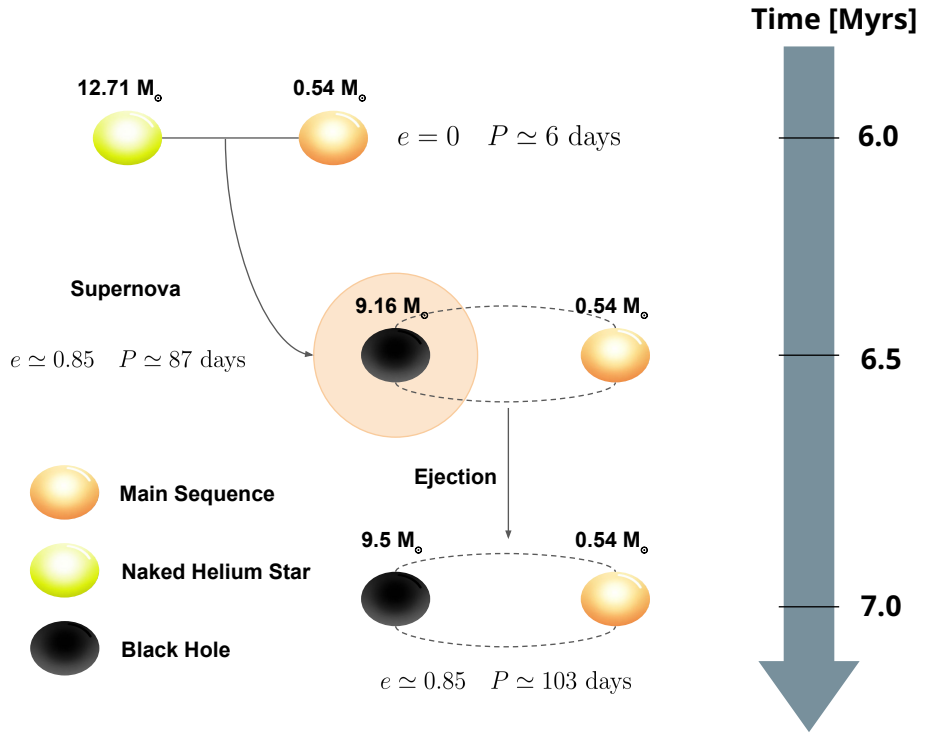


Figure 4.9: Formation pathway of the closest Gaia BH1-like system which was found in model Z2-M10-D3.

### 4.6.2 Best Gaia BH2 match

In this section, we describe the closest system to Gaia BH2, with the same criteria as in Section 4.6.1. The parameters of the closest system to Gaia BH2 are reported in Table 4.3.

The system is formed as a primordial binary in a dense cluster with $\rho_{\rm h} = 10^5$ M$_\odot$ pc$^{-3}$, $M_{\rm c} = 5 \times 10^4$ M$_\odot$, and $Z = 0.001$; the orbit has a medium eccentricity ($e = 0.43$) and a semi-major axis $a = 607.5$ R$_\odot$; the masses of the MS stars are $M_1 = 26.84$ M$_\odot$ and $M_2 = 6.80$ M$_\odot$. The most massive star quickly leaves the MS, starts burning He in the core evolving into a naked He star and losing 64% of its mass within 8 Myr. During this time, the more massive star fills its Roche lobe and then enters a CE phase that circularises and shrinks significantly the orbit ($e = 0.0$, $a = 11.2$ R$_\odot$). After 0.5 Myr, the massive star collapses and forms a BH with $M_{\rm BH} = 8.46$ M$_\odot$. Following another $\simeq 38.5$ Myr, the binary forms a stable triple with a tertiary BH ($M_{\rm BH} = 31.8$ M$_\odot$). The triple system is wide ($a_{\rm in}/a_{\rm out} \simeq 0.001$) and thus the inner binary orbital properties are not significantly perturbed by the tertiary. The binary is ejected from the cluster (with the tertiary still bound) as a BH-MS after 50 Myr, with an escape velocity $v_{\rm esc} = 11.4$ km s$^{-1}$. Soon after the ejection, the MS star crosses the HG, moving into the red giant phase and slowly stripping its envelope. During this phase, the mass loss from the evolving star widen

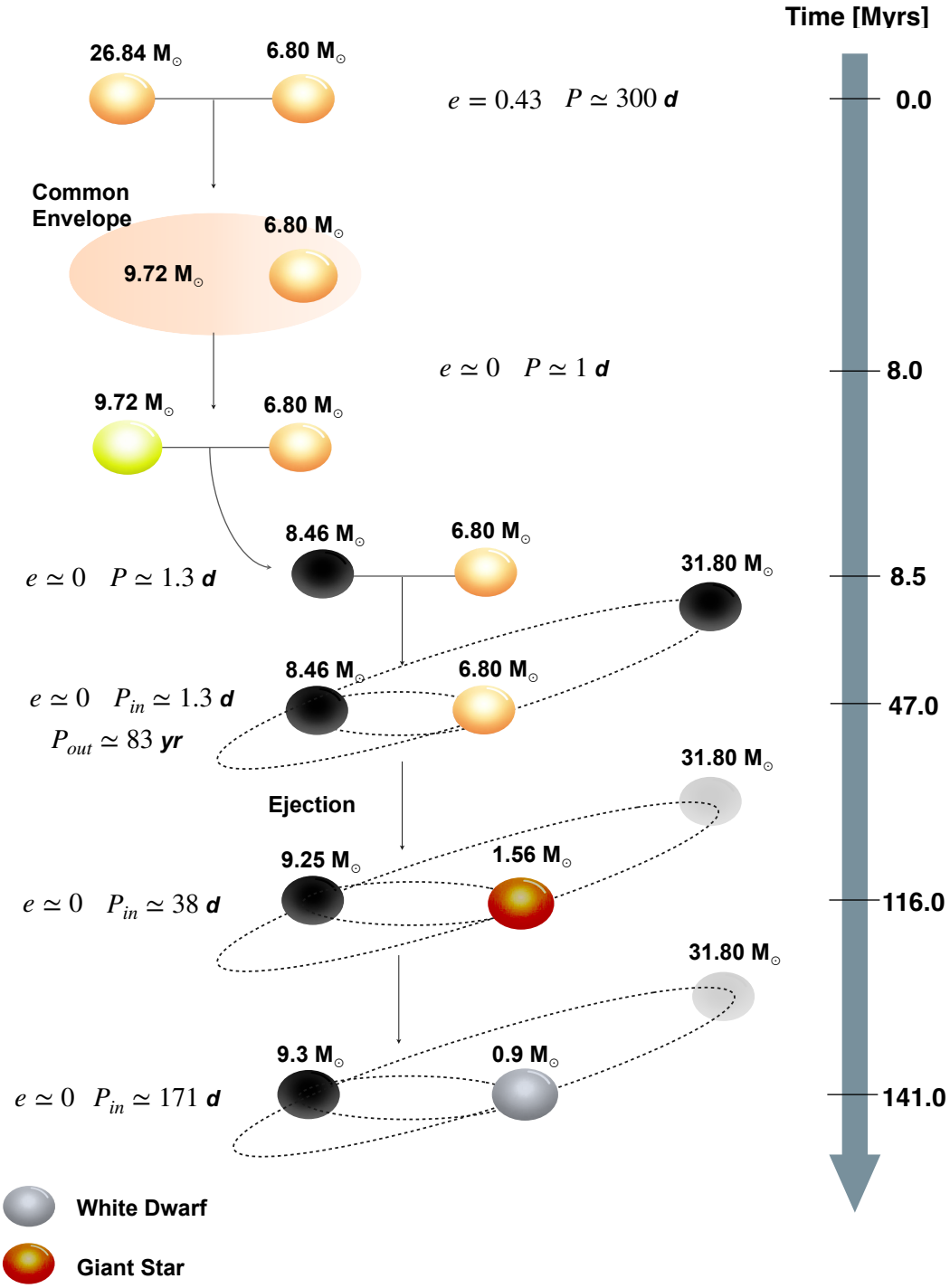


Figure 4.10: Formation pathway of the nearest Gaia BH2-like system; the inclination of the orbit is represented symbolically, with the actual inclination being 25°. The tertiary component after ejection is shaded to emphasise that evolution continues only for the inner binary, while the tertiary is disregarded post-ejection. This system is found in model Z2-M5-D5.

the orbit. Finally, 141 Myr from the start of the simulation, the star collapses into a Carbon-Oxygen WD with $M_{\rm WD} = 0.9$ M$_\odot$ in a circular orbit ($e \simeq 0$, $a = 281.4$ R$_\odot$, $P = 171.12$ days) with a BH of $M_{\rm BH} = 9.3$ M$_\odot$.

The schematic representation of this evolution is shown in Fig. 4.10. During the red giant phase, the properties of the system (reported at the closest moment in Table 4.3) are quite different from the ones measured for Gaia BH2. Moreover, the age of the system is $\simeq 116$ Myr, which is also different from the estimated age of Gaia BH2 ($\gtrsim 5$ Gyr).

# Chapter 5

# Conclusions

The goal of this thesis was to better understand the dynamics of COs within stellar clusters. Specifically, we aimed to explore how these dense stellar environments shape the BH and BBH populations, and how these populations contribute to the merging BBHs observed through GW detections. To achieve this, we employed both theoretical and numerical methods to model the formation and evolution of BHs, making predictions about the resultant populations. On the numerical side, we have utilised a variety of modern, highly sophisticated codes to simulate both the stellar evolution of single and binary stars, as well as the gravitational interactions within massive star clusters.

In this chapter we discuss in further detail the findings from the novel works presented in this thesis, highlighting the key conclusions from each.

## 5.1 The importance of primordial binaries

In Chapter 2 we have used the binary population synthesis code, `COMPAS` (Team COMPAS: Riley, J. et al., 2022; Vigna-Gómez et al., 2018; Stevenson et al., 2017) to characterise the population of BBHs that form through stellar processes in star clusters. Unlike dynamically formed BBHs, the properties (e.g., component masses, orbit) of such primordial binaries are set mostly by stellar evolution processes. After their formation, however, they can undergo dynamical interactions that change their orbit and their likelihood of becoming a detectable source of GW radiation. These binaries represent therefore a hybrid population, in the sense that they can be significantly affected by both stellar and dynamical processes.

We have presented simple analytical arguments together with binary evolution models and $N$-body simulations to study the formation and evolution of primordial BBHs in dense star clusters. These models represent a baseline for understanding their contribution to the population of merging BBHs detectable by LIGO-Virgo-Kagra. We briefly investigate how the choice of stellar ZAMS metallicity affects the binary properties of the BBHs that are formed. We then focus our efforts on

investigating the effect of placing the BBH and single BH populations in simplistic cluster models. Furthermore, we compare the kicks received during the SN; as well as the expected kicks due to many-body interactions, against a range of cluster escape velocities. From this, we estimate the fraction of BBHs and single BHs that could be retained within different-sized clusters, as well as the subpopulation of merging BBHs both inside and outside the cluster. Finally, we study the type of interactions these binaries are likely to experience when evolving in the dynamical environment of their parent cluster. The key conclusions we find are as follows:

(1) In clusters with escape velocity $v_{\rm esc} \lesssim 100$ km s$^{-1}$, BHs are predominantly found as BBH, with a significant fraction also being categorised as "hard" binaries. We expect therefore that primordial binaries might have a significant impact on the merger rate of BBHs formed in open and globular clusters. On the other hand, we expect their contribution to be smaller in higher velocity dispersion clusters such as nuclear star clusters.

(2) The retained BBH population can be further split into three distinct groups based on the binary separation compared to the ejection separation $a_{\rm ej}$, defined as the separation below which a dynamical interaction will eject the binary from the cluster.

- Pop I: These are binaries with $a < a_{\rm ej}$ that are so tightly bound that they either merge inside the cluster before an encounter can interfere with them, or they are ejected by the SN kick and merge outside the cluster.
- Pop II: These binaries also have $a \leq a_{\rm ej}$, however, they will experience a single interaction which ejects them from the cluster. This group may also merge in a Hubble time though is not defined to do so.
- Pop III: The final population are hard binaries with $a > a_{\rm ej}$ and will experience more than one interaction inside the cluster. This group has the most uncertain future as it could eventually be disrupted, become ejected or even merge.

(3) When further constraining Pop II and Pop III to those potentially merging in a Hubble time, we see that mergers in a cluster with $v_{\rm esc} \lesssim 100$ km s$^{-1}$ are predominantly Pop I and Pop II. Meanwhile, the Pop III mergers become dominant in the higher $v_{\rm esc}$ clusters.

(4) When using an $N$-body simulation code to evolve realistic cluster models, we find that the Pop I mergers are dominant with respect to the other two populations. Our models suggest that in clusters with escape velocity $v_{\rm esc} \leq 30$ km s$^{-1}$ dynamics play a secondary role in the production of BBH mergers.

(5) Interactions within the cluster are dominated by binary-binary encounters for cluster sizes up to $v_{\rm esc} \lesssim 100$ km s$^{-1}$ for $Z = 0.0001$, up to $v_{\rm esc} \lesssim 40$ km s$^{-1}$ for $Z = 0.001$, and up to $v_{\rm esc} \lesssim 10$ km s$^{-1}$ for Solar metallicity. This is of particular importance to Pop III BBHs which experience multiple interactions. For these, it becomes almost certain that at least one of the interactions they experience will be with another hard BBH.

In addition, we tested models with varied stellar evolution parameters to investigate how these new populations are impacted by the choice of evolution. Of particular note, we varied the BH natal kick prescription between a zero kick, fallback and reduced kick model. We find that in the zero kick case, Pop III becomes the dominant group down to $v_{\rm esc} = 4$ km s$^{-1}$. Whereas, in both the fallback and reduced kick models, Pop II become more significant at the small $v_{\rm esc}$ regime, with Pop III only rising to dominance at $v_{\rm esc} = 80$ km s$^{-1}$ with the reduced kicks, and $v_{\rm esc} = 14$ km s$^{-1}$ for the fallback model.

Our results indicate that primordial binaries can have a significant impact on the population of merging BBHs produced in dense star clusters. The initial BH population in clusters with sufficiently low escape velocities, $v_{\rm esc} \lesssim 30$ km s$^{-1}$, can be entirely in the form of hard BBHs that originate by stellar processes. The properties of the merging BBHs produced in these clusters are expected to be determined mostly by stellar evolution, with little or no effect from dynamics.

An implication is that the enhancement of the merger rate due to dynamics is expected to be negligible in these systems. In clusters with higher escape velocities, the primordial binary population becomes progressively less important. However, in the range $v_{\rm esc} \lesssim 100$ km s$^{-1}$, more than 10% of all BHs are still in hard binaries. A large fraction of these are so tight that they are ejected from the cluster after one dynamical interaction and then merge in the field. This population is of particular interest as their binary properties are set mostly by stellar evolution, but can include some influence due to the single interaction that ejects them. Finally, in higher escape velocity clusters, the single BH population becomes dominant as most of the binaries formed by stellar processes are soft and quickly disrupted.

## 5.2 BBHs in massive star clusters up to two million stars

Chapter 3 presented a detailed analysis on a suite of new $N$-body simulations produced using the $N-$body code `PeTar`. We produced 34 stellar clusters models which span a range of initial cluster masses from $10^4$ M$_\odot$ to $10^6$ M$_\odot$, initial half-mass density from 1200 M$_\odot$ pc$^{-3}$ to $10^5$ M$_\odot$ pc$^{-3}$ and metallicity values 0.0001, 0.001 and 0.01. For each cluster simulation, we ran two variations, one with no primordial binaries, and another with 100% binary fraction amongst massive ($\geq 20$ M$_\odot$) stars (see Table 3.1). We investigated the population of BBH mergers, identifying the impact

of the cluster environment and dynamical interactions on the binary properties and merger rate. We compared the results of our simulations to the predictions based on our theoretical understanding of BH dynamics in clusters. Our main conclusions are summarised in what follows:

(1) in clusters that start with a realistic population of massive binaries, the majority of BBH mergers originate from the primordial binary population rather than being paired by dynamical interactions (see Fig. 3.2, Fig. 3.3, and Fig. 3.4).

(2) This primordial BBH merger population is composed of two groups. One group is unaffected by the dynamical environment of the cluster either due to being ejected from it early on due to a natal kick, or because they are initially tight enough to merge before any interaction. The other group remains in the cluster for some time and undergoes at least one encounter which changes their orbital properties. We find that about 20% of all primordial BBH mergers are significantly *affected* by dynamics, in the sense that their merger timescale changes by at least a factor of 2 due to dynamical interactions (see Fig. 3.4). The two populations are characterised by statistically different distributions of component masses, delay times, eccentricities and mass-ratios (see Fig. 3.8).

(3) Due to the subdominant number of BBH mergers that are formed or affected by dynamical encounters in the cluster, the overall merger rate from the $N$-body models is essentially the same as if the cluster stars were evolved in isolation (see Fig. 3.5).

(4) Conclusion (3) depends on both the assumed prescription of CE evolution and metallicity. If binaries are assumed to merge when the CE is initiated by a star crossing the HG, then the merger rate for $Z = 0.01$ is increased due to dynamical interactions by $\simeq 3$ orders of magnitude. Under the same assumption and for $Z = 0.0001$, the effect of dynamics on the number of BBH mergers remains negligible (see Fig. 3.5).

(5) Almost all BBH mergers that are formed dynamically merge while the binary is still inside the parent cluster. This is in contrast to the theoretical expectation that about half of the mergers should occur outside the cluster. We argue that this is due to encounters involving systems with higher hierarchy such as triples and quadruples and/or multi-body interactions (beyond binary-binary and binary-single encounters) that are neglected in semi-analytical and Monte Carlo codes.

(6) We did not observe a clear correlation between the number of dynamically formed BBH mergers with cluster mass or density.

(7) We searched for higher multiplicity systems and found that $\simeq 10\%$ of the merging primordial BBHs are the inner binary of a stable triple BH system.

In contrast, dynamically formed BBHs can be found in approximately equal numbers in binaries and (stable) triples, as well as a small fraction $< 1\%$ in quadruples.

(8) We find several hierarchical BBH mergers with primary masses $> 45$ $M_\odot$, although these are overproduced in our models due to the lack of a GW recoil prescription in `PeTar`. However, we also find two instances of a first time BBH merger where the primary mass is above the PPI mass gap. Tracking the history of the most massive case we found the formation path for the primary involved several stellar mergers in succession, producing a massive star ($M = 397$ $M_\odot$) which is then swallowed by a BH ($M = 26.7$ $M_\odot$). This results in a very massive BH ($M = 225.2$ $M_\odot$) which then goes on to form a BBH and merge. This presents a potential mechanism for producing massive BHs well above the PPI mas limit.

The simulations presented in this work build on the collection of existing cluster simulations, exploring a more extreme region of parameter space than done before. In particular, we explored clusters with masses and densities that are comparable to those of present-day globular clusters and with an observationally motivated initial binary fraction. We compared the in-cluster merger fraction from our models with no primordial binaries, against previous studies. We show that our results are broadly consistent with the work of Banerjee et al. (2020) and Chattopadhyay et al. (2022), while they differ from Arca Sedda et al. (2024) who find a much lower in-cluster fraction. It is important to note that when comparing N-Body studies, the choice of initial conditions can significantly impact BBH formation and evolution. For example, in Arca Sedda et al. (2024), the mergers of primordial BBHs occur almost entirely outside the cluster, whereas in our work, we found a more even split between ejected and in-cluster mergers. One key difference between these studies lies in the initialization of the simulations, with Arca Sedda et al. (2024) opting for a lower cluster concentration ($W_0 = 6$). This implies a lower central escape velocity for a given cluster mass and density suggesting that binaries are susceptible to removal from the cluster through natal kicks, increasing the number of mergers amongst the ejected population.

Our findings have several significant implications. Firstly, they indicate that dense and massive clusters as the ones considered in this work might account for only a small portion of the overall BBH merger rate in the Universe. This is because most stars do not form within such dense clusters (Kruijssen, 2012; Krumholz et al., 2019), and the merger rate in our models with a primordial binary population is not substantially increased by the binary's presence in a dense cluster. We stress, however, that this conclusion is based on the results of massive binary evolution calculations that remain quite uncertain. Moreover, we showed that dynamically formed BBH mergers have larger masses and eccentricities than those formed in

isolation, making them a distinct and possibly identifiable population of mergers (see also Rodriguez & Loeb, 2018; Di Carlo et al., 2020; Torniamenti et al., 2022; Belczynski et al., 2022). The lack of a clear correlation between the number of dynamically formed BBH mergers with cluster properties is also interesting, and deserves further investigation which will require simulations extending the parameter space to even higher masses and densities.

Finally, our results cast doubts on conclusions derived from simplified models of cluster dynamics where binary-single and binary-binary encounters are assumed to be the main form of interactions leading to BBH mergers, as is discussed in Section 1.2.2. This is especially relevant to GW detections, as the fraction of eccentric BBH mergers originating from clusters is expected to scale with the number of in-cluster mergers. It is typically stated that $\sim 5\%$ of mergers from clusters will have a residual eccentricity at the moment they enter the $\gtrsim 10$ Hz window of current detectors (Samsing, 2018). The large number of in-cluster mergers found in our models is likely to imply a much higher number of eccentric mergers. Wile the reason for the discrepancy is unclear at the moment, we plan to carefully investigate this in future work.

## 5.3 Gaia BHs in massive clusters

The primary objective Chapter 4 was to characterise the population of ejected binaries from the `PeTar` cluster simulations presented in Chapter 3. We focussed our analysis on the ejected populations of BH-MS, BH-GS, BH-WD and NS-S binaries. After ejected from the cluster, these binaries are evolved in isolation up to a Hubble time using the `COSMIC` population synthesis code.

Compared to previous $N$-body simulations which focused on low mass clusters ($10^2$ M$_\odot \leq M_{\rm cl} \leq 10^4$ M$_\odot$), we have explored more massive clusters in the range $10^4$ M$_\odot \leq M_{\rm cl} \leq 10^6$ M$_\odot$. The formation of Gaia BH1 in low mass clusters was investigated in Rastello et al. (2023). They provide $3.5 \times 10^4$ direct $N$-body simulations of clusters with an initial mass between $3 \times 10^2$ M$_\odot$ and $3 \times 10^4$ M$_\odot$ at solar metallicity ($Z \simeq 0.02$) and define Gaia BH1 binaries with the similarity regions reported in Section 4.2. They find one ejected Gaia BH1 like system and compute a formation efficiency from all their models of $\eta \simeq 2 \times 10^{-7}$ M$_\odot^{-1}$. This result is compatible with the value of $\eta \simeq 4 \times 10^{-7}$ M$_\odot^{-1}$ found in our study. However, we note that we have not considered any eccentricity constraint and both our Gaia BH1 candidates come from sub-solar metallicity clusters ($Z = 0.001$).

Tanikawa et al. (2023a) studied the formation of Gaia BH1-like systems using 100 $N$-body simulations with cluster masses $\simeq 10^3$ M$_\odot$ and metallicity $Z = 0.005$. They define Gaia BH1-like binaries as those with properties such that $M_* \leq 1.1$ M$_\odot$, $P \in [100, 2000]$ days and $e \in [0.3, 0.9]$, and they find $\eta \simeq 10^{-5}$ M$_\odot^{-1}$. Adopting the same contours (and as before setting no constraint on eccentricity), for our BH-MS sample, we obtain a smaller $\eta \simeq 1.52 \times 10^{-6}$ M$_\odot^{-1}$. As previously underlined

in Rastello et al. (2023), the difference in the initial conditions in Tanikawa et al. (2023a) can have an impact on the number of Gaia BH-like systems and efficiencies. In particular, they set a binary fraction of 100% amongst all stars, whilst we opt for a total initial binary fraction of 0.25%, which is 100% amongst BH progenitors. Both these factors could explain the larger number of Gaia BH1-like systems formed in Tanikawa et al. (2023a).

Our simulations explore masses and densities similar to the models in Marín Pina et al. (2024), who used the Monte Carlo simulations from Kremer et al. (2020). Our total efficiency for high mass clusters ($M_{\rm c} = 10^5$ M$_\odot$) is $5 \times 10^{-5}$ M$_\odot^{-1}$, consistent although somewhat smaller than the efficiency of $\sim 10^{-4}$ M$_\odot^{-1}$ found by Marín Pina et al. (2024) for similar cluster masses and densities.

It is important to consider the impact of different initialisations of the stellar mass distribution across all of these studies. Half of our cluster models are initialised with all stars with $M_* \geq 20$ M$_\odot$ in a binary system, whilst in Rastello et al. (2023) all stars with $M_* \geq 5$ M$_\odot$ is in a binary. This choice causes the number of low mass binaries with no BH progenitor star to be higher in Rastello et al. (2023) compared to our simulations, possibly leading to a higher production efficiency of BH-S binaries through dynamical exchanges. In addition, Rastello et al. (2023) integrated their models for a larger number of initial cluster relaxation time, which was achievable due to their lower initial cluster masses. We note that for many of our models there still exists a significant BH population ($> 20$) within the cluster. Thus, these clusters can still be considered "alive" for the purposes of forming new binaries. Continuing the simulation of these clusters would likely produce many more Gaia-like BH systems (especially in our massive clusters with $\mathcal{O}(10^2)$ BHs still retained), increasing our formation efficiency.

We presented a qualitative analysis of the effects of RLO, CE evolution, tidal interactions and the presence of a stable tertiary on the eccentricity distribution of our population. We found that a large fraction of systems (always more than 20%) undergo a CE phase or a RLO event during the evolution, which leads to orbital circularisation and a peak at low eccentricities in the population distributions. The presence of a stable tertiary is found to be insufficient to significantly increase the inner binary eccentricity. On the other hand, the NS natal kick is the most efficient channel to produce eccentric binary systems with NS components.

We look for Gaia BH-like binaries in our sample (Section 4.6). We choose the regions of similarity for the three Gaia BH systems following previous literature (Rastello et al., 2023; Di Carlo et al., 2024; Tanikawa et al., 2023a; Marín Pina et al., 2024), and working under the assumption that the eccentricity of our systems is strongly influenced by the approximated prescription for CE and tides in `BSE` thus highly uncertain.

We present plausible candidates for Gaia BH1 and Gaia BH2 in our ejected sample, as well as a schematic of their formation pathways shown in Fig. 4.9 and

Fig. 4.10. We find that Gaia BH1-like systems can form dynamically in a dense and massive star cluster. For Gaia BH2-like systems, we find two binaries that are consistent with the properties of Gaia BH2. These binaries are formed from the primordial binary population and are not assembled dynamically. However, we find all Gaia-like binaries are formed in low-metallicity clusters, which is in contrast with the higher metallicity ([Fe/H]$\sim -0.2$) of the actual observed Gaia BH1 and Gaia BH2 systems. In regard to BH3, we found no system consistent with the properties of Gaia BH3, however see Marín Pina et al. (2024) who found Gaia BH3-like systems formed dynamically within globular clusters.

Our simulations indicate that clusters can generate a diverse population of binaries consisting of BH and stellar components. Many of these binaries align with at least some properties observed in Gaia BH binaries. The fact that only a limited number of our simulated systems align with all the characteristics of the observed systems is likely due to low-number statistics, given that our models generated only 120 ejected BH-stellar binaries, along with considerable theoretical uncertainties in modelling binary stellar evolution. Nevertheless, two key findings stand out. Firstly, most of the ejected BH-stellar binaries in our models originate from the primordial binary population (88% for BH-MS and 94% BH-GS binaries), rather than being formed dynamically. Secondly, dynamically formed binaries tend to occupy extreme regions of the parameter space, with distributions extending toward higher values of orbital periods and BH masses compared to primordial binaries. Moreover, the stellar masses in dynamically formed systems include both the heaviest and the lightest stars in our sample.

Finally, we investigate the dependence of the formation efficiency $\eta$ as a function of cluster properties finding comparable overall results with previous work by Rastello et al. (2023) and Marín Pina et al. (2024). Furthermore, we found a strong dependence of the formation efficiency on cluster metallicity and mass: a decreasing trend in accordance with Marín Pina et al. (2024), but with slightly lower values of $\eta$.

## 5.4 Future work

The work presented in this thesis represents another stepping stone towards the collective goal of better understanding the dynamical evolution of compact objects within star clusters. In particular, our new suite of $N$-body simulations adds to the growing catalogue of models produced by others in the field (e.g., Wang et al., 2015; Banerjee et al., 2020; Chattopadhyay et al., 2022; Arca Sedda et al., 2024) as we all strive to push these codes to there limits. Naturally, the work does not end here, and there are many exciting avenues for further studies which would better our understanding of star clusters in general as well as the specific results found in this work.

Regarding the simulations we have presented, there are two key areas for improvement. Firstly, although the `PeTar` code is incredibly sophisticated and a very powerful tool, the version available at the time of this work was purely Newtonian and lacked the inclusion of PN terms. Whilst this is unlikely to affect the majority of the dynamical encounters which are weak, distant interactions in the non-relativistic limit, the close encounters would be more significantly effected. In addition, we are missing out on exotic forms of dynamical interaction such as GW capture, whereby two BHs form a very highly eccentric binary following a particularly close encounter. These events are of particular interest since they typically form with very high eccentricity, and it is likely that they retain a non-negligible amount by the time they are emitting GWs in the observing band of our current detectors. GW recoil kicks are another process ignored in a purely Newtonian model, as they rely on the asymmetrical emission of GWs to impart a momentum kick on the remnant object. An understanding of these recoil kicks is paramount to understanding BH growth in clusters since it can effectively prohibit sequential BBH mergers. In this sense the number of BBH mergers we have presented here is likely an overestimate, with many of our hierarchical mergers being unlikely when recoil kicks are properly considered. The inclusion of PN terms in `PeTar` is something that is planned for future releases of the code.

The second direction for future work is the continued evolution of our $N$-body simulations such that every cluster is run until dissolution, or at least until several relaxation timescales have passed. This is especially true for our most massive cluster models, which, due to computational time constraints, could only be simulated to approximately one relaxation time, at which point they still contain a sizeable BH population. The limited physical simulation time is evident in the smaller number of BBH mergers found from the models, and it would be beneficial to study the population of merging BBHs throughout these clusters lifetimes. Moreover, further simulation studies exploring a wider range of initial cluster conditions, especially on the more massive side of things would go a long way in building our understanding of how very massive star clusters behave. How do they evolve? How do they couple to their BH populations? Can they facilitate the growth of intermediate mass BHs?

Finally, one of the key outcomes from this work was the importance of binary-binary and higher-order interactions within dense stellar clusters, especially with the introduction of a significant primordial binary population. Clearly, we require a stronger understanding of these complex, chaotic interactions, as they are important for the formation of stable triple and quadrupole BH systems, from which approximately half of all mergers from the dynamical binary population originated. These further studies could take the form of scattering experiments to investigate a wide range of possible encounter configurations, such as in Marín Pina & Gieles (2024), or draw from statistical theory to better understand the probability and rates of these types of interactions occurring in different stellar clusters.

# Bibliography


Aarseth S. J., 1963, Monthly Notices of the Royal Astronomical Society, 126, 223

Aarseth S. J., 1966, Monthly Notices of the Royal Astronomical Society, 132, 35

Aarseth S. J., 1999, Publications of the Astronomical Society of the Pacific, 111, 1333

Aarseth S. J., 2012, Monthly Notices of the Royal Astronomical Society, 422, 841

Aarseth S. J., Aarseth S. J., 2003, Gravitational N-body simulations: tools and algorithms. Cambridge University Press

Aarseth S., Heggie D., 1976, Astronomy and Astrophysics, vol. 53, no. 2, Dec. 1976, p. 259-265. Research supported by Trinity College., 53, 259

Aarseth S. J., Heggie D. C., 1998, Monthly Notices of the Royal Astronomical Society, 297, 794

Abbott B. P., et al., 2016a, Phys. Rev. Lett., 116, 061102

Abbott B. P., et al., 2016b, Physical review letters, 116, 241102

Abbott B. P., et al., 2019, Phys. Rev. X, 9, 031040

Abbott R., et al., 2021, Physical Review X, 11, 021053

Anagnostou O., Trenti M., Melatos A., 2020, Publications of the Astronomical Society of Australia, 37, e044

Antognini J. M. O., Thompson T. A., 2016, Monthly Notices of the Royal Astronomical Society, 456, 4219

Antonini F., Gieles M., 2020a, Physical Review D, 102, 123016

Antonini F., Gieles M., 2020b, Monthly Notices of the Royal Astronomical Society, 492, 2936

Antonini F., Perets H. B., 2012, The Astrophysical Journal, 757, 27

Antonini F., Rasio F. A., 2016, The Astrophysical Journal, 831, 187

Antonini F., Gieles M., Gualandris A., 2019, Monthly Notices of the Royal Astronomical Society, 486, 5008

Arca Sedda M., Amaro Seoane P., Chen X., 2021, A&A, 652, A54

Arca Sedda M., et al., 2023b, The Dragon-II simulations – I. Evolution of single and binary compact objects in star clusters with up to 1 million stars, `http://arxiv.org/abs/2307.04805`

Arca Sedda M., Kamlah A. W. H., Spurzem R., Rizzuto F. P., Giersz M., Naab T., Berczik P., 2023a, The Dragon-II simulations – III. Compact binary mergers in clusters with up to 1 million stars: mass, spin, eccentricity, merger rate and pair instability supernovae rate, `http://arxiv.org/abs/2307.04807`

Arca Sedda M., Kamlah A. W. H., Spurzem R., Rizzuto F. P., Naab T., Giersz M., Berczik P., 2023c, Monthly Notices of the Royal Astronomical Society, 526, 429

Arca Sedda M., Kamlah A. W., Spurzem R., Rizzuto F. P., Giersz M., Naab T., Berczik P., 2024, Monthly Notices of the Royal Astronomical Society, 528, 5140

Arca sedda M., Kamlah A. W. H., Spurzem R., Rizzuto F. P., Giersz M., Naab T., Berczik P., 2024, Monthly Notices of the Royal Astronomical Society, 528, 5140

Askar A., Szkudlarek M., Gondek-Rosińska D., Giersz M., Bulik T., 2017, Monthly Notices of the Royal Astronomical Society: Letters, 464, L36

Atallah D., Trani A. A., Kremer K., Weatherford N. C., Fragione G., Spera M., Rasio F. A., 2023, Monthly Notices of the Royal Astronomical Society, 523, 4227

Atallah D., Weatherford N. C., Trani A. A., Rasio F. A., 2024, The Astrophysical Journal, 970, 112

Balbinot, E. et al., 2024, A&A, 687, L3

Banerjee S., 2017, Monthly Notices of the Royal Astronomical Society, p. stw3392

Banerjee S., 2020, Monthly Notices of the Royal Astronomical Society, 500, 3002

Banerjee S., 2022, Astronomy & Astrophysics, 665, A20

Banerjee S., Belczynski K., Fryer C. L., Berczik P., Hurley J. R., Spurzem R., Wang L., 2020, Astronomy & Astrophysics, 639, A41

Barber J., Antonini F., 2025, Monthly Notices of the Royal Astronomical Society, p. staf279

Barber J., Chattopadhyay D., Antonini F., 2023, Monthly Notices of the Royal Astronomical Society, 527, 7363

Barkat Z., Rakavy G., Sack N., 1967, Physical Review Letters, 18, 379

Barnes J., Hut P., 1986, Nature, 324, 446

Bartos I., Kocsis B., Haiman Z., Márka S., 2017, The Astrophysical Journal, 835, 165

Belczynski K., Kalogera V., Bulik T., 2002, The Astrophysical Journal, 572, 407

Belczynski K., Bulik T., Fryer C. L., Ruiter A., Valsecchi F., Vink J. S., Hurley J. R., 2010, The Astrophysical Journal, 714, 1217

Belczynski K., et al., 2016, Astronomy & Astrophysics, 594, A97

Belczynski K., et al., 2020, åp, 636, A104

Belczynski K., Doctor Z., Zevin M., Olejak A., Banerje S., Chattopadhyay D., 2022, The Astrophysical Journal, 935, 126

Bhattacharya D., van den Heuvel E. P. J., 1991, Physics Reports, 203, 1

Binney J., Tremaine S., 1987, Galactic dynamics

Binney J., Tremaine S., 2008, Galactic Dynamics: Second Edition

Blaauw A., 1961, Bulletin of the Astronomical Institutes of the Netherlands, 15, 265

Blaes O., Lee M. H., Socrates A., 2002, The Astrophysical Journal, 578, 775

Bond J., Arnett W., Carr B. J., 1984b, Astrophysical Journal, Part 1 (ISSN 0004-637X), vol. 280, May 15, 1984, p. 825-847. Research supported by the Science and Engineering Research Council., 280, 825

Bond J. R., Arnett W. D., Carr B. J., 1984a, ApJ, 280, 825

Bowyer S., Byram E. T., Chubb T. A., Friedman H., 1965, Science, 147, 394

Brandt N., Podsiadlowski P., 1995, Monthly Notices of the Royal Astronomical Society, 274, 461

Breen P. G., Heggie D. C., 2013, Monthly Notices of the Royal Astronomical Society, 432, 2779

Breivik K., et al., 2020, The Astrophysical Journal, 898, 71

Broekgaarden F. S., et al., 2021, Monthly Notices of the Royal Astronomical Society, 508, 5028

Carr B. J., Hawking S. W., 1974, Monthly Notices of the Royal Astronomical Society, 168, 399

Carr B., Kühnel F., Sandstad M., 2016, Physical Review D, 94, 083504

Chakrabarti S., et al., 2023, The Astronomical Journal, 166, 6

Chandrasekhar S., 1943, ApJ, 97, 255

Chao W. Z., 1984, Phys. Rev. D, 30, 286

Chatterjee S., Fregeau J. M., Umbreit S., Rasio F. A., 2010, The Astrophysical Journal, 719, 915

Chattopadhyay D., Stevenson S., Hurley J. R., Rossi L. J., Flynn C., 2020, Monthly Notices of the Royal Astronomical Society, 494, 1587

Chattopadhyay D., Hurley J., Stevenson S., Raidani A., 2022, Monthly Notices of the Royal Astronomical Society, 513, 4527

Chattopadhyay D., Stegmann J., Antonini F., Barber J., Romero-Shaw I. M., 2023, Monthly Notices of the Royal Astronomical Society, 526, 4908

Chawla C., Chatterjee S., Breivik K., Moorthy C. K., Andrews J. J., Sanderson R. E., 2022, The Astrophysical Journal, 931, 107

Chen K.-J., Heger A., Woosley S., Almgren A., Whalen D. J., 2014, ApJ, 792, 44

Choudhury S., Sami M., 2025, Physical Research, 1103, 1

Coleman Miller M., Hamilton D. P., 2002, Monthly Notices of the Royal Astronomical Society, 330, 232

Costa G., Bressan A., Mapelli M., Marigo P., Iorio G., Spera M., 2021, Monthly Notices of the Royal Astronomical Society, 501, 4514

De Kool M., 1990, The Astrophysical Journal, 358, 189

De Mink S., Belczynski K., 2015, The Astrophysical Journal, 814, 58

Dehnen W., Read J. I., 2011, The European Physical Journal Plus, 126, 55

Di Carlo U. N., Giacobbo N., Mapelli M., Pasquato M., Spera M., Wang L., Haardt F., 2019, Monthly Notices of the Royal Astronomical Society, 487, 2947

Di Carlo U. N., et al., 2020, Monthly Notices of the Royal Astronomical Society, 498, 495

Di Carlo U. N., et al., 2021, Monthly Notices of the Royal Astronomical Society, 507, 5132

Di Carlo U. N., Agrawal P., Rodriguez C. L., Breivik K., 2024, The Astrophysical Journal, 965, 22

Djorgovski S., King I. R., 1986, ApJ, 305, L61

Dominik M., Belczynski K., Fryer C., Holz D. E., Berti E., Bulik T., Mandel I., O'shaughnessy R., 2012, The Astrophysical Journal, 759, 52

Dosopoulou F., Kalogera V., 2016a, The Astrophysical Journal, 825, 70

Dosopoulou F., Kalogera V., 2016b, The Astrophysical Journal, 825, 71

Duquennoy A., Mayor M., 1991, åp, 248, 485

Eggleton P., 2006, Evolutionary Processes in Binary and Multiple Stars

Einstein A., 1915, Preussische Akademie der Wissenschaften, Sitzungsberichte

Einstein A., et al., 1905, Annalen der physik, 17, 891

El-Badry K., 2024, The Open Journal of Astrophysics, 7

El-Badry K., et al., 2022, Monthly Notices of the Royal Astronomical Society, 518, 1057

El-Badry K., et al., 2023a, Monthly Notices of the Royal Astronomical Society, 518, 1057

El-Badry K., et al., 2023b, Monthly Notices of the Royal Astronomical Society, 521, 4323

Event Horizon Telescope Collaboration et al., 2019, ApJ, 875, L1

Fabj G., Samsing J., 2024, Monthly Notices of the Royal Astronomical Society, p. stae2499

Fantoccoli F., Barber J., Dosopoulou F., Chattopadhyay D., Antonini F., 2025, Monthly Notices of the Royal Astronomical Society, 538, 243

Farmer R., Renzo M., de Mink S. E., Marchant P., Justham S., 2019, ApJ, 887, 53

Farr W. M., Sravan N., Cantrell A., Kreidberg L., Bailyn C. D., Mandel I., Kalogera V., 2011, The Astrophysical Journal, 741, 103

Forastier B. R., Pina D. M., Gieles M., Zwart S. P., Antonini F., 2024, Binary-single interactions with different mass ratios, `http://arxiv.org/abs/2405.16999`

Ford E. B., Kozinsky B., Rasio F. A., 2000, The Astrophysical Journal, 535, 385

Fregeau J. M., Rasio F. A., 2007, The Astrophysical Journal, 658, 1047

Fregeau J. M., Cheung P., Portegies Zwart S., Rasio F., 2004, Monthly Notices of the Royal Astronomical Society, 352, 1

Fryer C. L., 1999, The Astrophysical Journal, 522, 413

Fryer C. L., Belczynski K., Wiktorowicz G., Dominik M., Kalogera V., Holz D. E., 2012, The Astrophysical Journal, 749, 91

Fuller J., Ma L., 2019, The Astrophysical Journal Letters, 881, L1

Fuller J., Piro A. L., Jermyn A. S., 2019, Monthly Notices of the Royal Astronomical Society, 485, 3661

Gaia Collaboration et al., 2024, Astronomy & Astrophysics, 686, L2

Garba L. G., Kassim H. A., Yusof N., 2022, Brazilian Journal of Physics, 52, 79

Giacobbo N., Mapelli M., 2018, Monthly Notices of the Royal Astronomical Society, 480, 2011

Giacobbo N., Mapelli M., Spera M., 2018, Monthly Notices of the Royal Astronomical Society, 474, 2959

Gieles M., Heggie D. C., Zhao H., 2011, Monthly Notices of the Royal Astronomical Society, 413, 2509

Giersz M., 1998, Monthly Notices of the Royal Astronomical Society, 298, 1239

Giersz M., 2006, Monthly Notices of the Royal Astronomical Society, 371, 484

Giersz M., Spurzem R., 2000, Monthly Notices of the Royal Astronomical Society, 317, 581

Giersz M., Heggie D. C., Hurley J. R., 2008, Monthly Notices of the Royal Astronomical Society, 388, 429

Giesers B., et al., 2018, Monthly Notices of the Royal Astronomical Society: Letters, 475, L15

Giesers B., et al., 2019, Astronomy & Astrophysics, 632, A3

Gilkis A., Mazeh T., 2024, Monthly Notices of the Royal Astronomical Society: Letters, 535, L44

Ginat Y. B., Perets H. B., 2024, Monthly Notices of the Royal Astronomical Society, 531, 739

Glanz H., Perets H. B., 2021, Monthly Notices of the Royal Astronomical Society, 507, 2659

González E., Kremer K., Chatterjee S., Fragione G., Rodriguez C. L., Weatherford N. C., Ye C. S., Rasio F. A., 2021, The Astrophysical Journal, 908, L29

Goodman J., Hut P., 1985, Dynamics of Star Clusters, 113

Goodman J., Hut P., 1989, Nature, 339, 40

Goodman J., Hut P., 1993, ApJ, 403, 271

Goswami S., Umbreit S., Bierbaum M., Rasio F. A., 2012, The Astrophysical Journal, 752, 43

Gröbner M., Ishibashi W., Tiwari S., Haney M., Jetzer P., 2020, A&A, 638, A119

Harris W. E., 2010, arXiv preprint arXiv:1012.3224

Harris W. E., Whitmore B. C., Karakla D., Okoń W., Baum W. A., Hanes D. A., Kavelaars J., 2006, The Astrophysical Journal, 636, 90

Heger A., Fryer C. L., Woosley S. E., Langer N., Hartmann D. H., 2003, ApJ, 591, 288

Heggie D. C., 1975, Monthly Notices of the Royal Astronomical Society, 173, 729

Heggie D. C., Hut P., 1993, Astrophysical Journal Supplement Series (ISSN 0067-0049), vol. 85, no. 2, p. 347-409., 85, 347

Heggie D., Hut P., 2003, The Gravitational Million-Body Problem: A Multidisciplinary Approach to Star Cluster Dynamics

Heggie D. C., Trenti M., Hut P., 2006, Monthly Notices of the Royal Astronomical Society, 368, 677

Hénon M., 1971a, in International Astronomical Union Colloquium. pp 151–167

Hénon M., 1971b, Astrophysics and Space Science, 13, 284

Hénon M., 1975, in Symposium-International Astronomical Union. pp 133–149

Hills J., 1975, Astronomical Journal, vol. 80, Oct. 1975, p. 809-825., 80, 809

Hills J. G., 1983, The Astrophysical Journal, 267, 322

Hobbs G., Lorimer D. R., Lyne A. G., Kramer M., 2005, Monthly Notices of the Royal Astronomical Society, 360, 974

Hockney R. W., Eastwood J. W., 1988, Computer simulation using particles. crc Press

Holley-Bockelmann K., Gültekin K., Shoemaker D., Yunes N., 2008, The Astrophysical Journal, 686, 829

Hong J., Vesperini E., Askar A., Giersz M., Szkudlarek M., Bulik T., 2018, Monthly Notices of the Royal Astronomical Society, 480, 5645

Hurley J. R., Pols O. R., Tout C. A., 2000, Monthly Notices of the Royal Astronomical Society, 315, 543

Hurley J. R., Tout C. A., Pols O. R., 2002, Monthly Notices of the Royal Astronomical Society, 329, 897

Hut P., 1981, A&A, 99, 126

Hut P., Bahcall J. N., 1983, Astrophysical Journal, Part 1 (ISSN 0004-637X), vol. 268, May 1, 1983, p. 319-341., 268, 319

Hypki A., Giersz M., 2013, Monthly Notices of the Royal Astronomical Society, 429, 1221

Hénon M., 1961, in Annales d'Astrophysique. p. 369

Hénon M., 1965, Annales d'Astrophysique, 28, 499

Iorio G., et al., 2024, The boring history of Gaia BH3 from isolated binary evolution (arXiv:2404.17568), https://arxiv.org/abs/2404.17568

Ivanova N., et al., 2013, The Astronomy and Astrophysics Review, 21, 59

Iwasawa M., Portegies Zwart S., Makino J., 2015, Computational Astrophysics and Cosmology, 2, 6

Iwasawa M., Tanikawa A., Hosono N., Nitadori K., Muranushi T., Makino J., 2016, Publications of the Astronomical Society of Japan, 68, 54

Iwasawa M., Oshino S., Fujii M. S., Hori Y., 2017, Publications of the Astronomical Society of Japan, 69, 81

Iwasawa M., Namekata D., Nitadori K., Nomura K., Wang L., Tsubouchi M., Makino J., 2020, Publications of the Astronomical Society of Japan, 72, 13

Joshi K. J., Rasio F. A., Zwart S. P., 2000, The Astrophysical Journal, 540, 969

Joshi K. J., Nave C. P., Rasio F. A., 2001, The Astrophysical Journal, 550, 691

Kalogera V., 1996, The Astrophysical Journal, 471, 352

King I. R., 1966, AJ, 71, 64

Kormendy J., 2013, in Thomas D., Pasquali A., Ferreras I., eds, IAU Symposium Vol. 295, The Intriguing Life of Massive Galaxies. pp 241–256, doi:10.1017/S174392131300495X

Kotko I., Banerjee S., Belczynski K., 2024, Monthly Notices of the Royal Astronomical Society, 535, 3577

Kremer K., et al., 2020, The Astrophysical Journal Supplement Series, 247, 48

Kroupa P., 2001, Monthly Notices of the Royal Astronomical Society, 322, 231

Kruckow M. U., Neunteufel P. G., Di Stefano R., Gao Y., Kobayashi C., 2021, The Astrophysical Journal, 920, 86

Kruckow M. U., et al., 2024, Astronomy & Astrophysics, 692, A141

Kruijssen J. D., 2012, Monthly Notices of the Royal Astronomical Society, 426, 3008

Krumholz M. R., McKee C. F., Bland-Hawthorn J., 2019, ARA&A, 57, 227

Kulkarni S., Hut P., McMillan S. J., 1993, Stellar black holes in globular clusters

Kustaanheimo P., Schinzel A., Davenport H., Stiefel E., 1965

Küpper A. H., Maschberger T., Kroupa P., Baumgardt H., 2011, Monthly Notices of the Royal Astronomical Society, 417, 2300

Law-Smith J. A. P., et al., 2022, Successful Common Envelope Ejection and Binary Neutron Star Formation in 3D Hydrodynamics, `http://arxiv.org/abs/2011.06630`

Lee H. M., 1995, Monthly Notices of the Royal Astronomical Society, 272, 605

Leveque A., Giersz M., Askar A., Arca-Sedda M., Olejak A., 2023, Monthly Notices of the Royal Astronomical Society, 520, 2593

Livio M., Soker N., 1988, ApJ, 329, 764

Makino J., Hut P., Kaplan M., Saygın H., 2006, New Astronomy, 12, 124

Mandel I., de Mink S. E., 2016, Monthly Notices of the Royal Astronomical Society, 458, 2634

Mapelli M., 2016, Monthly Notices of The Royal Astronomical Society, 459, 3432

Mapelli M., 2020, Frontiers in Astronomy and Space Sciences, 7, 38

Mapelli M., Ripamonti E., Zampieri L., Colpi M., Bressan A., 2010, Monthly Notices of the Royal Astronomical Society, 408, 234

Mapelli M., et al., 2021, Monthly Notices of the Royal Astronomical Society, 505, 339

Marchant P., Langer N., Podsiadlowski P., Tauris T. M., Moriya T. J., 2016, A&A, 588, A50

Marchant P., Renzo M., Farmer R., Pappas K. M., Taam R. E., De Mink S. E., Kalogera V., 2019, The Astrophysical Journal, 882, 36

Marchant P., Podsiadlowski P., Mandel I., 2024, Astronomy & Astrophysics, 691, A339

Marín Pina D., Gieles M., 2024, Monthly Notices of the Royal Astronomical Society, 527, 8369

Martin D., José J., Longland R., 2018, Computational Astrophysics and Cosmology, 5, 1

Marín Pina D., Rastello S., Gieles M., Kremer K., Fitzgerald L., Rando Forastier B., 2024, Astronomy & Astrophysics, 688, L2

Massevitch A., Yungelson L., 1975, Memorie della Societa Astronomica Italiana, 46, 217

McClintock J. E., Remillard R. A., 2006, in Lewin W. H. G., van der Klis M., eds, , Vol. 39, Compact stellar X-ray sources. pp 157–213, doi:10.48550/arXiv.astro-ph/0306213

McKernan B., et al., 2018, The Astrophysical Journal, 866, 66

Mikkola S., Tanikawa K., 1999, Monthly Notices of the Royal Astronomical Society, 310, 745

Miller M. C., Hamilton D. P., 2002, ApJ, 576, 894

Miller M. C., Lauburg V. M., 2009, The Astrophysical Journal, 692, 917

Mirabel F., 2017, New Astronomy Reviews, 78, 1

Mitchell J., 1784, Royal Society

Moe M., Di Stefano R., 2017, The Astrophysical Journal Supplement Series, 230, 15

Morscher M., Pattabiraman B., Rodriguez C., Rasio F. A., Umbreit S., 2015, The Astrophysical Journal, 800, 9

Namekata D., et al., 2018, Publications of the Astronomical Society of Japan, 70, 70

Neijssel C. J., et al., 2019, Monthly Notices of the Royal Astronomical Society, 490, 3740

Newton I., 1687, Royal Society

Nitadori K., Aarseth S. J., 2012, Monthly Notices of the Royal Astronomical Society, 424, 545

Ober W., El Eid M. F., Fricke K. J., 1983, Astronomy and Astrophysics, Vol. 119, P. 61, 1983, 119, 61

Oh S., Kroupa P., Pflamm-Altenburg J., 2015, The Astrophysical Journal, 805, 92

Olejak A., Belczynski K., 2021, The Astrophysical Journal Letters, 921, L2

Oshino S., Funato Y., Makino J., 2011, Publications of the Astronomical Society of Japan, 63, 881

Paczynski B., 1976, in Symposium-International Astronomical Union. Cambridge University Press, pp 75–80

Park D., Kim C., Lee H. M., Bae Y.-B., Belczynski K., 2017, Monthly Notices of The Royal Astronomical Society, 469, 4665

Pattabiraman B., Umbreit S., Liao W.-k., Choudhary A., Kalogera V., Memik G., Rasio F. A., 2013, The Astrophysical Journal Supplement Series, 204, 15

Pavlovskii K., Ivanova N., Belczynski K., Van K. X., 2017, Mon. Not. R. Astron. Soc., 465, 2092

Pavlík V., Vesperini E., 2021, Monthly Notices of the Royal Astronomical Society, 509, 3815

Peters P. C., 1964, Physical Review, 136, B1224

Peters P. C., Mathews J., 1963, Physical Review, 131, 435

Pfahl E., Rappaport S., Podsiadlowski P., 2002a, The Astrophysical Journal, 571, L37

Pfahl E., Rappaport S., Podsiadlowski P., 2002b, The Astrophysical Journal, 573, 283

Podsiadlowski P., Langer N., Poelarends A. J. T., Rappaport S., Heger A., Pfahl E., 2004, The Astrophysical Journal, 612, 1044

Portegies Zwart S. F., McMillan S. L. W., Hut P., Makino J., 2001, Monthly Notices of the Royal Astronomical Society, 321, 199

Portegies Zwart S. F., Baumgardt H., Hut P., Makino J., McMillan S. L. W., 2004, Nature, 428, 724

Portegies Zwart S. F., McMillan S. L., Gieles M., 2010, Annual review of astronomy and astrophysics, 48, 431

Qin Y., Hu R. C., Meynet G., Wang Y. Z., Zhu J. P., Song H. F., Shu X. W., Wu S. C., 2023, åp, 671, A62

Quinlan G. D., 1996, New Astronomy, 1, 35

Rantala A., Pihajoki P., Mannerkoski M., Johansson P. H., Naab T., 2020, Monthly Notices of the Royal Astronomical Society, 492, 4131

Rantala A., Naab T., Springel V., 2021, Monthly Notices of the Royal Astronomical Society, 502, 5546

Rantala A., Naab T., Rizzuto F. P., Mannerkoski M., Partmann C., Lautenschütz K., 2023, Monthly Notices of the Royal Astronomical Society, 522, 5180

Rantala A., Naab T., Lahén N., 2024, Monthly Notices of the Royal Astronomical Society, 531, 3770

Rastello S., Mapelli M., di Carlo U. N., Iorio G., Ballone A., Giacobbo N., Santoliquido F., Torniamenti S., 2021, Monthly Notices of the Royal Astronomical Society, 507, 3612

Rastello S., Iorio G., Mapelli M., Arca-Sedda M., Di Carlo U. N., Escobar G. J., Shenar T., Torniamenti S., 2023, Monthly Notices of the Royal Astronomical Society, 526, 740

Rees M. J., 1984, ARA&A, 22, 471

Riley J., Mandel I., Marchant P., Butler E., Nathaniel K., Neijssel C., Shortt S., Vigna-Gómez A., 2021, Monthly Notices of the Royal Astronomical Society, 505, 663

Riley J., et al., 2022, ApJS, 258, 34

Rizzuto F. P., et al., 2021, Monthly Notices of the Royal Astronomical Society, 501, 5257

Rodriguez C. L., Loeb A., 2018, The Astrophysical Journal Letters, 866, L5

Rodriguez C. L., Chatterjee S., Rasio F. A., 2016a, Physical Review D, 93, 084029

Rodriguez C. L., Haster C.-J., Chatterjee S., Kalogera V., Rasio F. A., 2016b, The Astrophysical Journal, 824, L8

Rodriguez C. L., Zevin M., Pankow C., Kalogera V., Rasio F. A., 2016c, The Astrophysical Journal Letters, 832, L2

Rodriguez C. L., Amaro-Seoane P., Chatterjee S., Rasio F. A., 2018a, Physical Review D, 98, 123005

Rodriguez C. L., Amaro-Seoane P., Chatterjee S., Rasio F. A., 2018b, Phys. Rev. Lett., 120, 151101

Rodriguez C. L., et al., 2022, The Astrophysical Journal Supplement Series, 258, 22

Samsing J., 2018, Physical Review D, 97, 103014

Samsing J., D'Orazio D. J., 2018, Monthly Notices of the Royal Astronomical Society, 481, 5445

Samsing J., MacLeod M., Ramirez-Ruiz E., 2014, The Astrophysical Journal, 784, 71

Sana H., et al., 2012, Science, 337, 444

Schnittman J. D., Buonanno A., 2007, ApJ, 662, L63

Scholz F. W., Stephens M. A., 1987, Journal of the American Statistical Association, 82, 918

Sedda M. A., Askar A., Giersz M., 2019, MOCCA-SURVEY Database I. Intermediate mass black holes in Milky Way globular clusters and their connection to supermassive black holes, `http://arxiv.org/abs/1905.00902`

Sepinsky J. F., Willems B., Kalogera V., Rasio F. A., 2007, ApJ, 667, 1170

Shao Y., Li X.-D., 2022, The Astrophysical Journal, 930, 26

Shields G. A., 1999, PASP, 111, 661

Shikauchi M., Kumamoto J., Tanikawa A., Fujii M. S., 2020, Publications of the Astronomical Society of Japan, 72, 45

Sigurdsson S., Phinney E. S., 1993, ApJ, 415, 631

Soberman G., Phinney E., Van Den Heuvel E., 1997, Astronomy and Astrophysics, v. 327, p. 620-635, 327, 620

Spera M., Mapelli M., 2017, Monthly Notices of the Royal Astronomical Society, 470, 4739

Spera M., Mapelli M., Giacobbo N., Trani A. A., Bressan A., Costa G., 2019, Monthly Notices of the Royal Astronomical Society, 485, 889

Spitzer L., 1987, Dynamical evolution of globular clusters

Spitzer Jr. L., Hart M. H., 1971, The Astrophysical Journal, 164, 399

Stegmann J., Antonini F., Moe M., 2022, Monthly Notices of the Royal Astronomical Society, 516, 1406

Stevenson S., Vigna-Gómez A., Mandel I., Barrett J. W., Neijssel C. J., Perkins D., de Mink S. E., 2017, Nature Communications, 8, 14906

Stevenson S., Sampson M., Powell J., Vigna-Gómez A., Neijssel C. J., Szécsi D., Mandel I., 2019, The Astrophysical Journal, 882, 121

Stodolkiewicz J., 1982, Acta Astronomica, vol. 32, no. 1-2, 1982, p. 63-91., 32, 63

Stodolkiewicz J., 1986, Acta Astronomica (ISSN 0001-5237), vol. 36, no. 1, 1986, p. 19-41., 36, 19

Stone N. C., Metzger B. D., Haiman Z., 2017, Mon. Not. R. Astron. Soc., 464, 946

Strader J., Chomiuk L., Maccarone T. J., Miller-Jones J. C., Seth A. C., 2012, Nature, 490, 71

Tanikawa A., Cary S., Shikauchi M., Wang L., Fujii M. S., 2023a, Monthly Notices of the Royal Astronomical Society, 527, 4031

Tanikawa A., Hattori K., Kawanaka N., Kinugawa T., Shikauchi M., Tsuna D., 2023b, The Astrophysical Journal, 946, 79

Tauris T. M., Takens R. J., 1998, åp, 330, 1047

Tauris T., Van Den Heuvel E., 2006, Compact stellar X-ray sources, 39, 623

Tauris T. M., Langer N., Podsiadlowski P., 2015, Monthly Notices of the Royal Astronomical Society, 451, 2123

Tauris T., et al., 2017, The Astrophysical Journal, 846, 170

Team COMPAS: Riley, J. et al., 2022, The Astrophysical Journal Supplement Series, 258, 34

Terlevich E., 1987, Monthly Notices of the Royal Astronomical Society, 224, 193

The LIGO Scientific Collaboration et al., 2021, arXiv e-prints, p. arXiv:2111.03606

Thompson T. A., et al., 2019, Science, 366, 637

Thorne K. S., 1980, Reviews of Modern Physics, 52, 299

Toonen S., Claeys J., Mennekens N., Ruiter A., 2014, Astronomy & Astrophysics, 562, A14

Torniamenti S., Rastello S., Mapelli M., Di Carlo U. N., Ballone A., Pasquato M., 2022, Monthly Notices of the Royal Astronomical Society, 517, 2953

Torniamenti S., Mapelli M., Périgois C., Arca Sedda M., Artale M. C., Dall'Amico M., Vaccaro M. P., 2024, A&A, 688, A148

Trenti M., Hut P., 2008, Scholarpedia, 3, 3930

Trenti M., Heggie D. C., Hut P., 2007, Monthly Notices of the Royal Astronomical Society, 374, 344

Tutukov A., Yungelson L., 1973, Nauchnye Informatsii, 27, 70

Van Den Heuvel E. P. J., Portegies Zwart S. F., De Mink S. E., 2017, Monthly Notices of the Royal Astronomical Society, 471, 4256

Vigna-Gómez A., et al., 2018, Monthly Notices of the Royal Astronomical Society, 481, 4009

Vinciguerra S., et al., 2020, Monthly Notices of the Royal Astronomical Society, 498, 4705

Von Hoerner S., 1960, Z. Astrophys. 50, 184-214, 50

Wang L., 2020, Monthly Notices of the Royal Astronomical Society, 491, 2413

Wang L., Spurzem R., Aarseth S., Nitadori K., Berczik P., Kouwenhoven M. B. N., Naab T., 2015, Monthly Notices of the Royal Astronomical Society, 450, 4070

Wang L., et al., 2016, Monthly Notices of the Royal Astronomical Society, 458, 1450

Wang L., Kroupa P., Jerabkova T., 2019, Monthly Notices of the Royal Astronomical Society, 484, 1843

Wang L., Nitadori K., Makino J., 2020a, Monthly Notices of the Royal Astronomical Society, 493, 3398

Wang L., Iwasawa M., Nitadori K., Makino J., 2020b, Monthly Notices of the Royal Astronomical Society, 497, 536

Wang L., Tanikawa A., Fujii M. S., 2021, Monthly Notices of the Royal Astronomical Society, 509, 4713

Weatherford N. C., Chatterjee S., Kremer K., Rasio F. A., 2020, The Astrophysical Journal, 898, 162

Webbink R., 1984, The Astrophysical Journal, 277, 355

Wiktorowicz G., Wyrzykowski L., Chruslinska M., Klencki J., Rybicki K. A., Belczynski K., 2019, The Astrophysical Journal, 885, 1

Woosley S., 2017, The Astrophysical Journal, 836, 244

Woosley S., 2019, The Astrophysical Journal, 878, 49

Woosley S., Heger A., 2021, The Astrophysical Journal Letters, 912, L31

Woosley S. E., Heger A., Weaver T. A., 2002, Reviews of modern physics, 74, 1015

Woosley S. E., Blinnikov S., Heger A., 2007, Nature, 450, 390

Xu X.-J., Li X.-D., 2010, The Astrophysical Journal, 716, 114

Yungelson L. R., van den Heuvel E. P. J., Vink J. S., Portegies Zwart S. F., de Koter A., 2008, A&A, 477, 223

Zevin M., Samsing J., Rodriguez C., Haster C.-J., Ramirez-Ruiz E., 2019, The Astrophysical Journal, 871, 91

Zwart S. P., Boekholt T., 2014, The Astrophysical Journal Letters, 785, L3

Zwart S. F. P., Makino J., McMillan S. L. W., Hut P., 1999, A&A, 348, 117

du Buisson L., et al., 2020, Monthly Notices of the Royal Astronomical Society, 499, 5941

Özel F., Psaltis D., Narayan R., McClintock J. E., 2010, The Astrophysical Journal, 725, 1918